EFFECT OF ENGINE POSITION AND HIGH-LIFT DEVICES ON AERODYNAMIC CHARACTERISTICS OF AN EXTERNAL-FLOW JET-FLAP STOL MODEL

by Charles C. Smith, Jr.

Langley Research Center
Hampton, Va. 23365

NATIONAL AERONAUTICS AND SPACE ADMINISTRATION • WASHINGTON, D. C. • MARCH 1971

1. Report No.	2. Government Accession No.	3. Recipient's Catalog No.
NASA TN D-6222		

4. Title and Subtitle	5. Report Date
EFFECT OF ENGINE POSITION AND HIGH-LIFT DEVICES ON AERODYNAMIC CHARACTERISTICS OF AN EXTERNAL-FLOW JET-FLAP STOL MODEL	March 1971
	6. Performing Organization Code

7. Author(s)	8. Performing Organization Report No.
Charles C. Smith, Jr.	L-7581
	10. Work Unit No.
9. Performing Organization Name and Address	721-01-11-06
NASA Langley Research Center Hampton, Va. 23365	11. Contract or Grant No.
	13. Type of Report and Period Covered
12. Sponsoring Agency Name and Address	Technical Note
National Aeronautics and Space Administration Washington, D.C. 20546	14. Sponsoring Agency Code

15. Supplementary Notes

16. Abstract

An investigation has been conducted to provide some basic information on the aerodynamic design parameters of an external-flow jet-flap configuration. Included in the investigation were static force tests to determine the effects of engine vertical and longitudinal position, jet-exhaust deflectors, flap size and type, leading-edge slat chord and deflection, and gap and overlap of the slats and flaps. The force tests were made in the Langley full-scale tunnel with a model having an unswept untapered wing and powered by four simulated high-bypass-ratio turbofan engines.

17. Key Words (Suggested by Author(s))	18. Distribution Statement
External-flow jet flap High lift Stability and control STOL	Unclassified – Unlimited

19. Security Classif. (of this report)	20. Security Classif. (of this page)	21. No. of Pages	22. Price*
Unclassified	Unclassified	140	$3.00

*For sale by the National Technical Information Service, Springfield, Virginia 22151

EFFECT OF ENGINE POSITION AND HIGH-LIFT DEVICES ON AERODYNAMIC CHARACTERISTICS OF AN EXTERNAL-FLOW JET-FLAP STOL MODEL

By Charles C. Smith, Jr.
Langley Research Center

SUMMARY

An investigation has been conducted to provide some basic information on the aerodynamic design parameters of an external-flow jet-flap configuration. Included in the investigation were static force tests to determine the effects of engine vertical and longitudinal position, jet-exhaust deflectors, flap size and type, leading-edge slat chord and deflection, and gap and overlap of the slats and flaps. The force tests were made in the Langley full-scale tunnel with a model having an unswept untapered wing and powered by four simulated high-bypass-ratio turbofan engines.

The results of the investigation showed that higher lift and better turning of the jet were obtained with the engines up close to the wing rather than well below the wing. Exhaust deflectors improved the lift and turning of the jet for a given installed engine thrust especially for the engine positions well below the wing. Large-chord flaps were found to produce more lift for a given installed engine thrust than small-chord flaps. Leading-edge slat deflections and chords slightly larger than those used for more normal lift operation were found to be necessary for high-lift jet-flap operation. Double-slotted-flap and leading-edge slat gaps and overlaps generally used for normal lift operation were also found to be effective for high-lift jet-flap operation.

INTRODUCTION

At the present time considerable interest is being shown in jet-powered STOL (short take-off and landing) aircraft. One promising means of achieving the high lift required for operation of such aircraft is the external-flow jet-augmented flap. Early experimental work demonstrated the lift capability of this concept. (For example, see refs. 1 to 5.) Recent extension of this research into the area of high-thrust-weight-ratio turbofan aircraft has shown that the external-flow jet flap effectively produces the high lift required for STOL operation (refs. 6 to 9).

Although considerable wind-tunnel research has been conducted on the external-flow jet-augmented flap, the main objective of most of the work in the past has been to explore

the general area of performance and stability and control with particular reference to problem areas and to finding practical solutions to the problems, so that the overall feasibility of the concept in terms of practical reliable application could be accurately assessed. This research has provided the necessary information to show that the external-flow jet-augmented flap effectively produces high lift on turbofan STOL aircraft but has provided very little information relative to the optimization of the jet-flap parameters involved. Because of the increased interest at the present time in the jet-flap concept, there is now a need for more detailed information for the rational design of such systems. A program has been started at the Langley Research Center to provide basic design information on the effects of geometric variables such as wing planform, engine location, jet-exhaust deflectors, flap span, flap size and type, leading-edge high-lift devices, and horizontal- and vertical-tail locations. The program will consist mainly of static force tests but will also include pressure distribution measurements for determining lift distribution along the wing chord and span.

This paper presents the results of part of the general investigation and consists of static force tests made to determine the effects of engine position, thrust deflectors, and leading-edge and trailing-edge flap geometry on the aerodynamic characteristics of an external-flow jet-flap configuration without vertical- and horizontal-tail surfaces. The model used in the investigation was powered by four simulated high-bypass-ratio turbofan engines and was equipped with an unswept untapered wing with double-slotted flaps. The tests were made over an angle-of-attack range for several thrust coefficients and for several flap deflections.

SYMBOLS

The data are referred to the stability-axis system with the origin at the center-of-gravity location (0.40 mean aerodynamic chord) shown in figure 1. Measurements were made in the U.S. Customary Units; they are presented herein in the International System of Units (SI) with the equivalent values in the U.S. Customary Units given parenthetically.

C_D drag coefficient, F_D/qS

C_L lift coefficient, F_L/qS

$C_{L,trim}$ trim lift coefficient, $C_L + \frac{C_m}{l/c}$

C_m pitching-moment coefficient, M_Y/qSc

C_μ gross-thrust coefficient, T/qS

c	local wing chord, 0.254 m (0.833 ft)
F_A	net axial force, N (lb)
F_D	drag force, N (lb)
F_L	lift force, N (lb)
F_N	normal force, N (lb)
l	tail length (assumed), m (ft)
M_Y	pitching moment, m-N (ft-lb)
q	free-stream dynamic pressure, N/m^2 (lb/ft^2)
S	wing area, 0.45 m^2 (4.86 ft^2)
T	total installed engine thrust, N (lb)
x	longitudinal coordinate of airfoil chord, percent vane or flap chord
y_u	airfoil upper surface ordinate, percent vane or flap chord
y_l	airfoil lower surface ordinate, percent vane or flap chord
α	angle of attack, deg
γ	flight-path angle, deg
δ_f	total deflection of double-slotted flap, $\delta_{f1} + \delta_{f2}$, deg
δ_{f1}	deflection of vane from wing chord, deg
δ_{f2}	deflection of flap from vane chord, deg
δ_j	jet or flap turning angle, $\tan^{-1} \frac{F_N}{F_A}$, deg

δ_s deflection of leading-edge slat from wing chord, deg

η flap turning efficiency, $\frac{\sqrt{F_N^2 + F_A^2}}{T}$

MODEL AND APPARATUS

The investigation was conducted on the four-engine high-wing model illustrated in figure 1. The wing was unswept and untapered and incorporated a leading-edge slat and double-slotted trailing-edge flaps. An NACA 4415 airfoil section was used on the wing. The airfoil sections for the vane and flap were identical, and their coordinates are presented in table I. Detailed sketches of the wing-leading-edge slat and trailing-edge flap assembly are shown in figure 2. Also shown is the position of the moment reference center relative to the wing. Changes in the leading-edge slat and trailing-edge flap deflections, overlaps, and gaps were obtained by using special brackets for each setting. In all tests with flaps deflected, $\delta_{f1} = \delta_{f2}$. No vertical- or horizontal-tail surfaces were used in the present investigation.

The model engines represented high-bypass-ratio fan-jet engines, and compressed-air-driven turbines drove the fans. The basic engine is illustrated in figure 3(a) and details of the jet-exhaust deflectors used in some tests are shown in figure 3(b). The deflector design was based on that of the small deflectors discussed in reference 6. Four sets of engine pylons were provided to give four different engine positions relative to the wing leading edge. (See fig. 4.)

The model was sting mounted on a six-component strain-gage balance in the 9.1- by 18.3-m (30- by 60-ft) test section of the Langley full-scale tunnel.

TESTS AND PROCEDURES

In preparation for the tests, engine calibrations were made to determine gross thrust as a function of engine rotational speed in the static condition (zero angle of attack with the thrust deflectors off). These calibrations were made with bellmouth inlets installed on the engines. The tests were then run by setting the engine rotational speed to give the desired thrust and holding these speeds constant over the angle-of-attack range.

Tests were made at zero airspeed to determine flap turning angles δ_j and turning efficiencies η under static conditions. These tests and the wind-on tests were made with the small-vane—large-flap configuration deflected 35°, 55°, and 70°. The trailing-edge flap and leading-edge slat parameters used in these tests were as follows:

Vane, 0.02c gap
Flap, 0.02c gap
Slat, Overlap, 0.02c gap
Slat chord, 0.19c
Slat deflection, 55^{o}

For flap deflections of 35^{o} and 70^{o}, four different engine positions with and without exhaust deflectors were tested. For a flap deflection of 55^{o}, only engine positions 1 and 4 were tested.

Tests to determine the effect of wing-flap geometry were made with the flap deflected at 55^{o} only. In these tests, various changes were made to the double-slotted-flap element gaps and overlaps, flap chord and element arrangement, and leading-edge geometry.

All the wind-on tests were made over an angle-of-attack range from -4^{o} to 31^{o} at gross-thrust coefficients C_{μ} of 0, 1.38, 2.75, 4.13, and 5.50. The free-stream dynamic pressure was 154.17 N/m^2 (3.22 psf) which corresponds to an airspeed of 15.85 m/sec (52 ft/sec). The Reynolds number was 2.78×10^5 based on the wing chord.

No wind-tunnel jet-boundary corrections were considered necessary since the model was very small relative to the test-section size.

RESULTS AND DISCUSSION

The longitudinal aerodynamic characteristics of the model with flaps retracted ($\delta_f = 0^{o}$), with engine position 4, and without exhaust deflectors are presented in figure 5 as an aid in analysis of the test results.

Effect of Engine Position on Static Turning

Since the effectiveness of a jet-flap system is dependent to a large degree upon the capability of the system for turning and spreading the jet exhaust efficiently, static turning tests were first made of all the configurations included in the present investigation to identify the relative performance of each. Results of these tests (figs. 6 and 7) show that jet turning angles were higher for the engines positioned vertically close to the wing (positions 1 and 2). For engines positioned low and forward of the wing (positions 3 and 4), tilting the engine nose down (position 4) produced some improvement in jet turning angle. For almost all the engine positions, jet-exhaust deflectors used to direct the exhaust toward the leading edge of the flap system improved the turning angle. The ratio of normal force to thrust F_N/T is plotted as a function of the ratio of net axial forces to thrust F_A/T in figure 7. The data indicate that the average losses caused by turning and spreading the jet were about 20 percent for 35^{o} flap deflection, about 35 percent for

55° flap deflection, and about 40 percent for 70° flap deflection. The deflectors were generally detrimental to the turning efficiency, but this effect was not consistent since for some engine positions at the high flap deflections the deflectors actually increased the flap turning efficiency.

Effect of Engine Position on Aerodynamic Characteristics

The basic aerodynamic data for the model with engine positions 1 to 4 with and without exhaust deflectors are presented in figures 8 and 9 for 35° flap deflection, in figures 10 and 11 for 55° flap deflection, and in figures 12 and 13 for 70° flap deflection. These data show that increasing the thrust coefficient caused an increase in stall angle of attack, maximum lift coefficient, and nose-down pitching moments. For the highest flap deflection ($\delta_f = 70°$), maximum lift coefficients up to about 12 (untrimmed) could be produced for a gross-thrust coefficient of 5.50.

In order to show the effects of engine position on the longitudinal aerodynamic characteristics more clearly, the data of figures 8 to 13 have been replotted in summary form for two values of C_μ (2.75 and 5.50) in figures 14 to 19. These data indicate that generally the highest lift was obtained with the engines vertically up close to the wing (positions 1 and 2) for all test conditions. For the 35° flap deflection (figs. 14 and 15), moving the engines forward from position 1 to position 2 actually increased the lift performance slightly; whereas, for the 70° flap deflection (figs. 18 and 19), moving the engines from position 1 to position 2 caused an appreciable drop in lift. The deterioration in lift performance for engine position 2 with increasing flap deflection is probably the result of an excessive amount of the jet exhaust being induced over the top of the wing by the high circulation lift. Previous investigations (for example, ref. 7) have revealed that when this condition exists, there is a tendency for the flow to break away from the wing at the flap instead of turning and following the flap as it does for lower surface blowing. For the low engine positions, having the engine exhaust directed straight back generally proved to be ineffective in producing high lift. This was particularly true for the low flap deflections because most of the jet exhaust passed beneath the flap. Tilting the engines so that the exhaust was directed more toward the leading edge of the flaps (position 4) considerably improved the lift effectiveness of the low engine arrangements. Exhaust deflectors used with the engines in the low positions generally produced an increase in lift. For example, figures 16 and 17, in which a more representative landing-approach flap setting ($\delta_f = 55°$) is used, show that the aerodynamic characteristics for engine positions 1 and 4 are similar as a result of the use of exhaust deflectors. Another point, which is illustrated by the data in figure 20, is that a larger favorable effect on the aerodynamic characteristics of the model was produced by the exhaust deflectors with the engines in position 4 than with the engines in position 1. The engines in position 1 were up close to the wing and the flaps were therefore well immersed in the jet exhaust without the use of

deflectors. The deflectors were needed, however, for engine position 4 to direct the jet over more of the flap for better spreading and turning.

One means of determining the overall efficiencies of jet-flap configurations is to compare the thrust-weight ratio T/W required to fly in level flight. In the present investigation, the term $\frac{C_\mu + C_D}{C_{L,trim}}$ was used to provide a measure of this efficiency. The term $\frac{C_\mu + C_D}{C_{L,trim}}$ is approximately equal to the thrust-weight ratio required to fly in level flight at an angle of attack of 0° and provides a convenient method for making a comparison when data are not available for the exact flap angle required for trim drag conditions. The $C_{L,trim}$ is the tail-off lift coefficient C_L corrected for pitch trim, that is, $C_{L,trim} = C_L + \frac{C_m}{l/c}$ with a tail arm l/c of 3.5 being assumed.

The data of figure 21 indicate that the most desirable positions of the engines from the standpoint of lift produced for a given installed thrust is up close to the wing (position 1) or low and tilted (position 4) for both low and high flap deflections. The low engine position without tilt (position 3) was undesirable for low flap deflections and the forward position (position 2) was undesirable for high flap deflections.

Effect of Flap Element Size

The longitudinal aerodynamic characteristics of the model with several different double-slotted-flap arrangements are presented in figures 22 to 27. These data are for a flap deflection δ_f of 55°, engine positions 1 and 4 with and without exhaust deflectors, and a range of thrust coefficient from 0 to 5.50. Four different arrangements of the double-slotted-flap elements were tested; they are illustrated in figure 2. The original leading-edge slat shown in figure 2 was used for these tests. For convenience in analyzing the results, summary plots of the basic data are presented in figures 28 and 29. These data show that, as might be expected, the largest chord flap produced the most lift and the smallest chord flap produced the least lift. The flap combination of small and large elements appeared to be most effective when the small vane was forward of the flap. With this arrangement, good lift was achieved with reduced pitching moments. When the small vane was to the rear of the flap, the lift decreased apparently because of relatively poor turning, but the pitching moments were high. To provide a better understanding of the total performance of the jet-flap configurations tested, the force test results are presented in figure 30 in terms of $\frac{C_\mu + C_D}{C_{L,trim}}$ and $C_{L,trim}$. The plots show that for a given thrust-weight ratio $\frac{C_\mu + C_D}{C_{L,trim}}$, the configurations with the largest chord flap generally

produced the most lift and the smallest chord flap, the least lift. This result indicates that a large-chord flap is necessary on a jet-flap wing not only to achieve good turning but also to achieve good spreading and, therefore, good span loading. The turning and spreading of the jet exhaust is the least for the model with small-chord flap and exhaust deflectors off because most of the jet exhaust passes underneath the flap. For the flap combination of small and large elements, there was no consistent difference in favor of having the smaller chord element as the vane or the flap.

In addition to the tests to determine the effect of flap element size with the double-slotted-flap arrangements, a few tests were also made with one of the flap slots sealed to simulate a single-slotted-flap arrangement. These data (fig. 31) show that for a given thrust coefficient C_μ, all the flap configurations had about the same drag; this indicates similar turning angles. However, the double-slotted flap was more efficient at producing lift, although this lift was accompanied by larger diving moments.

Effect of Flap Gap and Overlap

The longitudinal aerodynamic characteristics of the model for several combinations of overlap and gap of the double-slotted-flap elements are presented in figures 32 to 45 for a flap deflection δ_f of 55° and engine positions 1 and 4 with and without exhaust deflectors. Summary plots of the data for the thrust coefficient of 5.50 are presented in figures 46 to 51. Presented in figures 52 to 55 are values of $\frac{C_\mu + C_D}{C_{L,trim}}$ (equivalent to thrust-weight ratio) required to fly in level flight at an angle of attack of 0° and a lift coefficient of 5. The data of figures 46 to 51 show that increasing the gaps of the flap or the vane generally increased the lift, drag, and the diving moments. Increases in the overlap from -0.02c to 0.02c also generally increased the lift and drag and caused reductions in the diving moments. The significance of these changes in aerodynamic characteristics with changes in gap and overlap is shown in the summary plots presented as figures 52 to 55. In these figures it is seen that increases in gap size of the vane or flap generally caused increases in the thrust required to fly at a given lift coefficient $\left(C_{L,trim} = 5.0\right)$, particularly for the large vane gaps. Increases in the overlap of the flap from -0.02c to 0.02c were generally beneficial to the thrust requirements, although this effect was relatively small. The limited data obtained with variations in vane overlap (fig. 55) show no consistent trends in aerodynamic characteristics as a result of vane overlap changes but do show minimum thrust requirements for this condition near a vane overlap of zero percent wing chord.

Effect of Leading-Edge Slat Size, Gap, and Overlap

The basic longitudinal aerodynamic data for variations in leading-edge-slat geometry are presented in figures 56 to 65 and are summarized in figures 66 to 71. These data were measured mostly for the configuration with engine position 4 and exhaust deflectors on. The data of figures 66 and 67 show that changes in gap size from 0.01c to 0.03c and changes in overlap from 0 to 0.02c had little effect on the aerodynamic characteristics of the model. Changes in leading-edge slat deflection from 45^{o} to 65^{o} (fig. 68) extended the stall to a slightly higher angle of attack and caused the lift curve to break less abruptly. Figures 69 to 71 show that extending the chord of the slat from 0.19c to 0.25c generally increased the maximum lift coefficient for the higher thrust coefficients. For the lower thrust coefficients $\left(C_{\mu} = 2.75\right)$, there was no appreciable effect of extending the chord of the leading-edge slat except for an increase in lift coefficient above the stall. The data presented in figure 72 show that, in general, the leading-edge slats tested were more effective than the leading-edge flaps formed by sealing the slots of the slats.

Effect of Engine-Out Condition

The longitudinal aerodynamic characteristics of the model with one or more of the engines inoperative are presented in figure 73 for the model with engines in position 1 and exhaust deflectors off. Summary plots of these characteristics for maximum thrust $\left(C_{\mu} = 5.50\right)$ with all four engines operating, and for various engine-out conditions are presented in figure 74. These plots show that the loss of an engine causes little or no change in the longitudinal stability but produces large changes in pitch trim, lift, and drag. The effect of one or more engines being inoperative on the lift and drag is best shown by the summary plot of trim lift coefficient $C_{L,trim}$ as a function of thrust coefficient C_{μ} presented as figure 75. These data show that the loss of the inboard engine causes a larger reduction in lift for a given C_{μ} than does the loss of the outboard engine. As might be expected, the loss of both outboard engines causes a considerable reduction in trim lift coefficient $C_{L,trim}$ for a given thrust coefficient. This effect is basically the effect of a reduction in effective aspect ratio.

CONCLUSIONS

From a wind-tunnel investigation to determine the effects of engine position and wing trailing-edge and leading-edge geometry on the aerodynamic characteristics of an external-flow jet-flap STOL model, the following conclusions are drawn:

1. Better turning of the jet and higher lift for a given installed engine thrust was obtained with the engines up close to the wing rather than well below or forward of the

wing. Tilting the engines when in the low position result in better spreading of the jet exhaust over the flap and improves the lift.

2. Engine exhaust deflectors improved the turning of the jet and increased the lift for a given installed engine thrust especially for the low engine positions.

3. Large-chord double-slotted flaps were found to be more efficient in producing lift for a given installed engine thrust than were small-chord double-slotted flaps.

4. Leading-edge slat deflections and chords slightly larger than those used for more normal lift operation were found to be necessary for effective high-lift jet-flap operation.

5. Double-slotted-flap and leading-edge slat gaps and overlaps generally used for normal lift operation were also found to be effective for high-lift jet-flap operation.

Langley Research Center,
National Aeronautics and Space Administration,
Hampton, Va., February 11, 1971.

REFERENCES

1. Campbell, John P.; and Johnson, Joseph L., Jr.: Wind-Tunnel Investigation of an External-Flow Jet-Augmented Slotted Flap Suitable for Application to Airplanes With Pod-Mounted Jet Engines. NACA TN 3898, 1956.

2. Lowry, John G.; Riebe, John M.; and Campbell, John P.: The Jet-Augmented Flap. Preprint No. 715, S.M.F. Fund Paper, Inst. Aeronaut. Sci., Jan. 1957.

3. Johnson, Joseph L., Jr.: Wind-Tunnel Investigation of a Small-Scale Sweptback-Wing Jet-Transport Model Equipped With an External-Flow Jet-Augmented Double Slotted Flap. NASA MEMO 3-8-59L, 1959.

4. Johnson, Joseph L., Jr.: Wind-Tunnel Investigation of the Static Longitudinal Stability and Trim Characteristics of a Sweptback-Wing Jet-Transport Model Equipped With an External-Flow Jet-Augmented Flap. NACA TN 4177, 1958.

5. Fink, Marvin P.: Aerodynamic Characteristics, Temperature, and Noise Measurements of a Large-Scale External-Flow Jet-Augmented-Flap Model With Turbojet Engines Operating. NASA TN D-943, 1961.

6. Freeman, Delma C., Jr.; Parlett, Lysle P.; and Henderson, Robert L.: Wind-Tunnel Investigation of a Jet Transport Airplane Configuration With an External-Flow Jet Flap and Inboard Pod-Mounted Engines. NASA TN D-7004, 1970.

7. Parlett, Lysle P.; and Shivers, James P.: Wind-Tunnel Investigation of an STOL Aircraft Configuration Equipped With an External-Flow Jet Flap. NASA TN D-5364, 1969.

8. Parlett, Lysle P.; Freeman, Delma C., Jr.; and Smith, Charles C., Jr.: Wind-Tunnel Investigation of a Jet Transport Airplane Configuration With High Thrust-Weight Ratio and an External-Flow Jet Flap. NASA TN D-6058, 1970.

9. Parlett, Lysle P.; Fink, Marvin P.; and Freeman, Delma C., Jr. (With appendix by Marion O. McKinney and Joseph L. Johnson, Jr.): Wind-Tunnel Investigation of a Large Jet Transport Model Equipped With an External-Flow Jet Flap. NASA TN D-4928, 1968.

TABLE I.- VANE AND FLAP AIRFOIL COORDINATES

[Percent vane and flap chord]

x	y_u	y_l
0	0	0
5	9.8	-3.3
10	13.0	-4.1
15	15.0	-3.8
20	16.0	-3.8
25	17.2	-3.5
30	17.3	-3.3
40	17.0	-2.8
50	15.2	-2.2
60	12.5	-1.7
70	10.0	-1.3
80	7.1	-.8
90	4.0	.7
100	1.2	.3

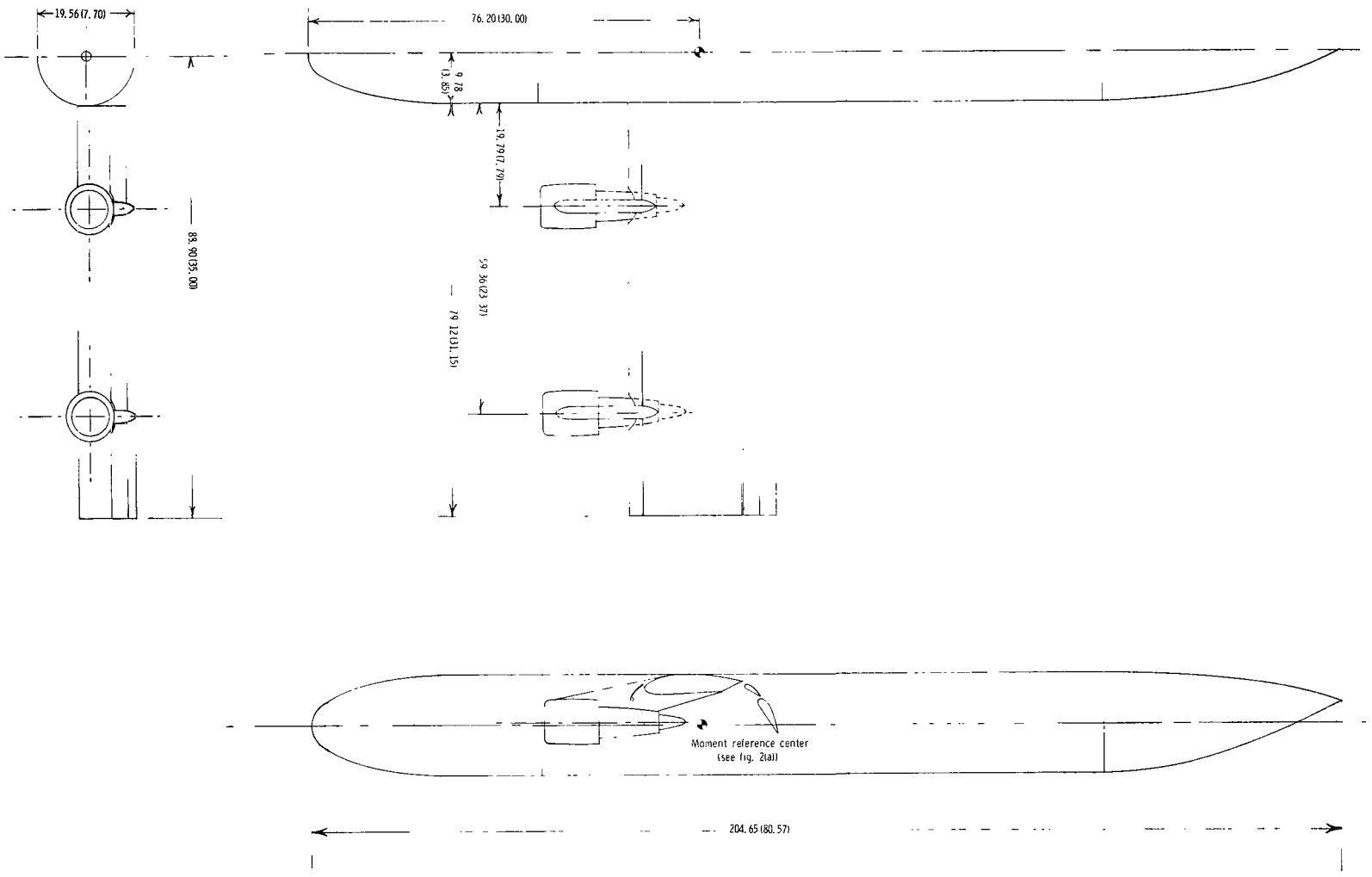

Figure 1.- Three-view drawing of model used in investigation. Dimensions are in centimeters (inches).

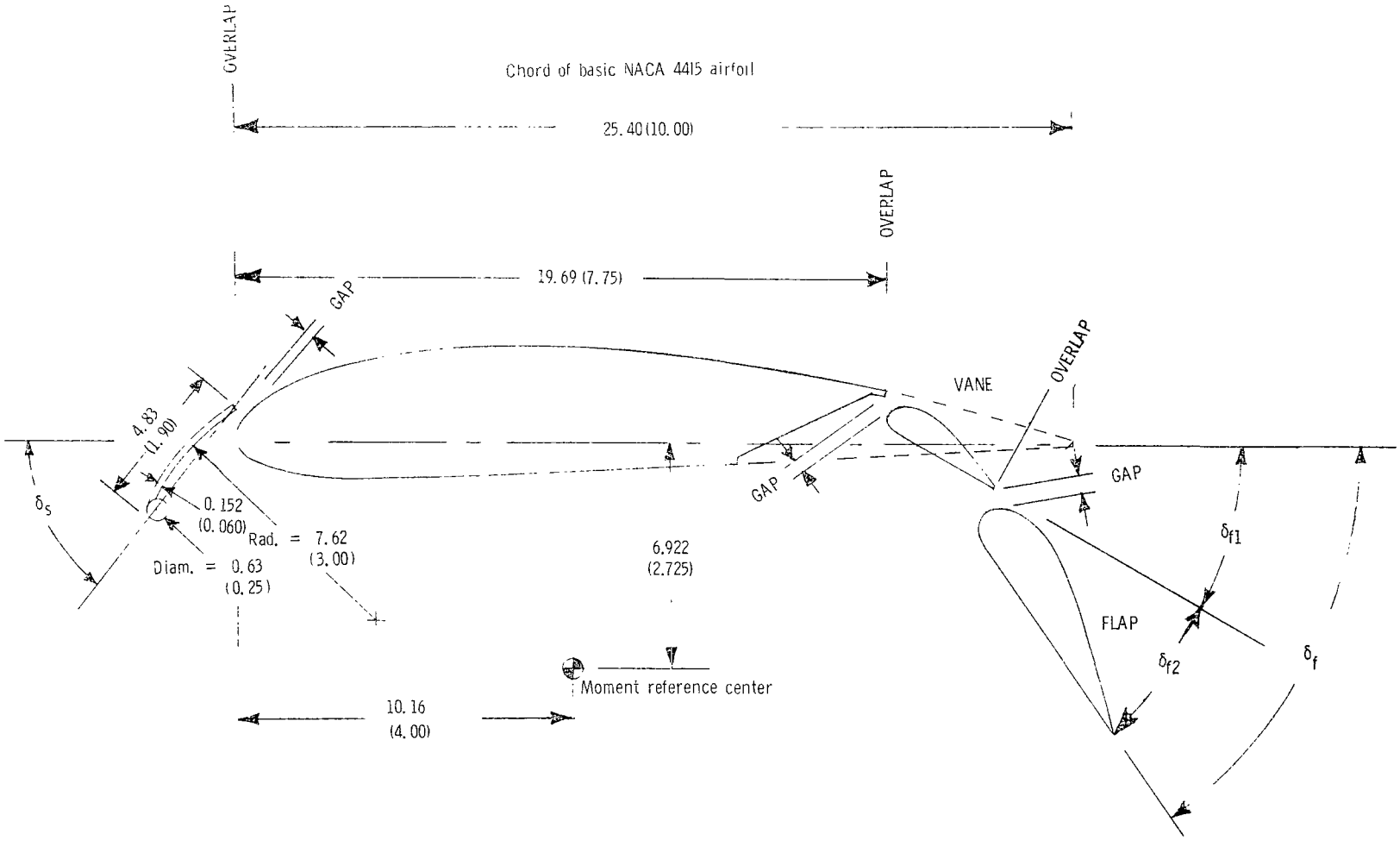

(a) Slat details and general arrangement of flaps. $\delta_{f1} = \delta_{f2}$.

Figure 2.- Details of slats and flaps. Dimensions are in centimeters (inches).

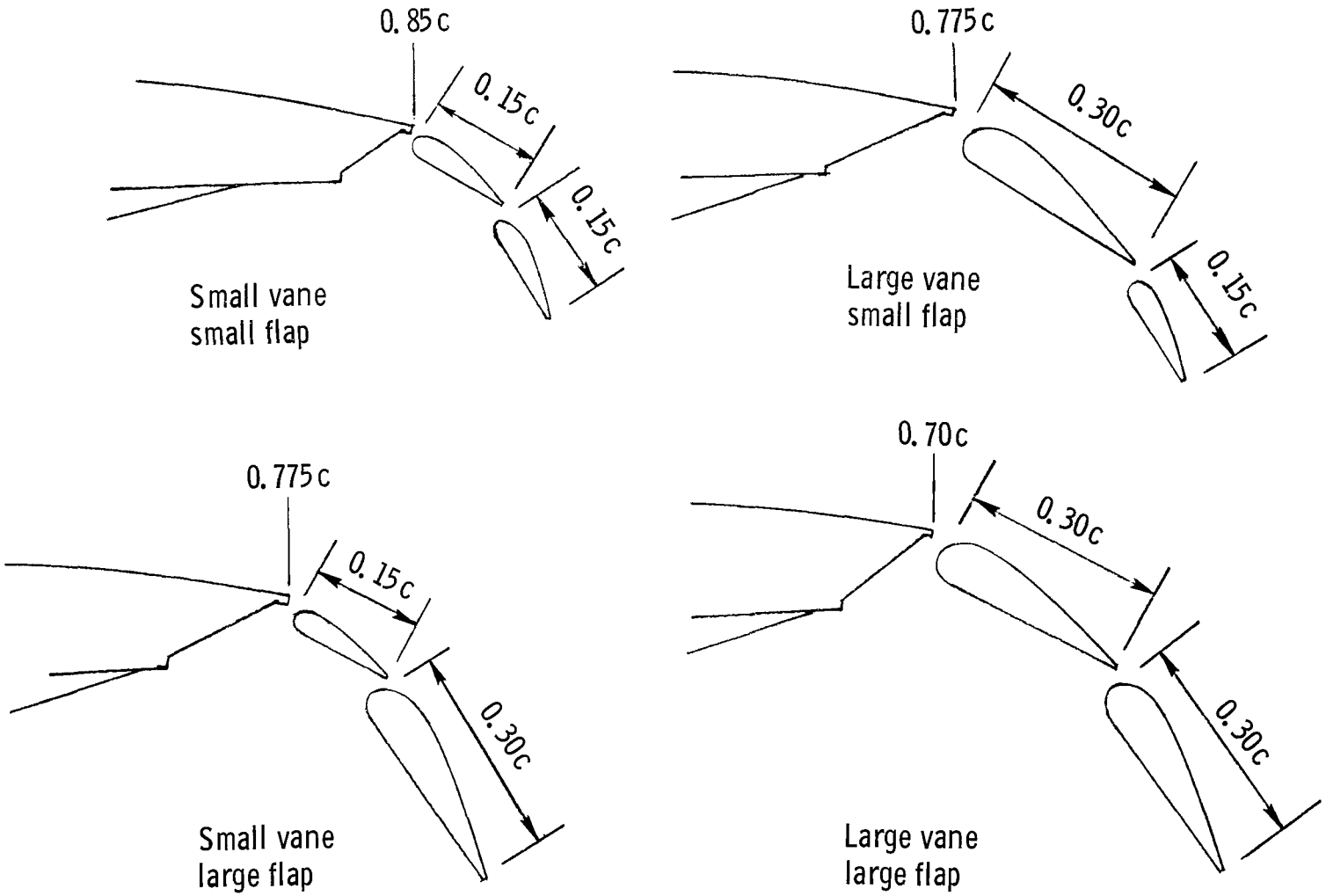

(b) Flap configurations used in investigation.

Figure 2.- Concluded.

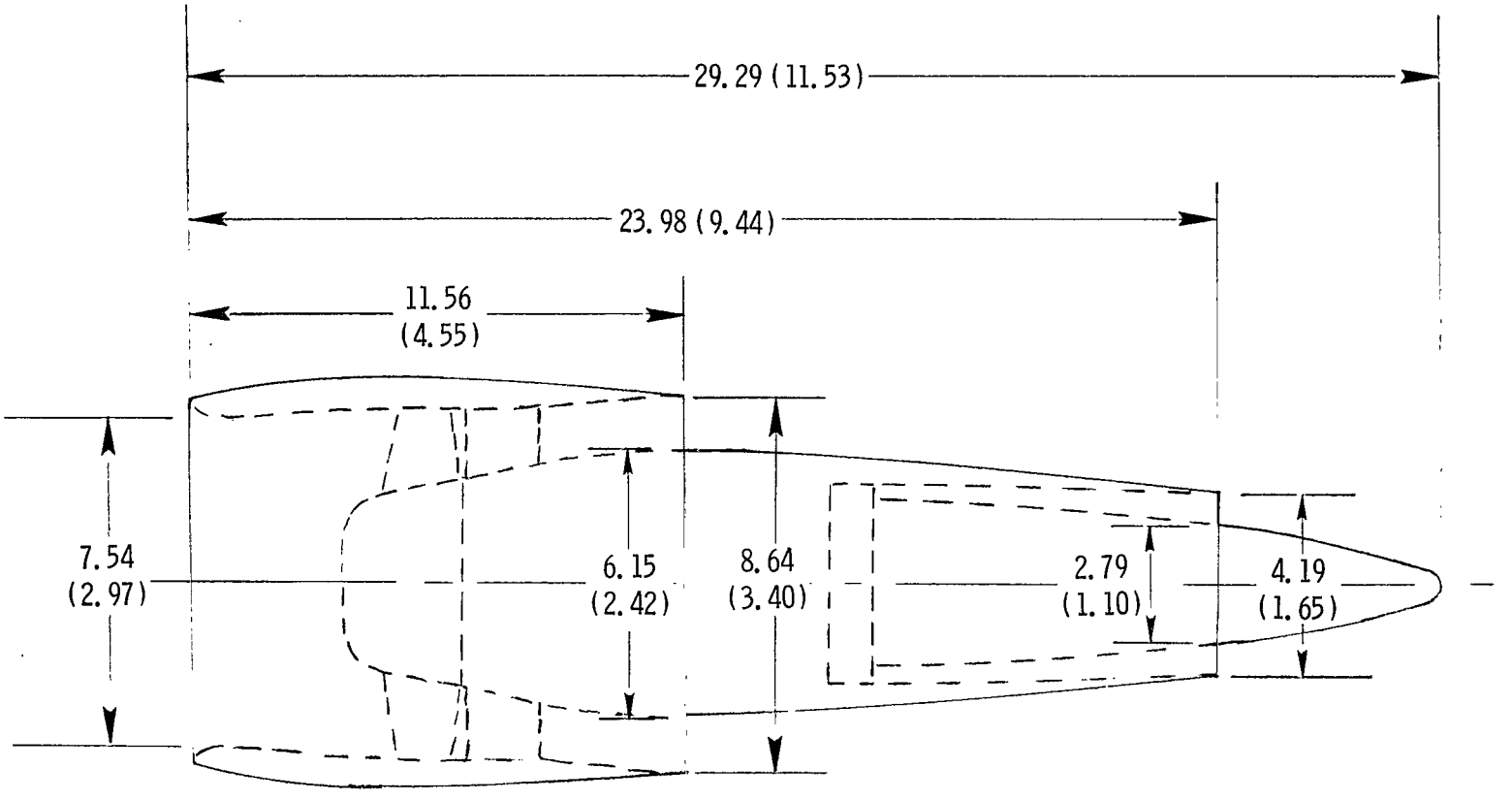

(a) Basic engine.

Figure 3.- Engine and exhaust deflectors. Dimensions are in centimeters (inches).

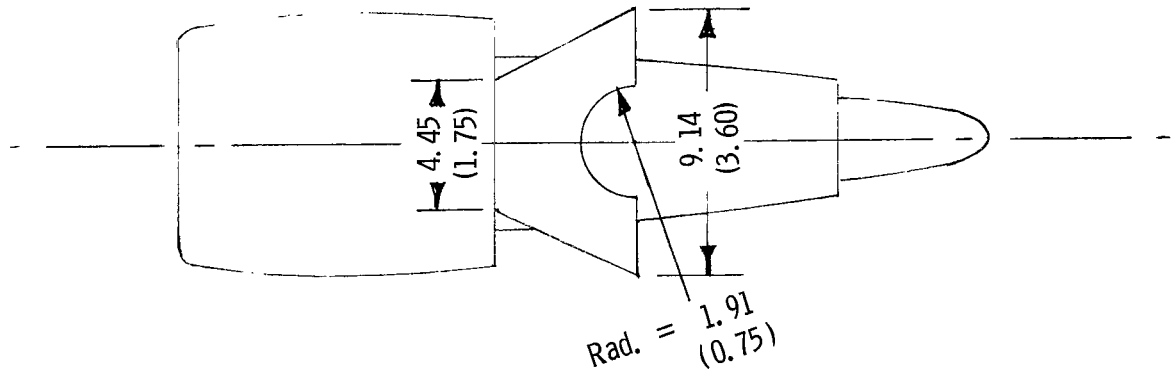

Bottom view

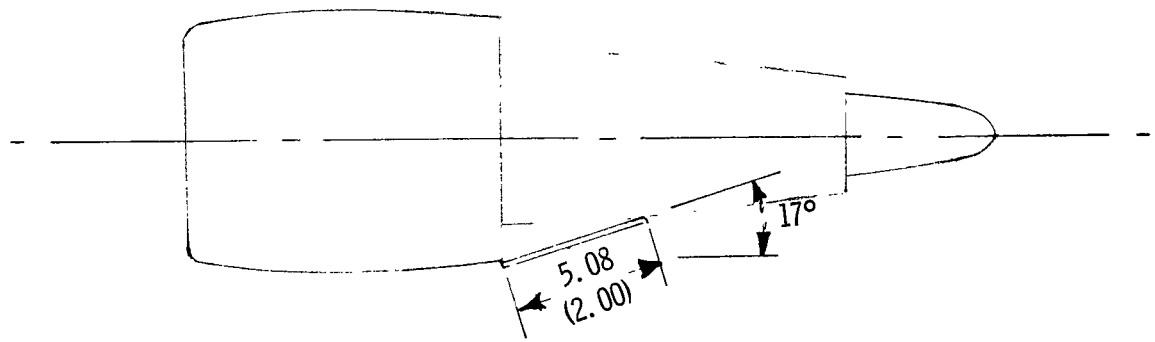

Side view

(b) Details of exhaust deflectors.

Figure 3.- Concluded.

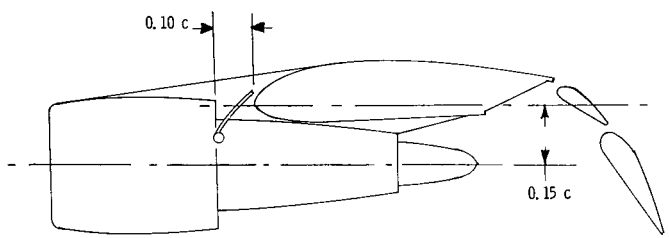

Engine Position 1

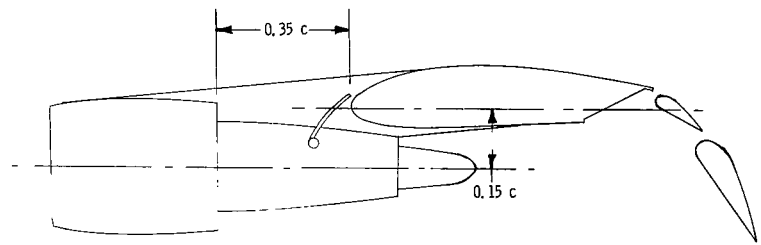

Engine Position 2

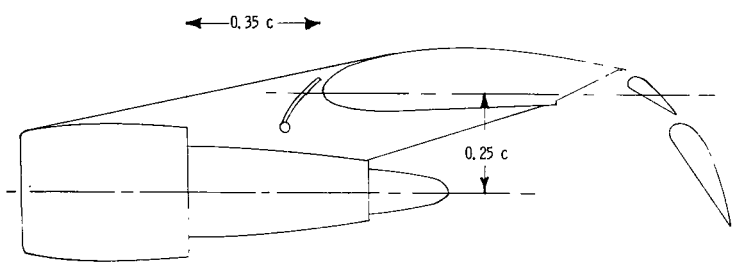

Engine Position 3

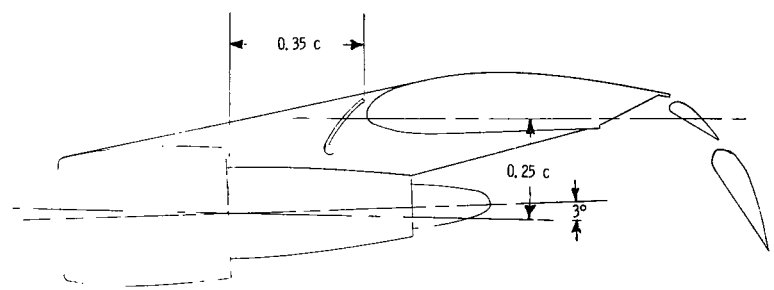

Engine Position 4

Figure 4.- Engine positions used in investigation.

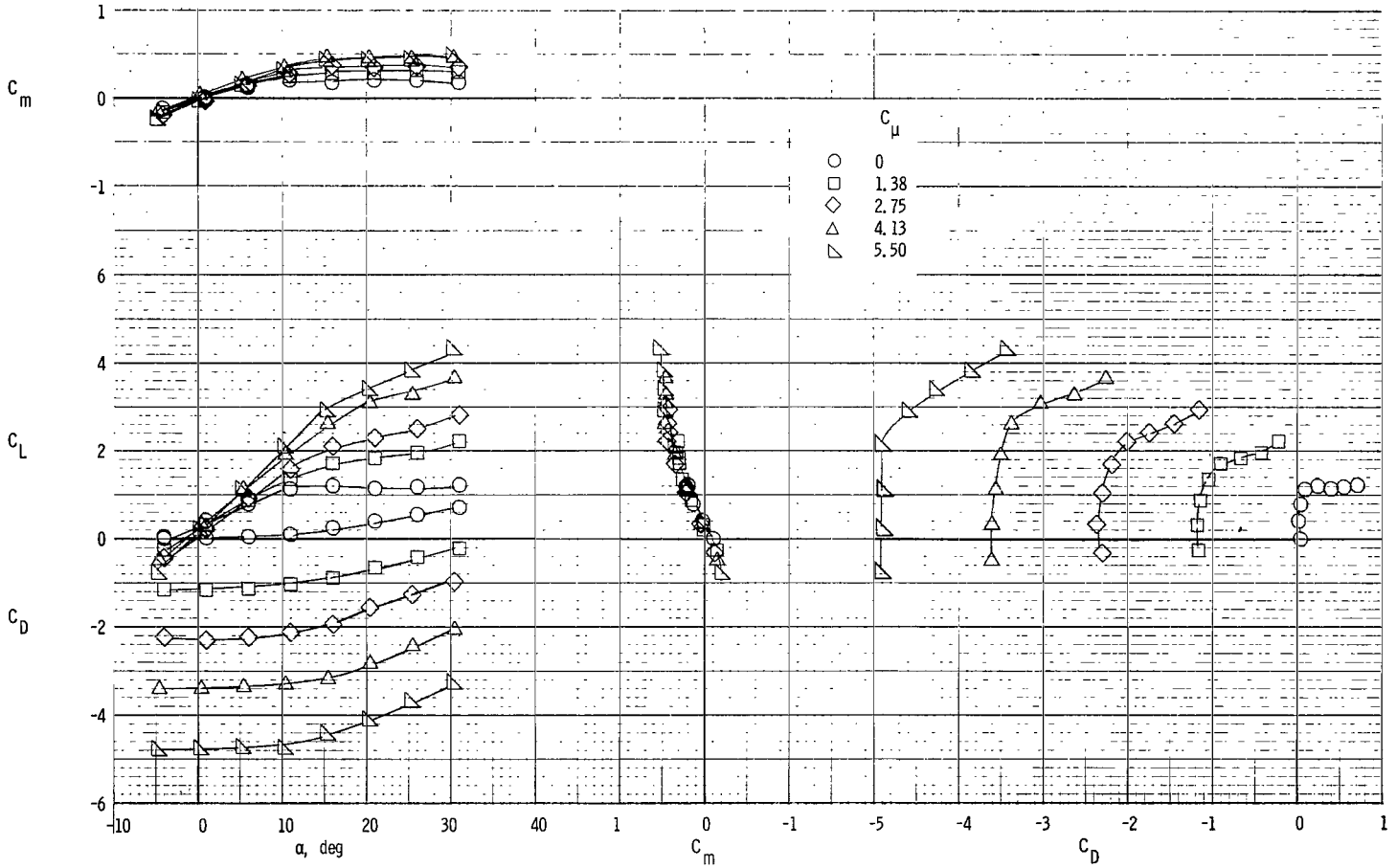

Figure 5.- Longitudinal aerodynamic characteristics of model in the cruise condition. $\delta_f = 0^o$; engine position 4; exhaust deflectors off.

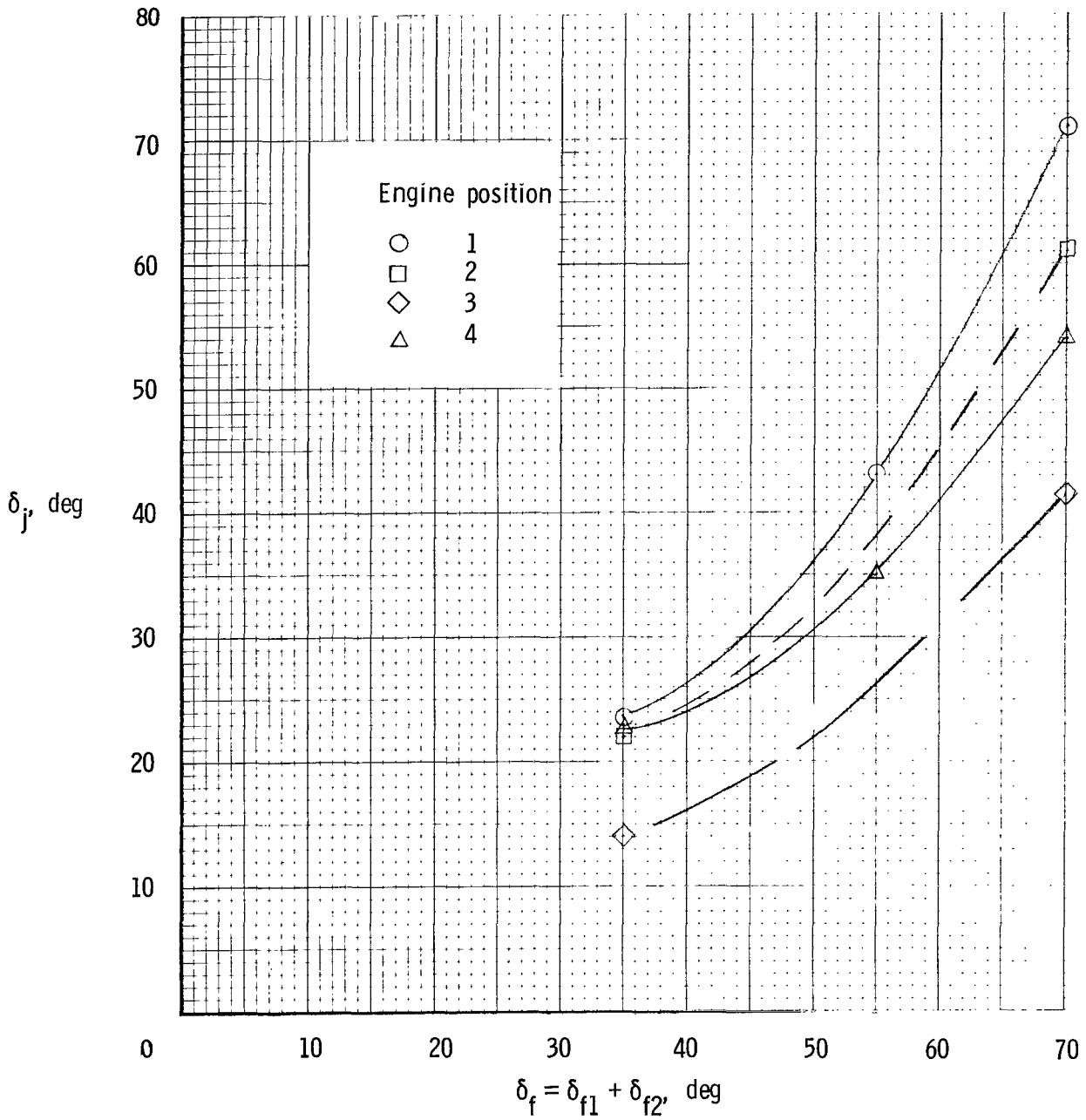

(a) Exhaust deflectors off.

Figure 6.- Calibration of jet deflection angles.

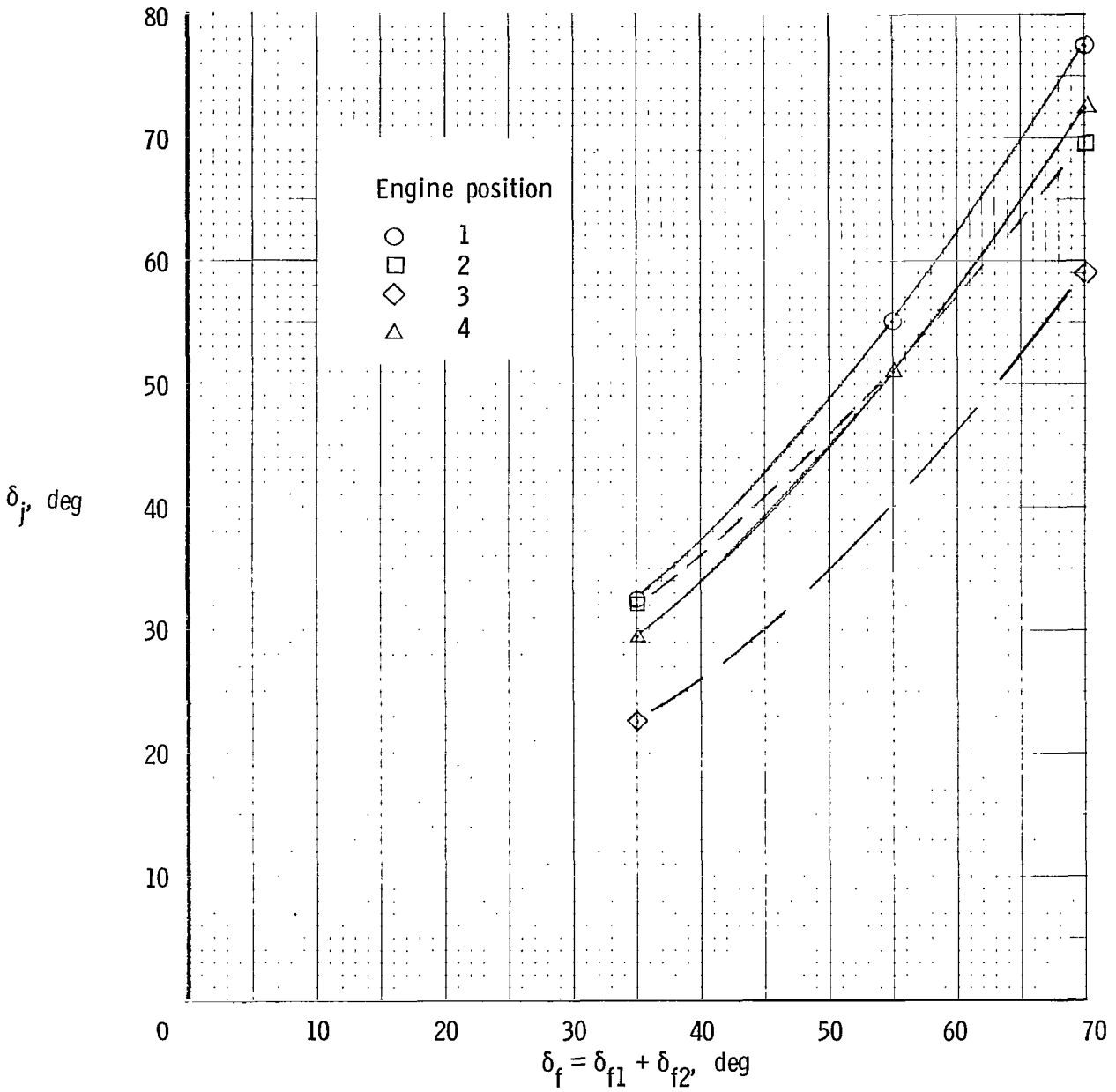

(b) Exhaust deflectors on.

Figure 6.- Concluded.

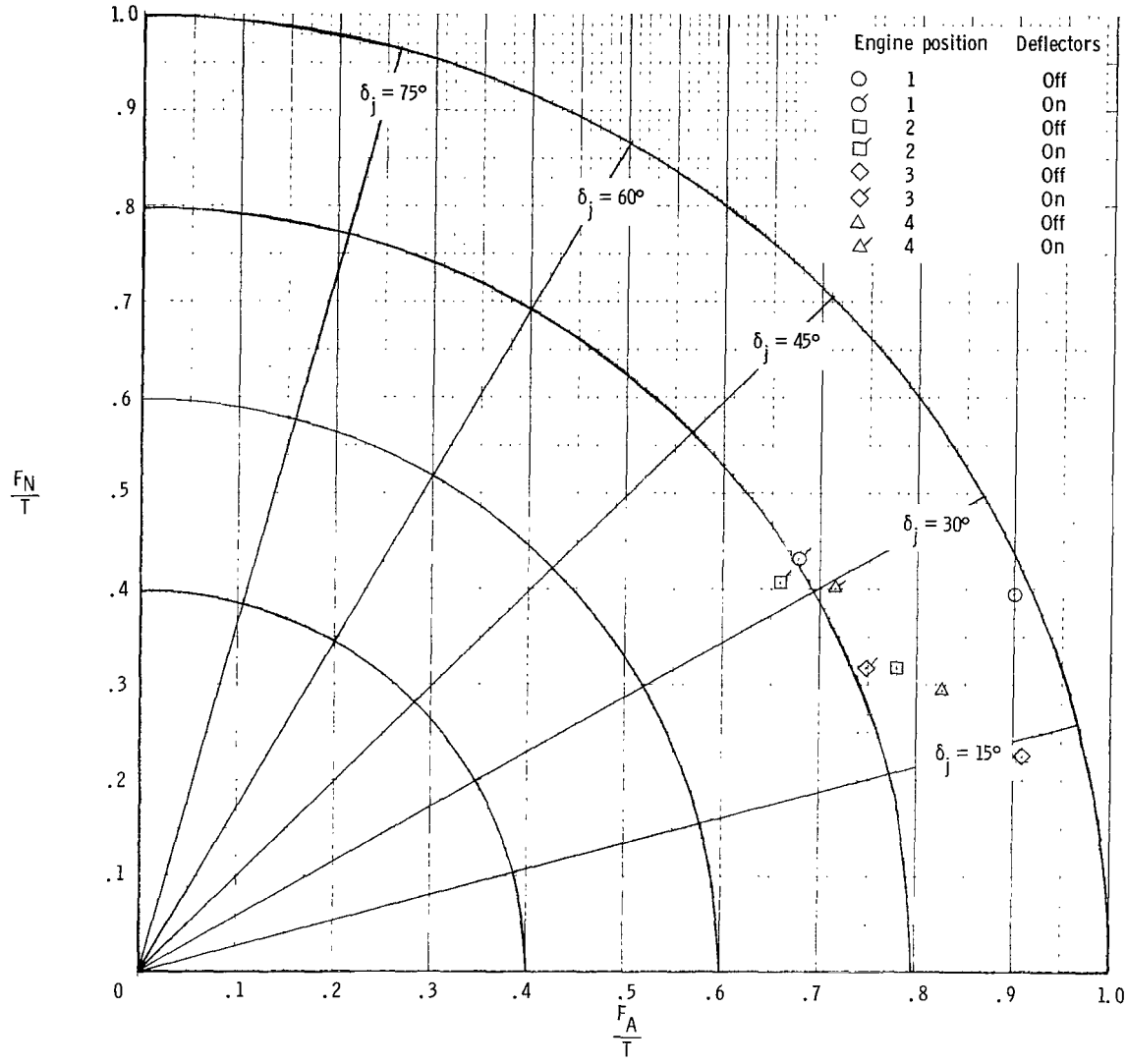

(a) $\delta_f = 35^o$.

Figure 7.- Summary of flap turning efficiency and turning angle.

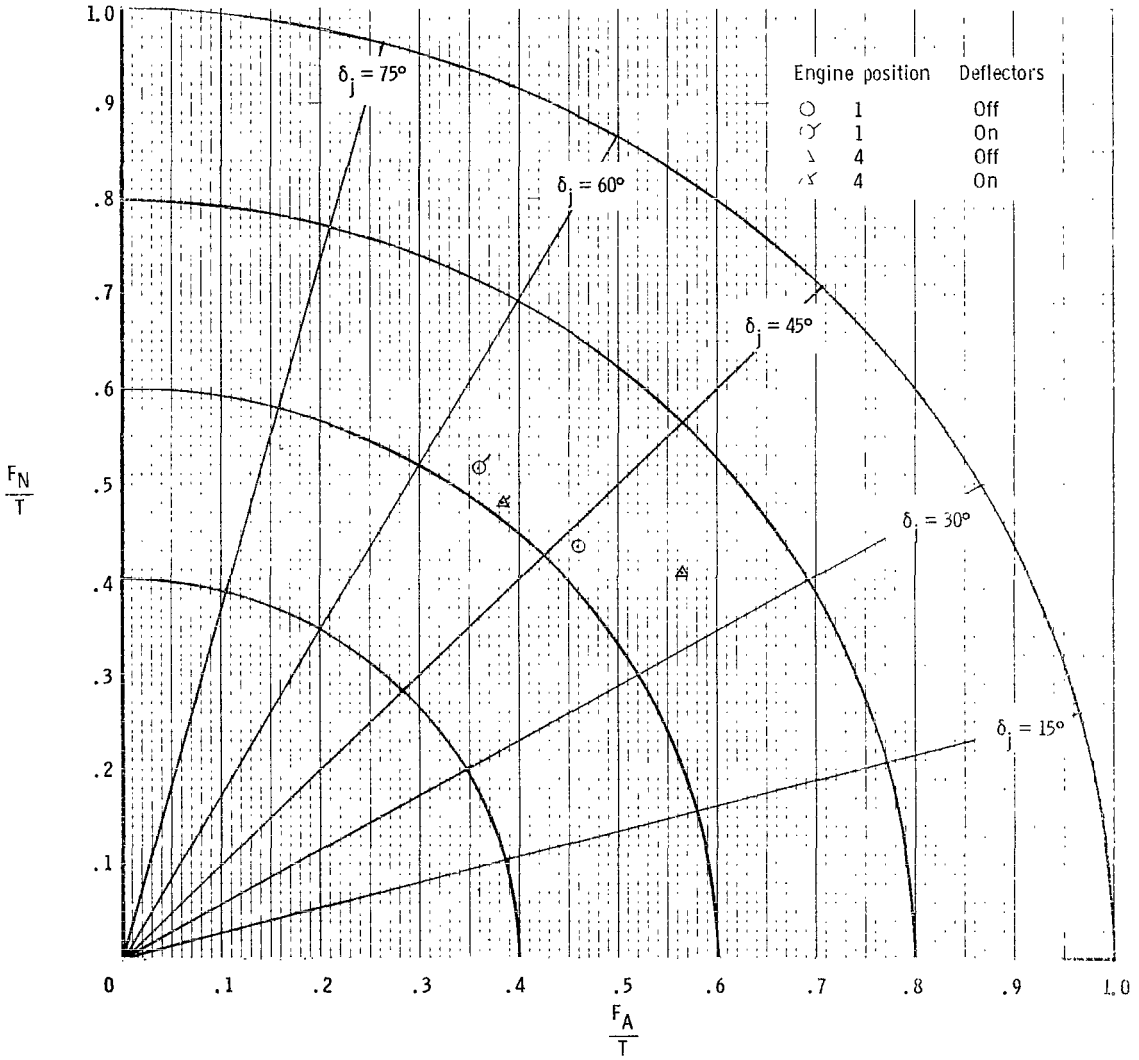

(b) $\delta_f = 55°$.

Figure 7.- Continued.

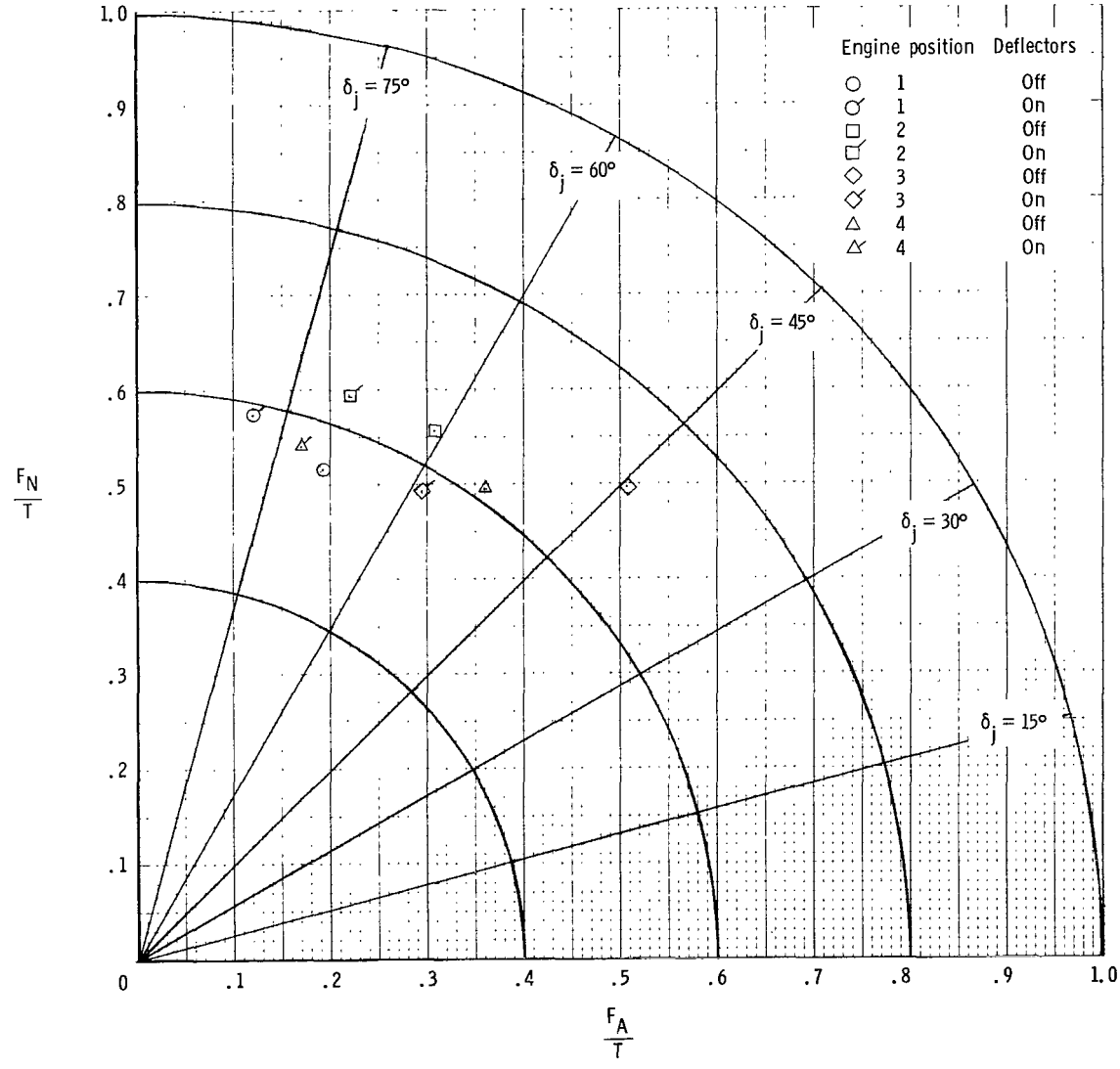

(c) $\delta_f = 70°$.

Figure 7.- Concluded.

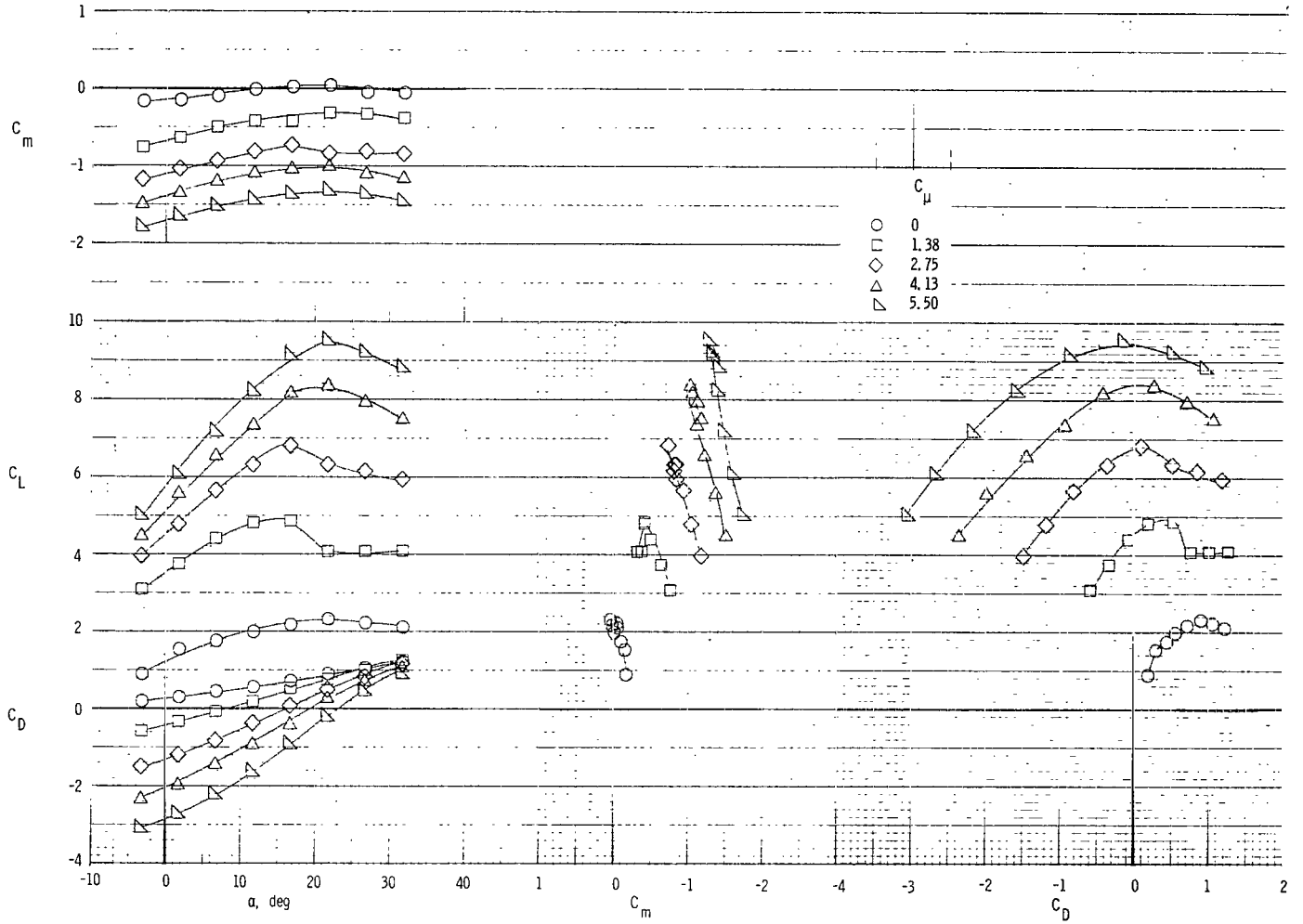

(a) Engine position 1.

Figure 8.- Longitudinal aerodynamic characteristics of model without exhaust deflectors. $\delta_f = 35^o$.

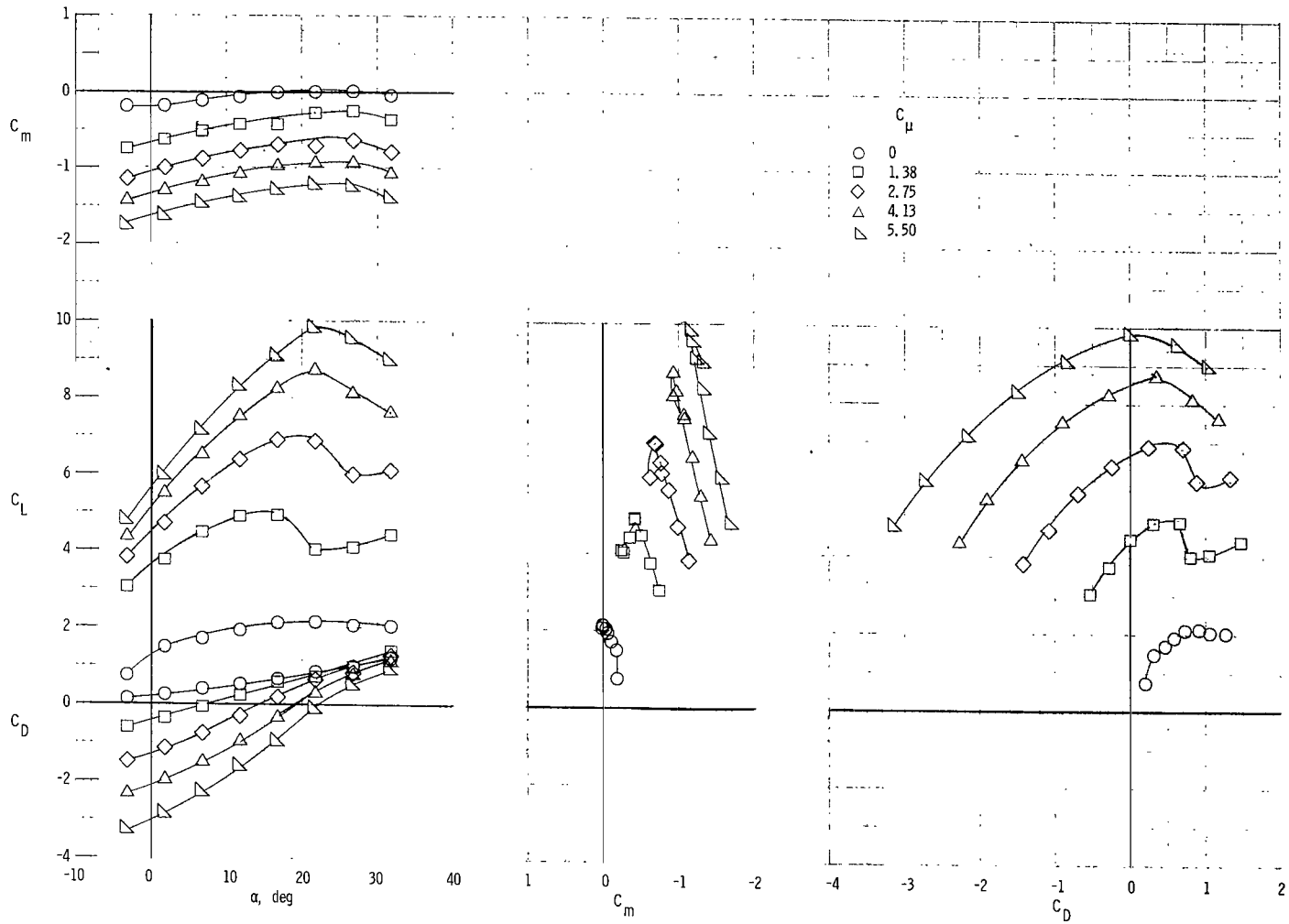

(b) Engine position 2.

Figure 8.- Continued.

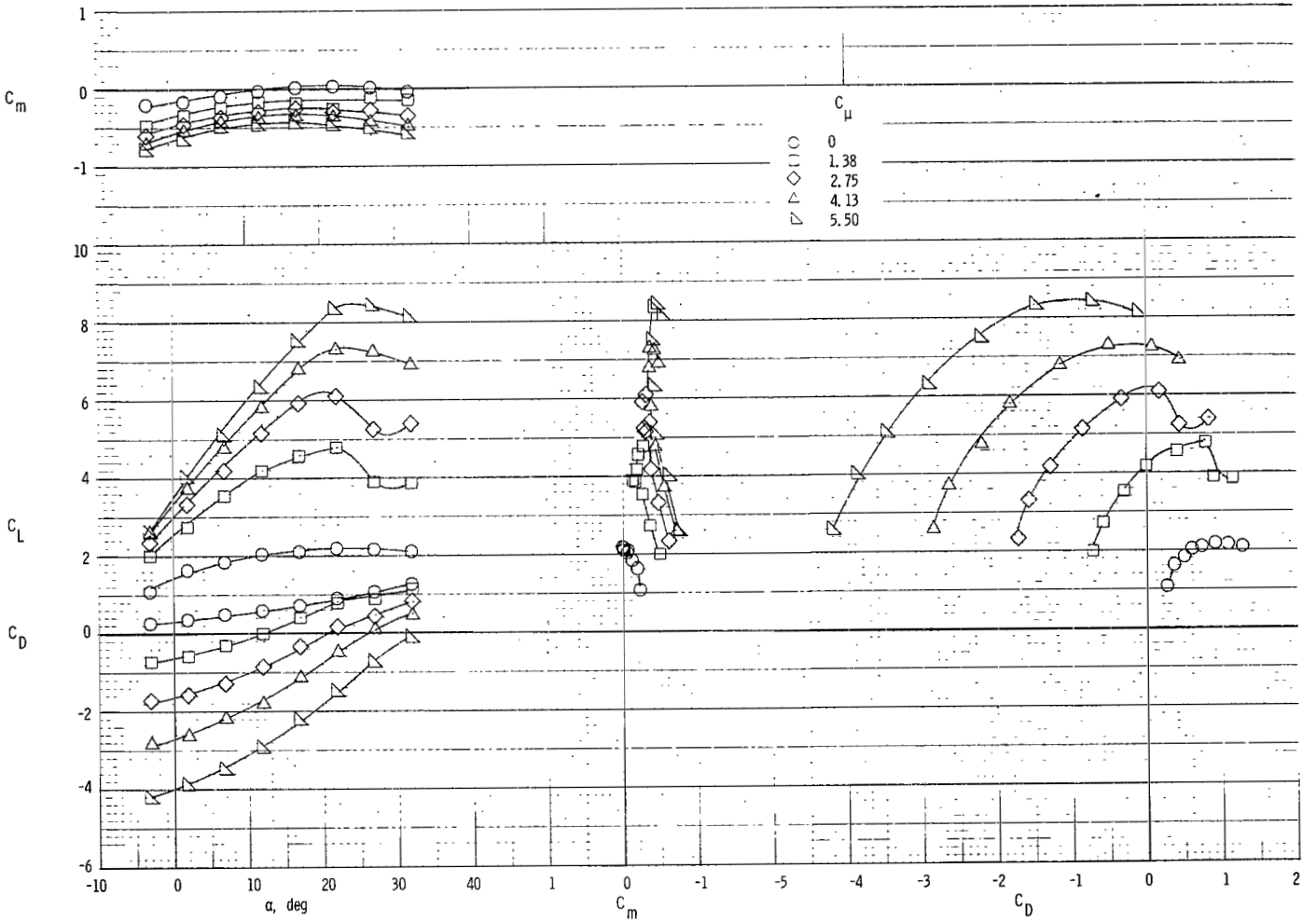

(c) Engine position 3.

Figure 8.- Continued.

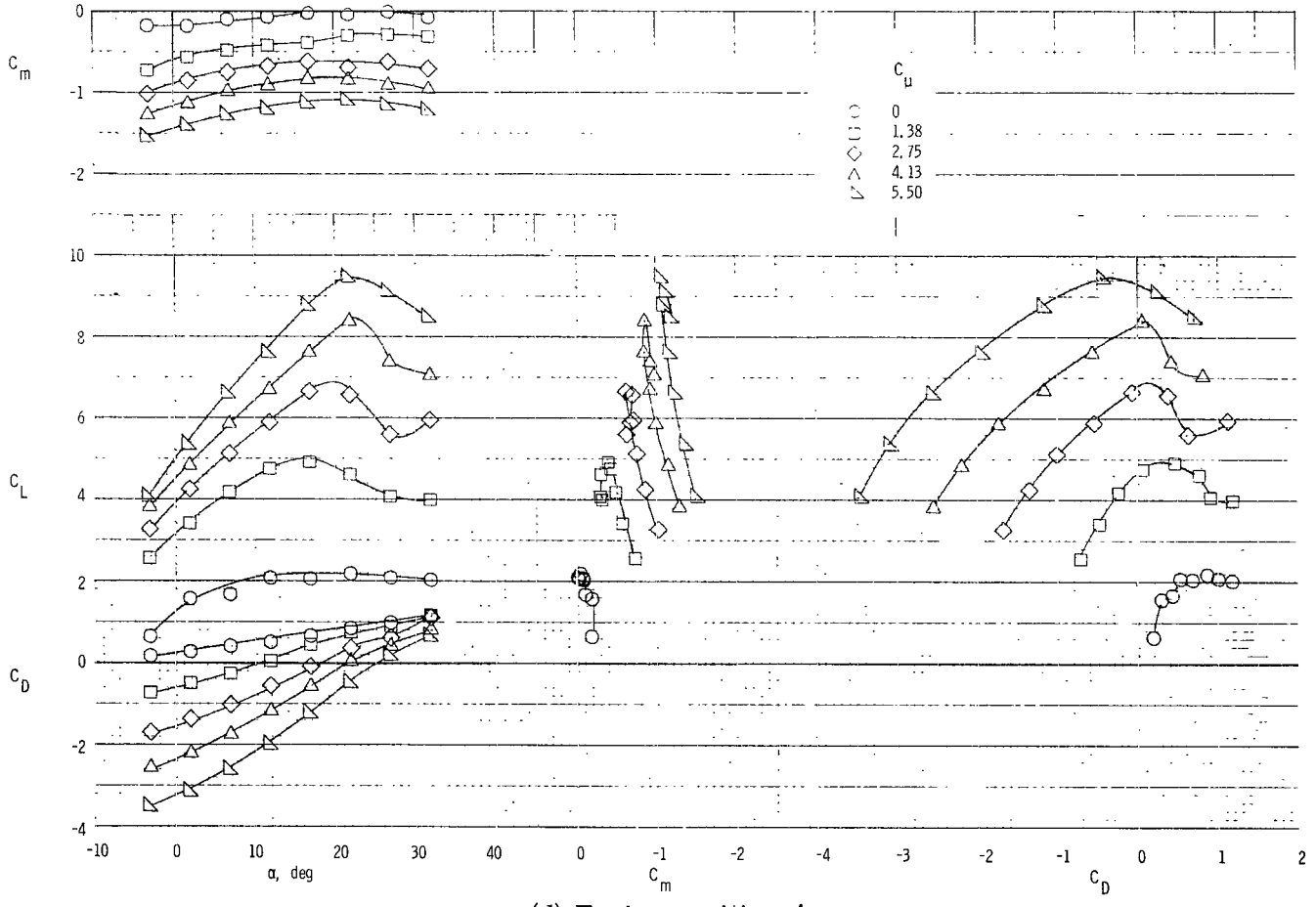

(d) Engine position 4.

Figure 8.- Concluded.

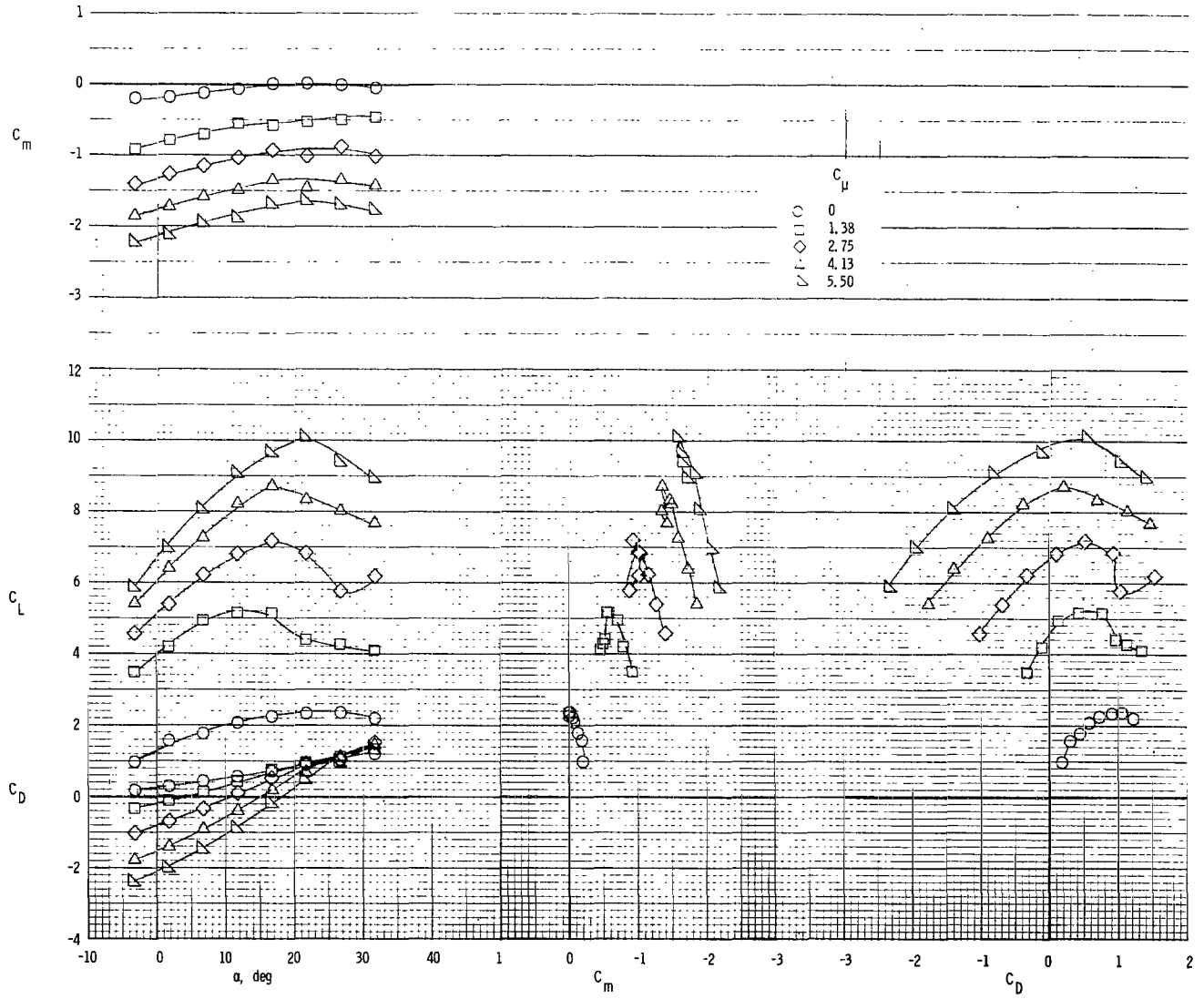

(a) Engine position 1.

Figure 9.- Longitudinal aerodynamic characteristics of model with exhaust deflectors. $\delta_f = 35^o$.

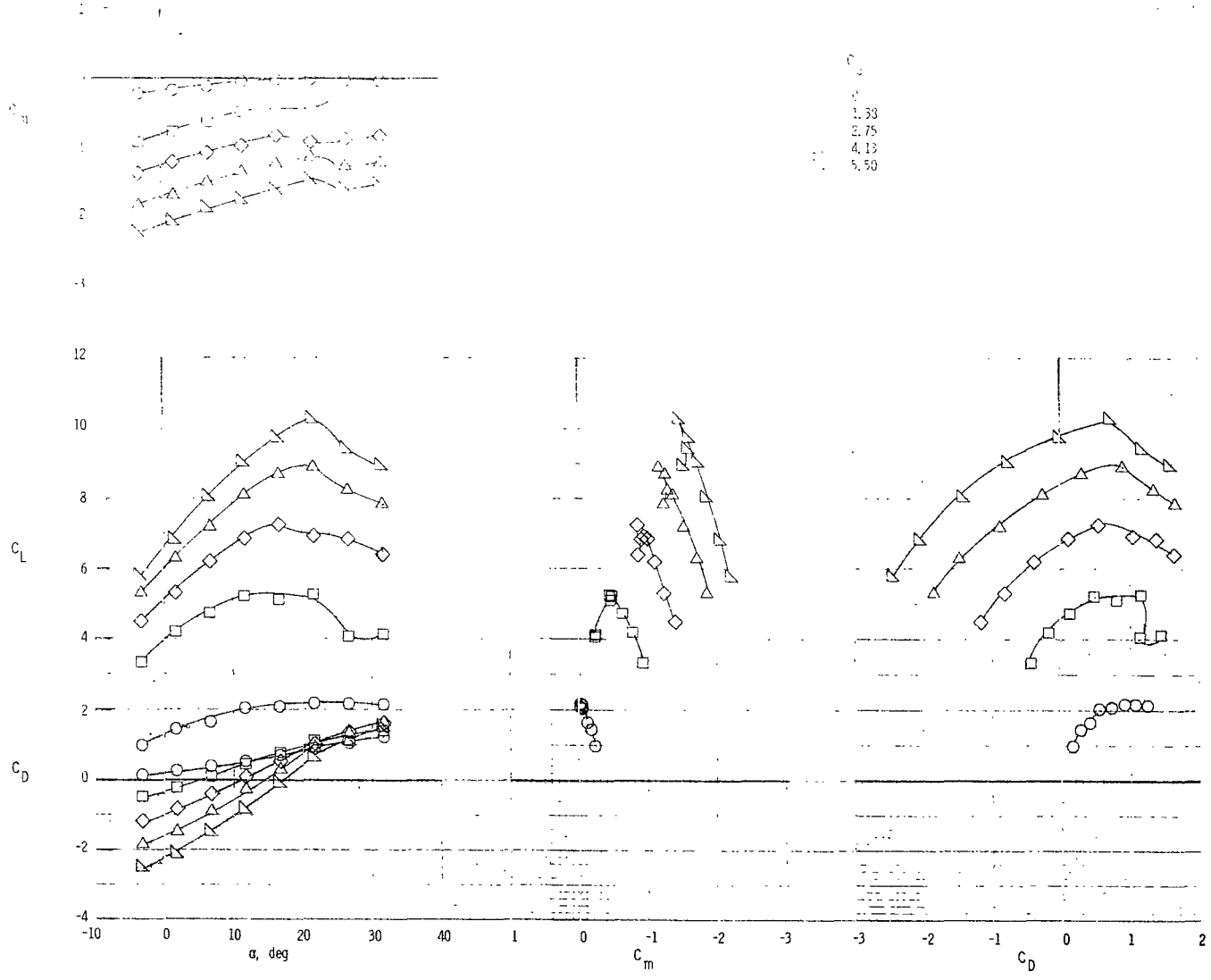

(b) Engine position 2.

Figure 9.- Continued.

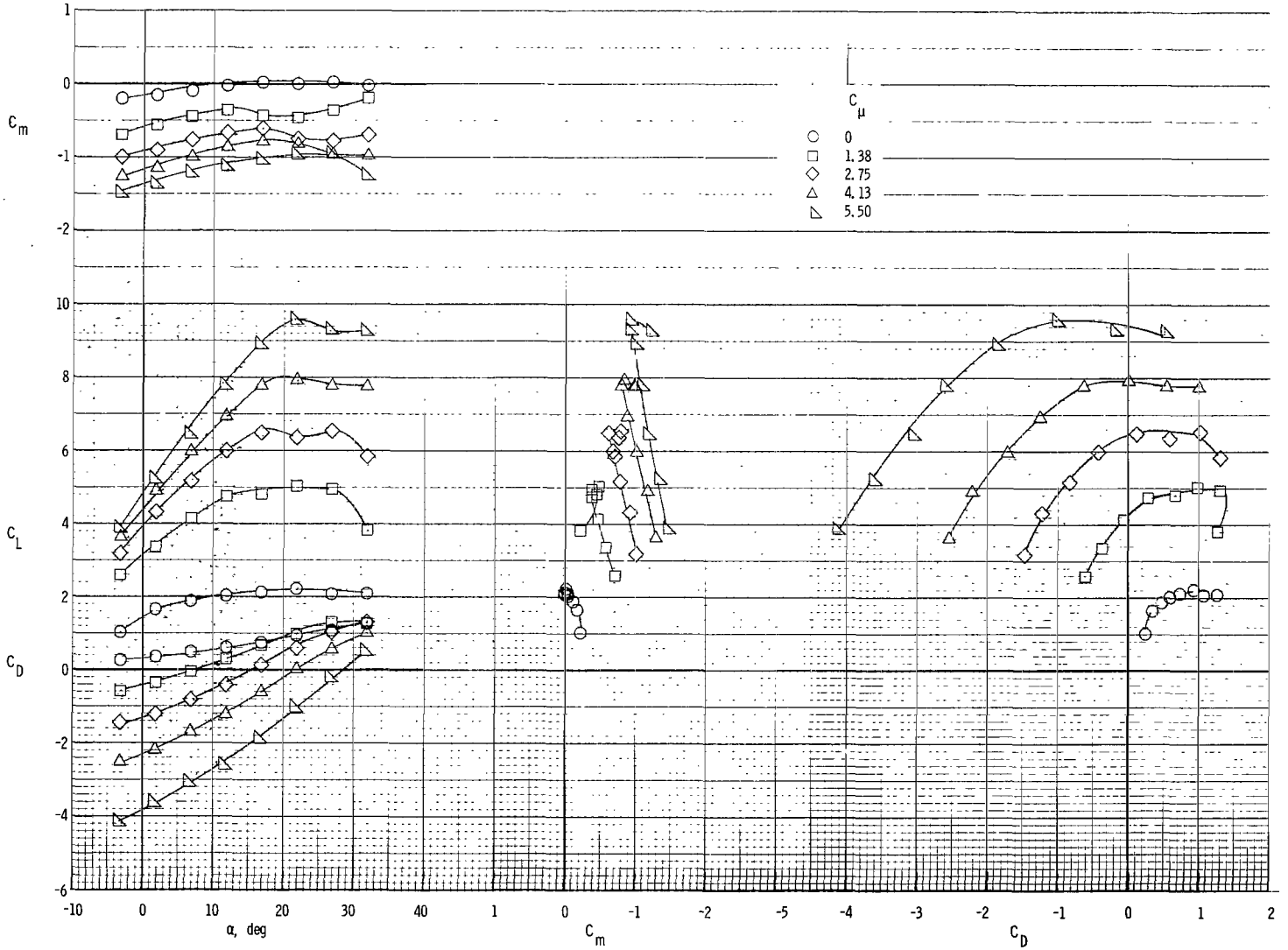

(c) Engine position 3.

Figure 9.- Continued.

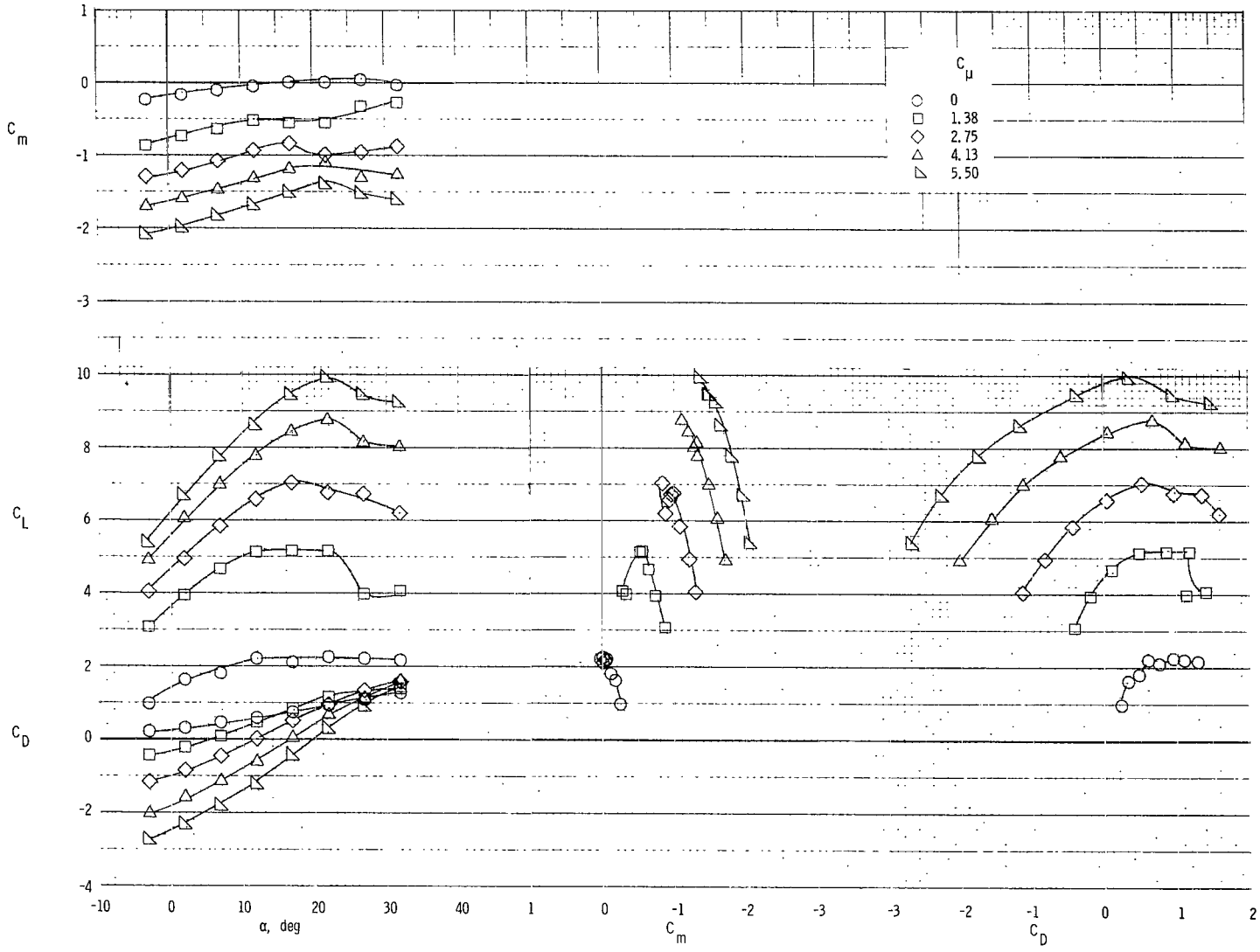

(d) Engine position 4.

Figure 9.- Concluded.

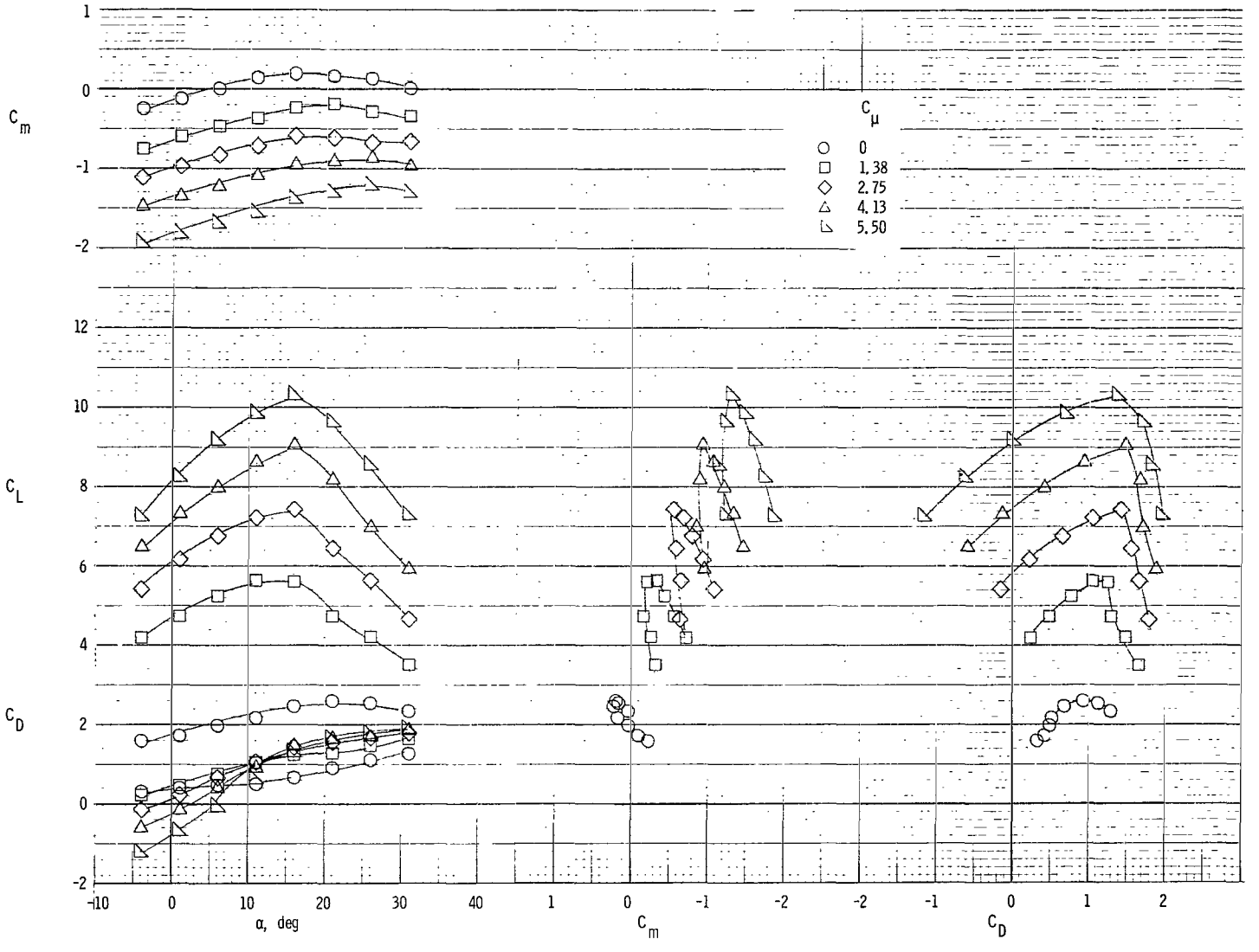

(a) Engine position 1.

Figure 10.- Longitudinal aerodynamic characteristics of the model without exhaust deflectors. $\delta_f = 55^o$.

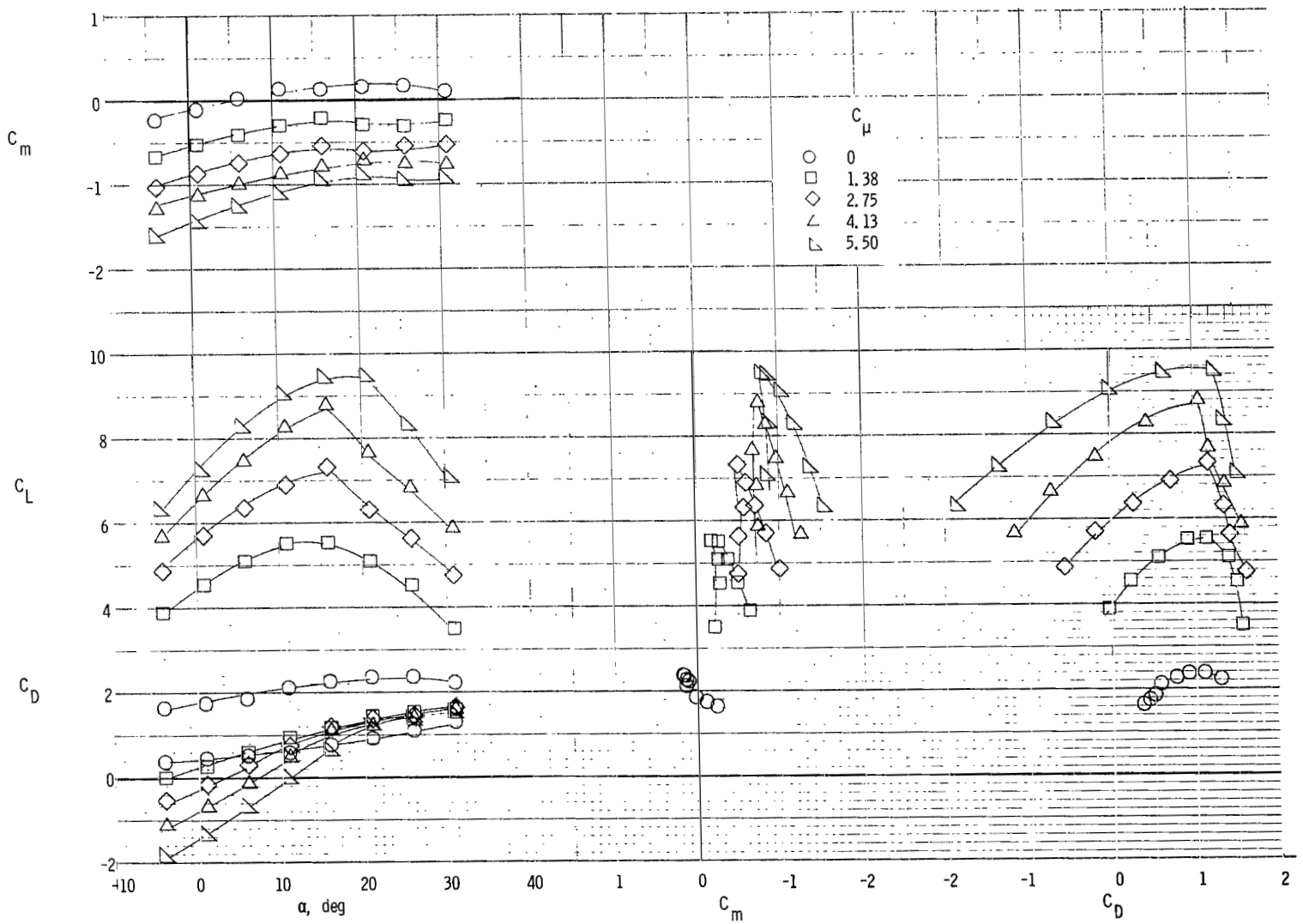

(b) Engine position 4.

Figure 10.- Concluded.

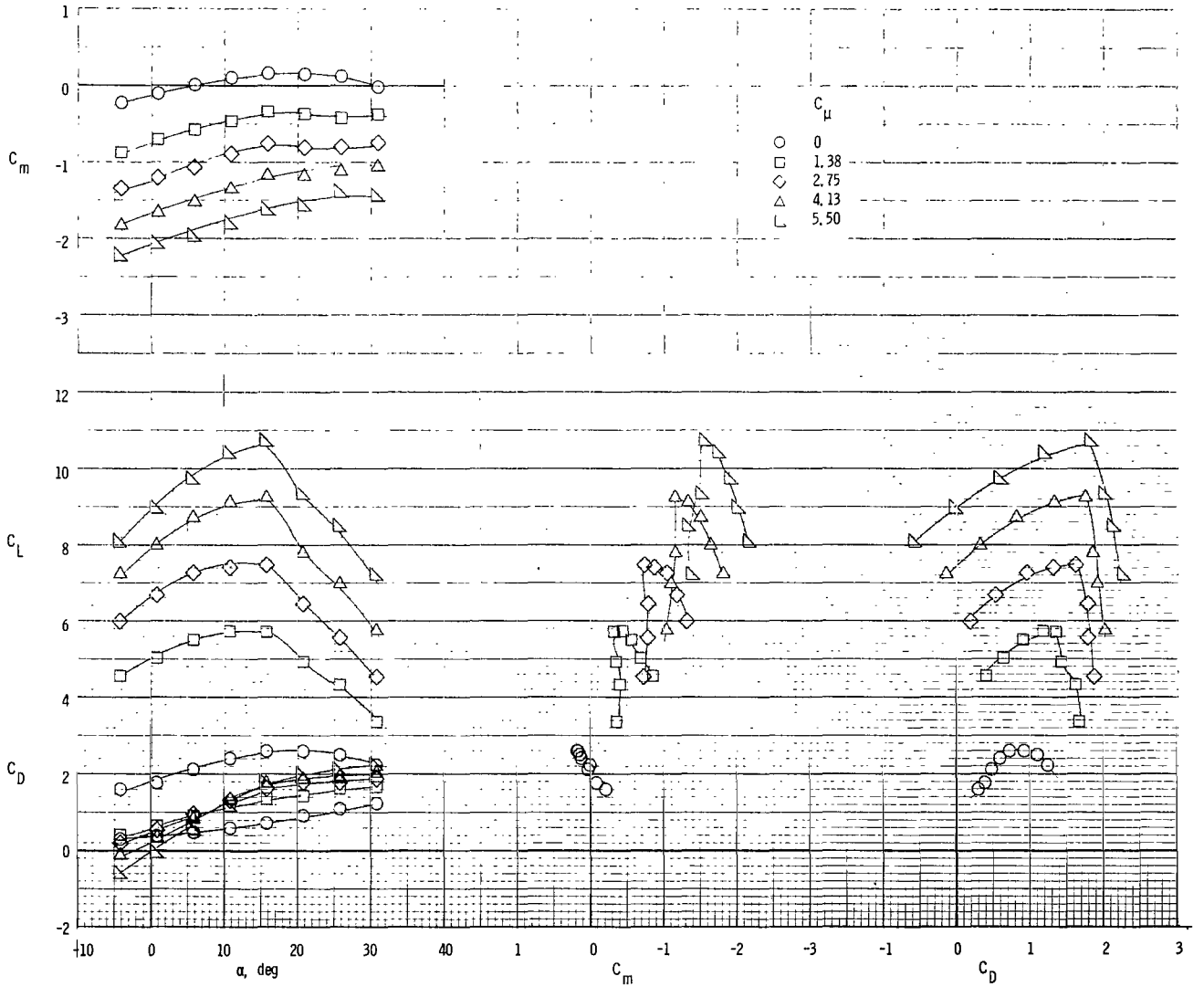

(a) Engine position 1.

Figure 11.- Longitudinal aerodynamic characteristics of the model with exhaust deflectors. $\delta_f = 55^o$.

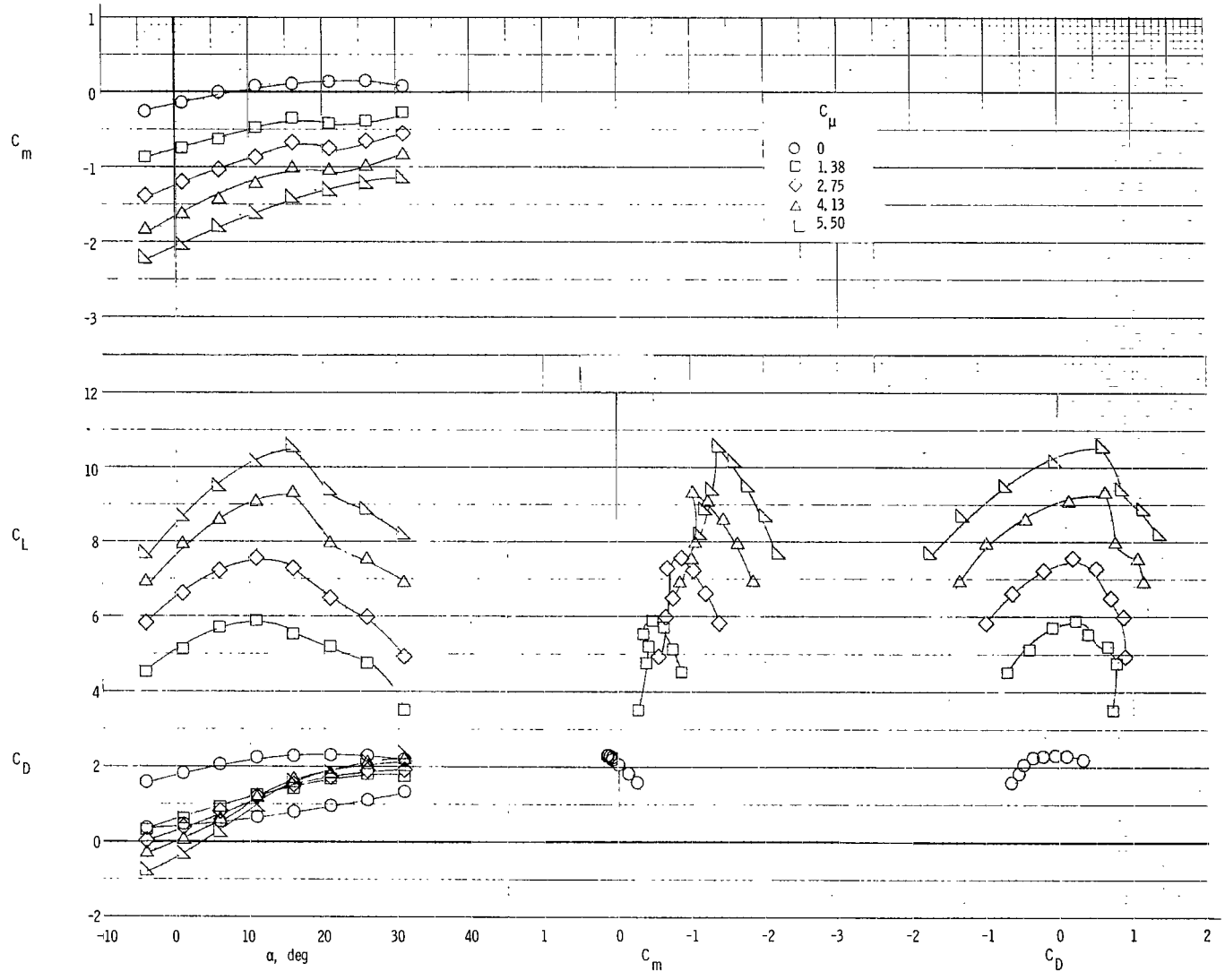

(b) Engine position 4.

Figure 11.- Concluded.

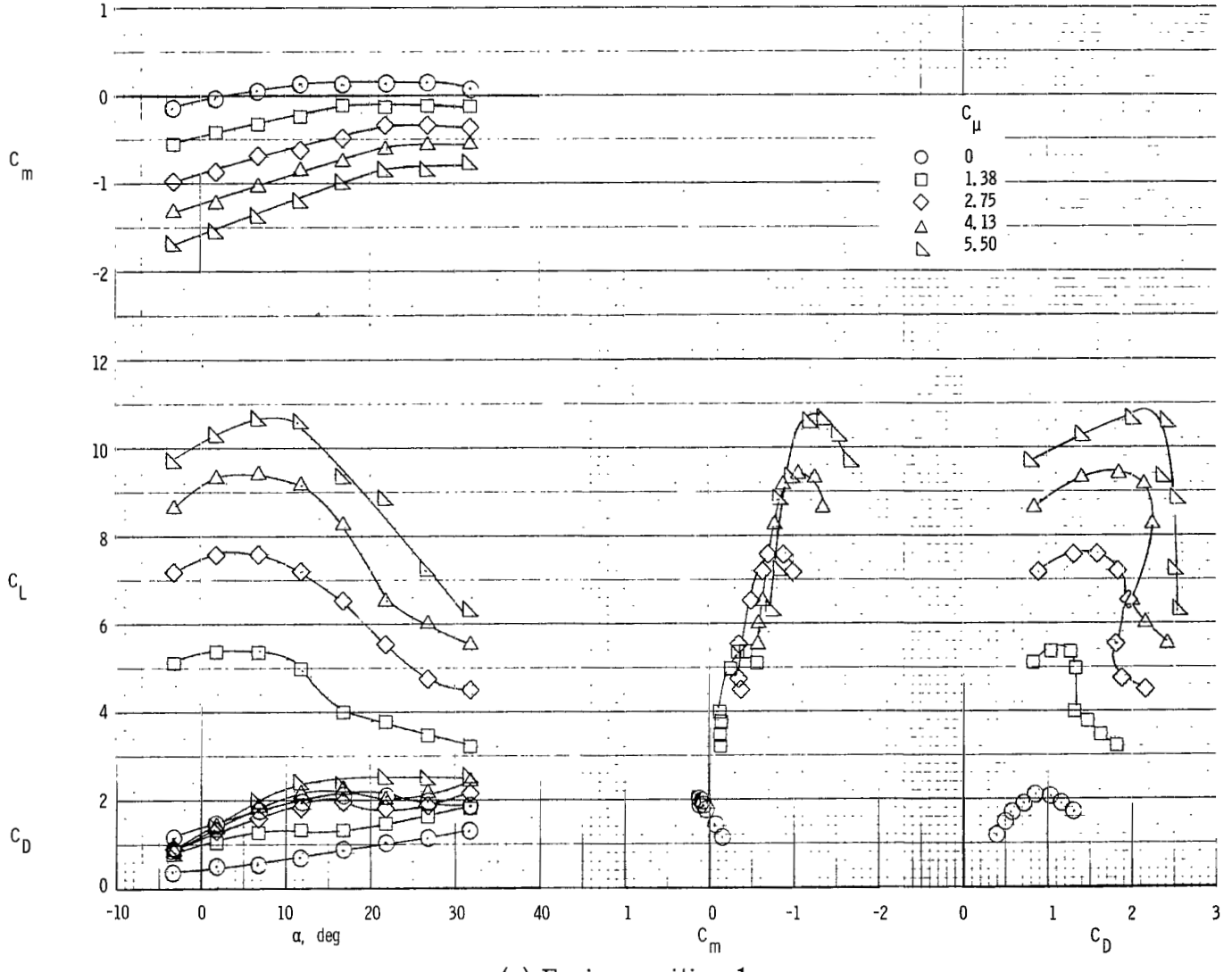

(a) Engine position 1.

Figure 12.- Longitudinal aerodynamic characteristics of the model without exhaust deflectors. $\delta_f = 70^o$.

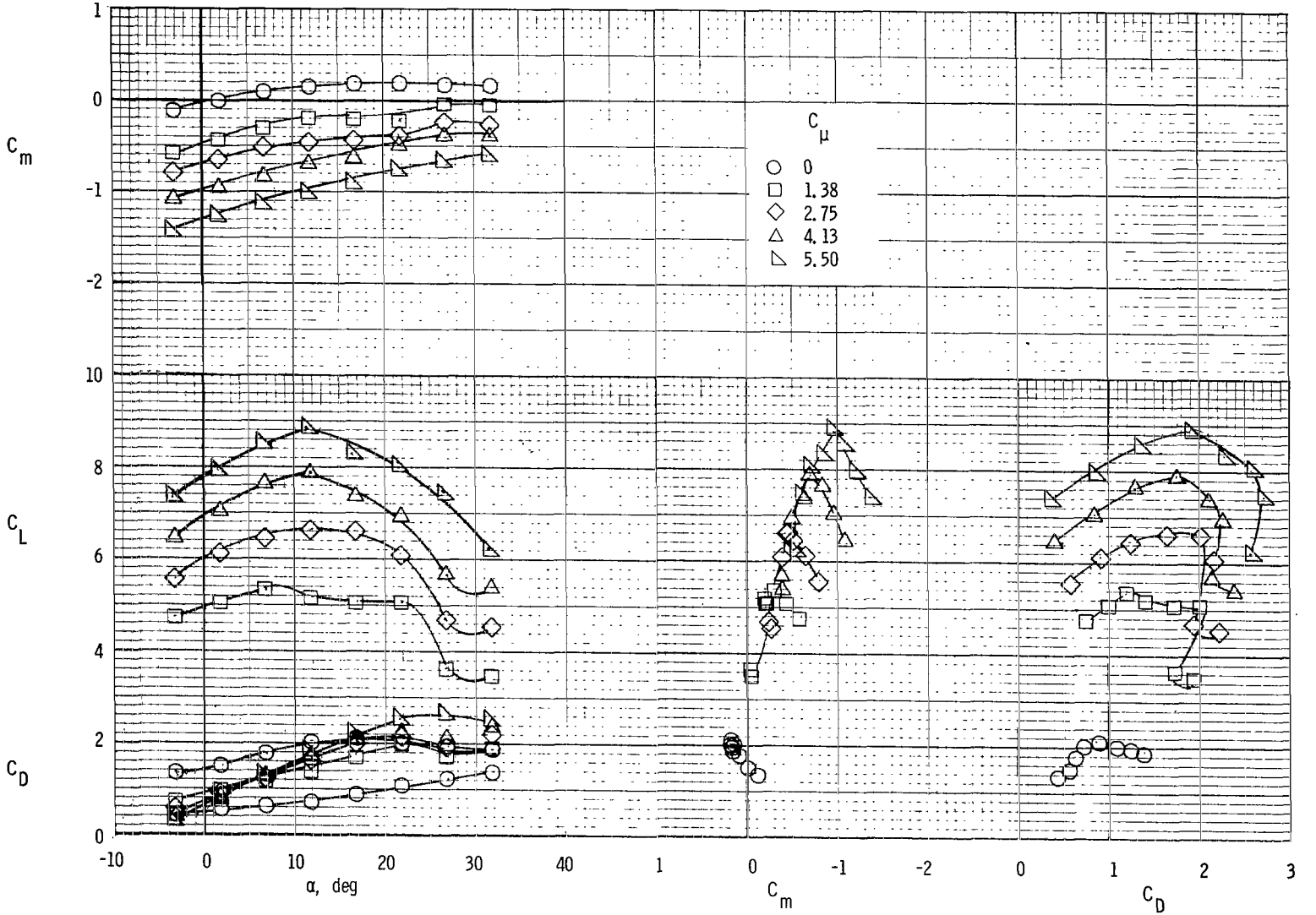

(b) Engine position 2.

Figure 12.- Continued.

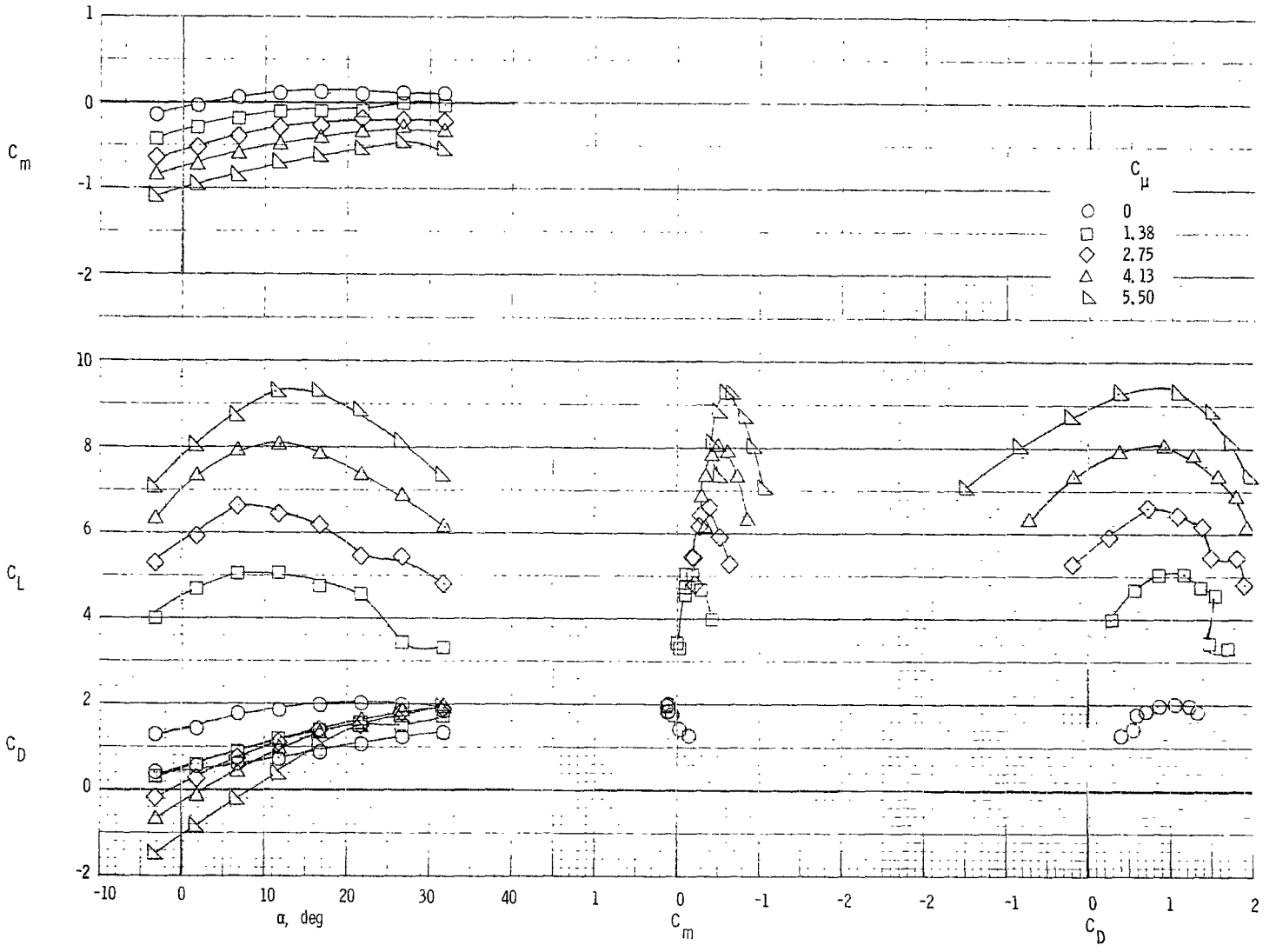

(c) Engine position 3.

Figure 12.- Continued.

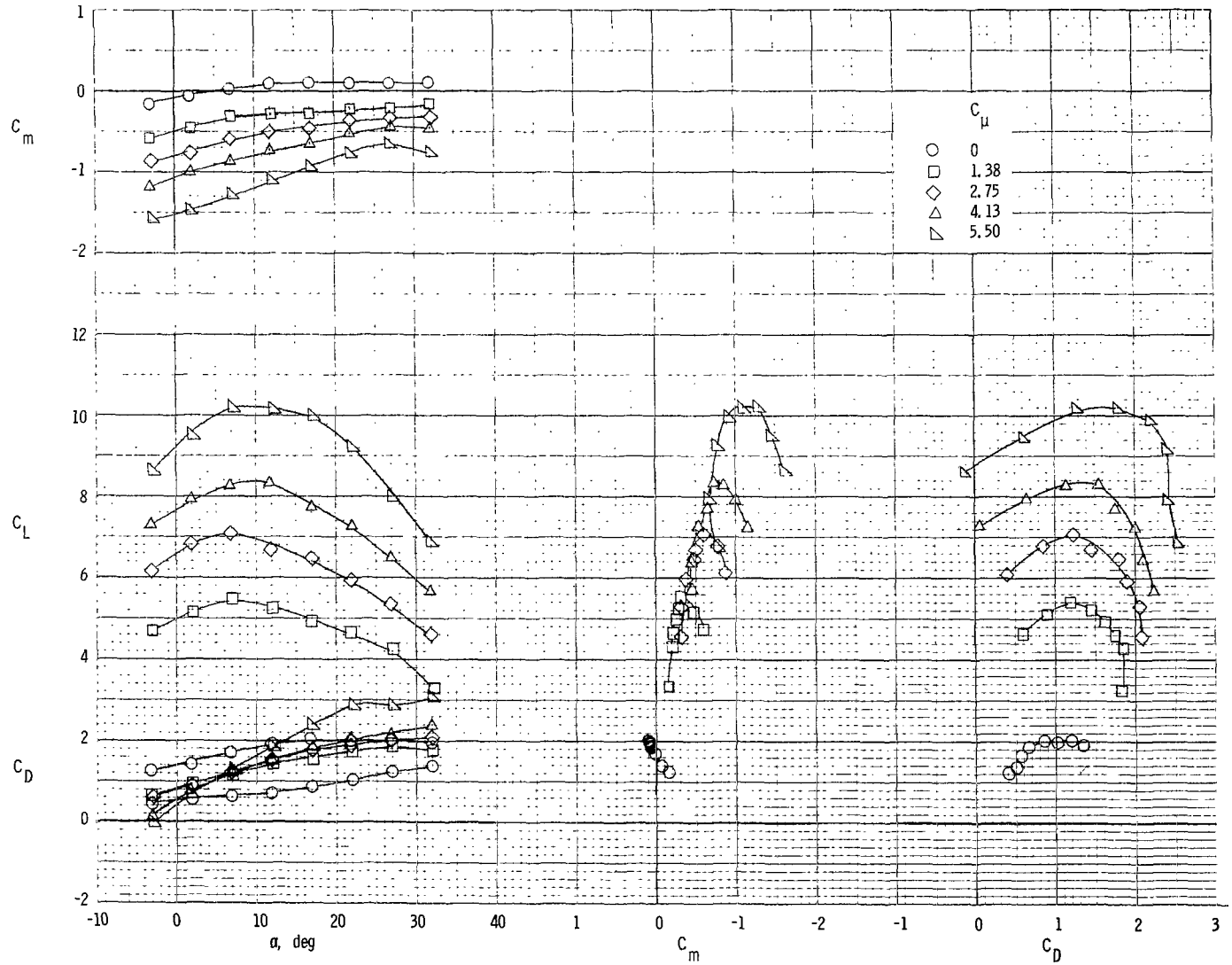

(d) Engine position 4.

Figure 12.- Concluded.

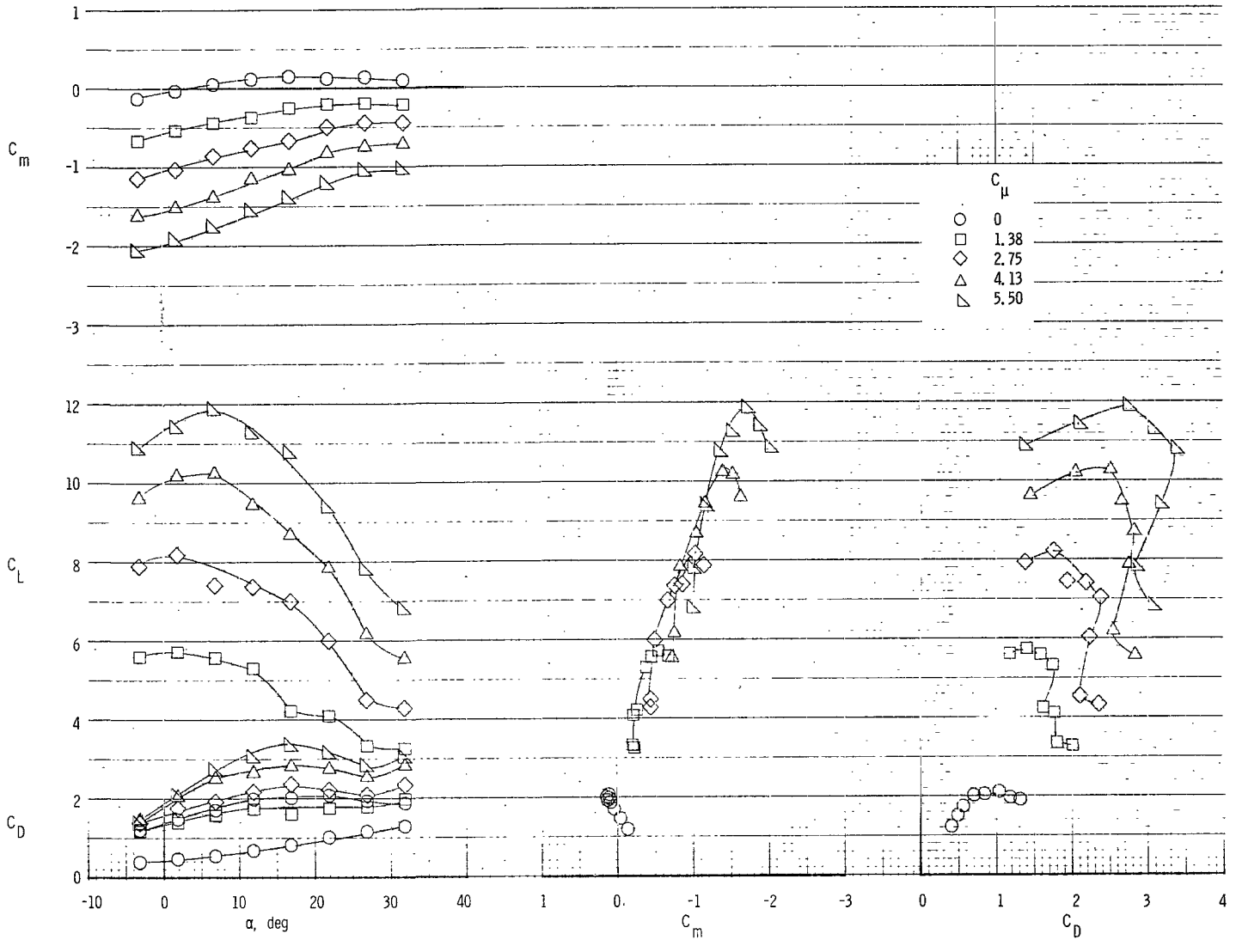

(a) Engine position 1.

Figure 13.- Longitudinal aerodynamic characteristics of the model with exhaust deflectors. $\delta_f = 70^o$.

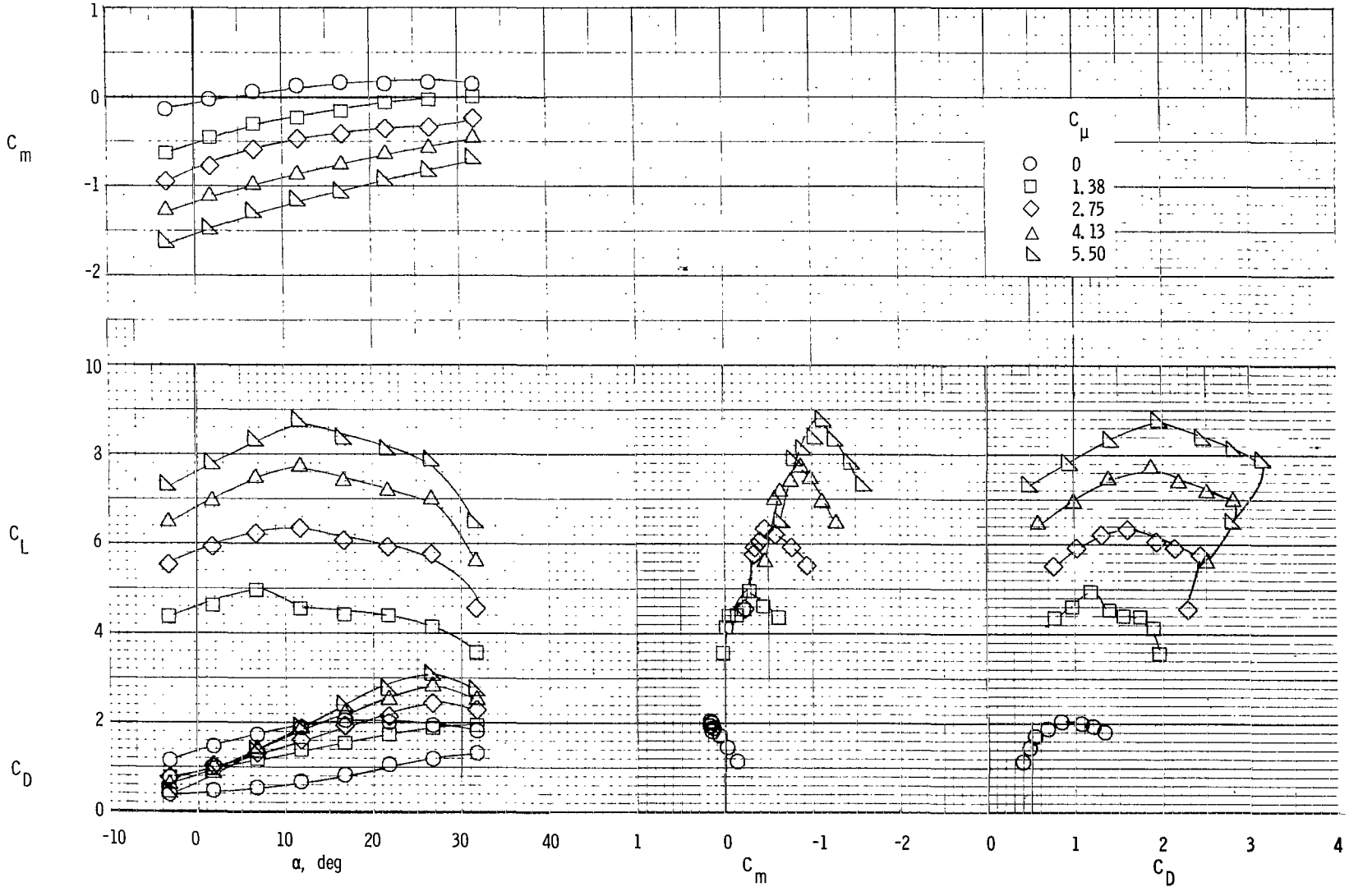

(b) Engine position 2.

Figure 13.- Continued.

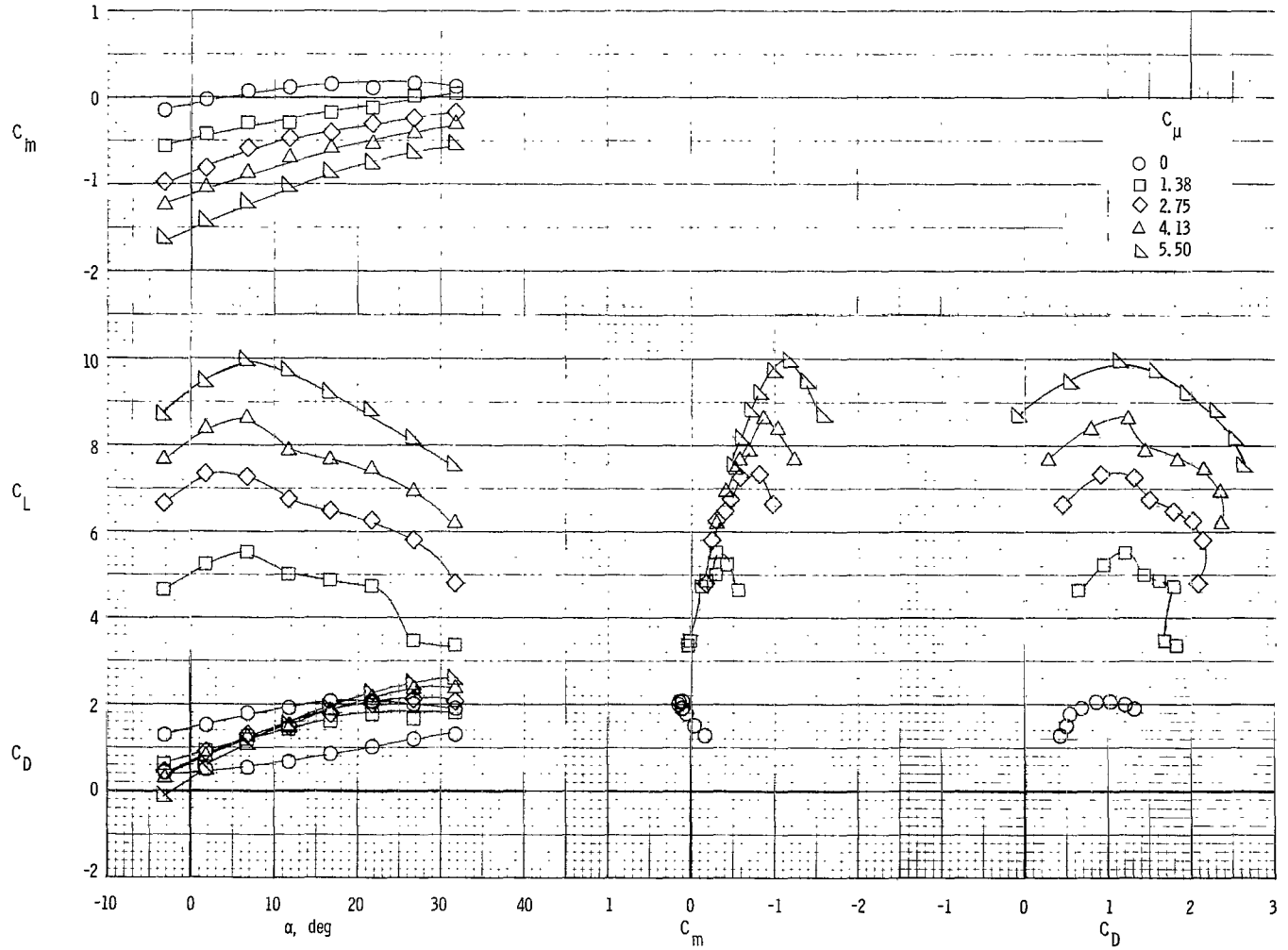

(c) Engine position 3.

Figure 13.- Continued.

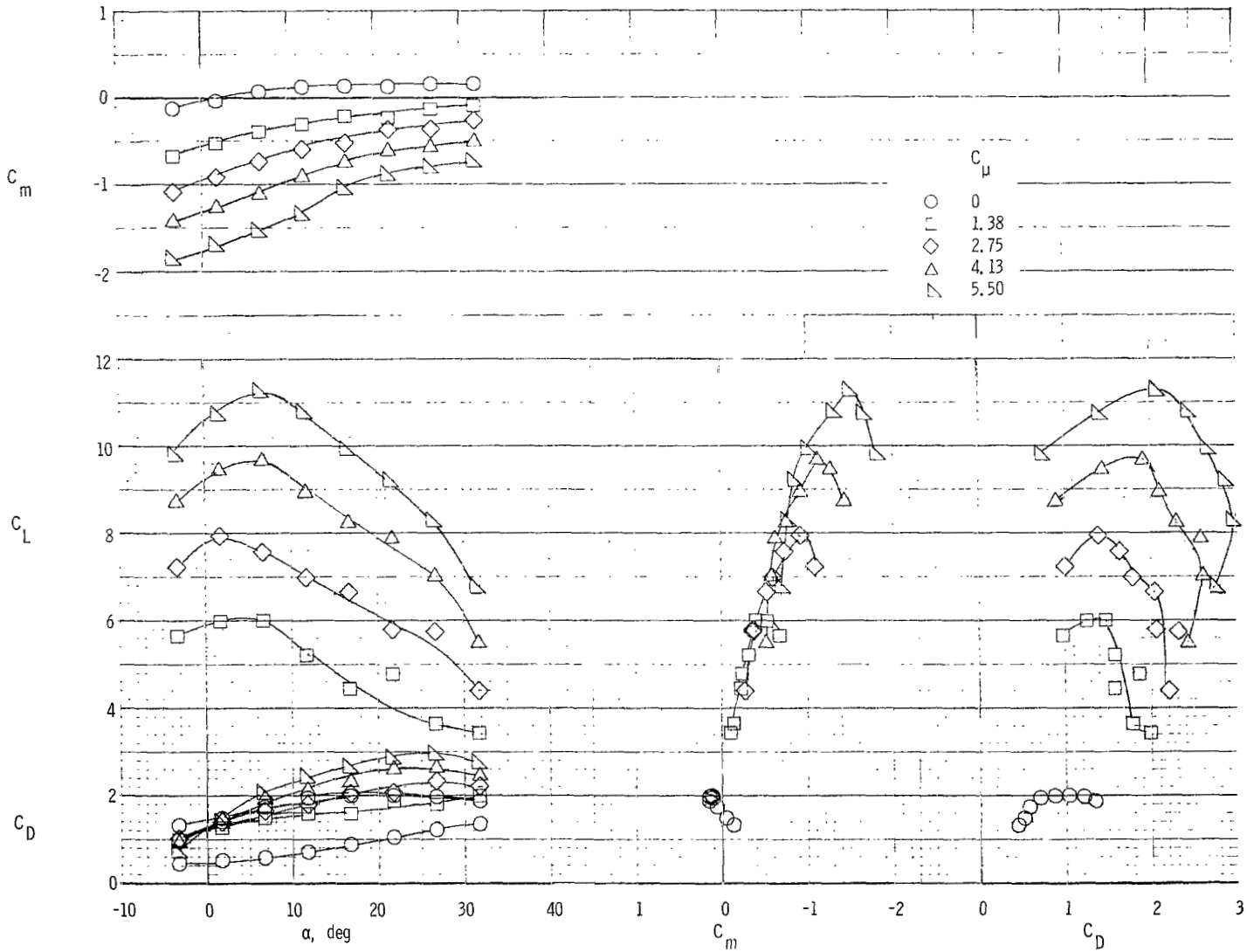

(d) Engine position 4.

Figure 13.- Concluded.

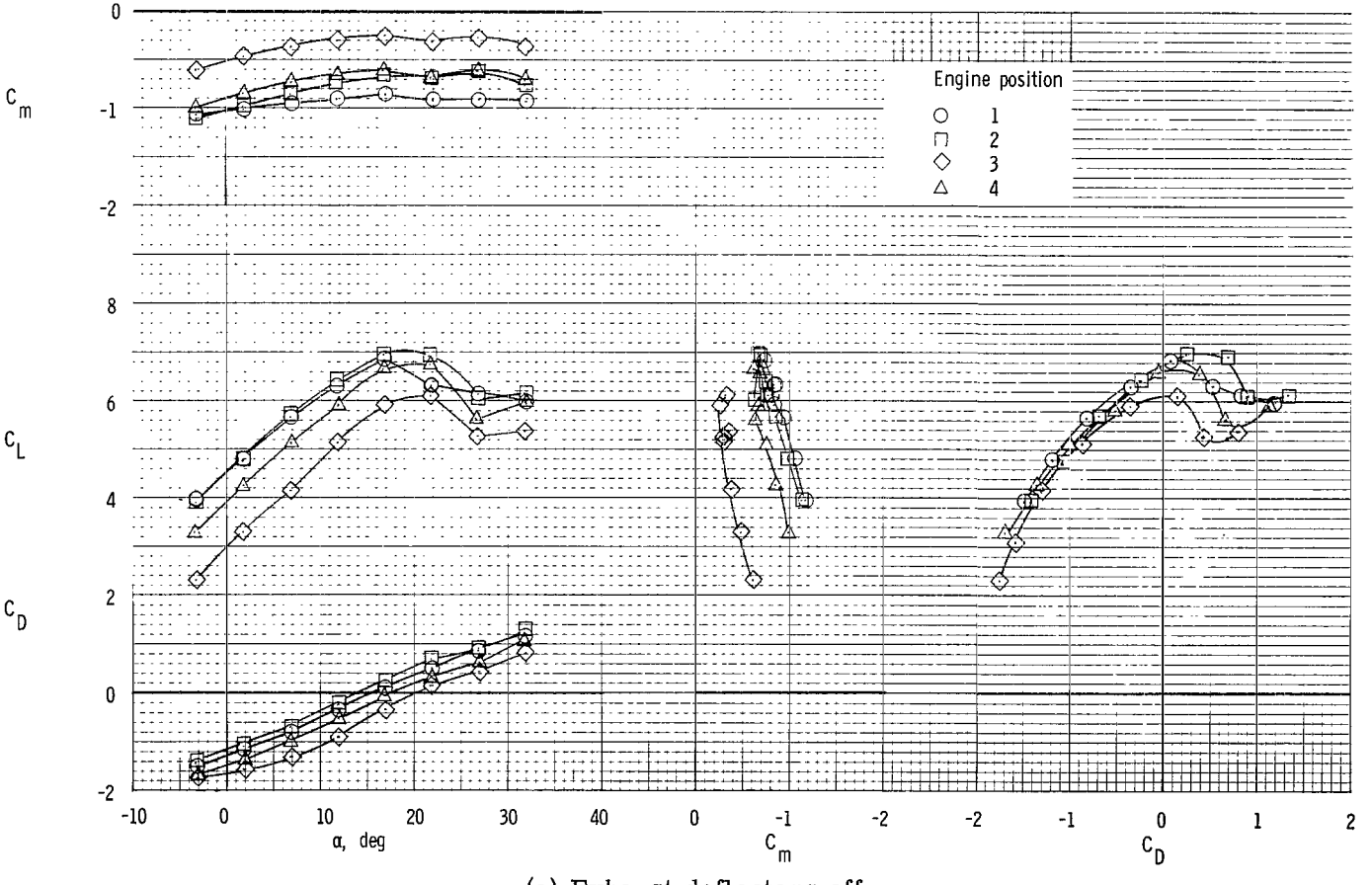

(a) Exhaust deflectors off.

Figure 14.- Effect of engine position. $\delta_f = 35^o$; $C_\mu = 2.75$.

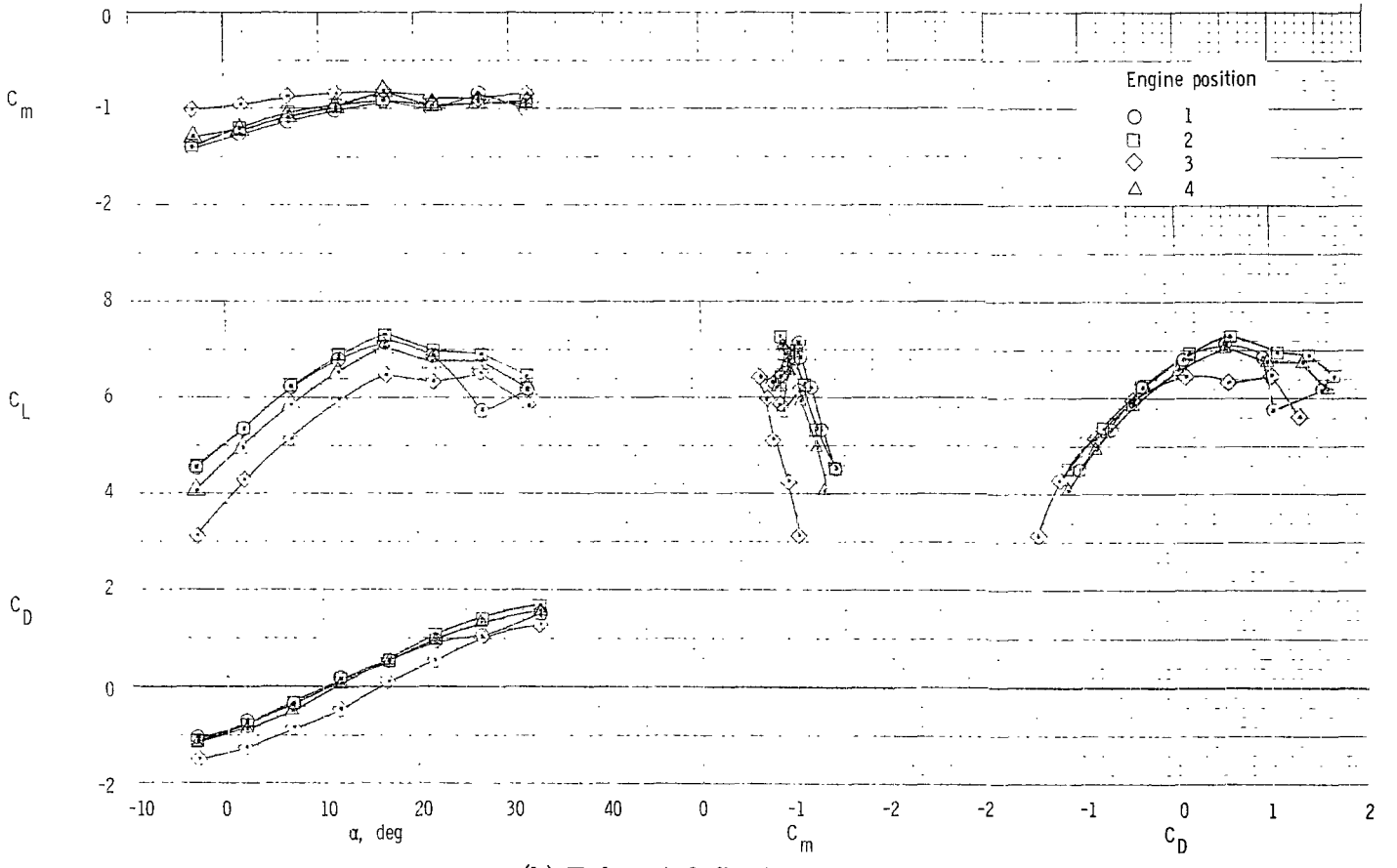

(b) Exhaust deflectors on.

Figure 14.- Concluded.

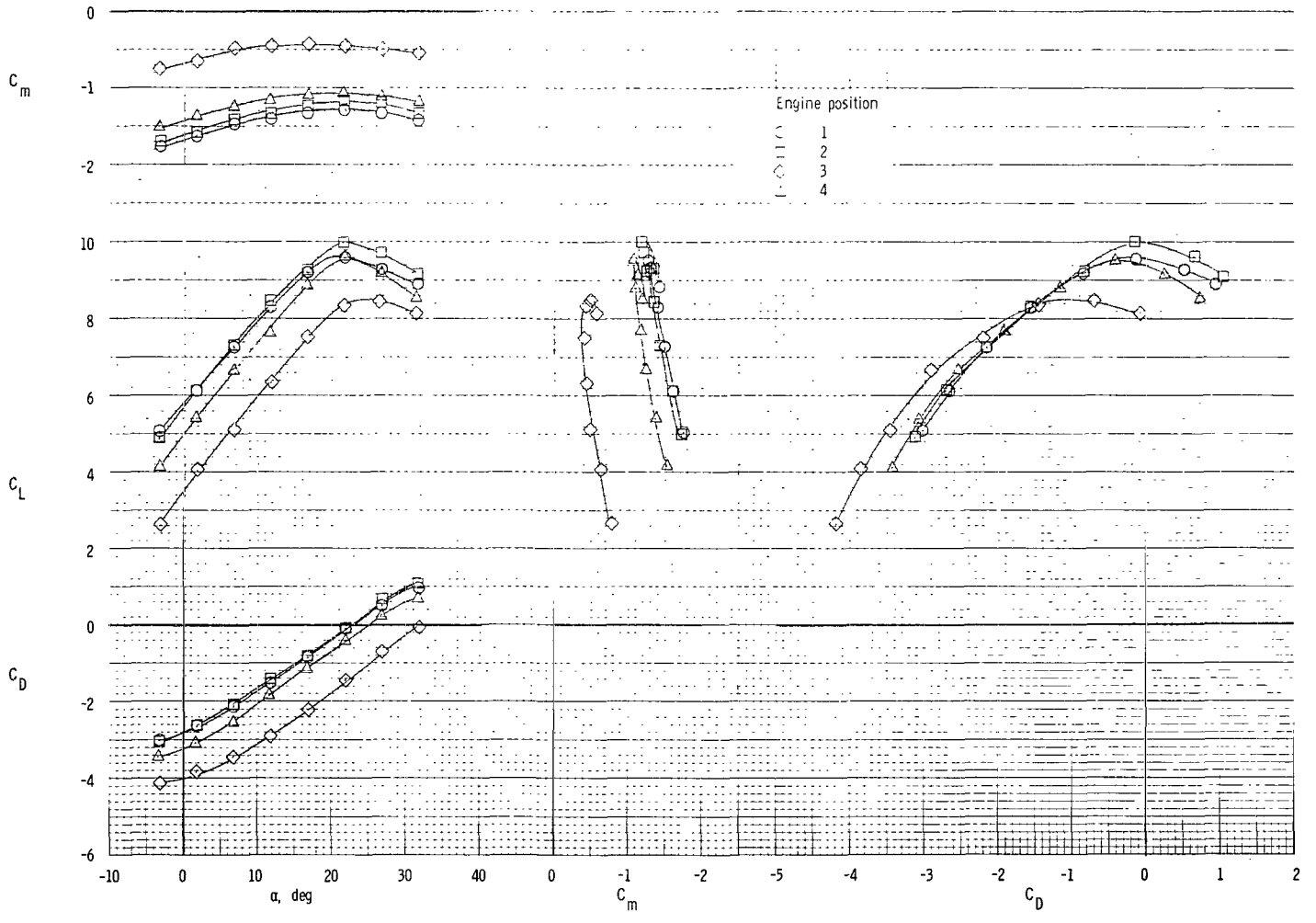

(a) Exhaust deflectors off.

Figure 15.- Effect of engine position. $\delta_f = 35^o$; $C_\mu = 5.50$.

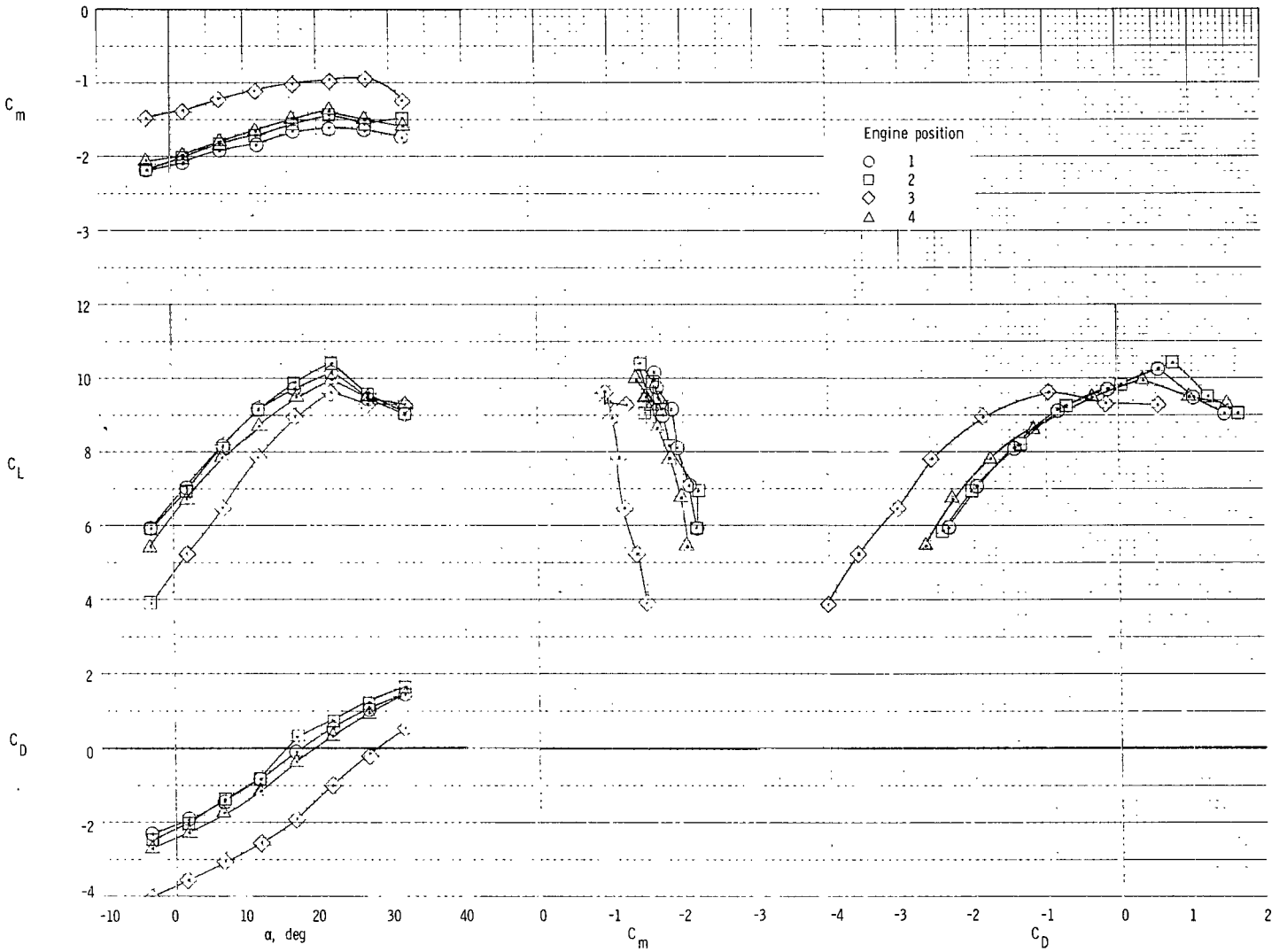

(b) Exhaust deflectors on.

Figure 15.- Concluded.

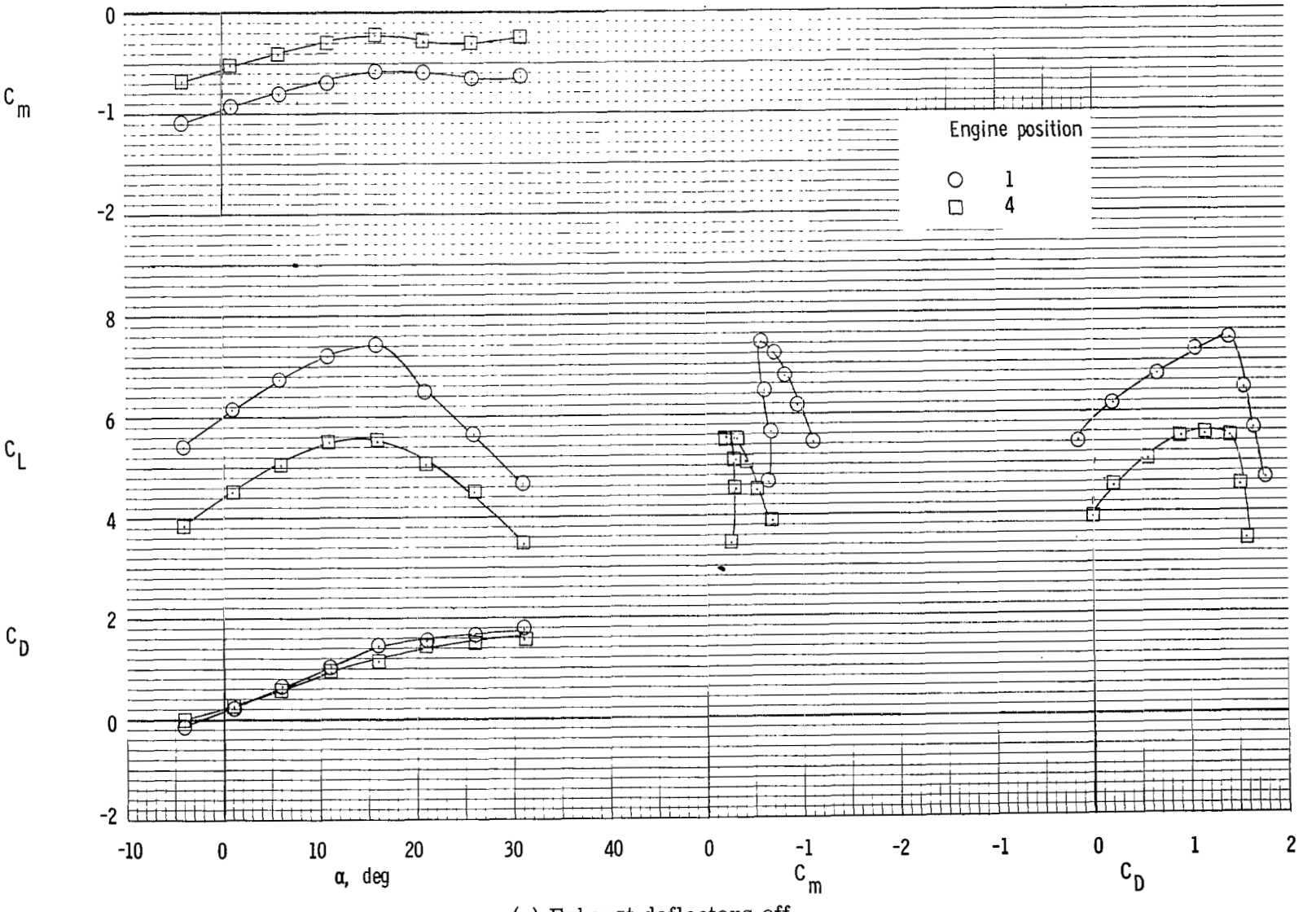

(a) Exhaust deflectors off.

Figure 16.- Effect of engine position. $\delta_f = 55^o$; $C_\mu = 2.75$.

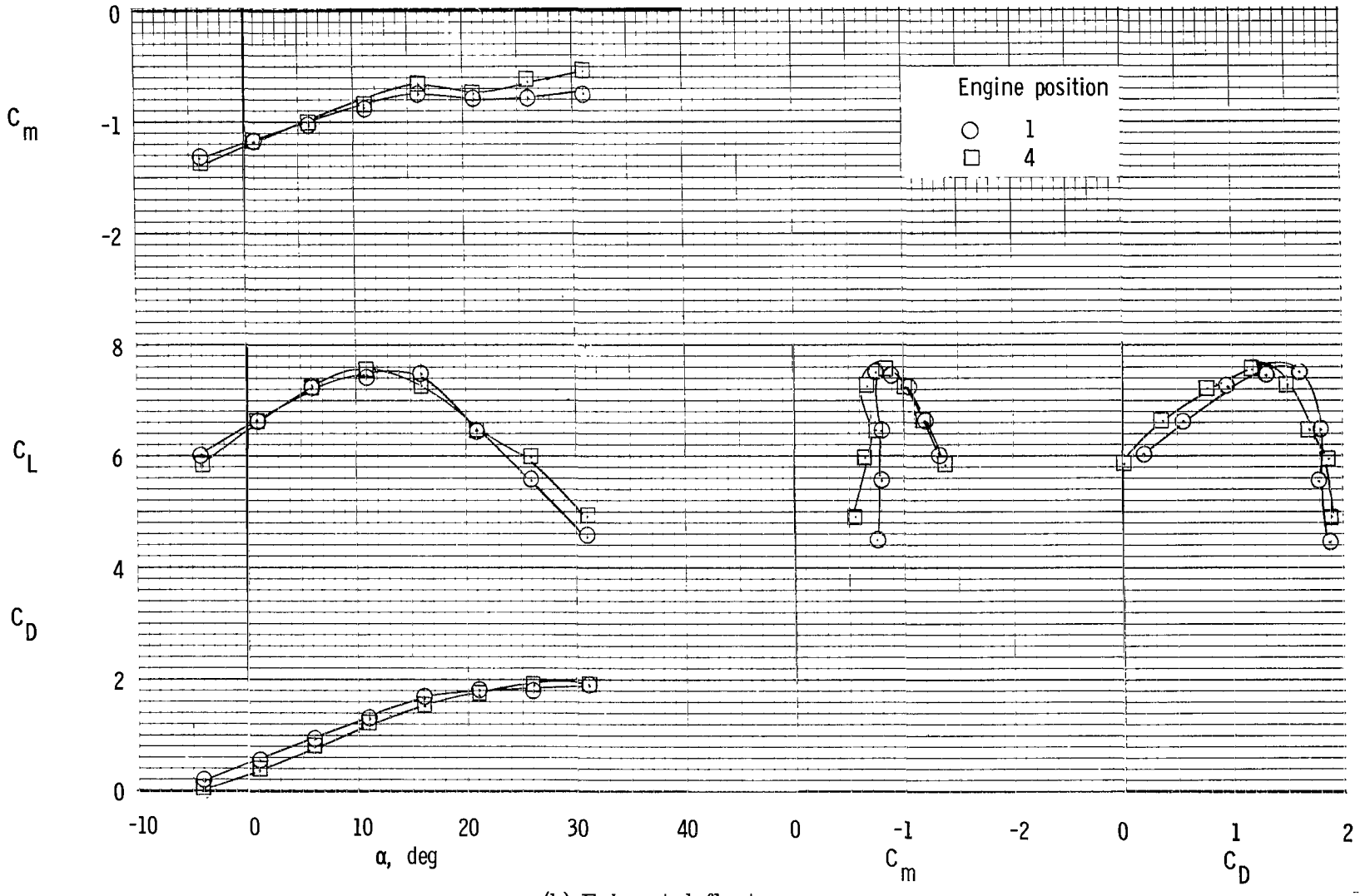

(b) Exhaust deflectors on.

Figure 16.- Concluded.

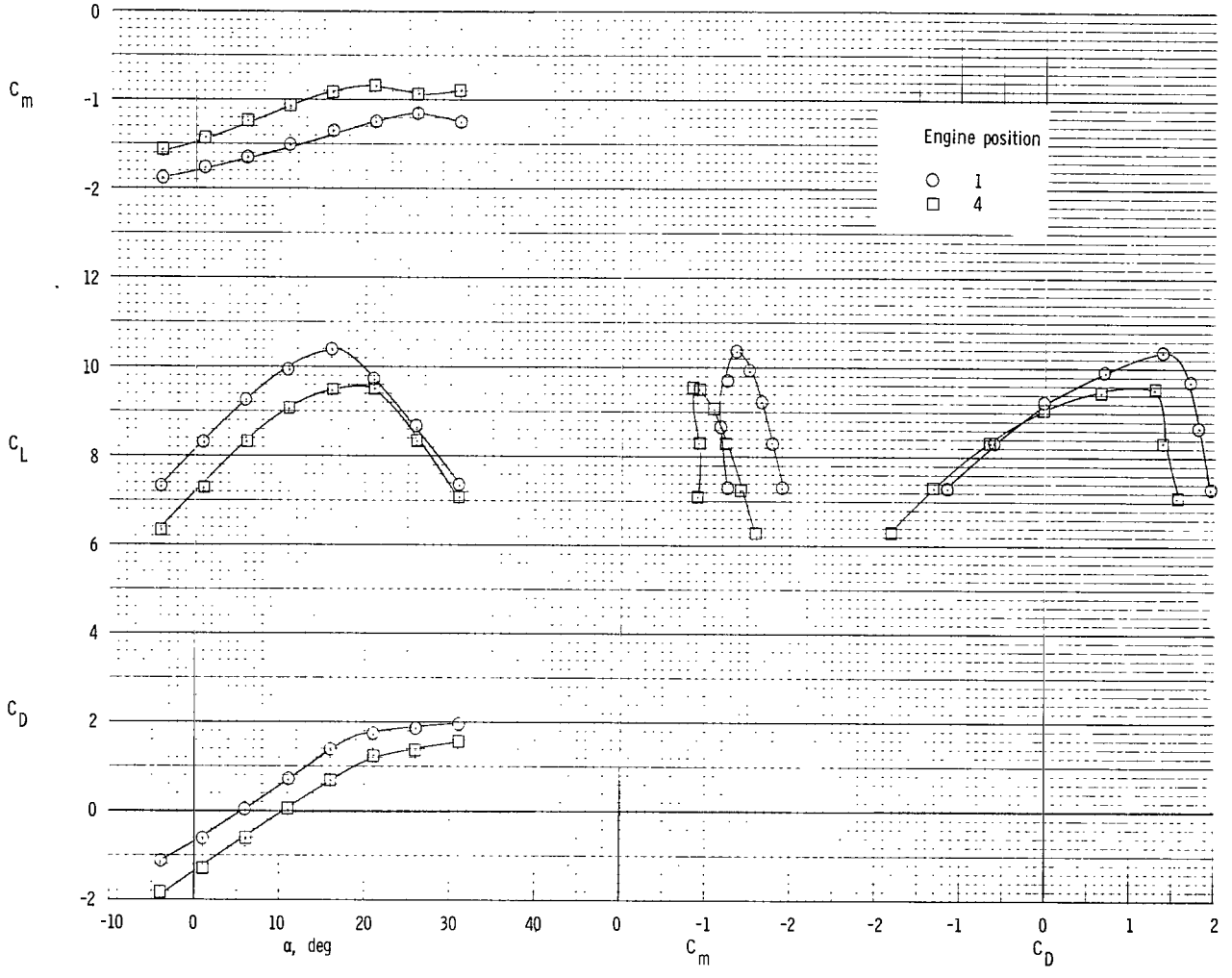

(a) Exhaust deflectors off.

Figure 17.- Effect of engine position. $\delta_f = 55^o$; $C_\mu = 5.50$.

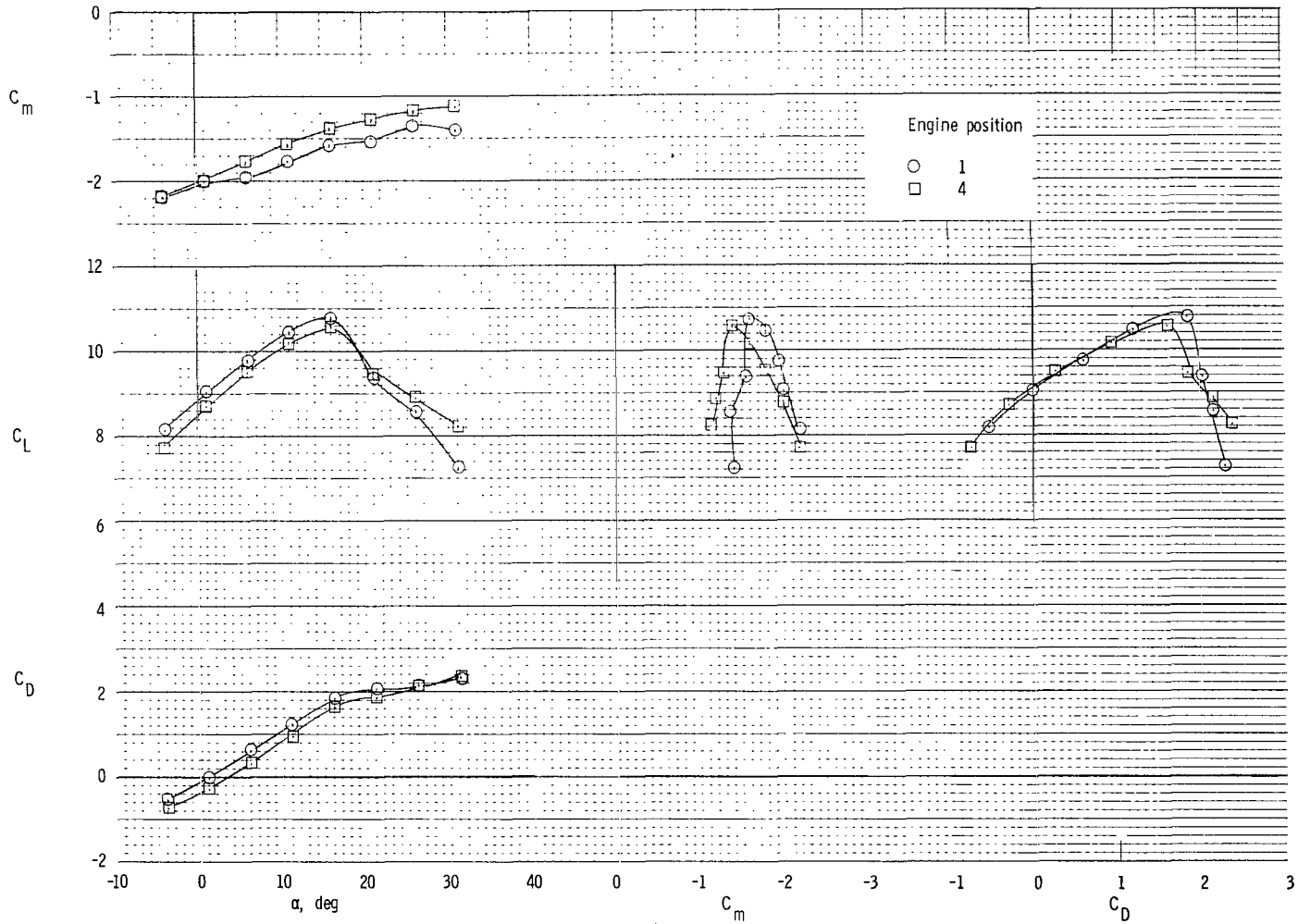

(b) Exhaust deflectors on.

Figure 17.- Concluded.

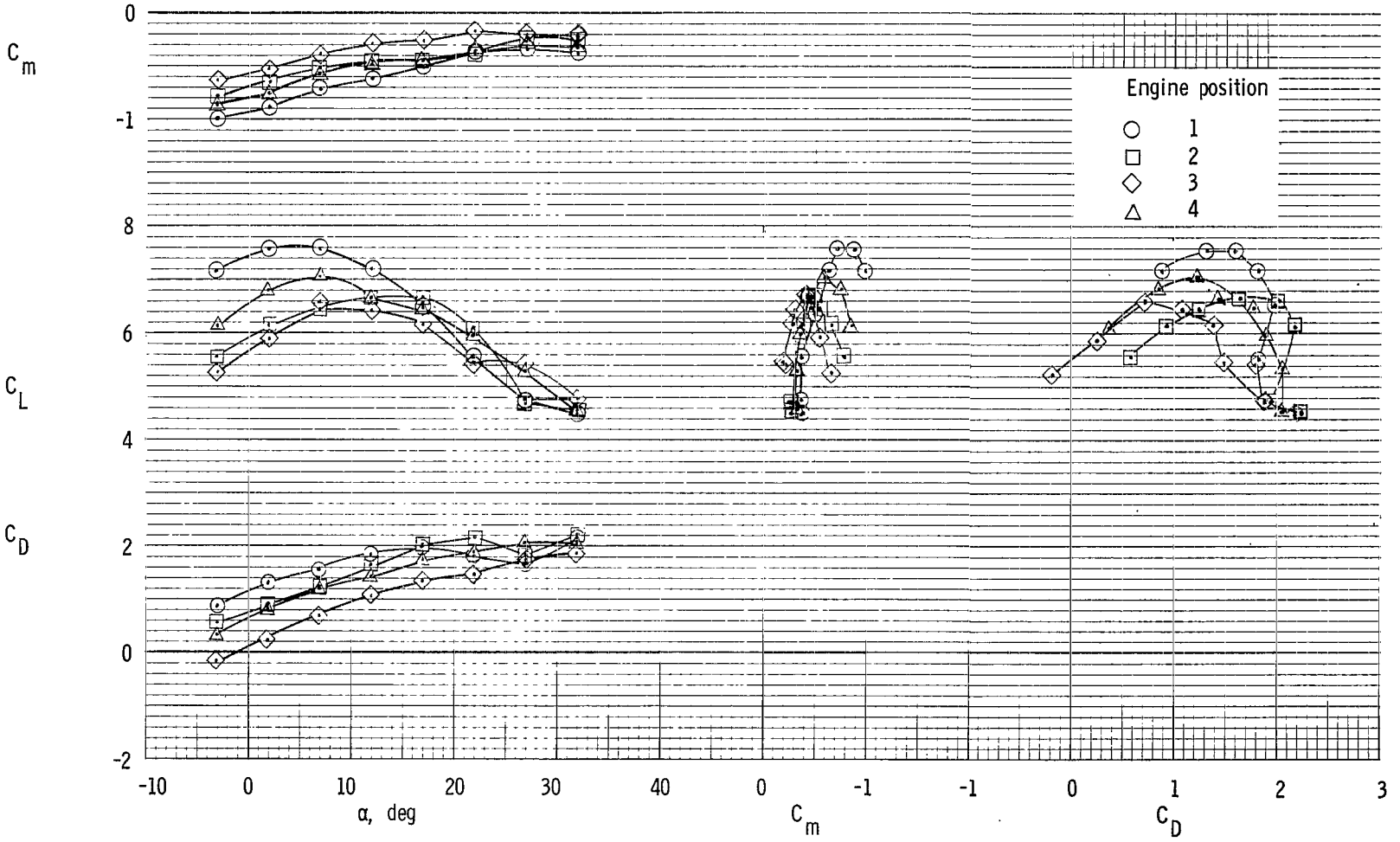

(a) Exhaust deflectors off.

Figure 18.- Effect of engine position. $\delta_f = 70^o$; $C_\mu = 2.75$.

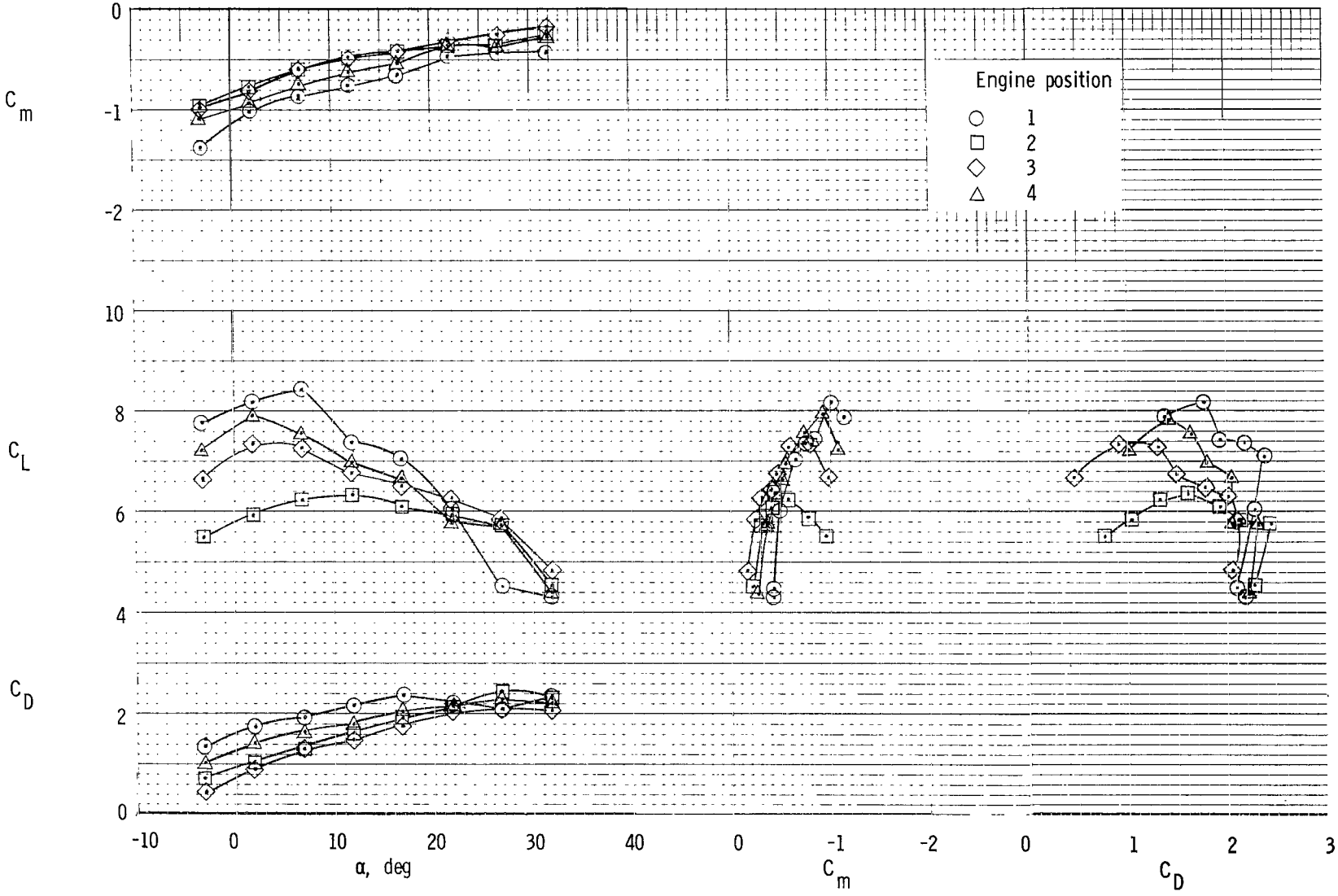

(b) Exhaust deflectors on.

Figure 18.- Concluded.

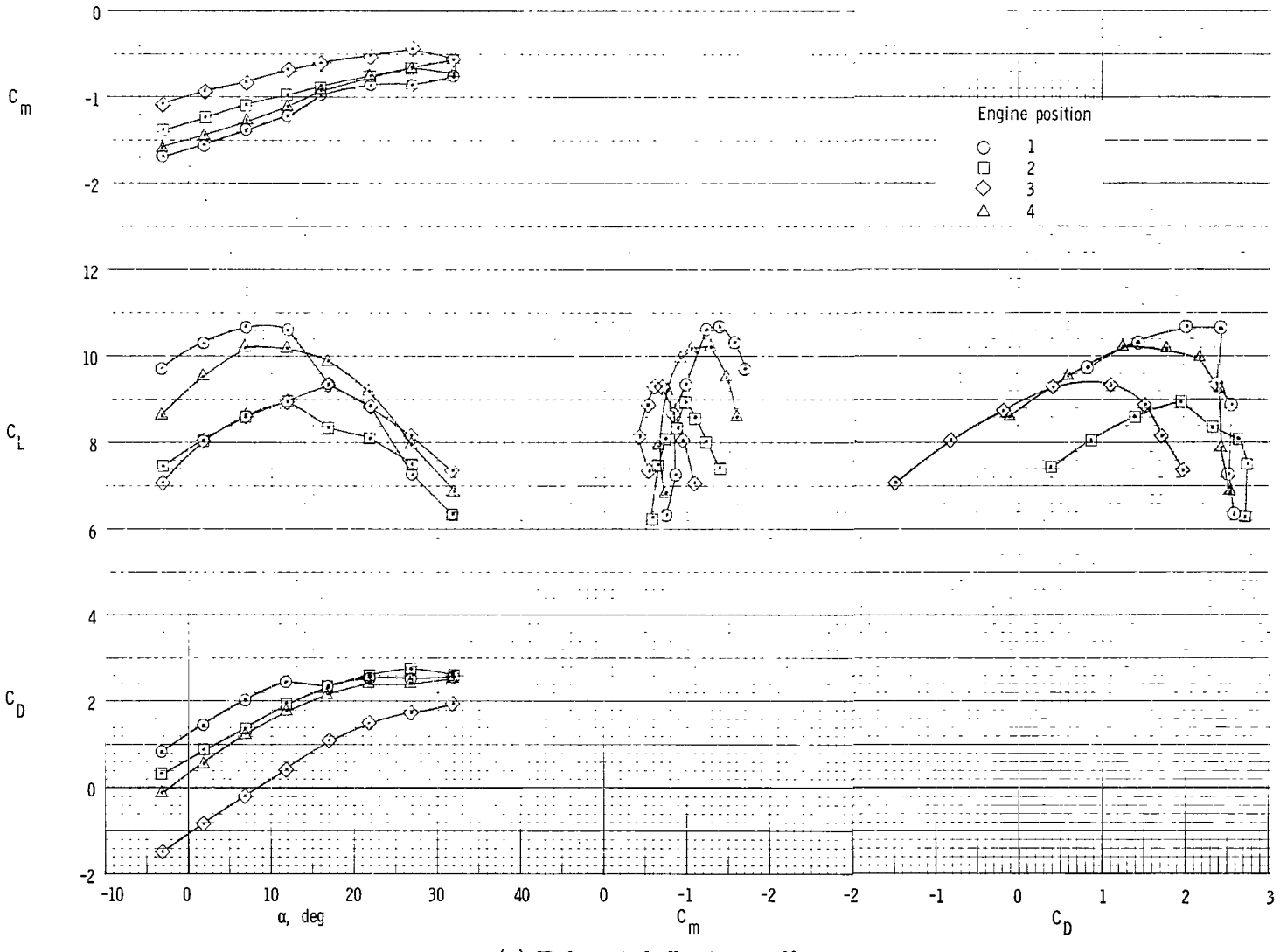

(a) Exhaust deflectors off.

Figure 19.- Effect of engine position. $\delta_f = 70^o$; $C_\mu = 5.50$.

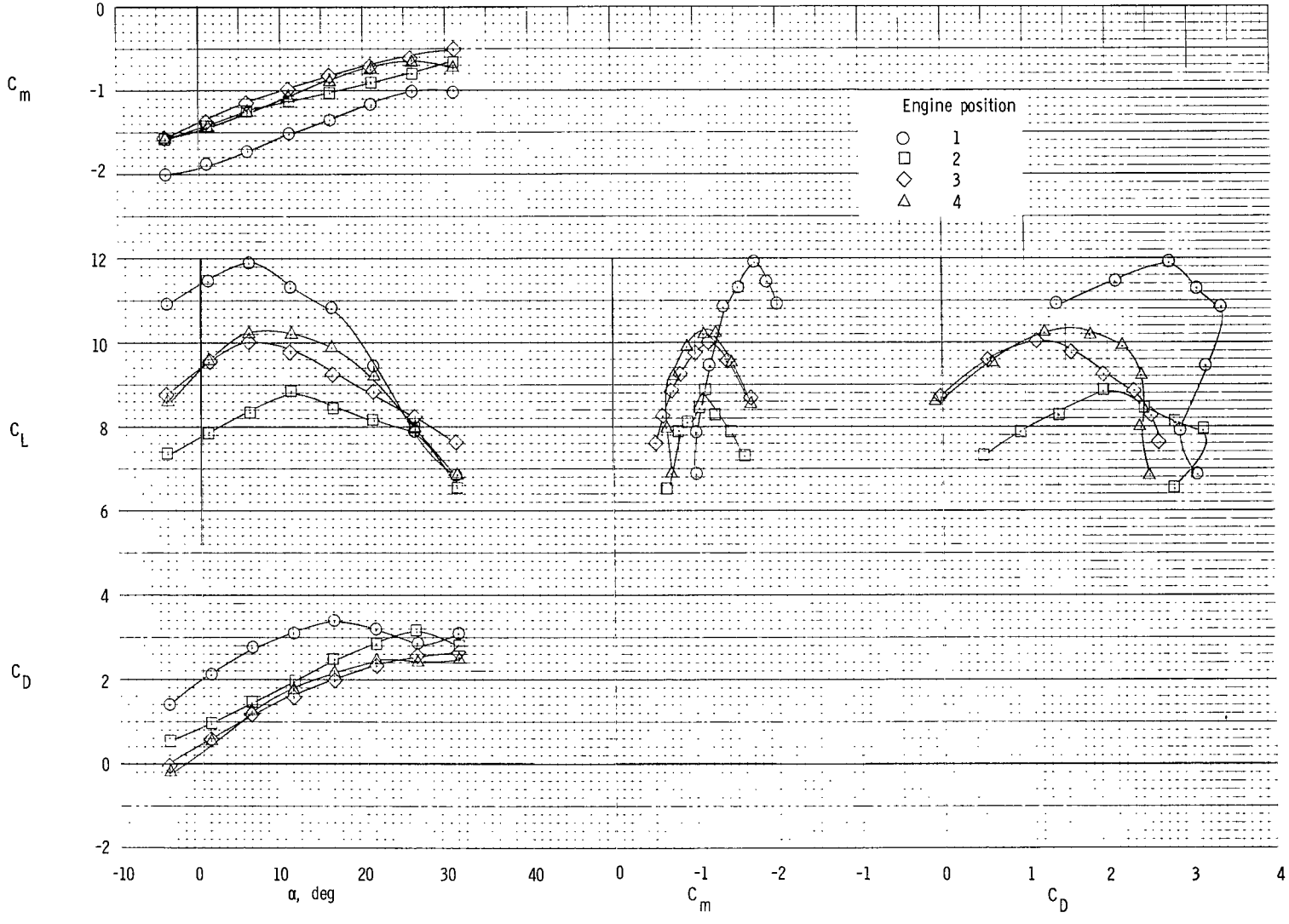

(b) Exhaust deflectors on.

Figure 19.- Concluded.

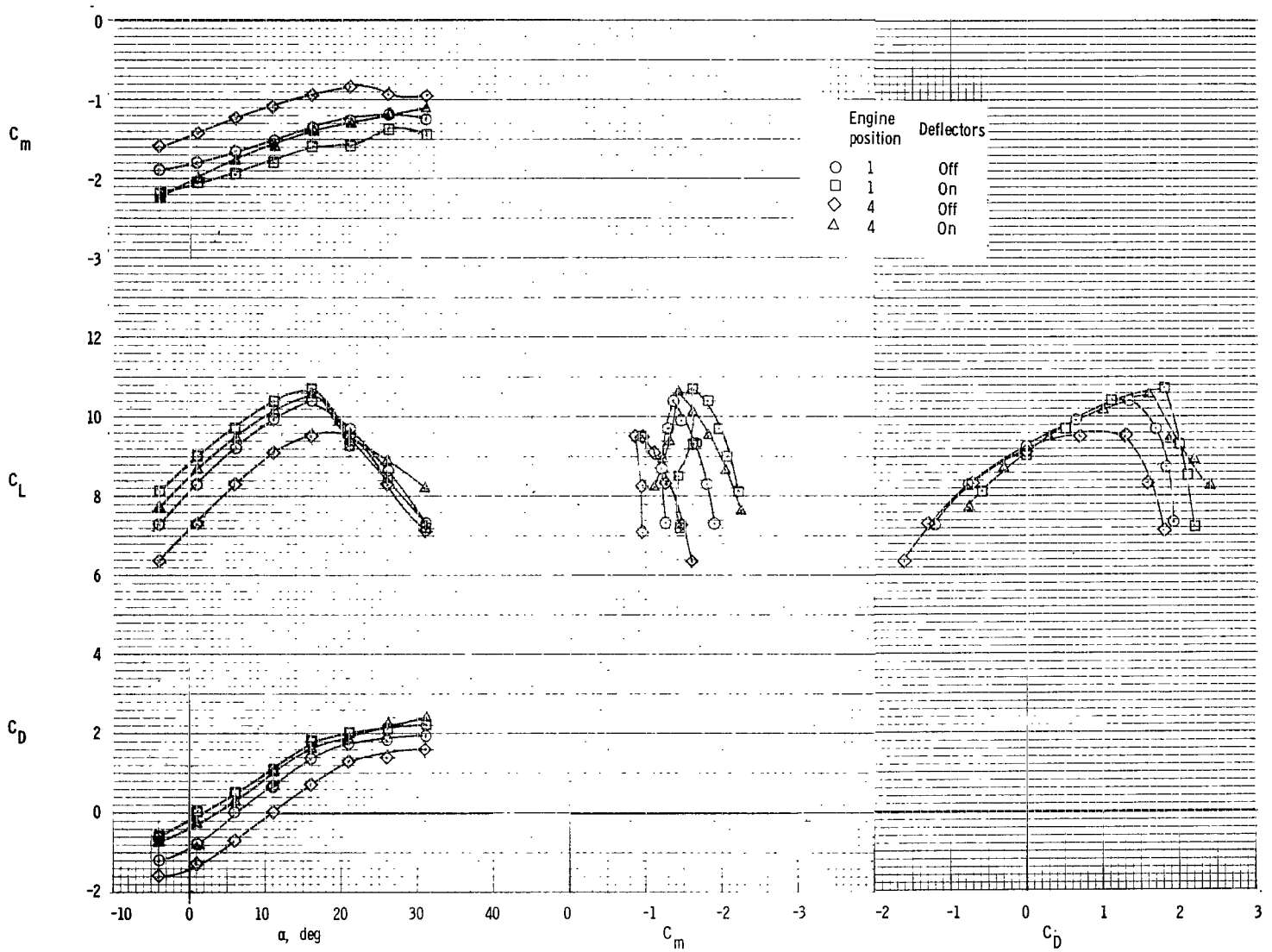

Figure 20.- Effect of exhaust deflectors. $\delta_f = 55^o$; $C_\mu = 5.50$.

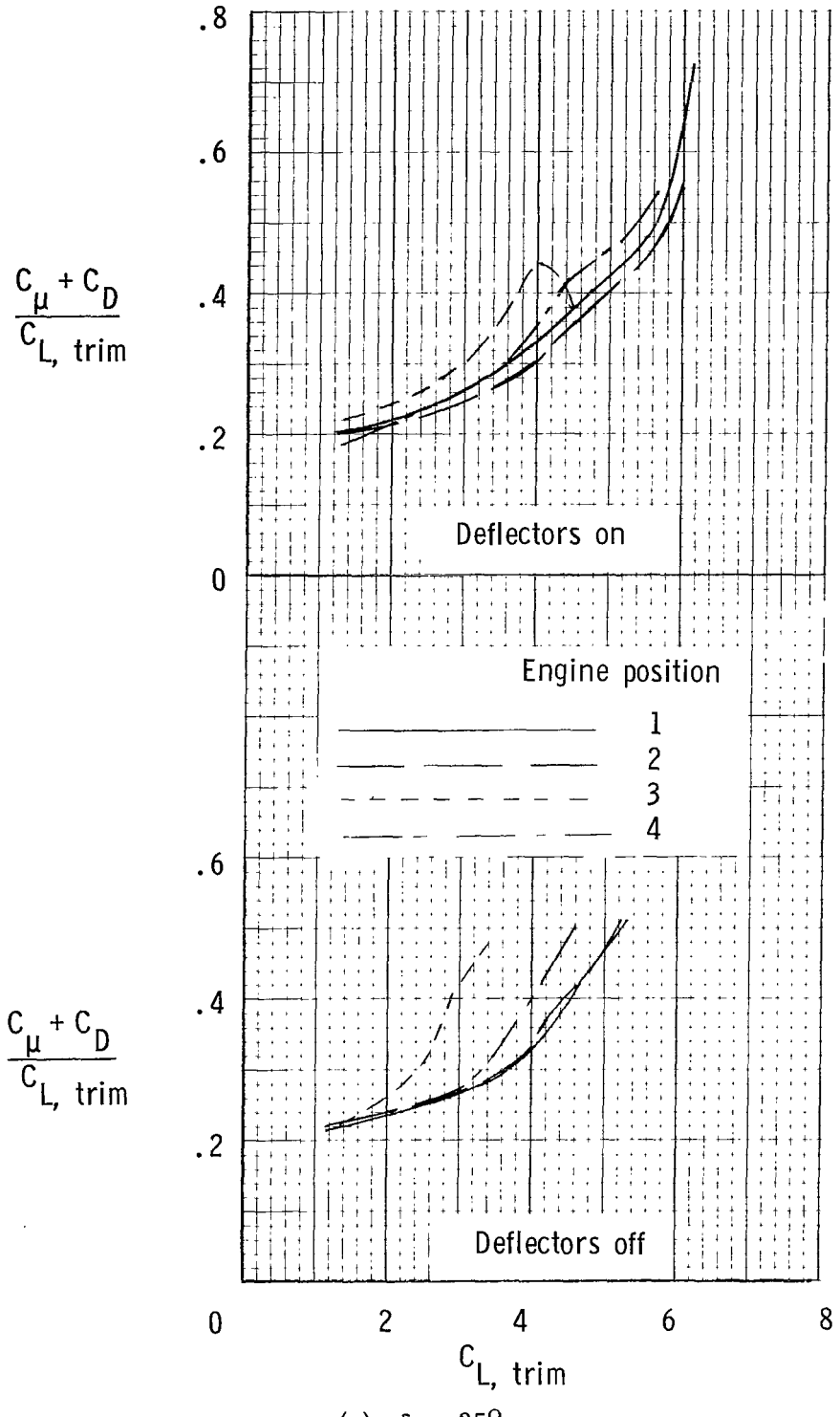

(a) $\delta_f = 35^o$.

Figure 21.- Summary of effect of engine position on longitudinal aerodynamic characteristics of model. $\alpha = 0^o$.

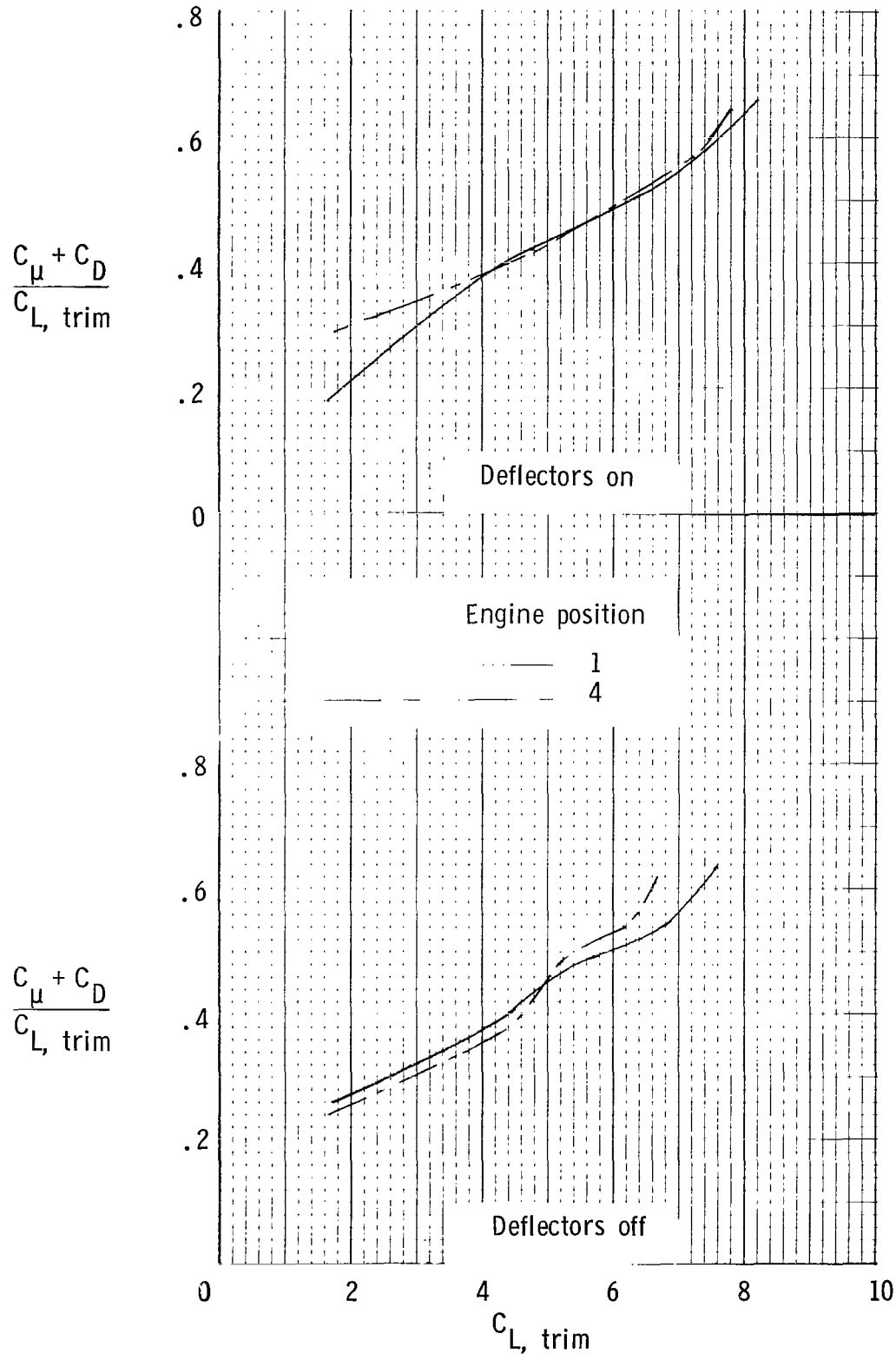

(b) $\delta_f = 55^o$.

Figure 21.- Continued.

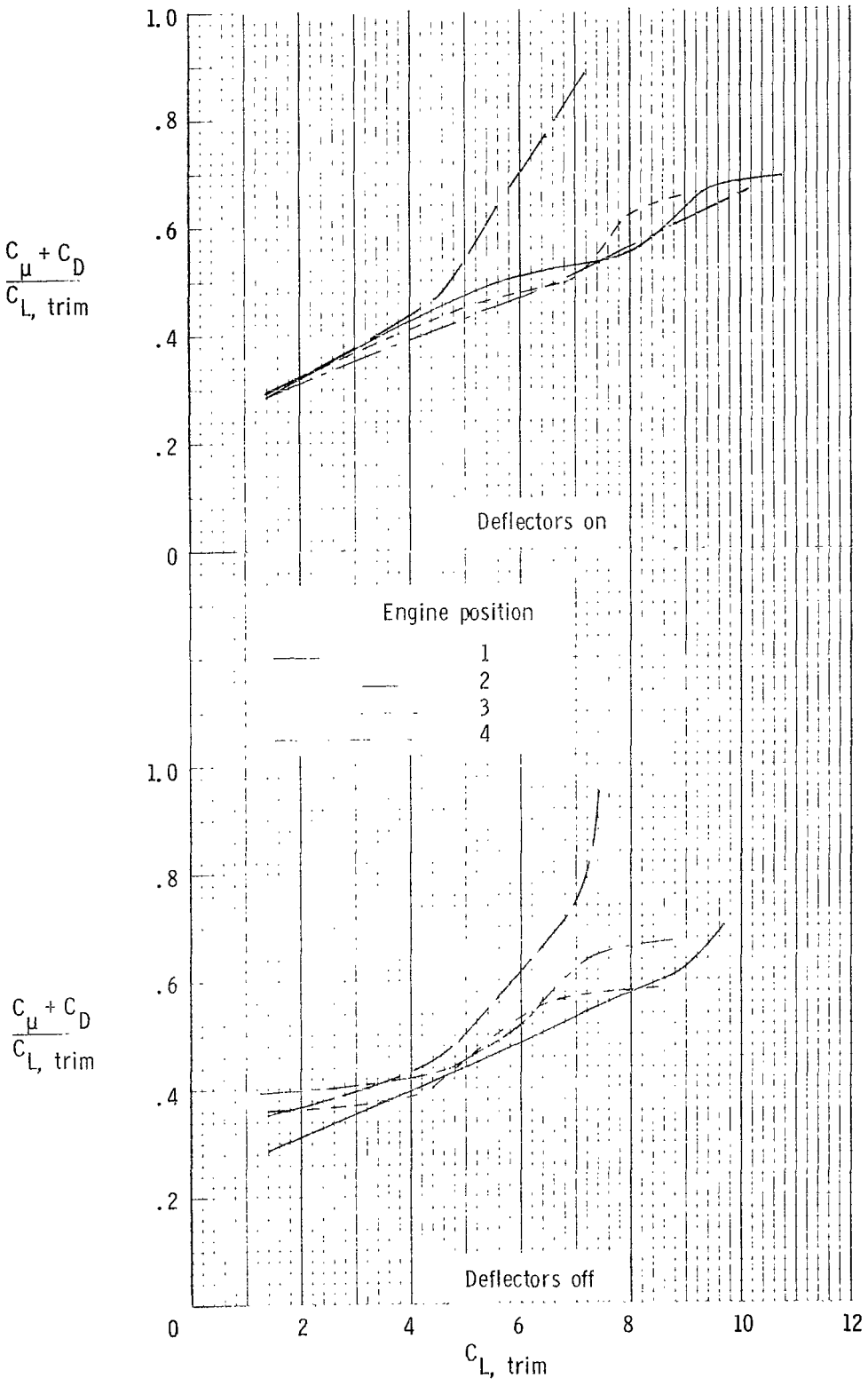

(c) $\delta_f = 70^o$.

Figure 21.- Concluded.

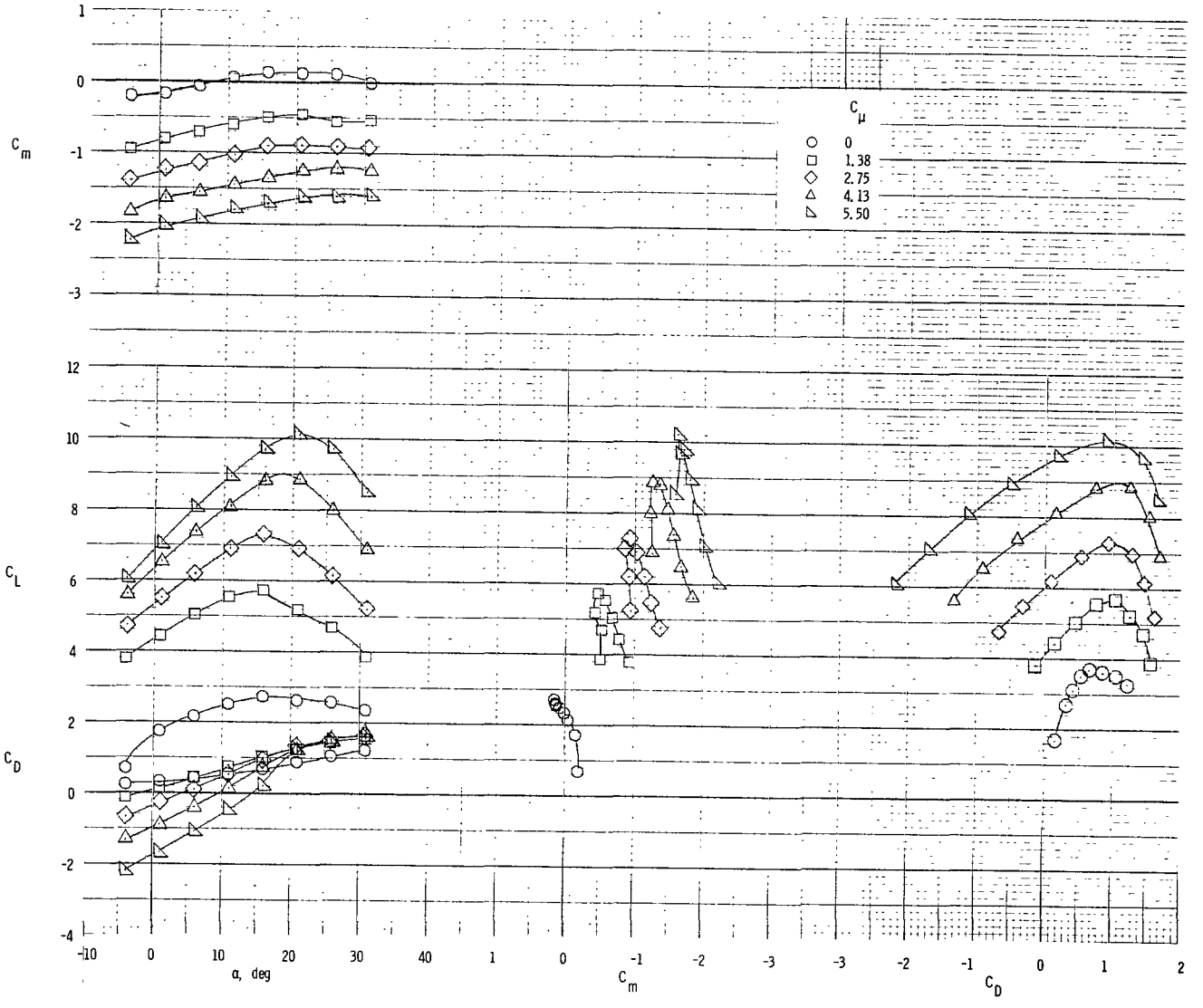

(a) Exhaust deflectors off.

Figure 22.- Longitudinal aerodynamic characteristics of model. Engine position 1; large vane and small flap; $\delta_f = 55^o$; original leading-edge slat.

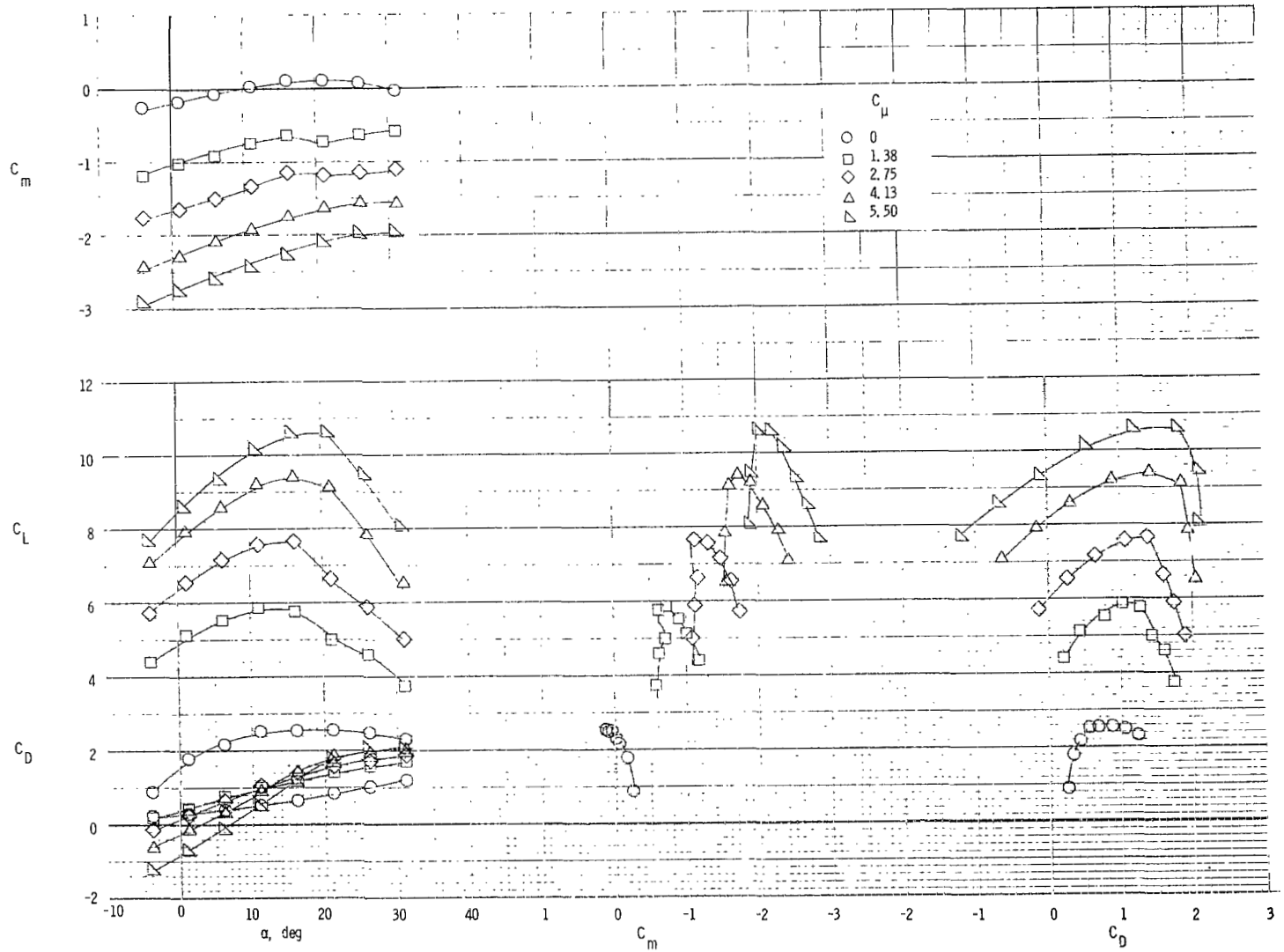

(b) Exhaust deflectors on.

Figure 22.- Concluded.

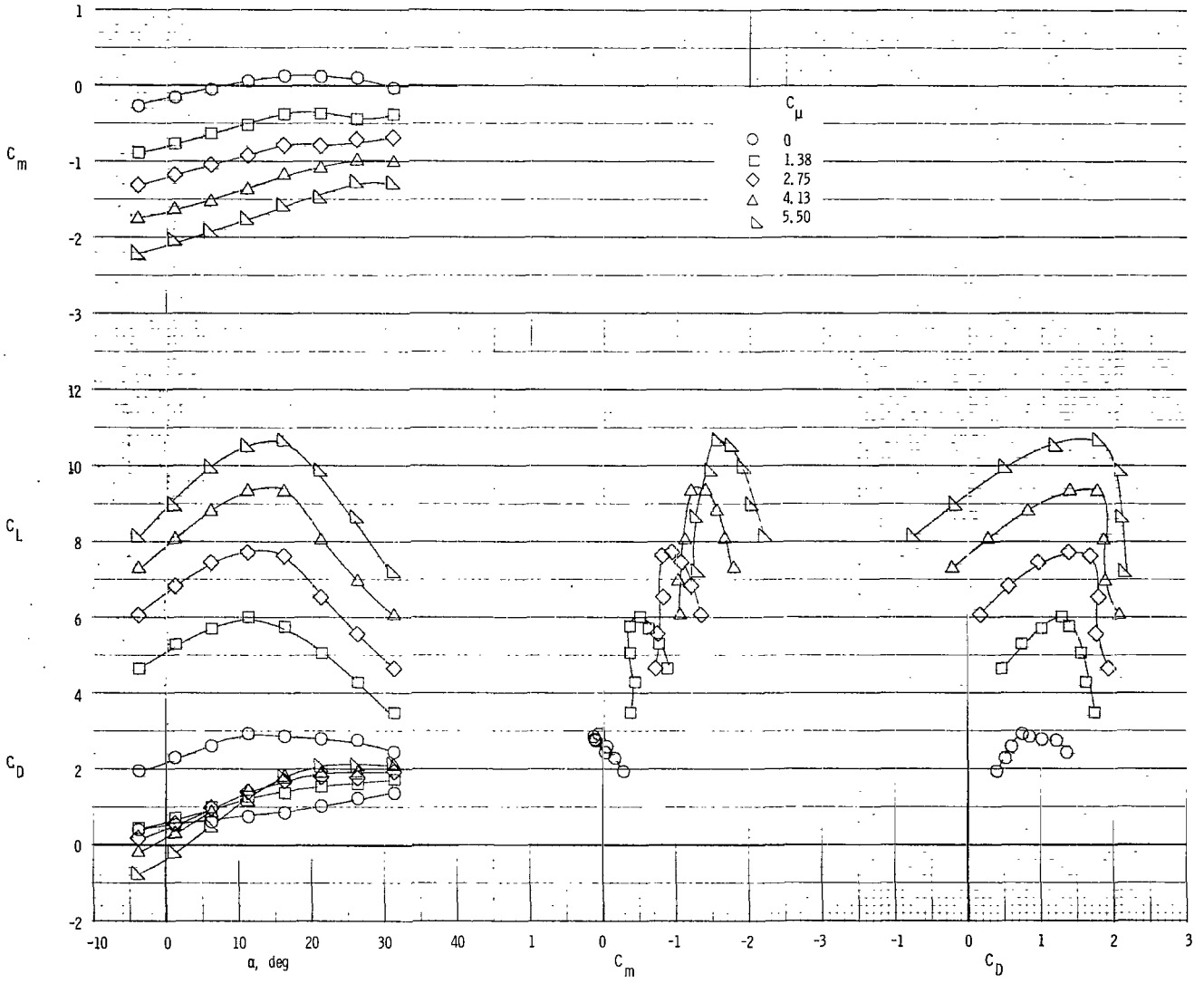

(a) Exhaust deflectors off.

Figure 23.- Longitudinal aerodynamic characteristics of model. Engine position 1; large vane and large flap; $\delta_f = 55^o$; original leading-edge slat.

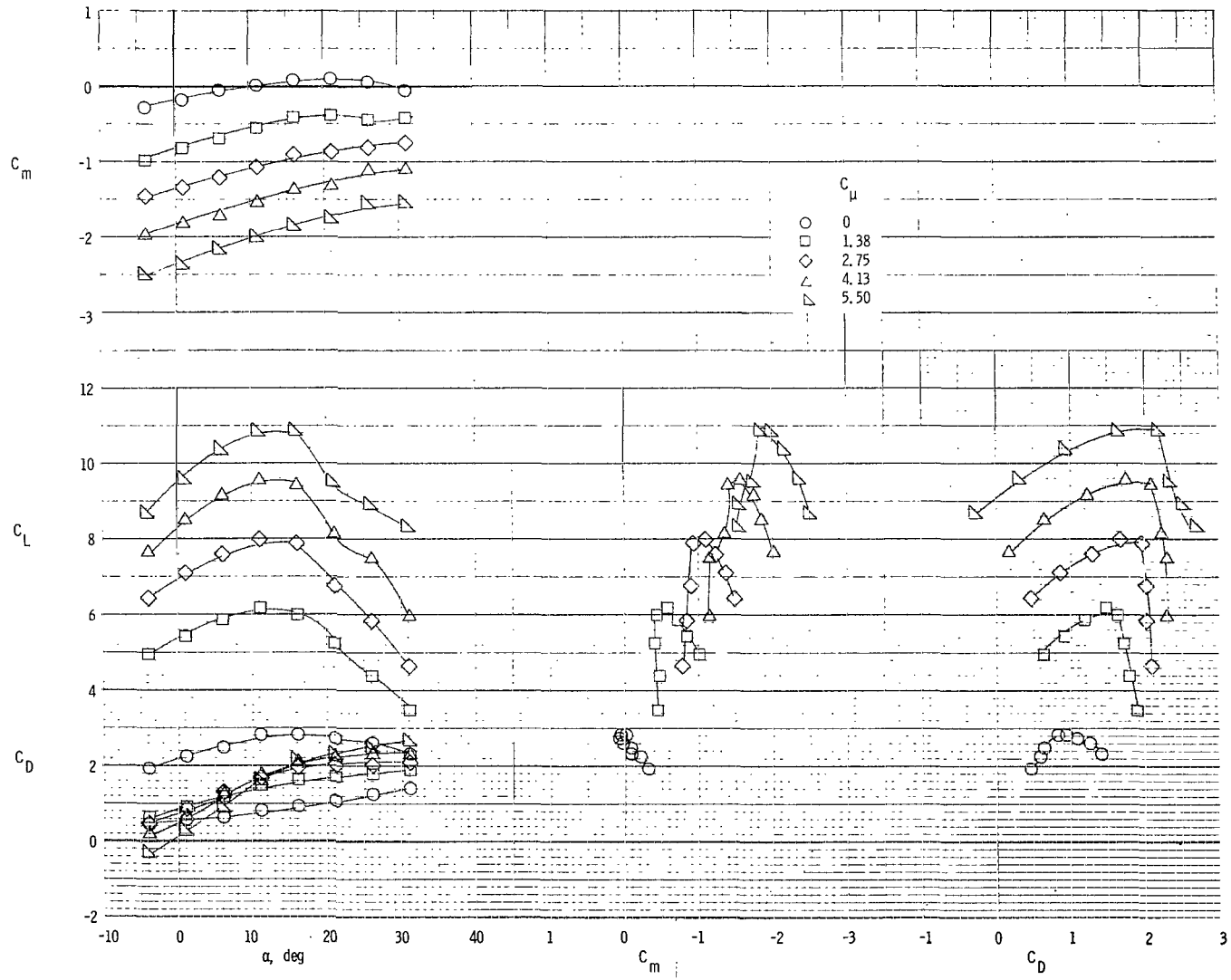

(b) Exhaust deflectors on.

Figure 23.- Concluded.

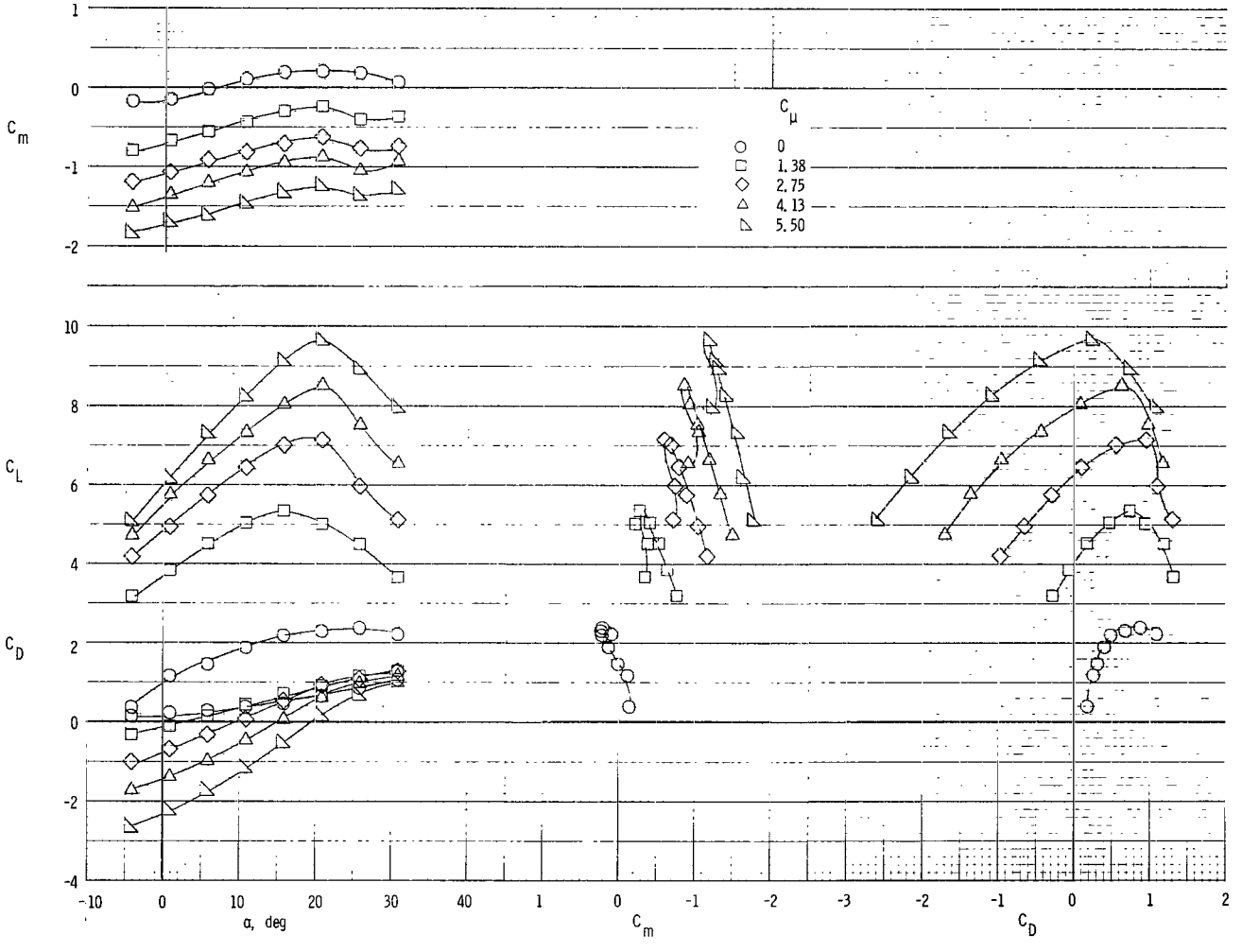

(a) Exhaust deflectors off.

Figure 24.- Longitudinal aerodynamic characteristics of model. Engine position 1; small vane and small flap; $\delta_f = 55^o$; original leading-edge slat.

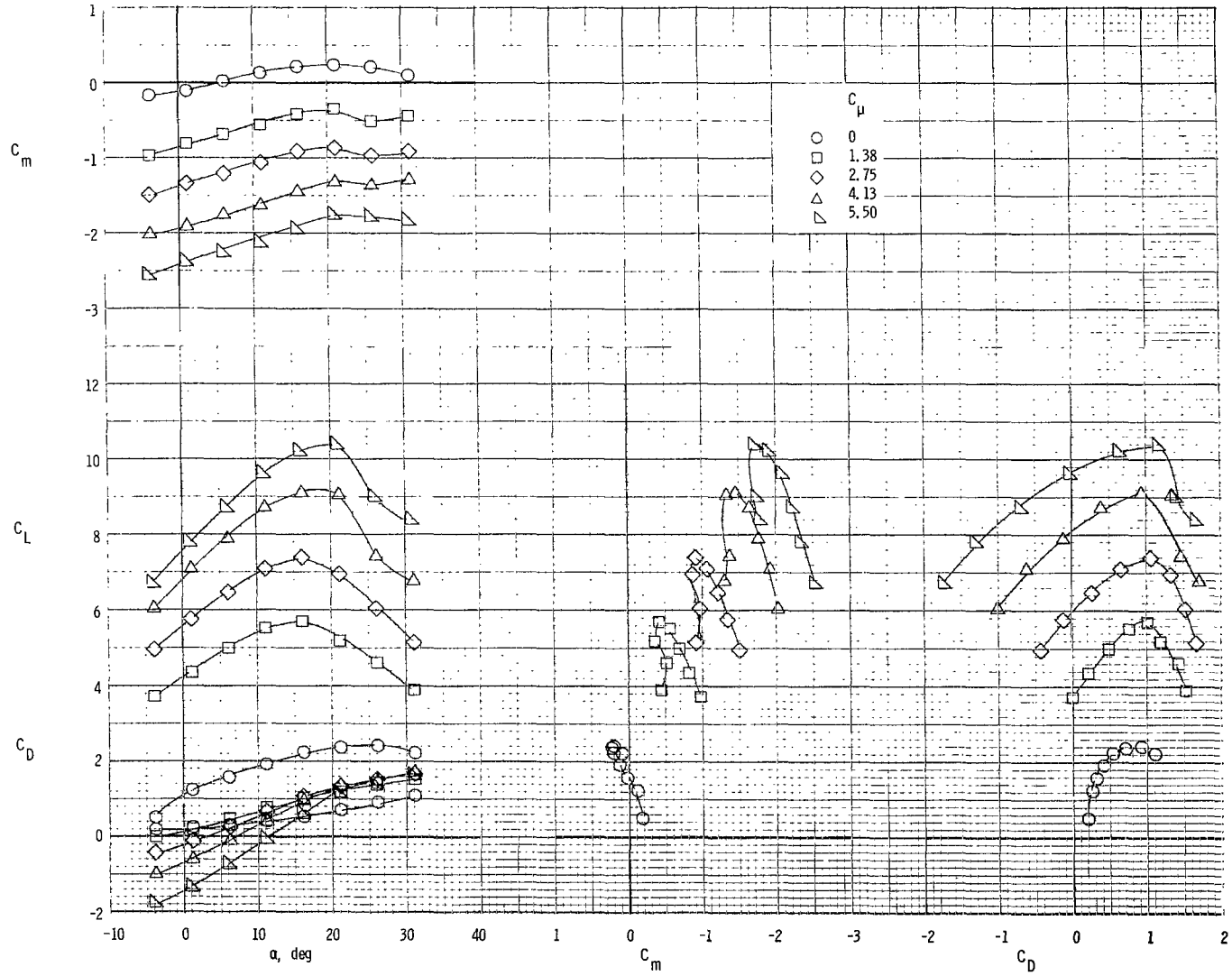

(b) Exhaust deflectors on.

Figure 24.- Concluded.

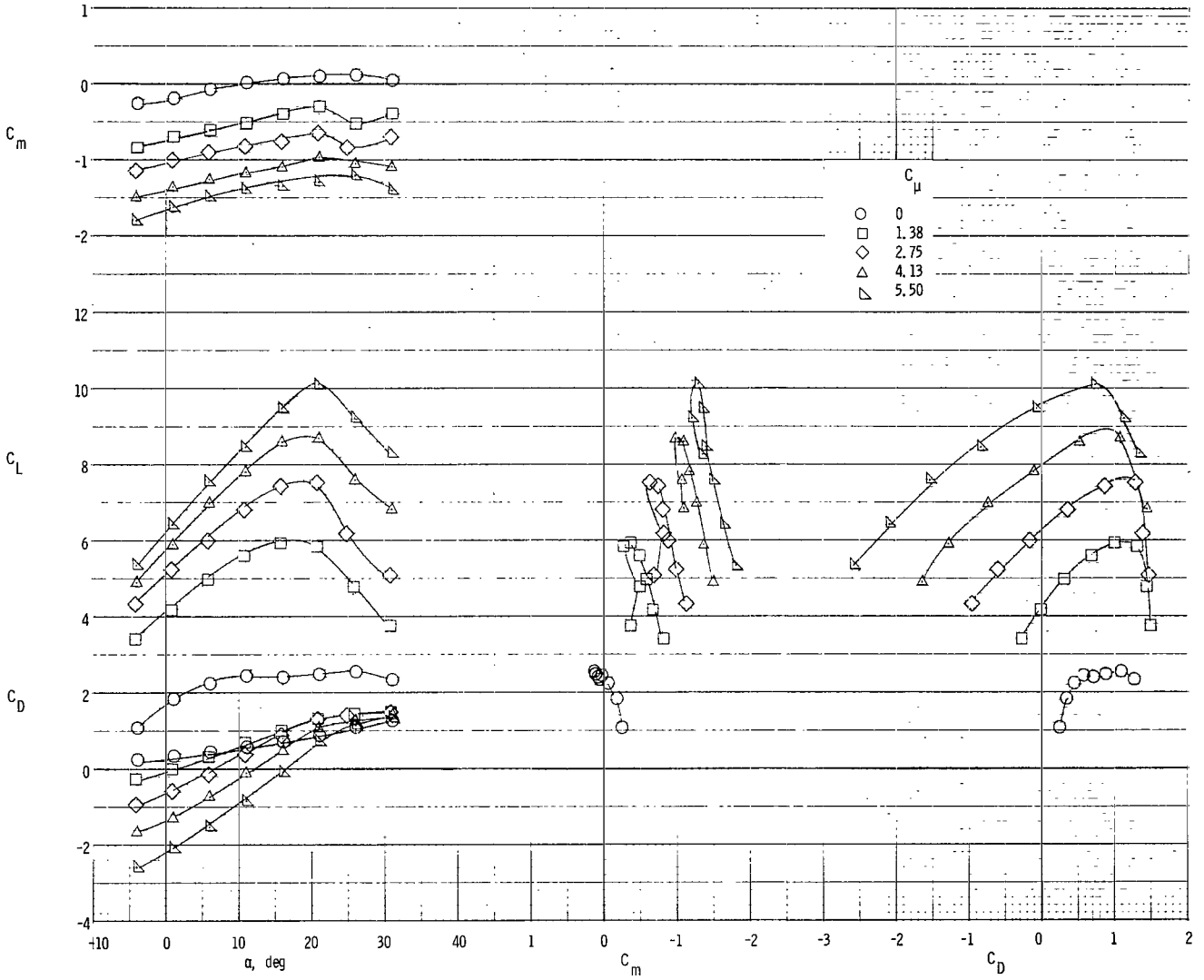

(a) Exhaust deflectors off.

Figure 25.- Longitudinal aerodynamic characteristics of model. Engine position 4; large vane and small flap; $\delta_f = 55^o$; original leading-edge slat.

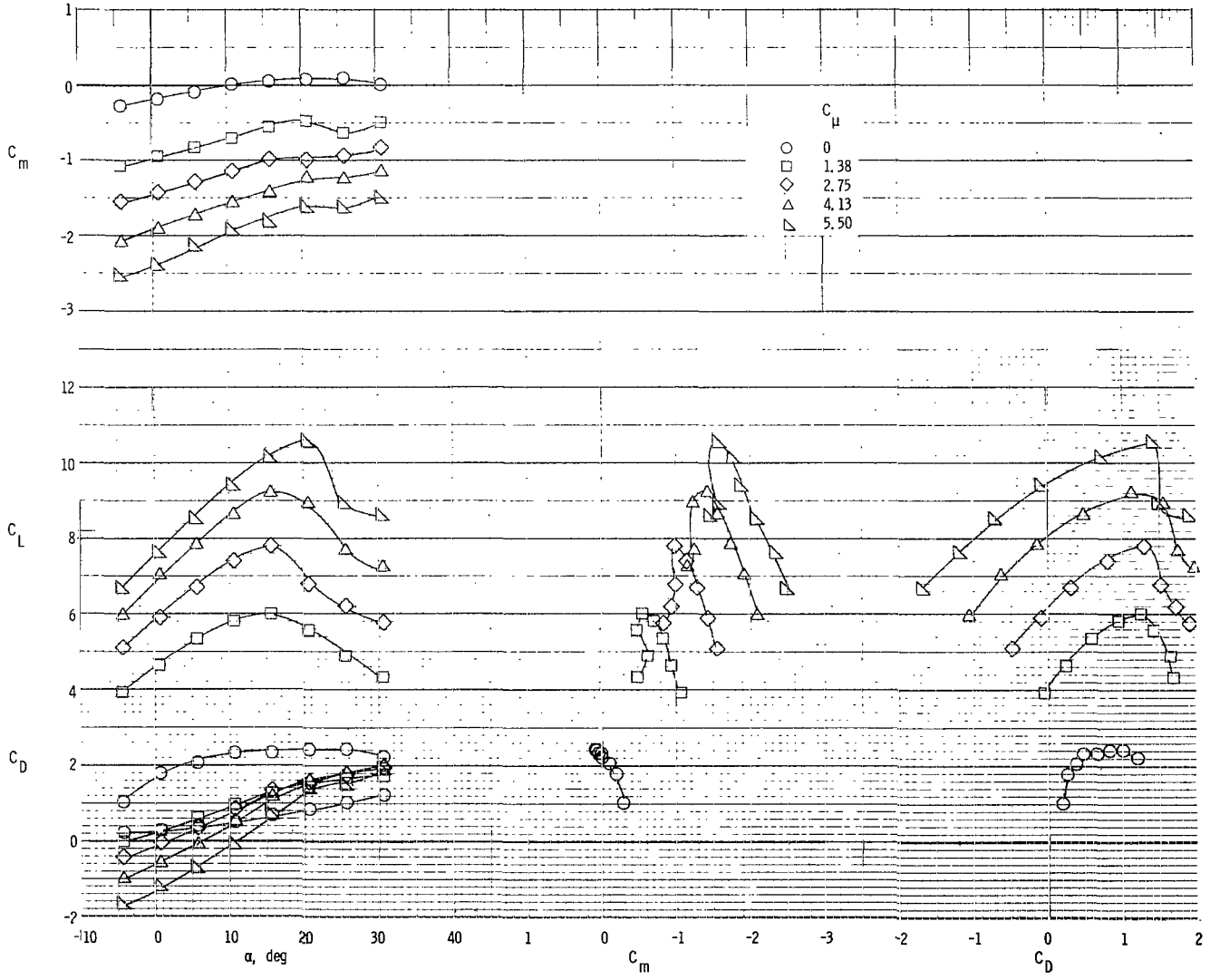

(b) Exhaust deflectors on.

Figure 25.- Concluded.

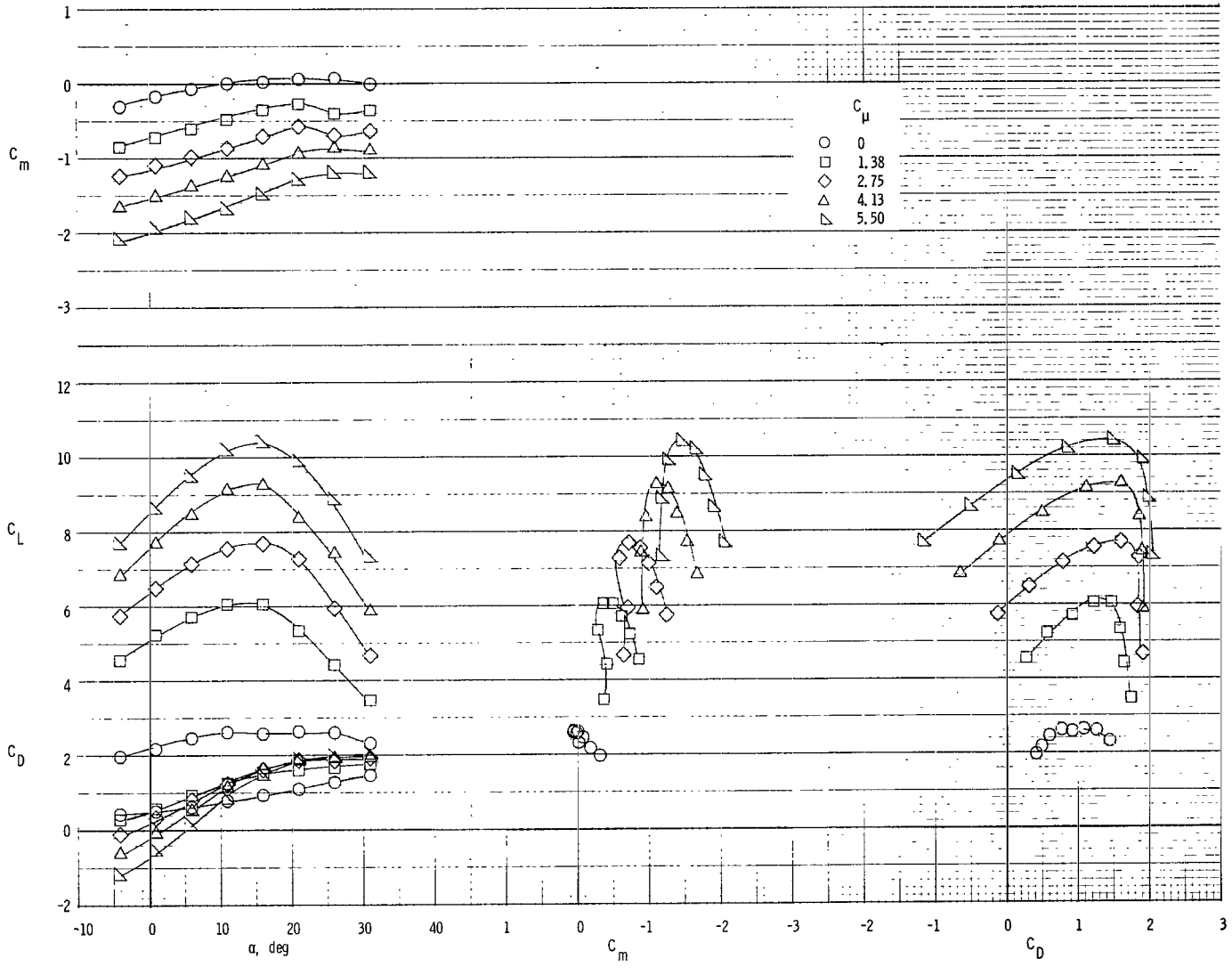

(a) Exhaust deflectors off.

Figure 26.- Longitudinal aerodynamic characteristics of model. Engine position 4; large vane and large flap; $\delta_f = 55^o$; original leading-edge slat.

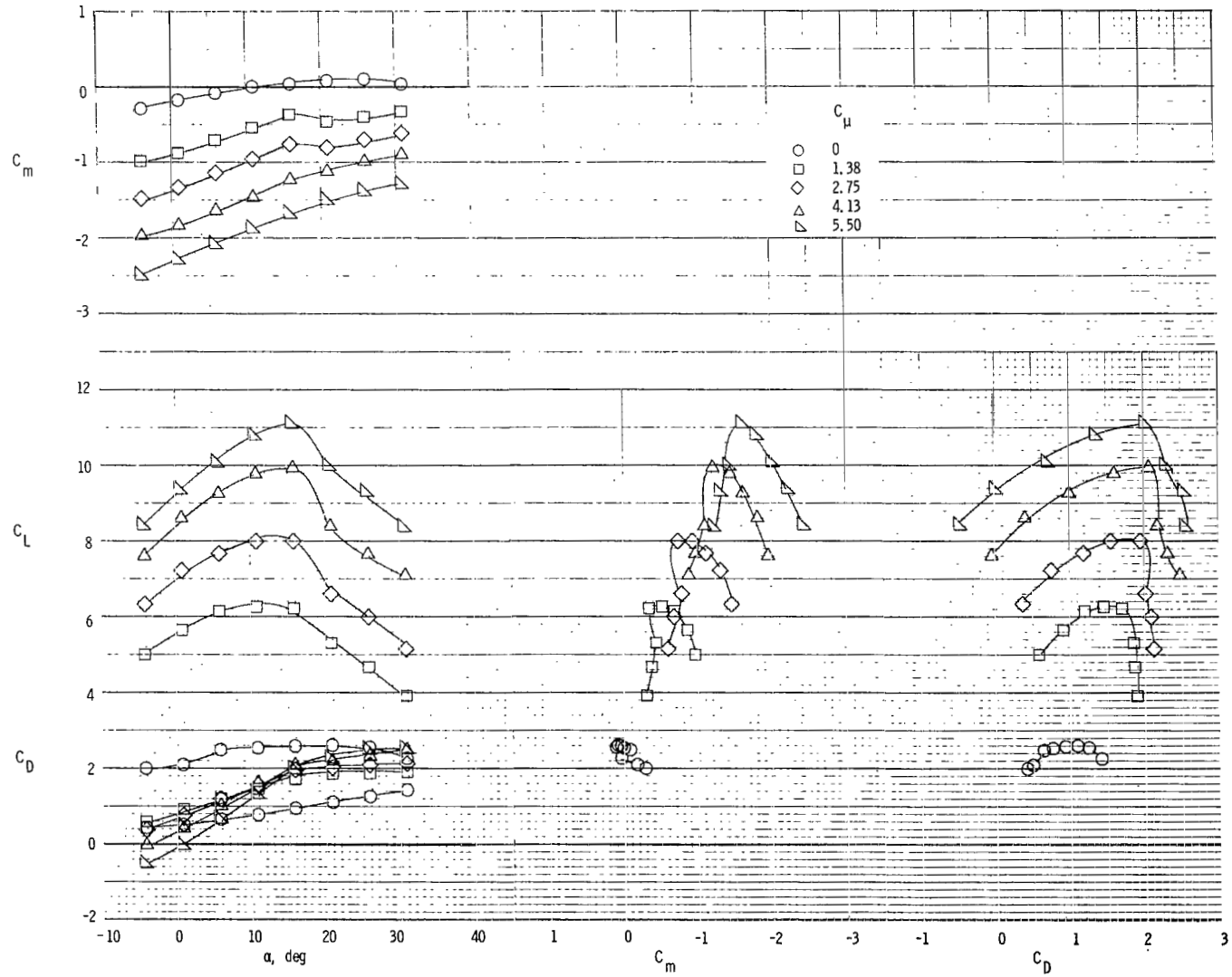

(b) Exhaust deflectors on.

Figure 26.- Concluded.

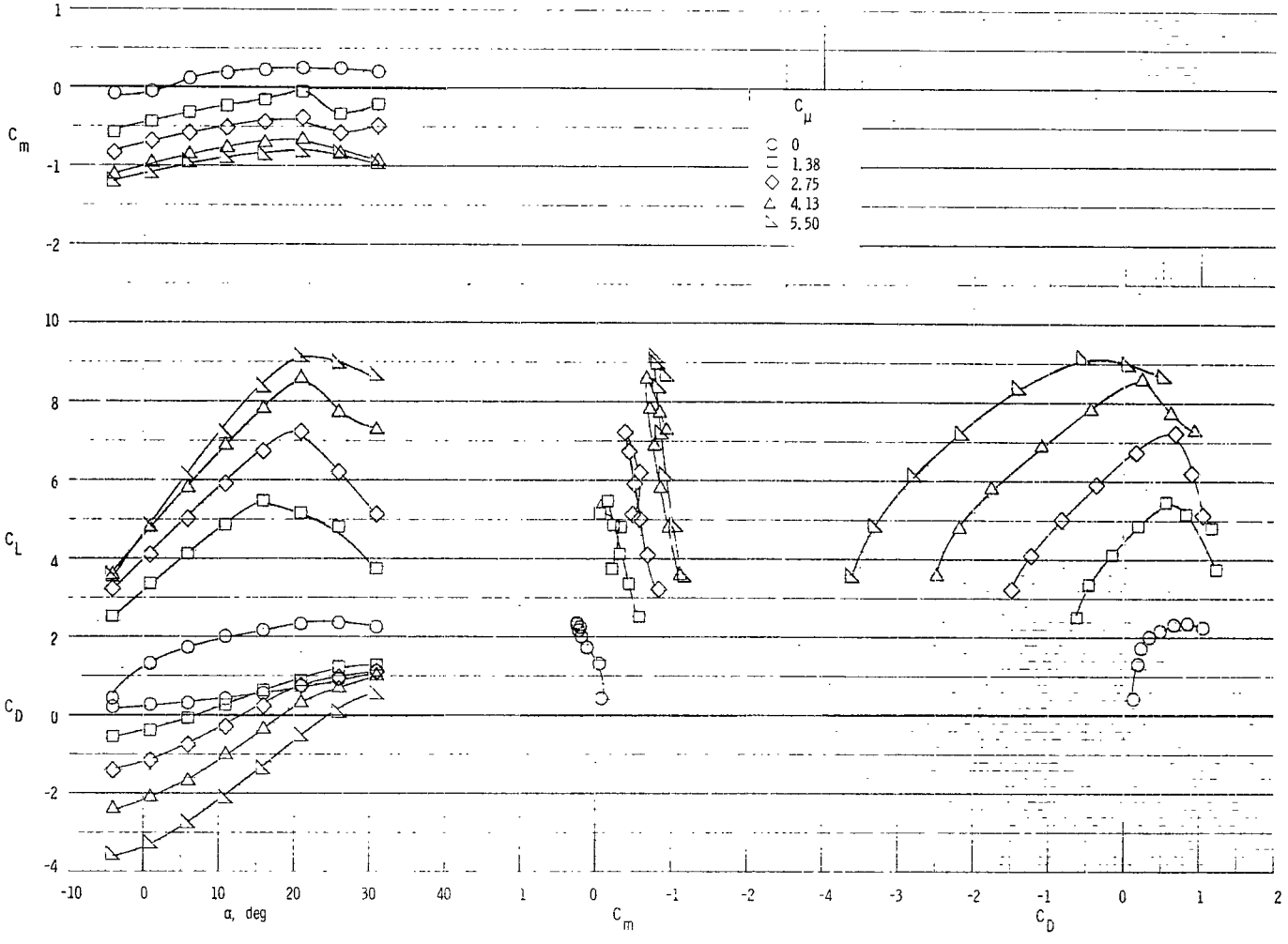

(a) Exhaust deflectors off.

Figure 27.- Longitudinal aerodynamic characteristics of model. Engine position 4; small vane and small flap; $\delta_f = 55^o$; original leading-edge slat.

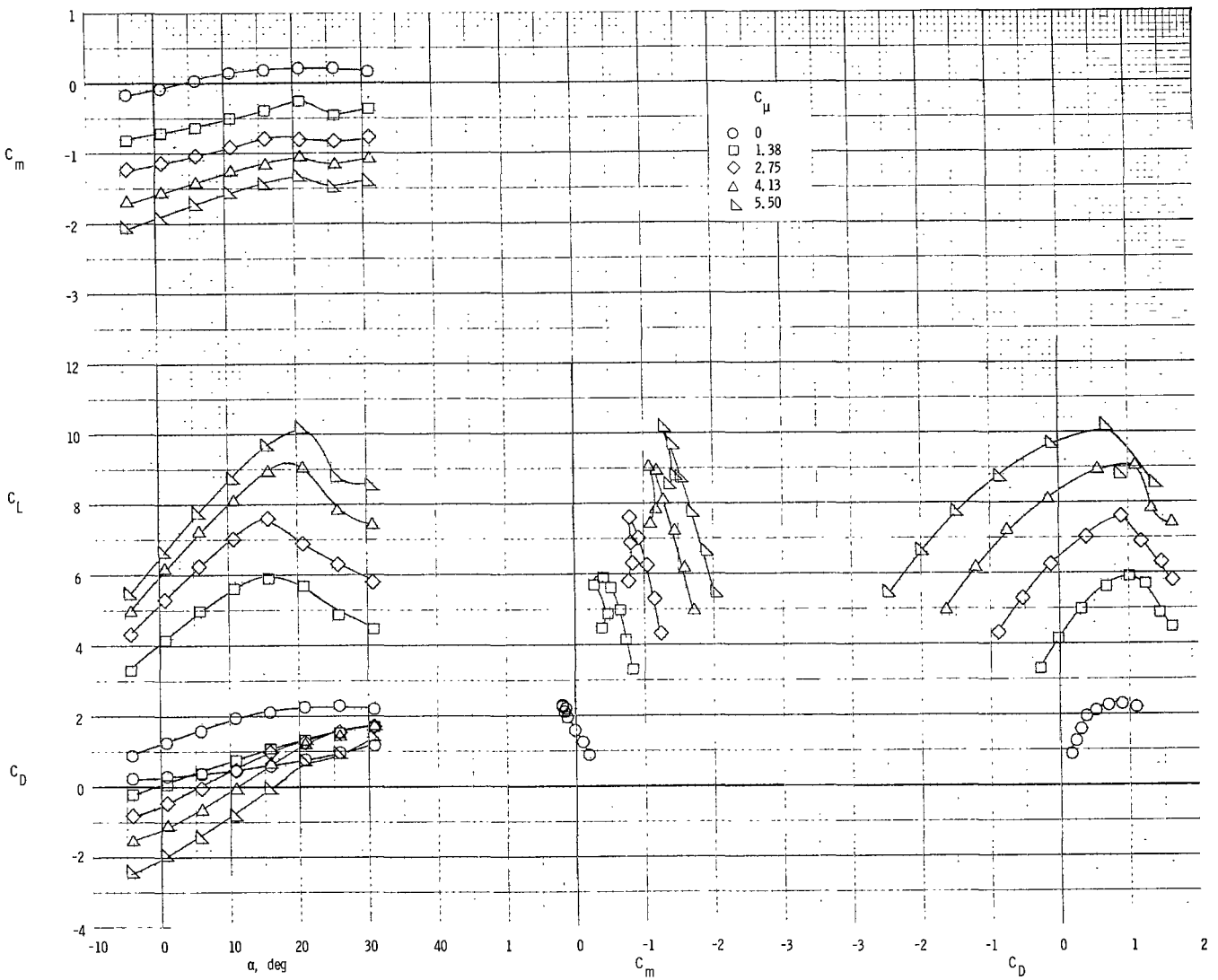

(b) Exhaust deflectors on.

Figure 27.- Concluded.

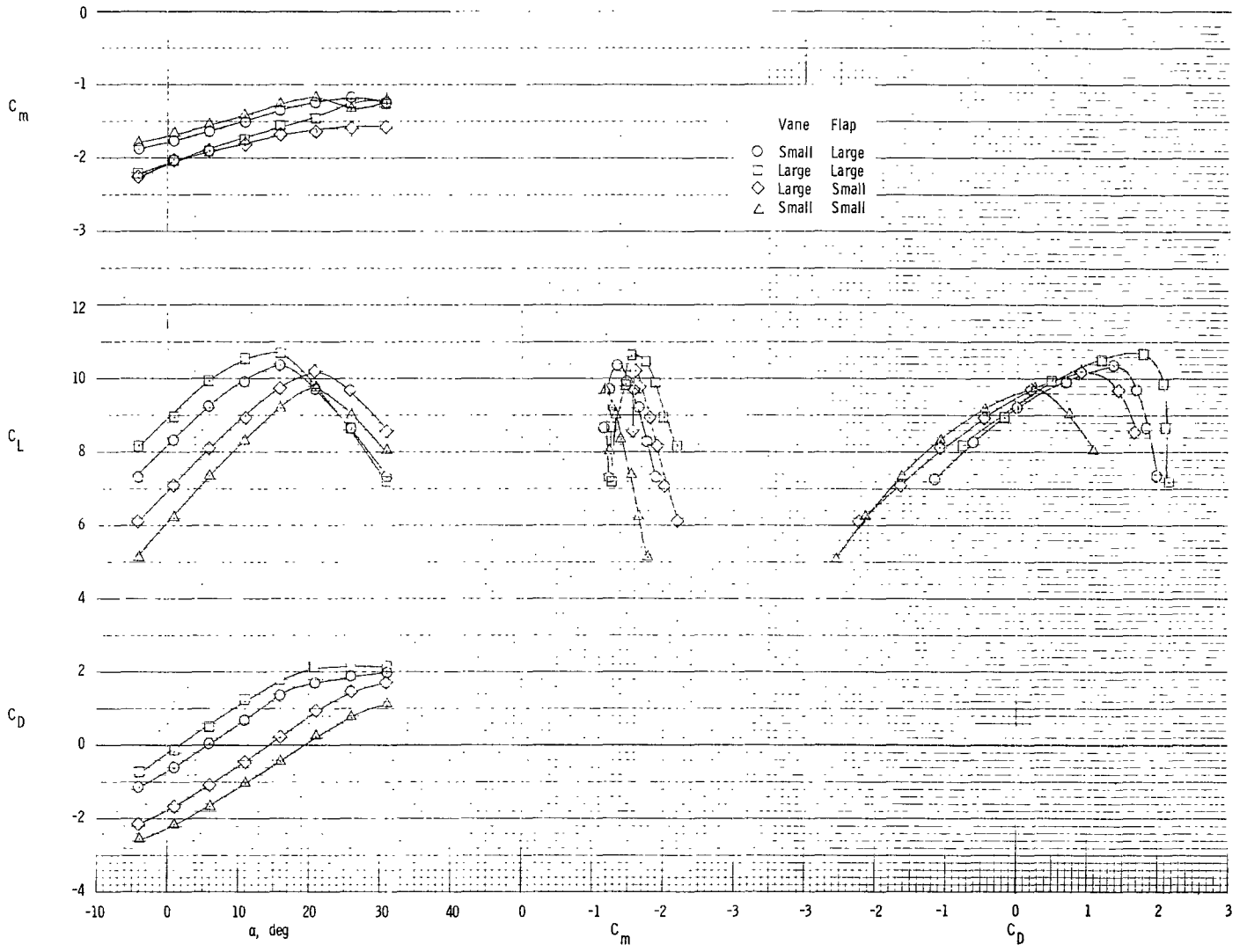

(a) C_μ = 5.50.

Figure 28.- Effect of vane and flap size and arrangement on longitudinal aerodynamic characteristics of model. Engine position 1; $\delta_f = 55^o$; deflectors off.

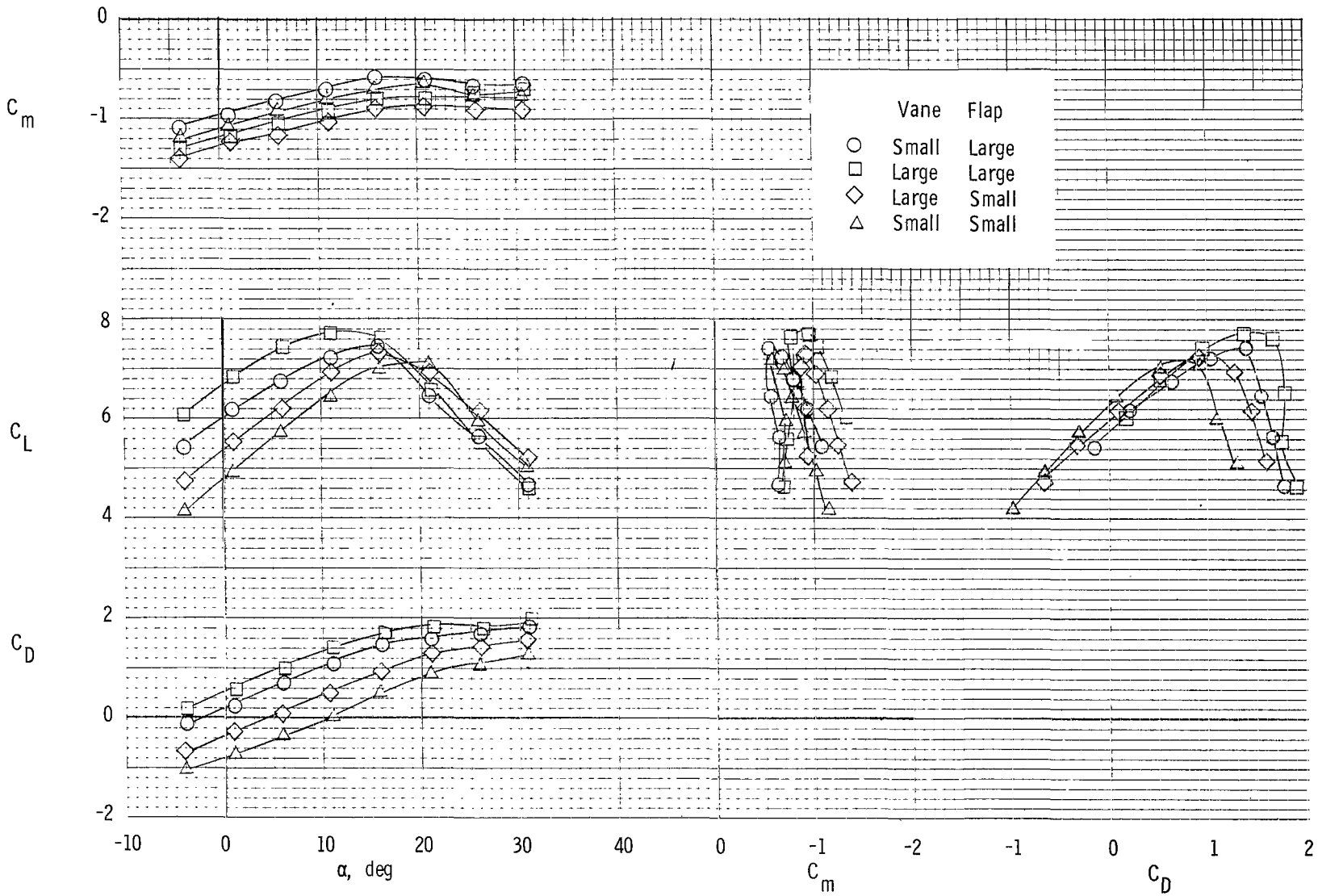

(b) $C_\mu = 2.75$.

Figure 28.- Concluded.

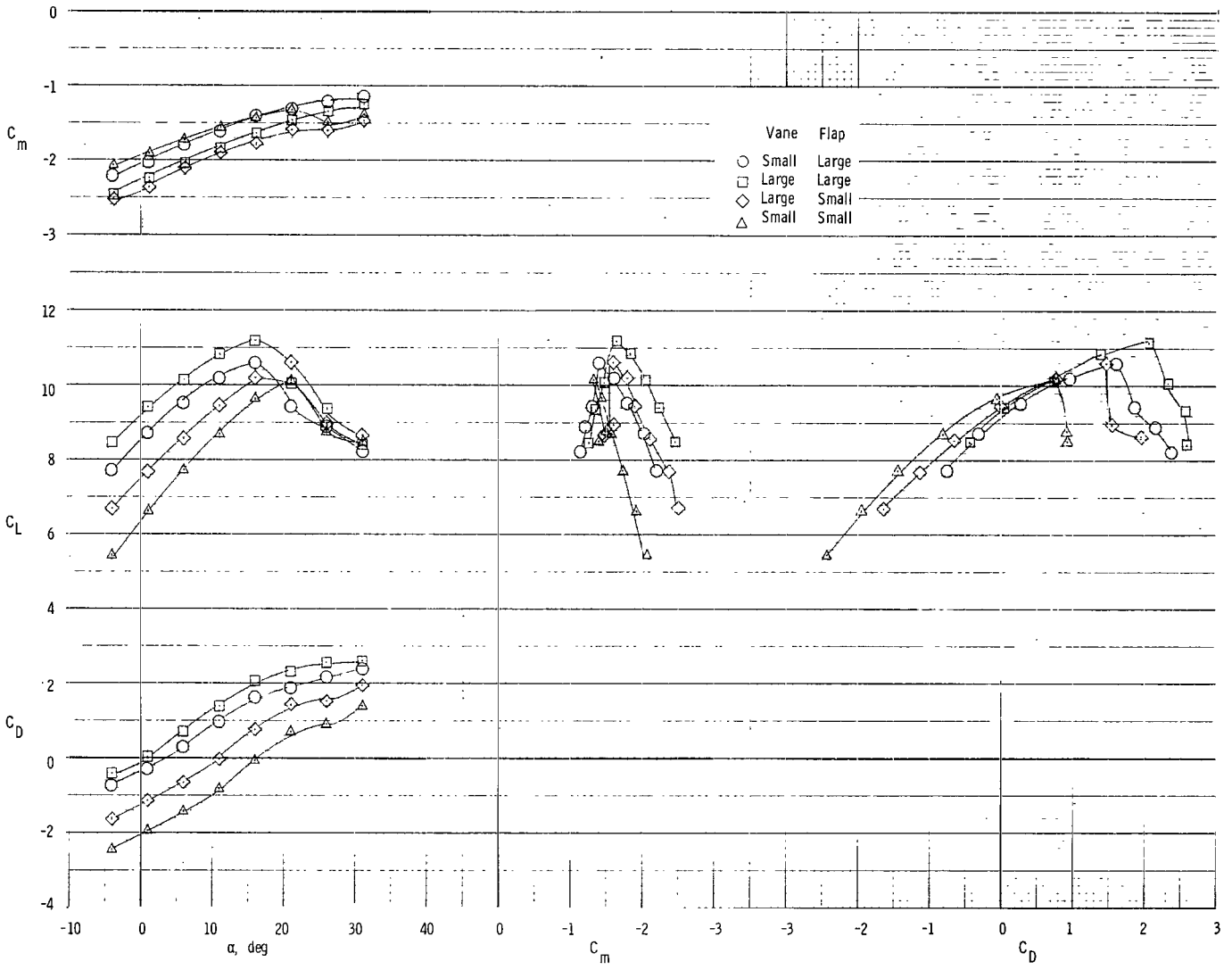

(a) C_μ = 5.50.

Figure 29.- Effect of vane and flap size and arrangement on longitudinal aerodynamic characteristics of model. Engine position 4; $\delta_f = 55^o$; exhaust deflectors off.

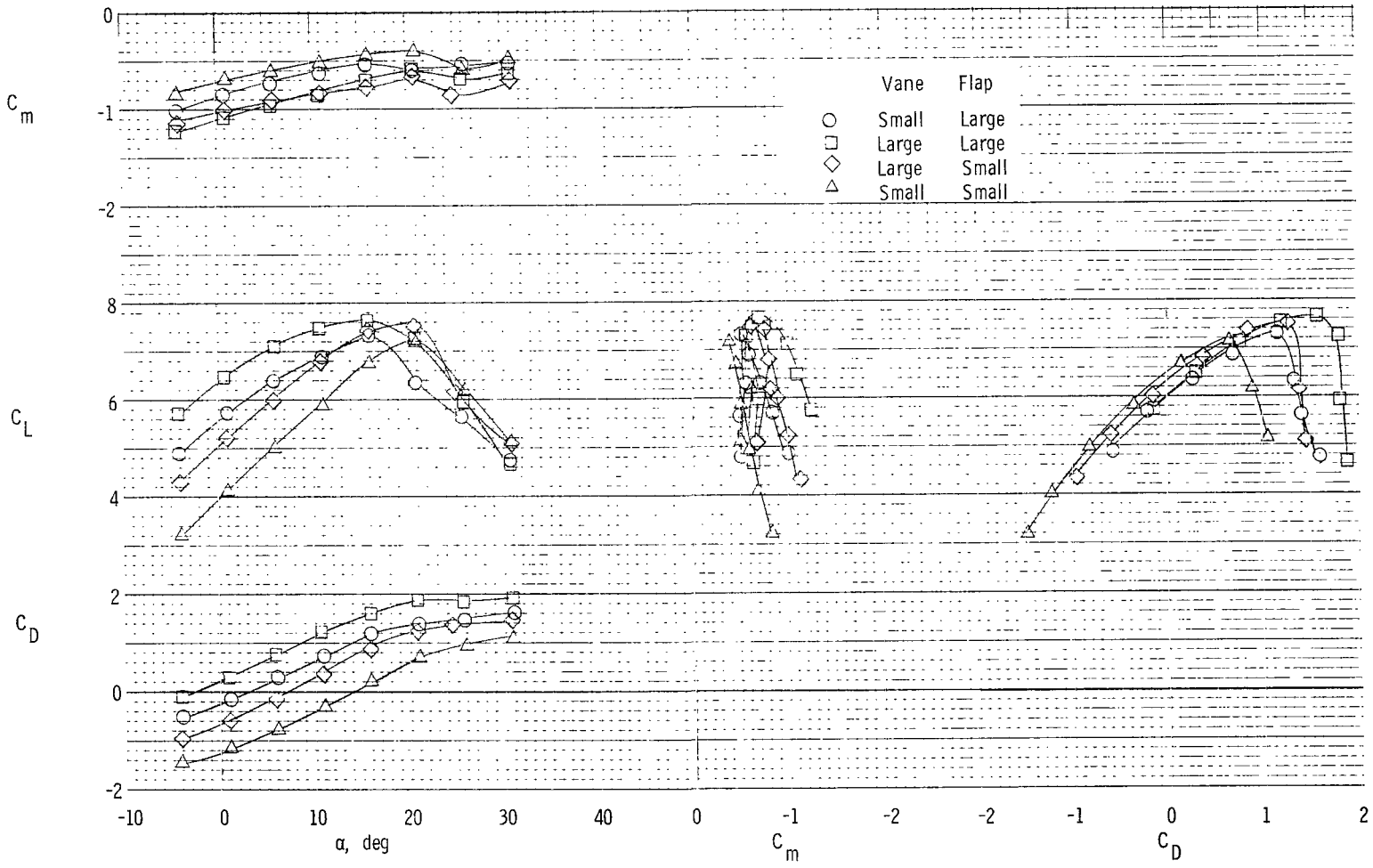

(b) C_μ = 2.75.

Figure 29.- Concluded.

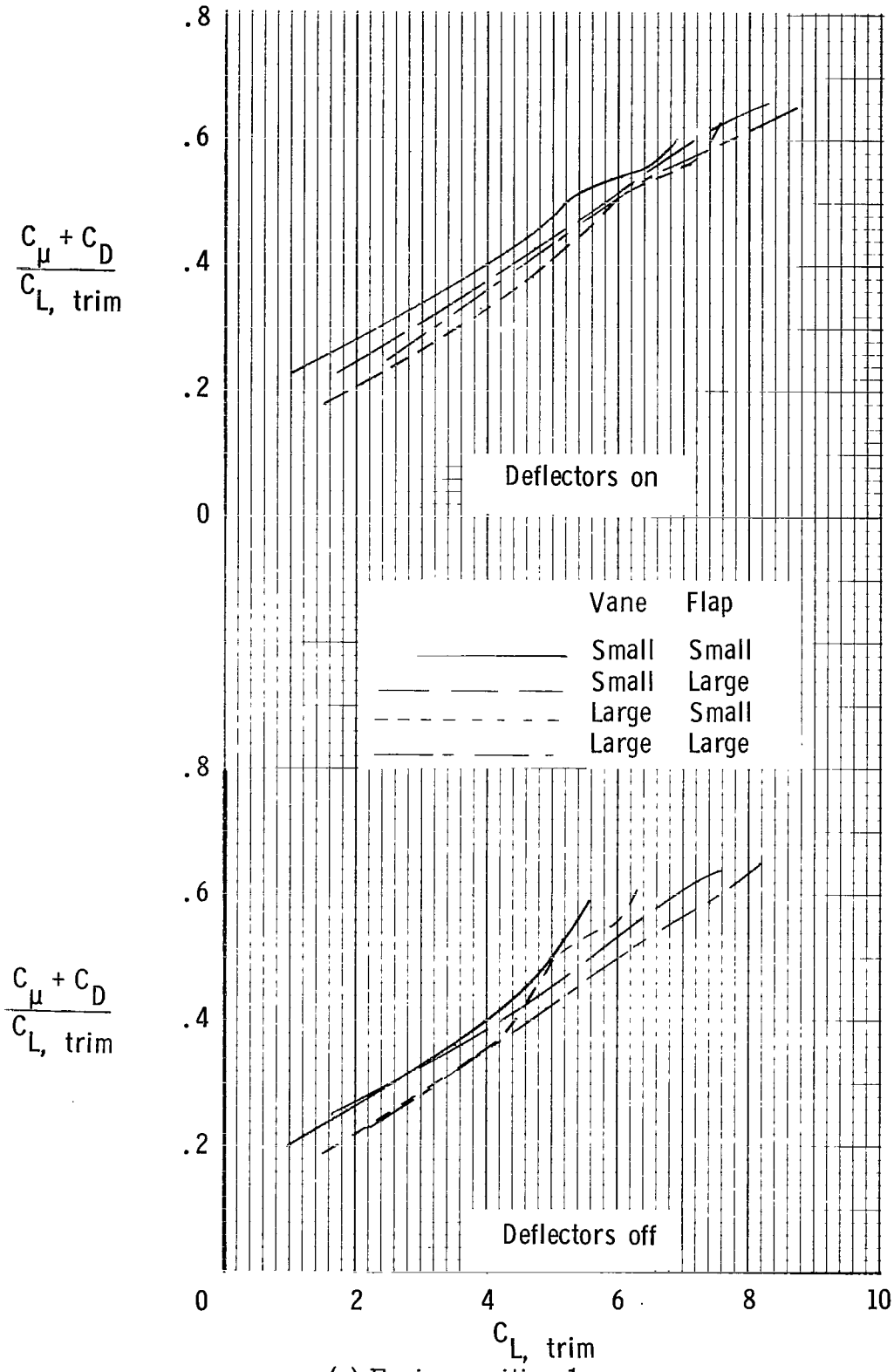

(a) Engine position 1.

Figure 30.- Effect of flap configuration on longitudinal aerodynamic characteristics of model. $\delta_f = 55^o$; original leading-edge slat; $\alpha = 0^o$.

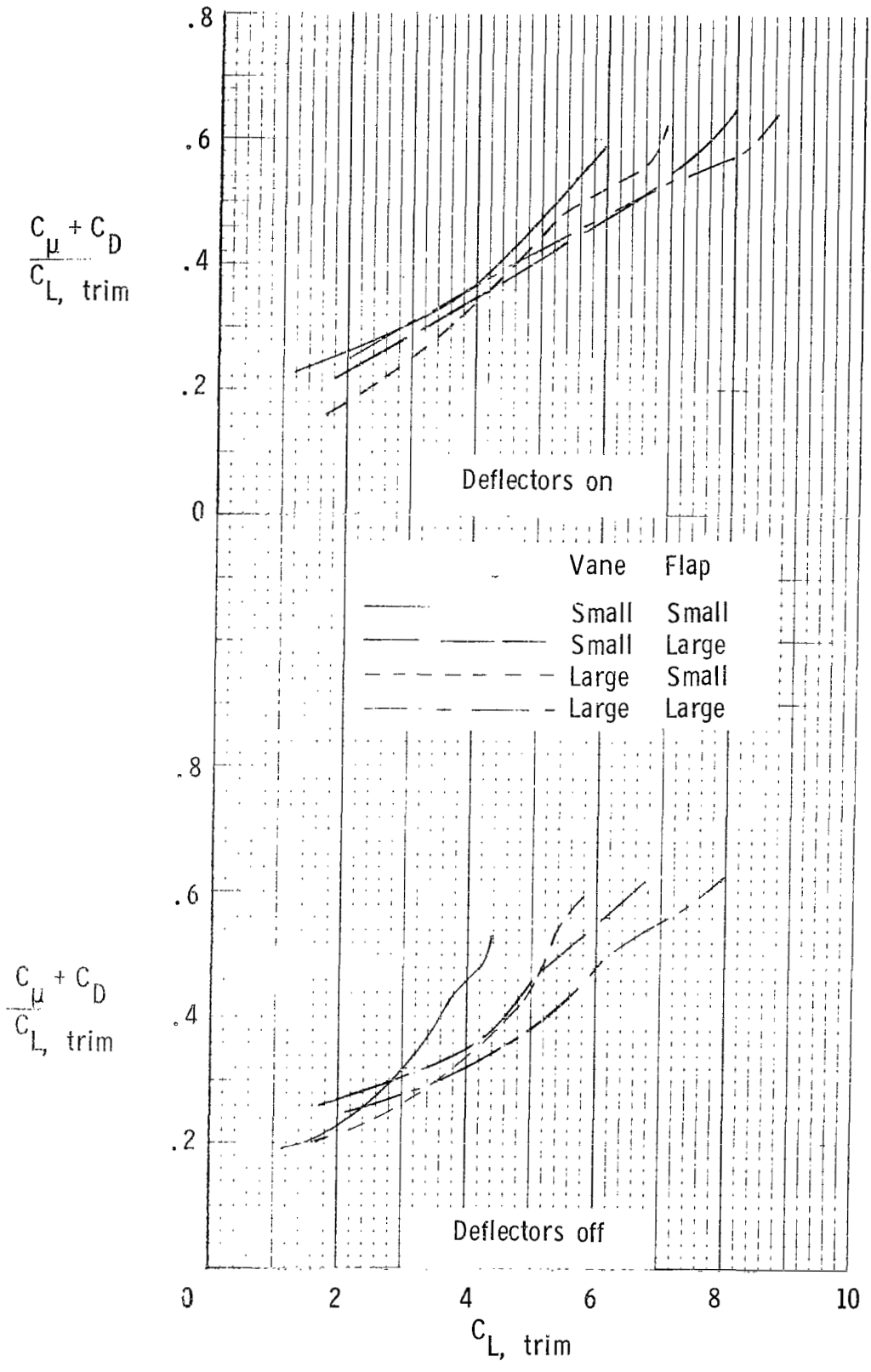

(b) Engine position 4.

Figure 30.- Concluded.

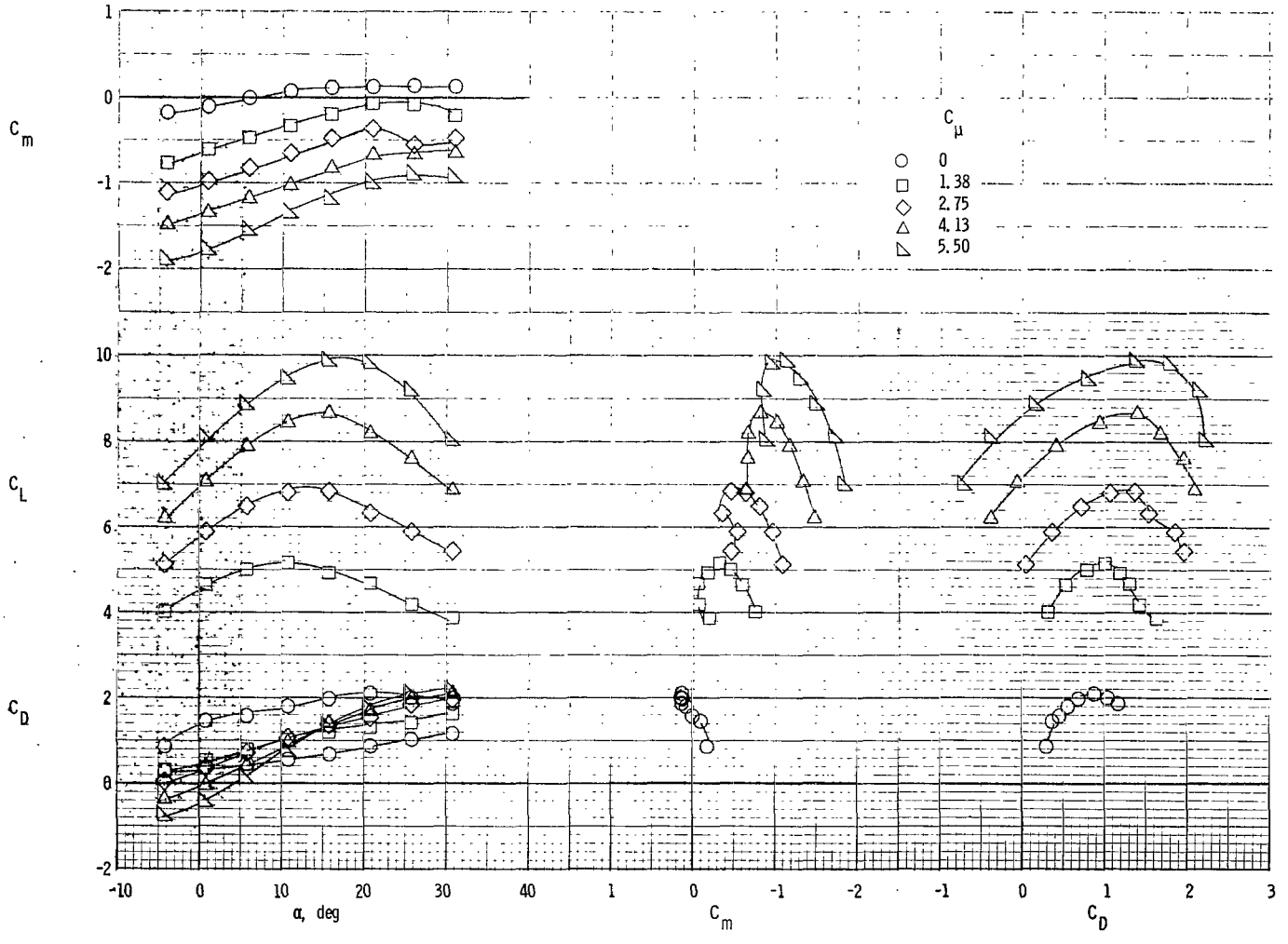

(a) Vane-flap gap sealed.

Figure 31.- Effect of sealing gaps in double-slotted flap on longitudinal aerodynamic characteristics of model. Engine position 4; $\delta_f = 55^o$; leading-edge-slat deflection, 65^o; exhaust deflectors on.

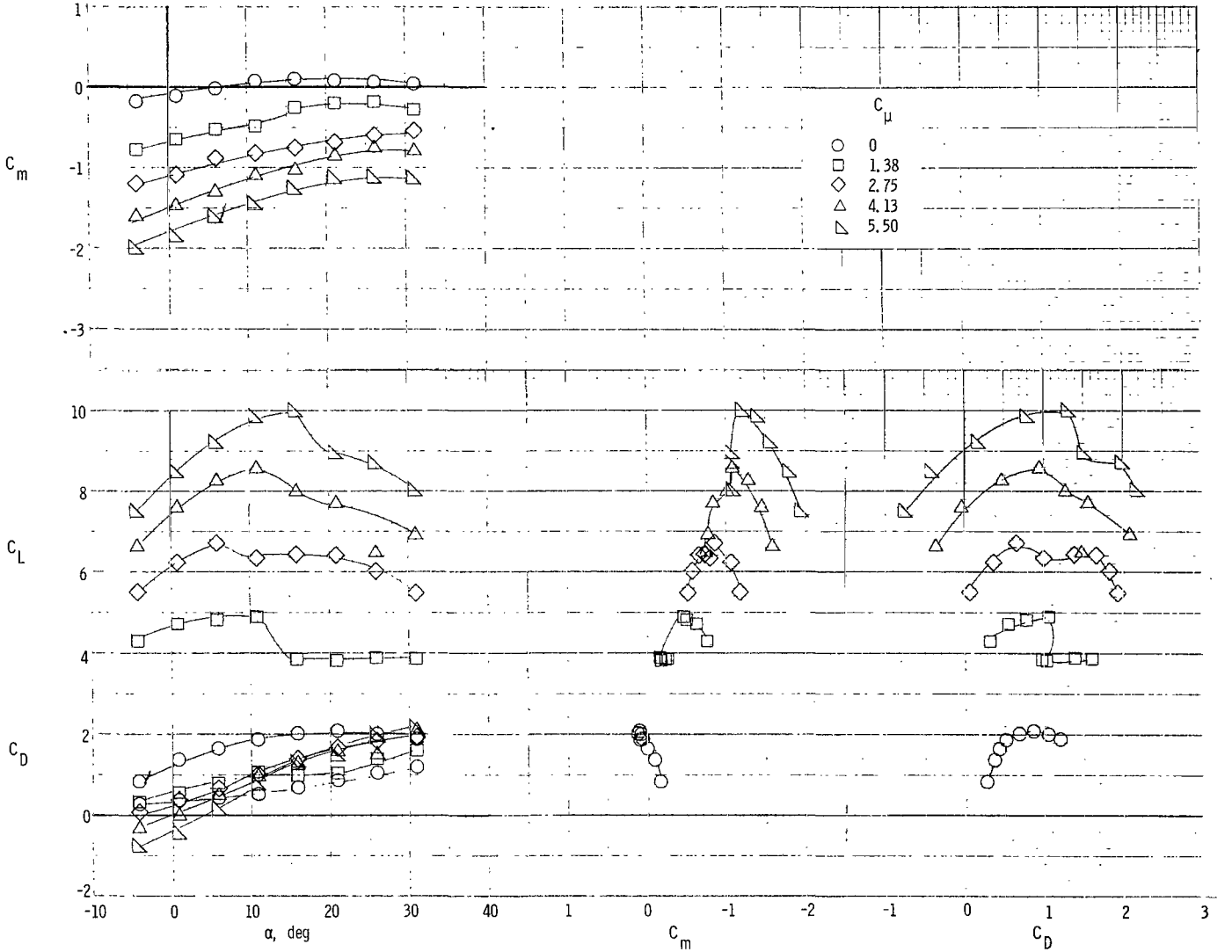

(b) Wing-vane gap sealed.

Figure 31.- Continued.

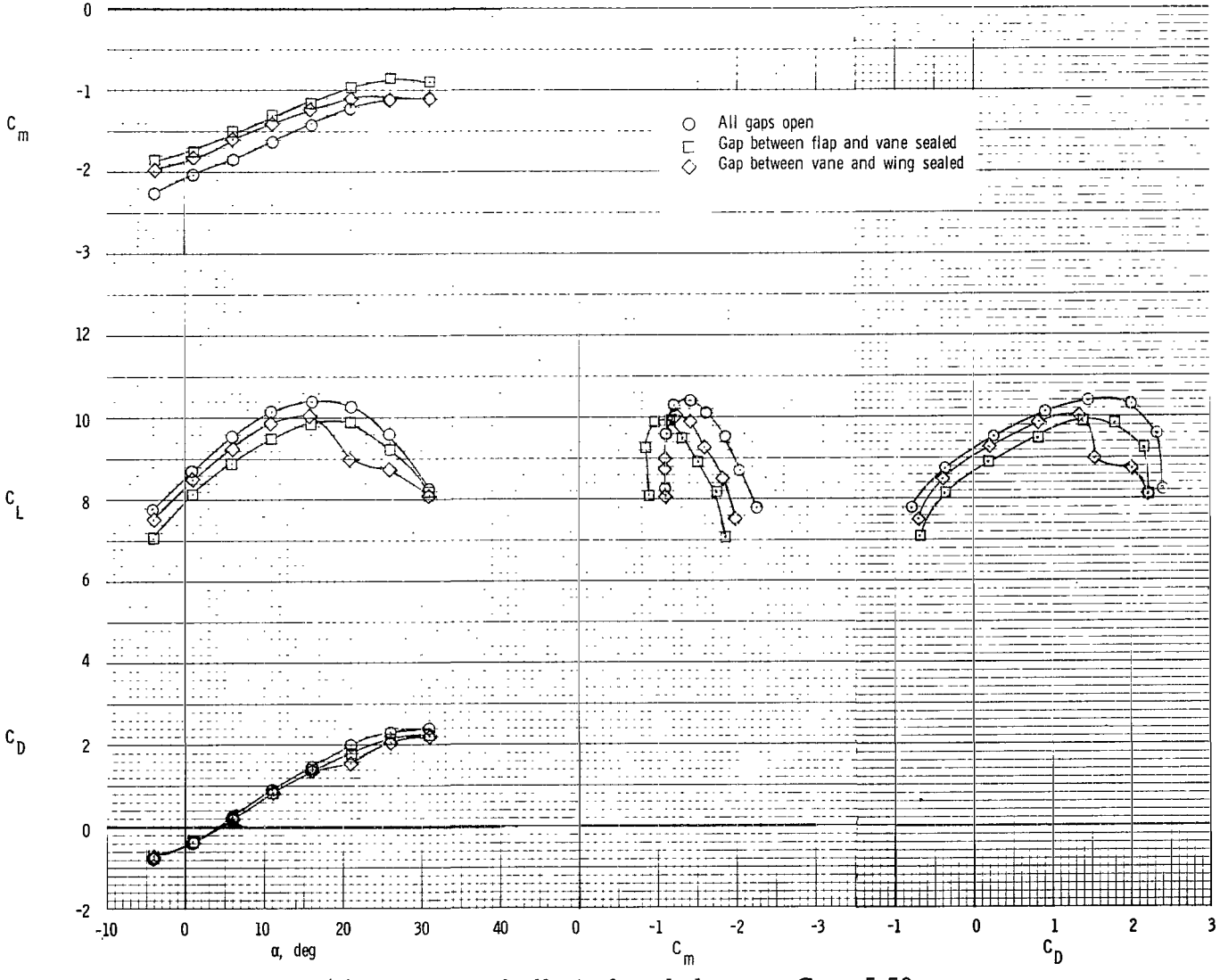

(c) Summary of effect of sealed gaps. C_μ = 5.50.

Figure 31.- Concluded.

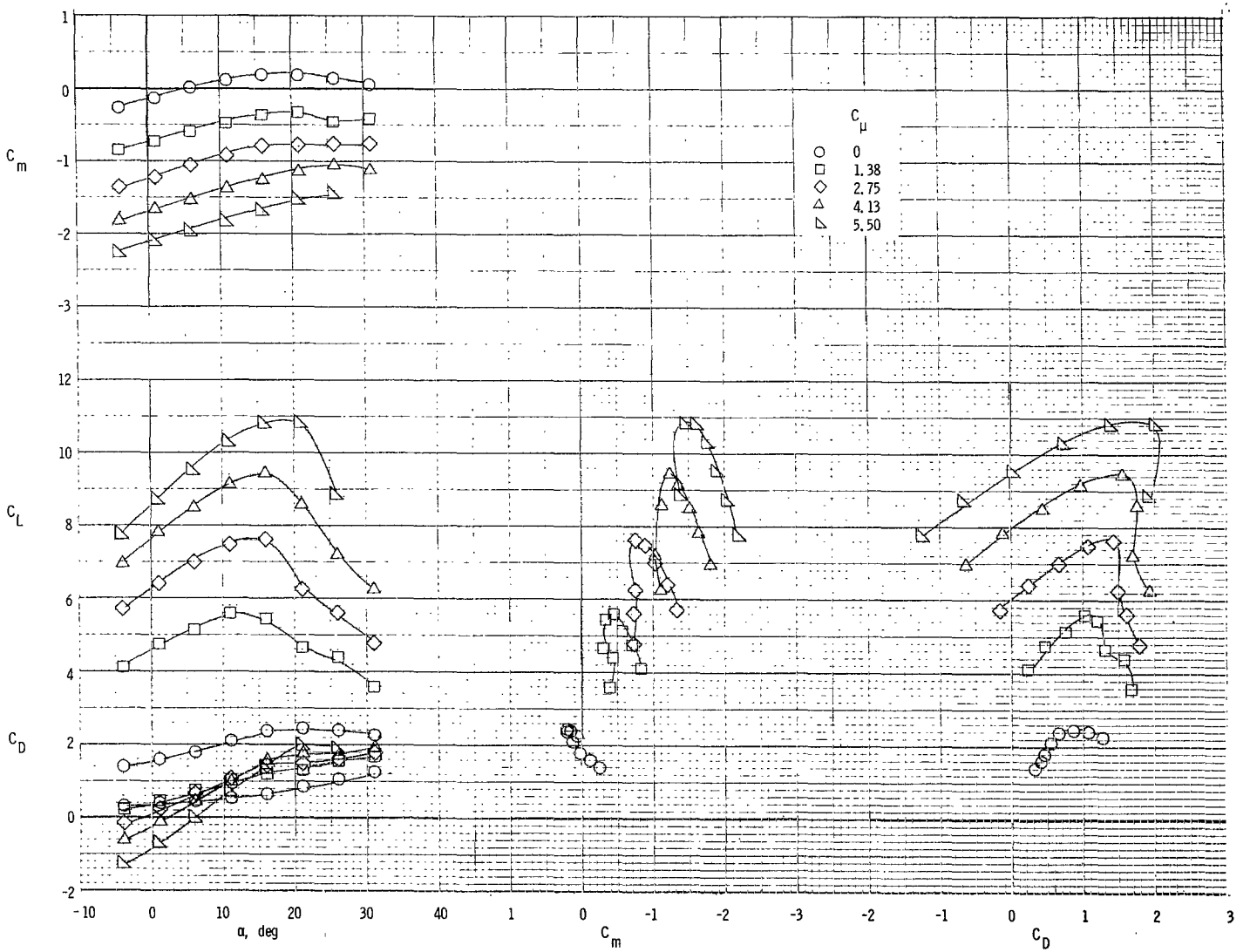

(a) Exhaust deflectors off.

Figure 32.- Longitudinal aerodynamic characteristics of model with engine position 1 and 0.04c flap gap. $\delta_f = 55^o$; original leading-edge slat.

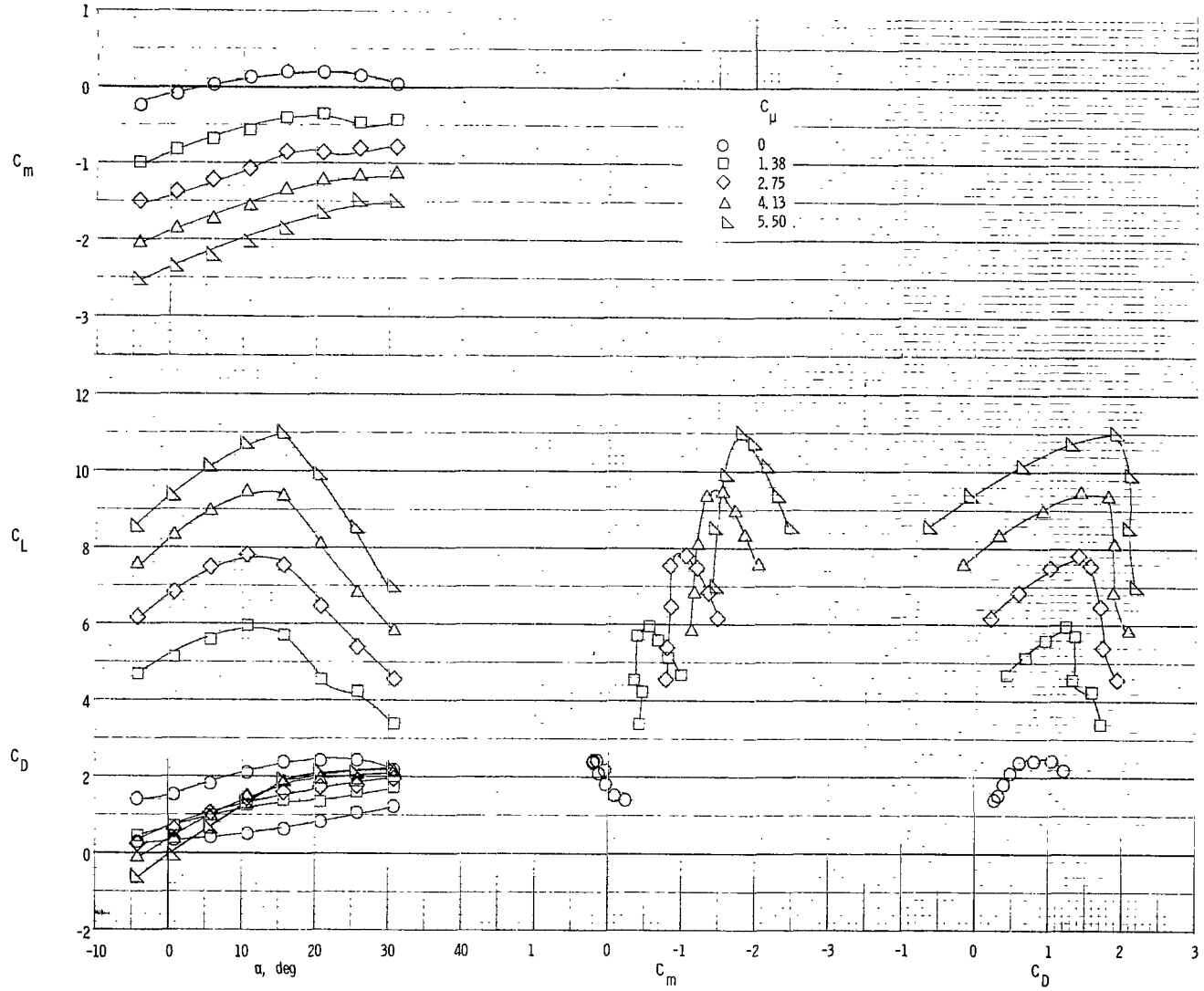

(b) Exhaust deflectors on.

Figure 32.- Concluded.

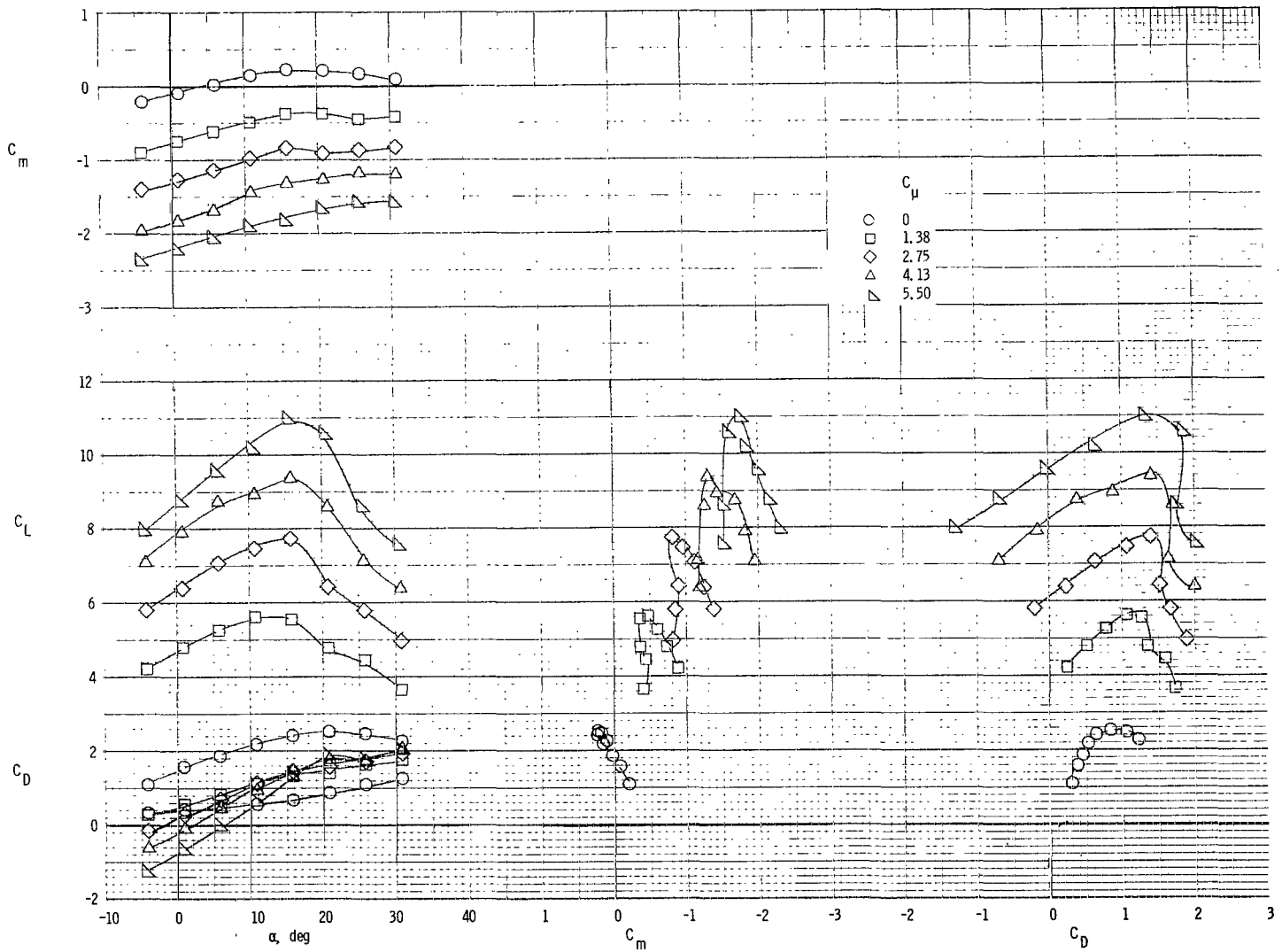

(a) Exhaust deflectors off.

Figure 33.- Longitudinal aerodynamic characteristics of model with engine position 1 and 0.06c flap gap. $\delta_f = 55^o$; original leading-edge slat.

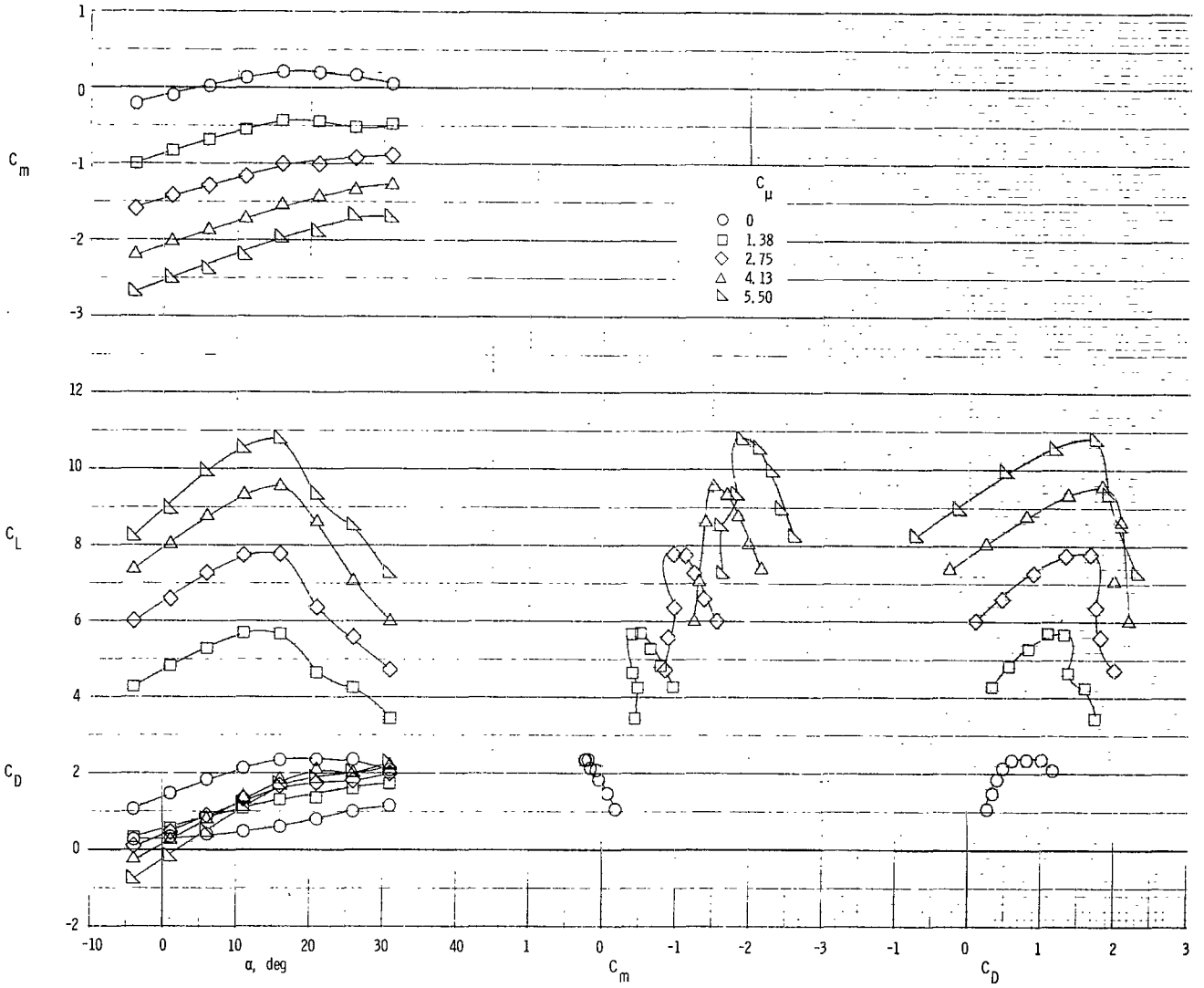

(b) Exhaust deflectors on.

Figure 33.- Concluded.

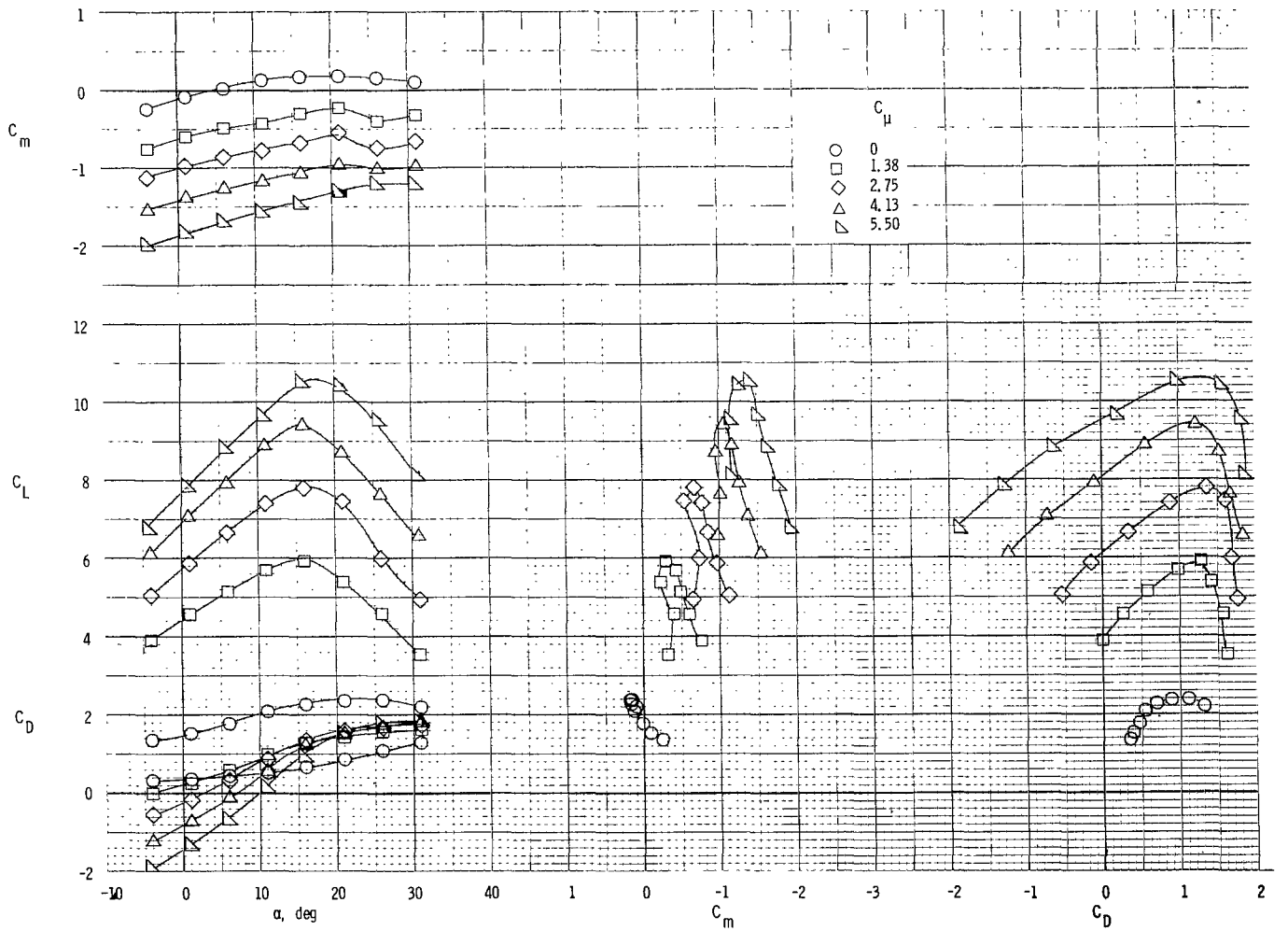

(a) Exhaust deflectors off.

Figure 34.- Longitudinal aerodynamic characteristics of model with engine position 4 and 0.04c flap gap. $\delta_f = 55^o$; original leading-edge slat.

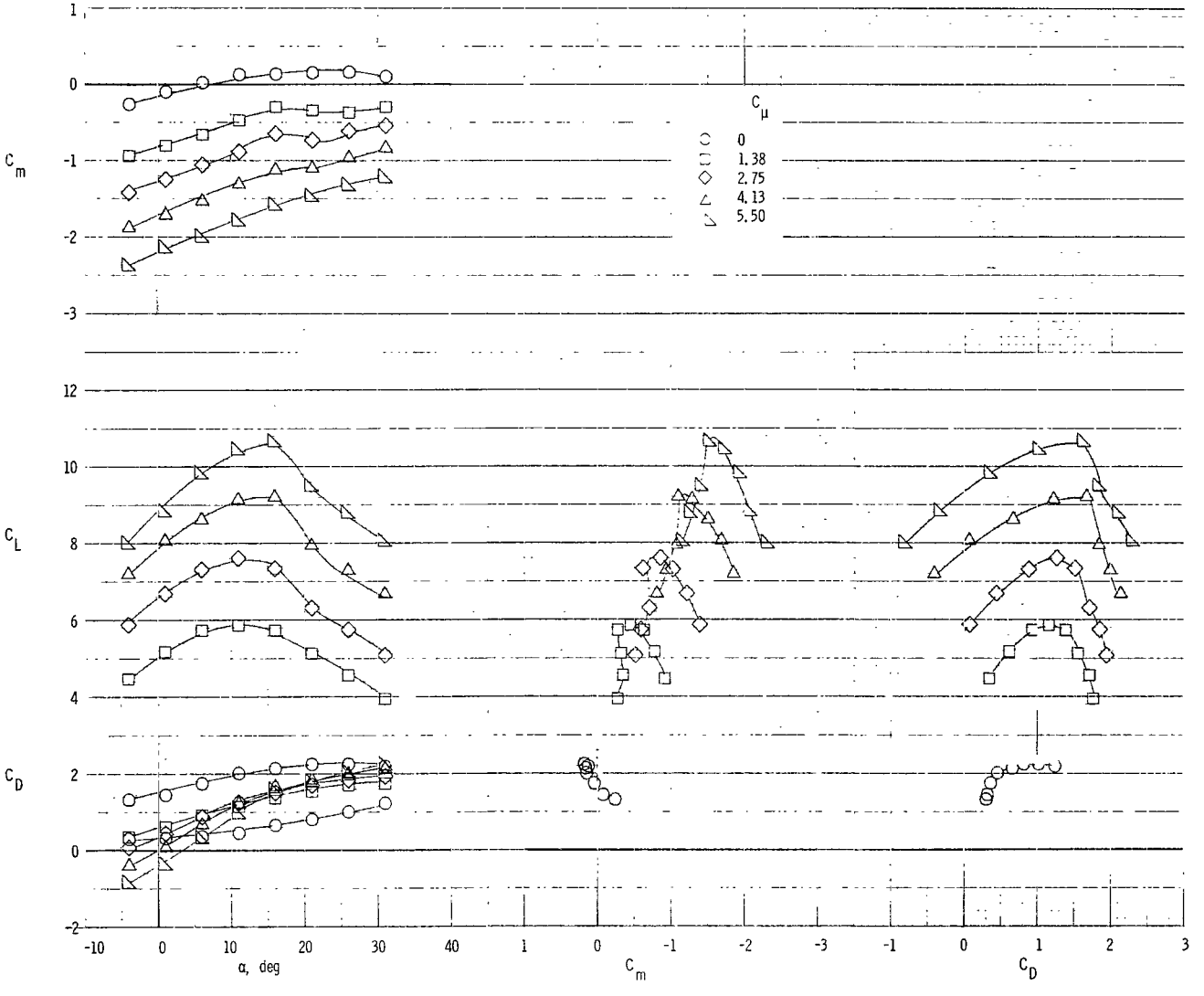

(b) Exhaust deflectors on.

Figure 34.- Concluded.

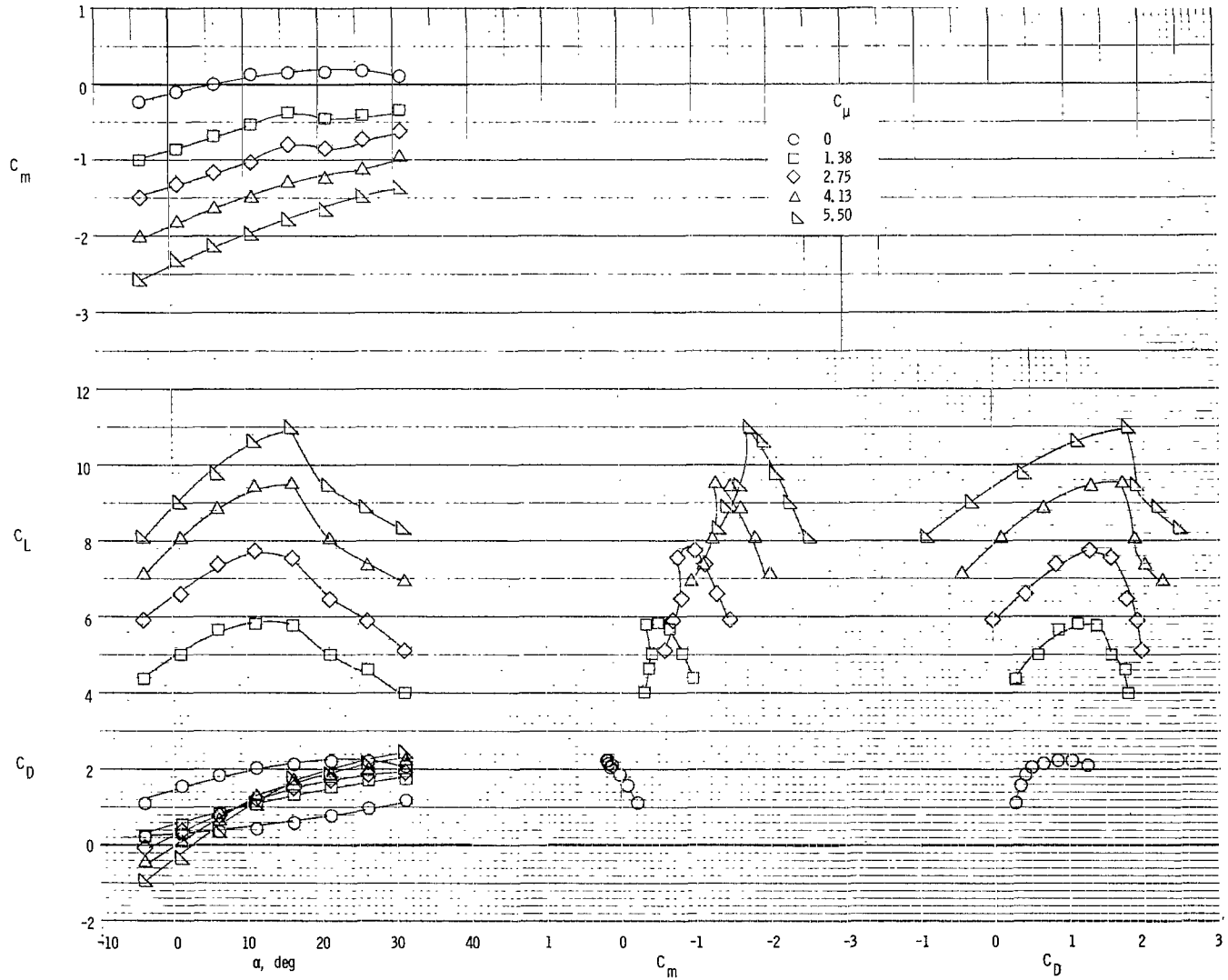

Figure 35.- Longitudinal aerodynamic characteristics of model with engine position 4 and 0.06c flap gap. $\delta_f = 55^o$; deflectors on; original leading-edge slat.

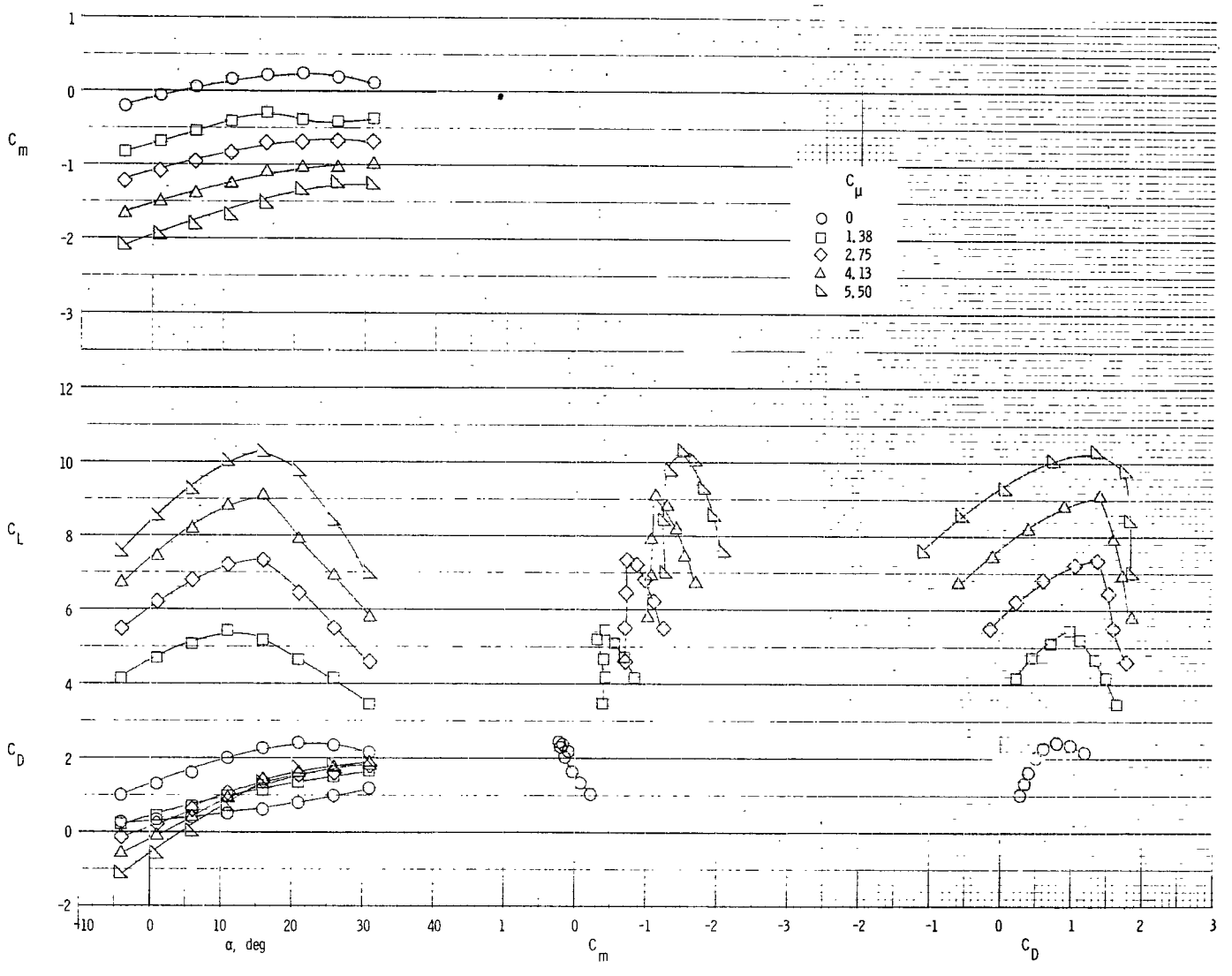

(a) Exhaust deflectors off.

Figure 36.- Longitudinal aerodynamic characteristics of model with engine position 1 and 0.04c vane gap. $\delta_f = 55^o$; original leading-edge slat.

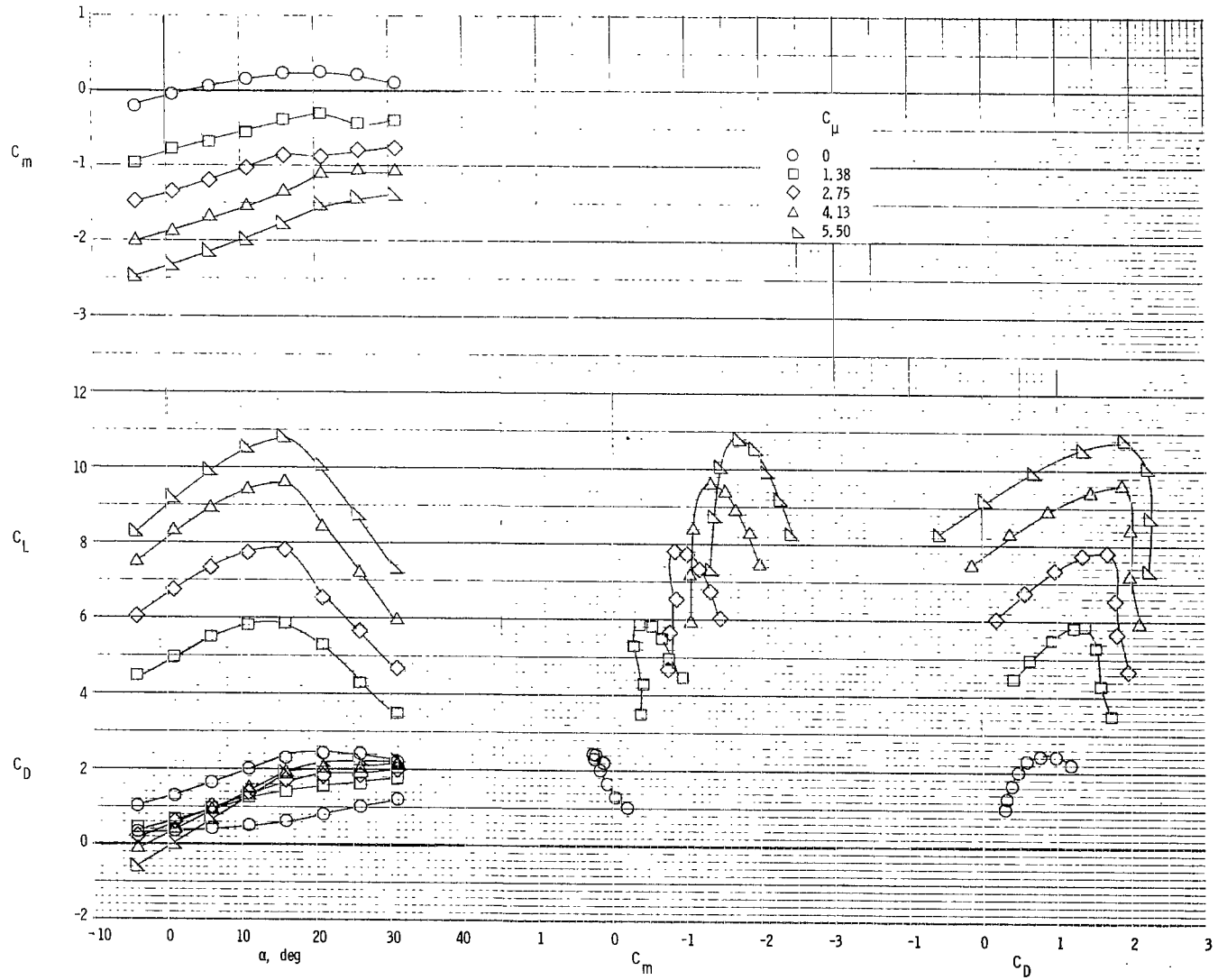

(b) Exhaust deflectors on.

Figure 36.- Concluded.

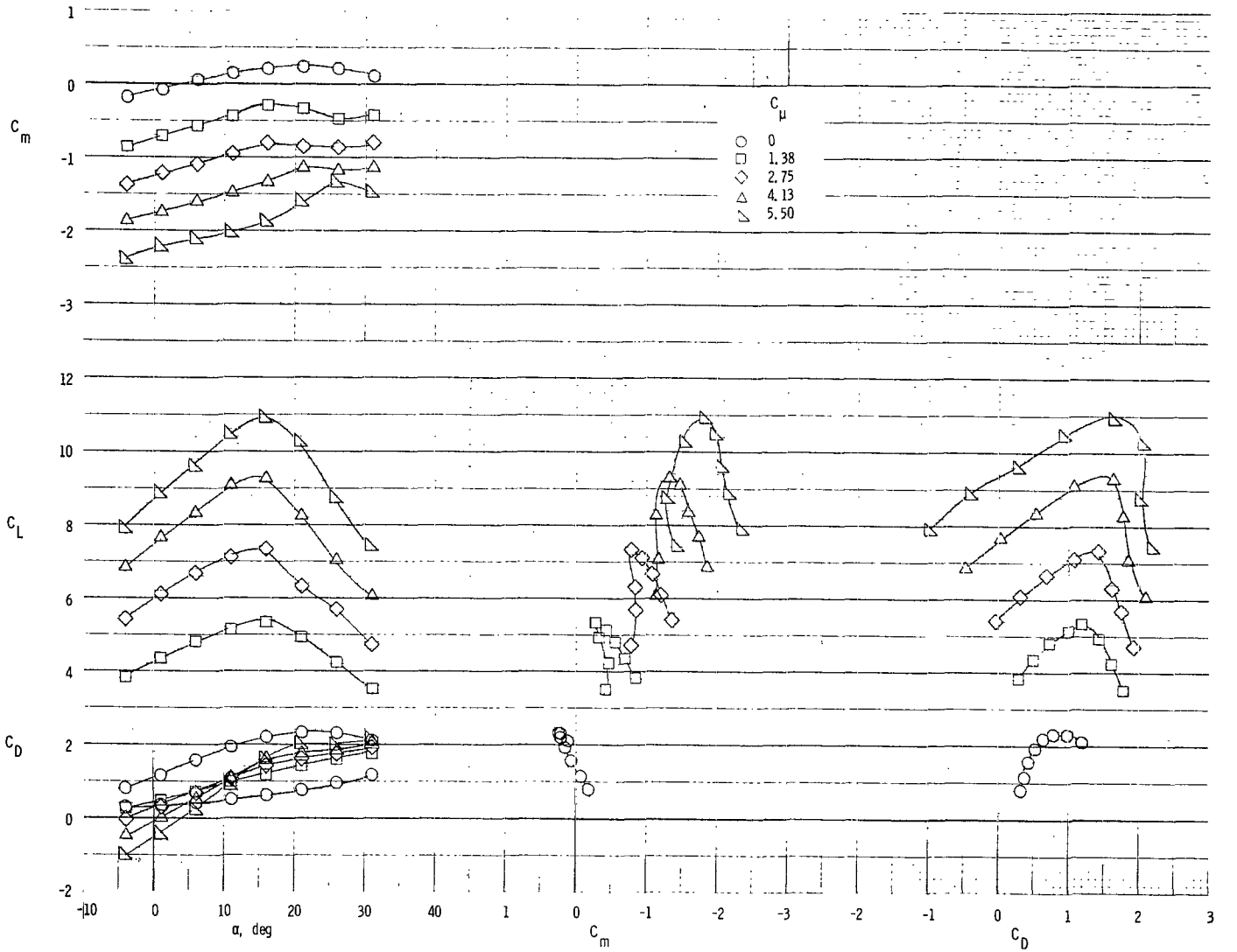

(a) Exhaust deflectors off.

Figure 37.- Longitudinal aerodynamic characteristics of model with engine position 1 and 0.06c vane gap. $\delta_f = 55^o$; original leading-edge slat.

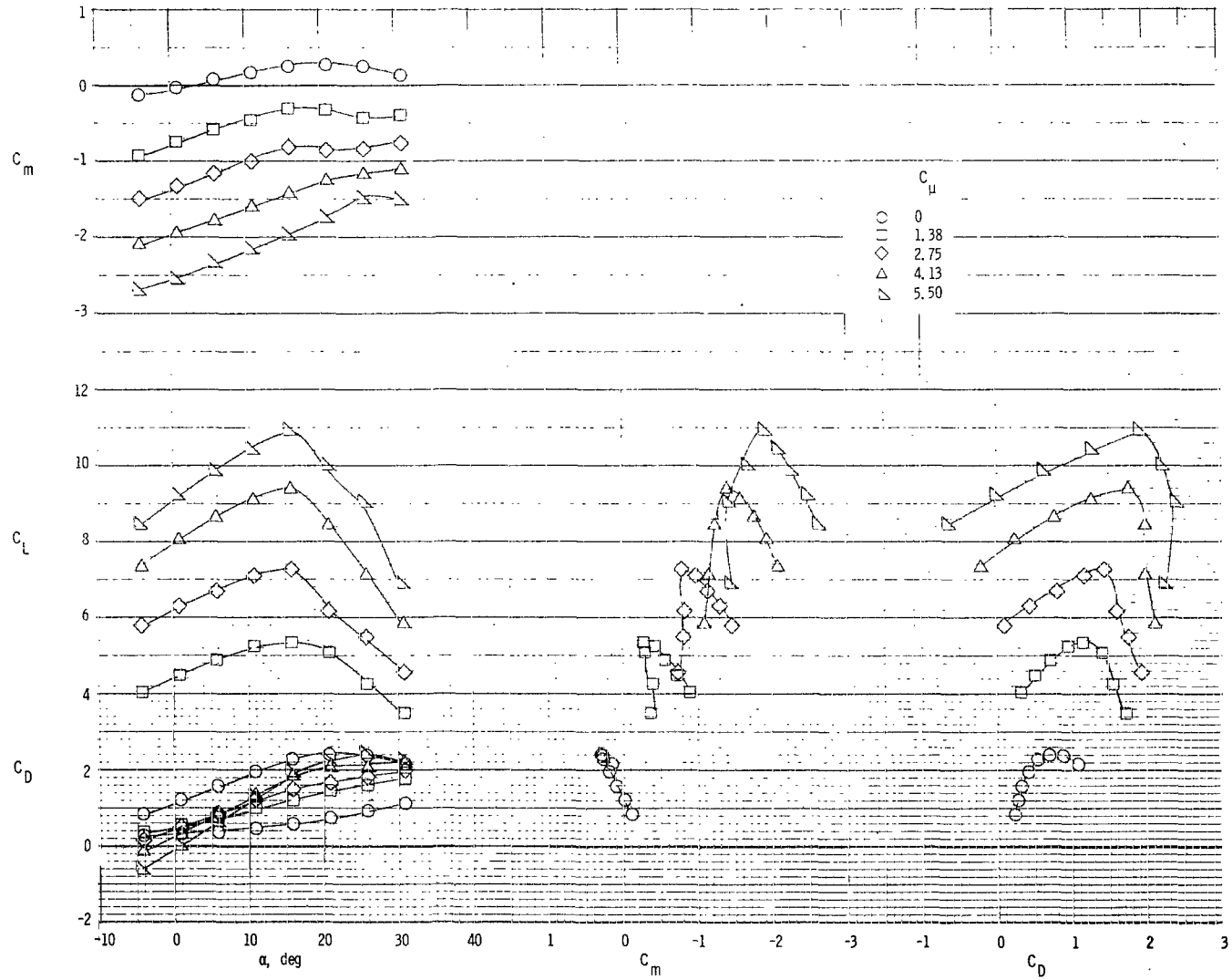

(b) Exhaust deflectors on.

Figure 37.- Concluded.

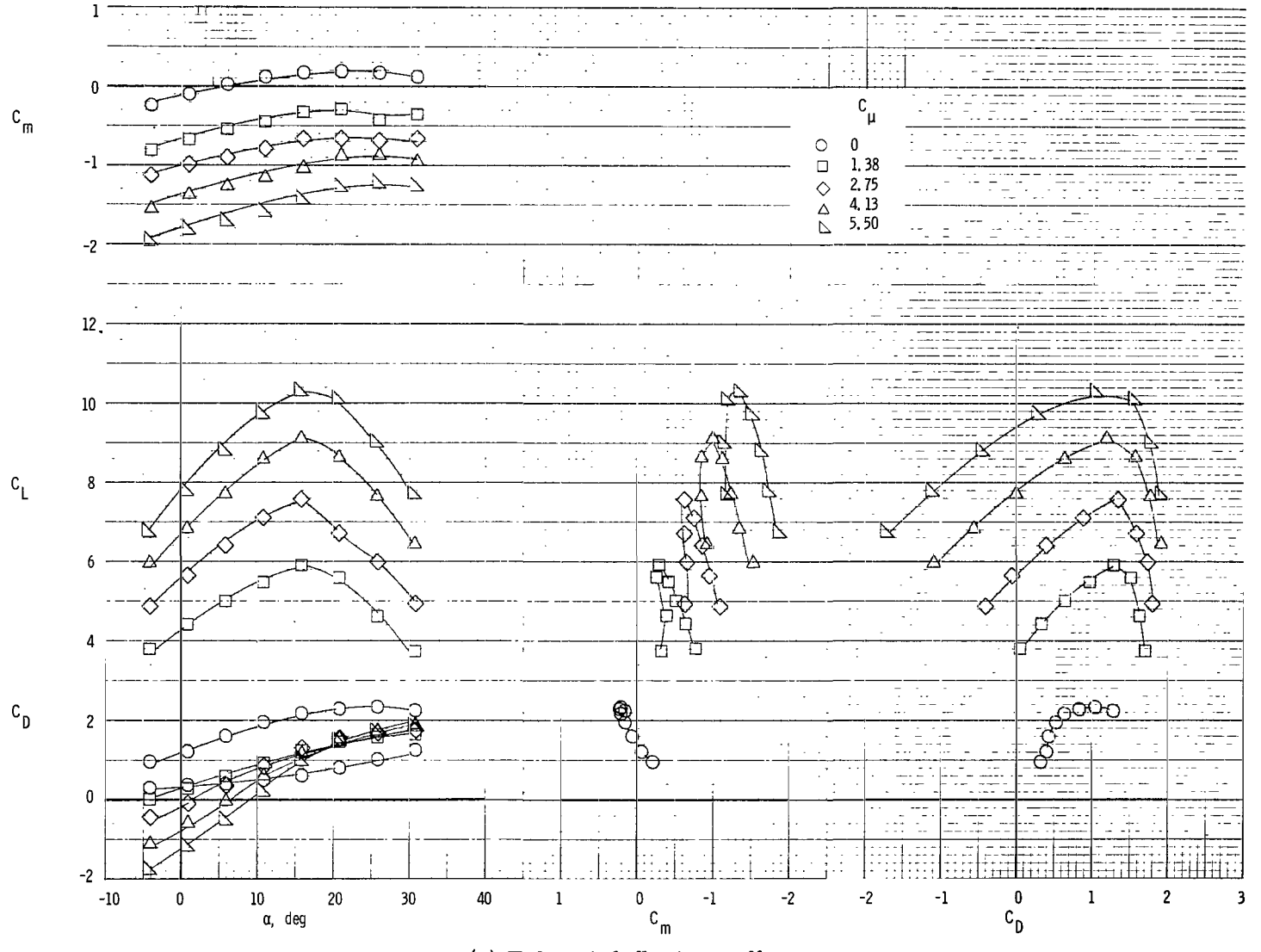

(a) Exhaust deflectors off.

Figure 38.- Longitudinal aerodynamic characteristics of model with engine position 4 and 0.04c vane gap. $\delta_f = 55^o$; original leading-edge slat.

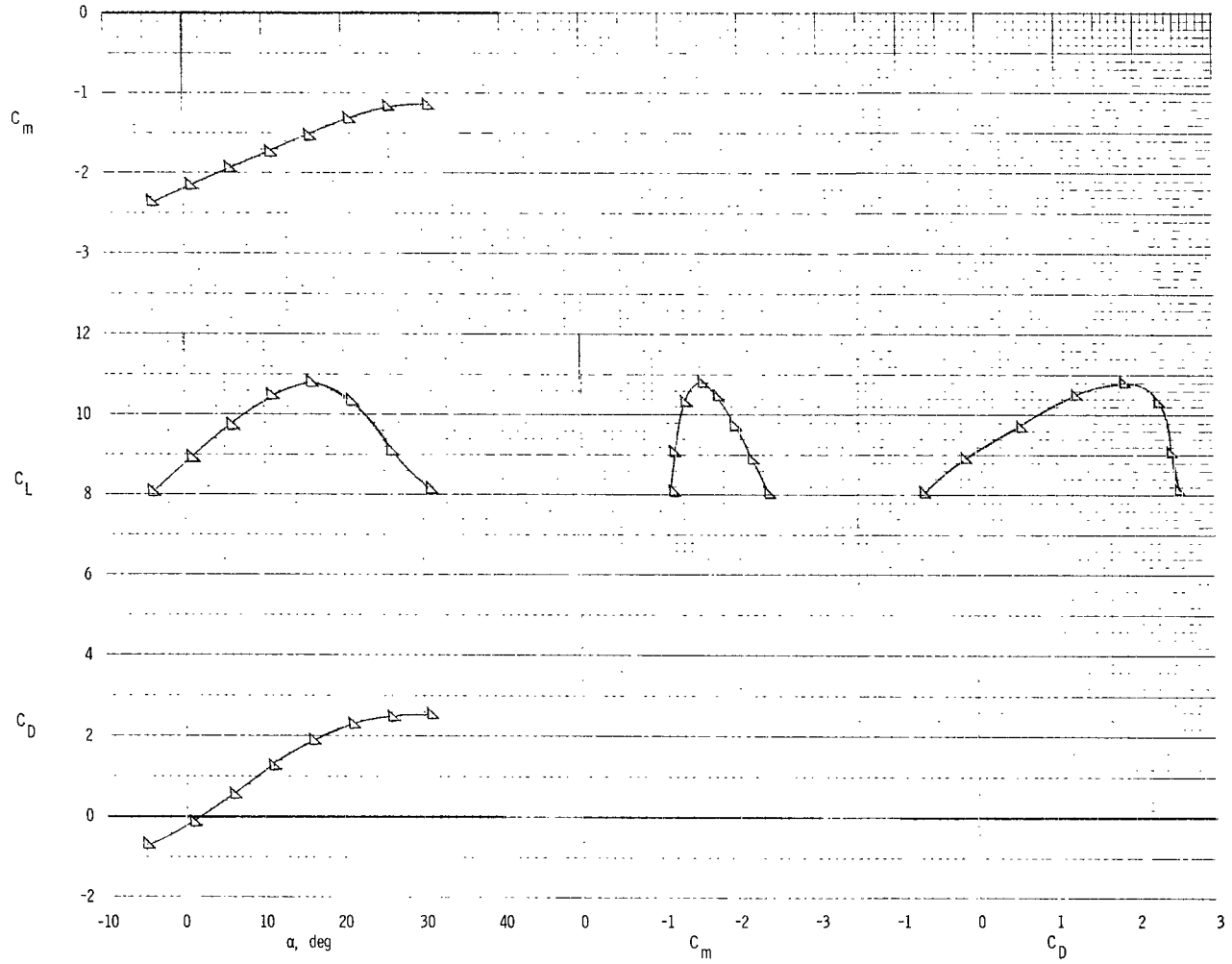

(b) Exhaust deflectors on. $\left(C_\mu = 5.5 \quad \text{only.}\right)$

Figure 38.- Concluded.

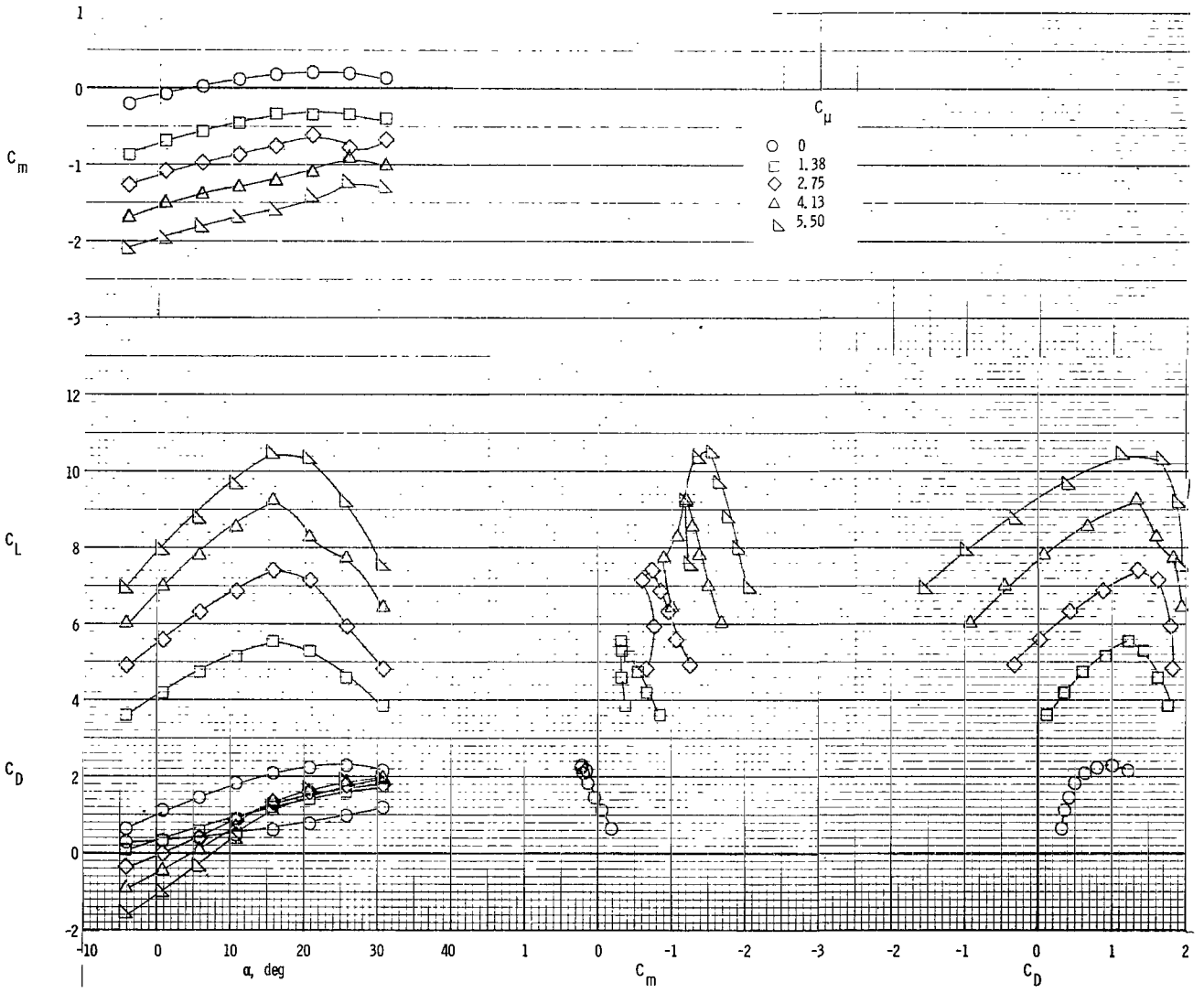

(a) Exhaust deflectors off.

Figure 39.- Longitudinal aerodynamic characteristics of model with engine position 4 and 0.06c vane gap. $\delta_f = 55^o$; original leading-edge slat.

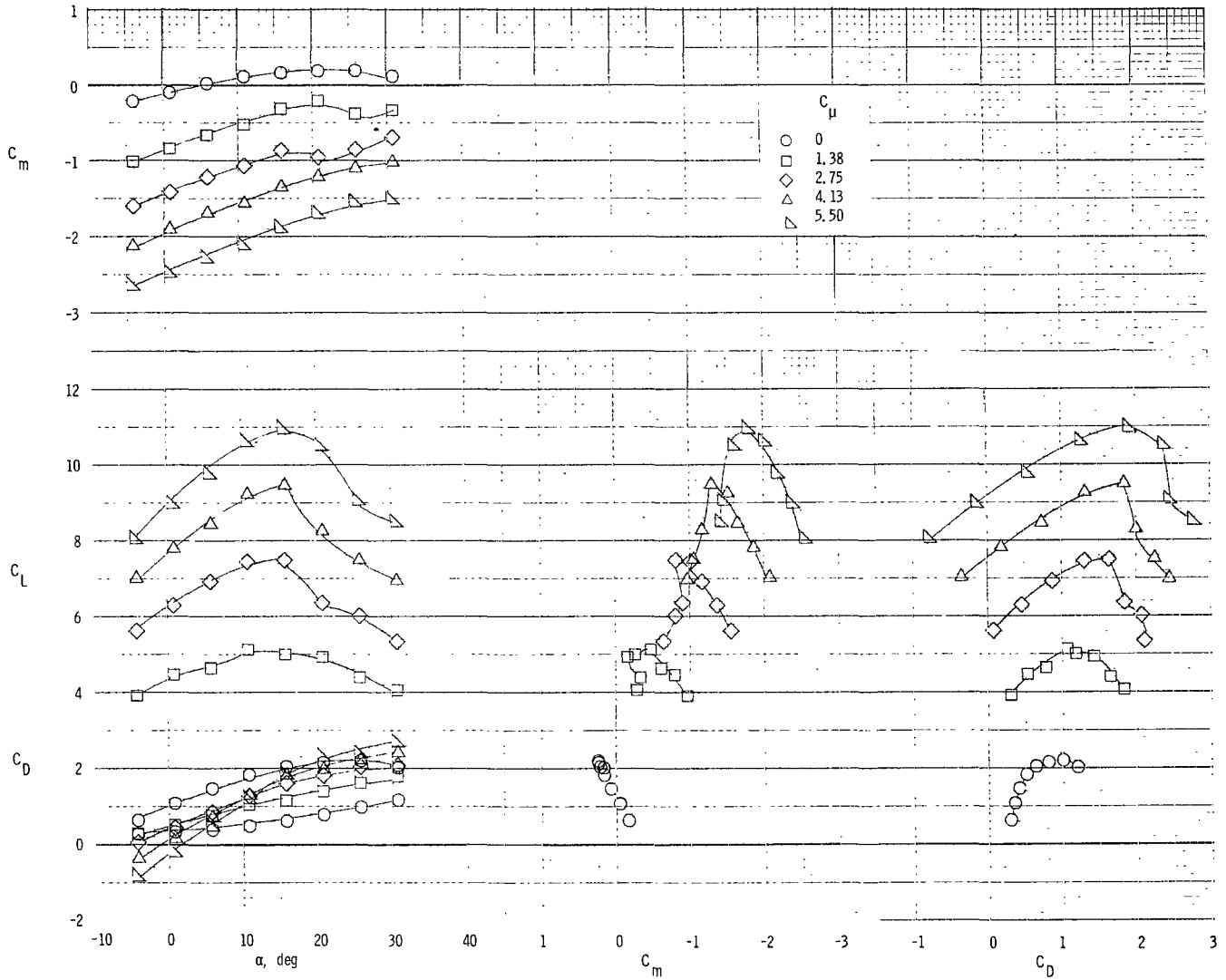

(b) Exhaust deflectors on.

Figure 39.- Concluded.

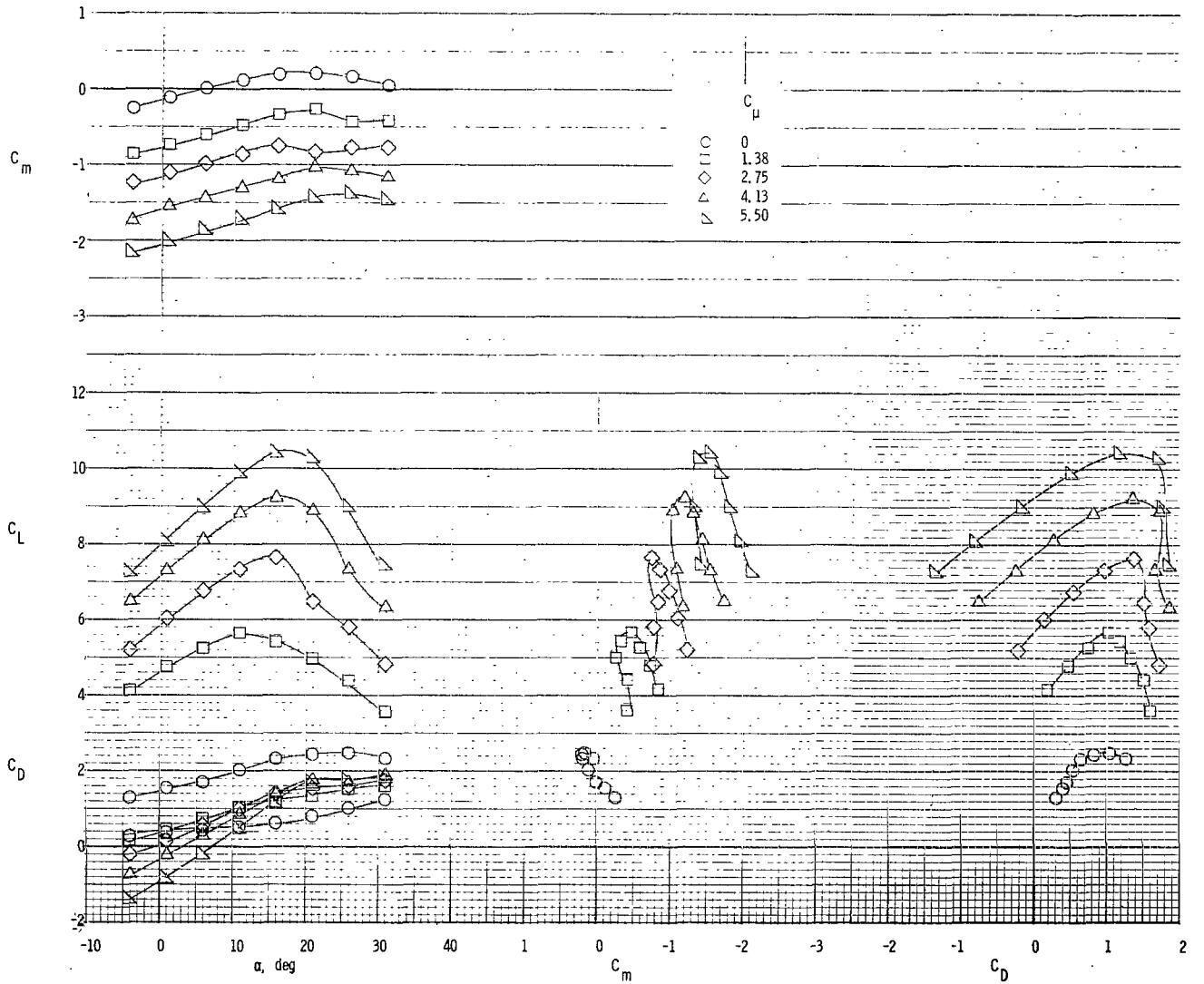

(a) Exhaust deflectors off.

Figure 40.- Longitudinal aerodynamic characteristics of model with engine position 1 and -0.02c flap overlap. $\delta_f = 55^o$; original leading-edge slat.

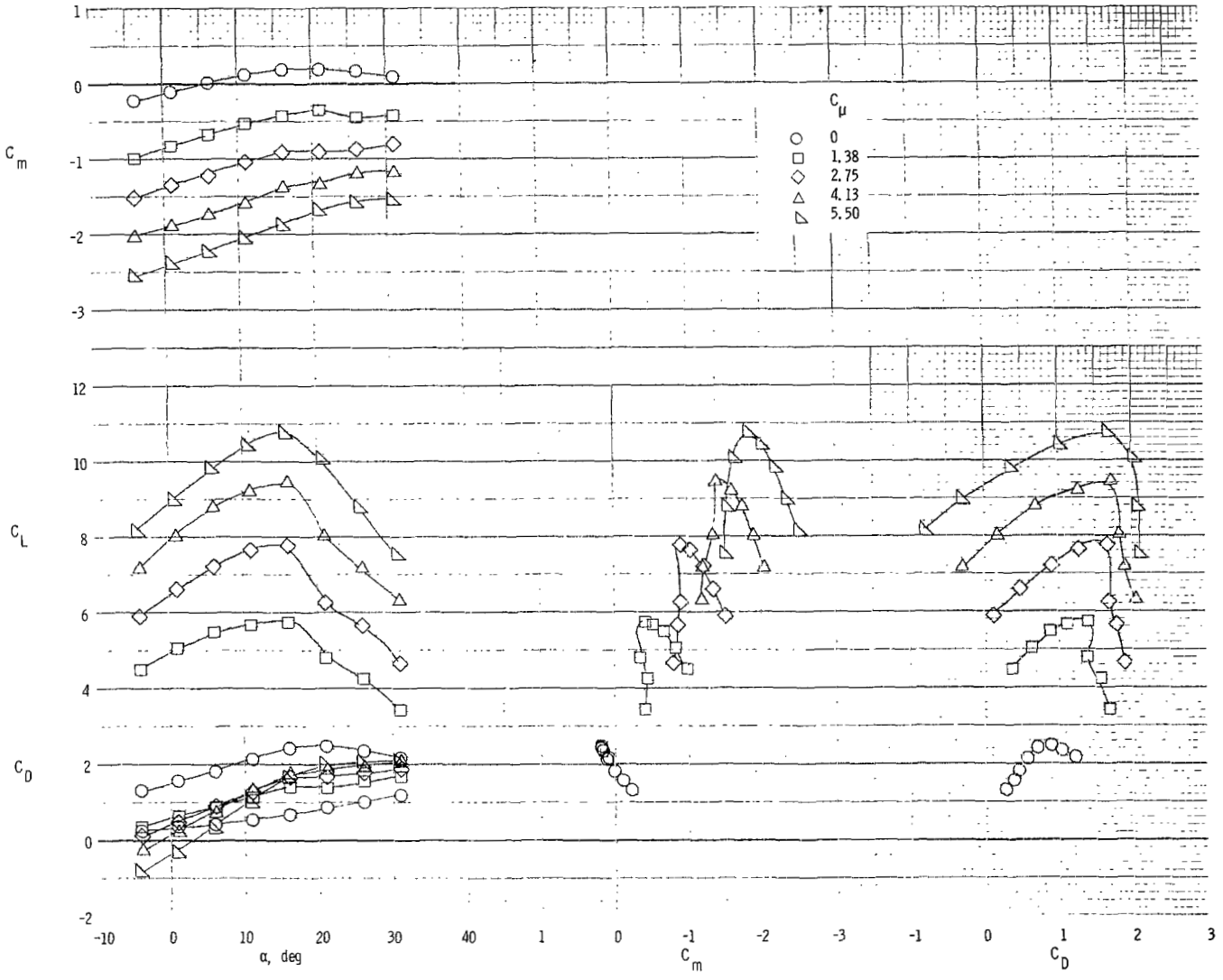

(b) Exhaust deflectors on.

Figure 40.- Concluded.

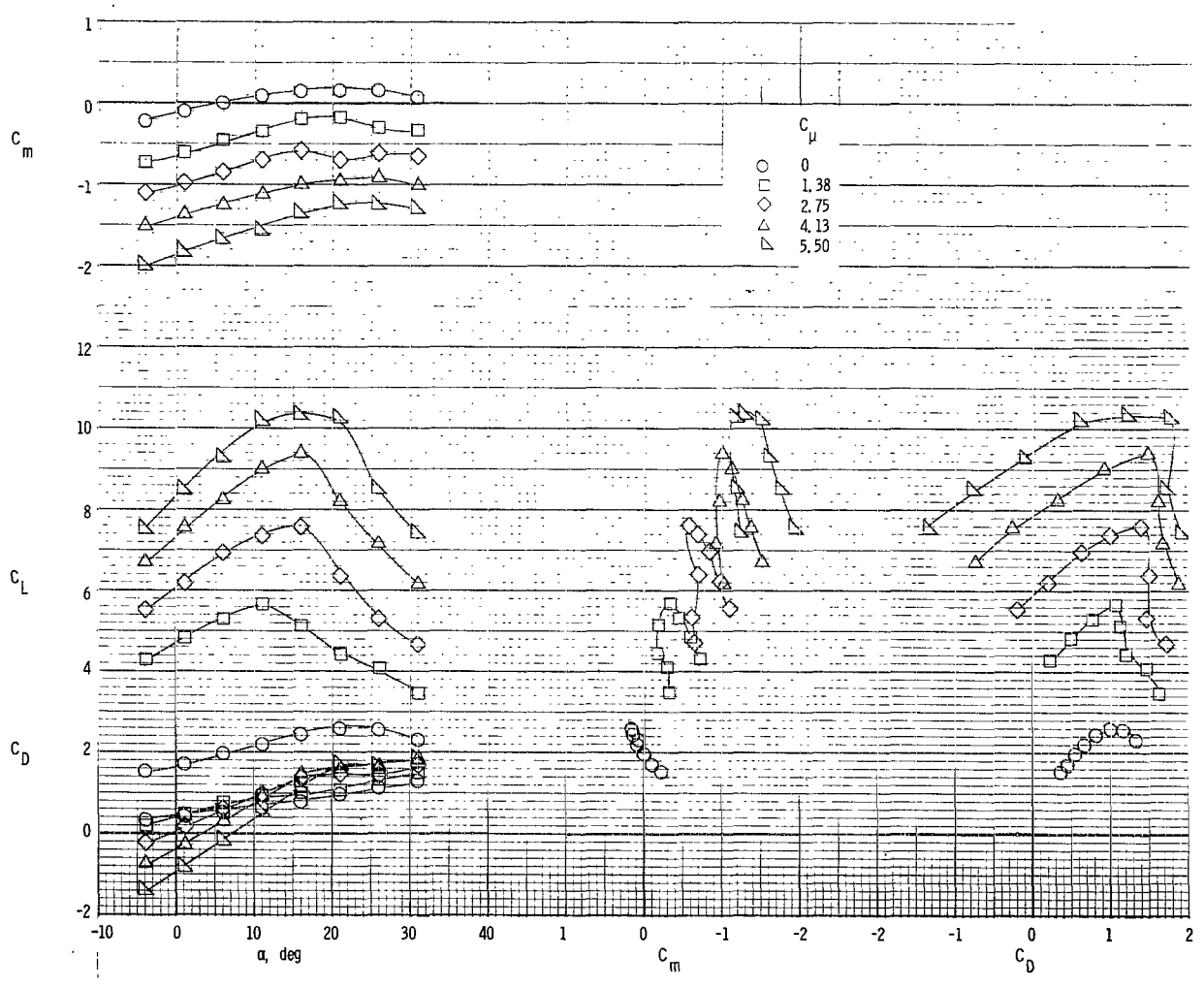

(a) Exhaust deflectors off.

Figure 41.- Longitudinal aerodynamic characteristics of model with engine position 1 and 0.02c flap overlap. $\delta_f = 55^o$; original leading-edge slat.

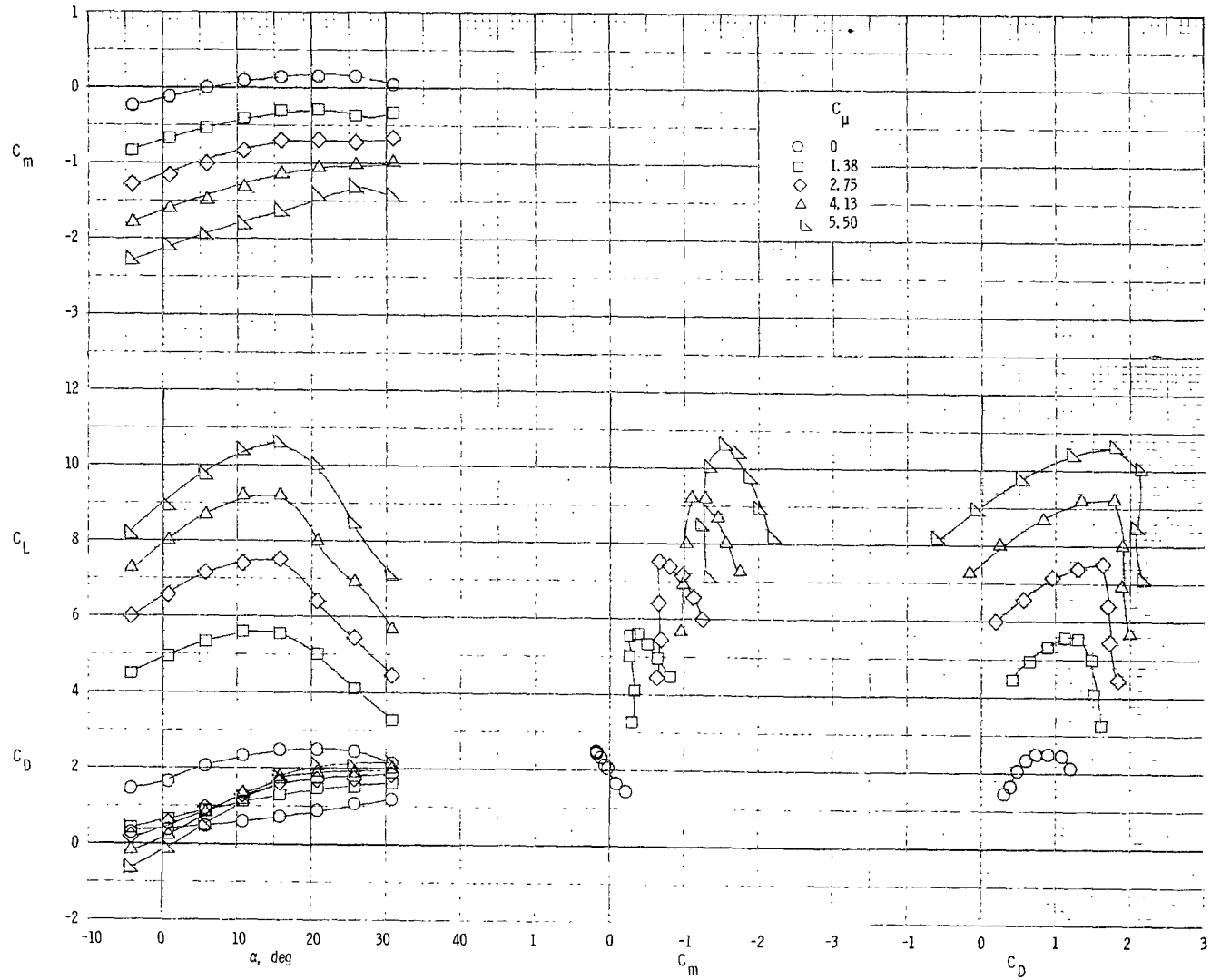

(b) Exhaust deflectors on.

Figure 41.- Concluded.

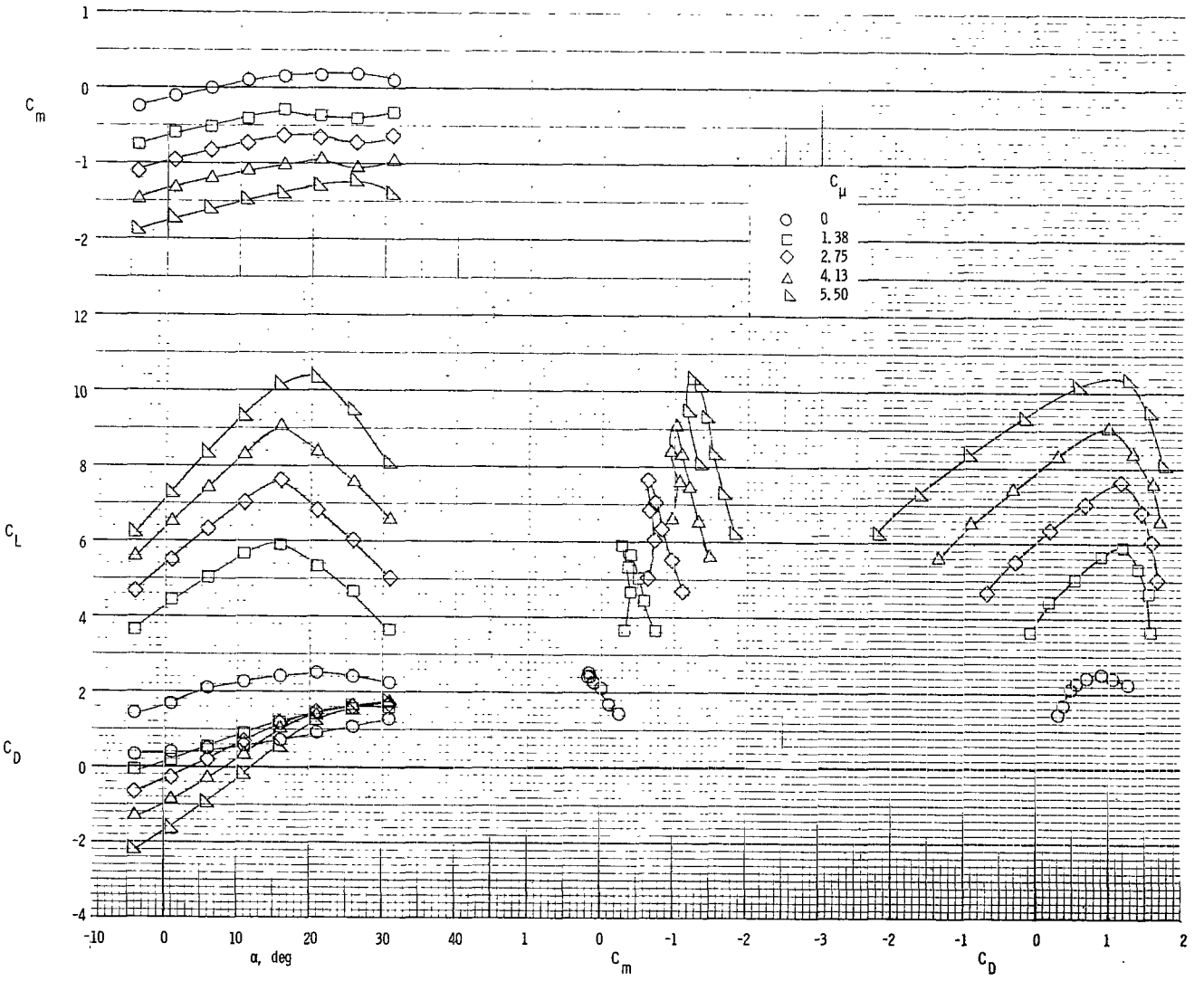

(a) Exhaust deflectors off.

Figure 42.- Longitudinal aerodynamic characteristics of model with engine position 4 and -0.02c flap overlap. $\delta_f = 55^o$; original leading-edge slat.

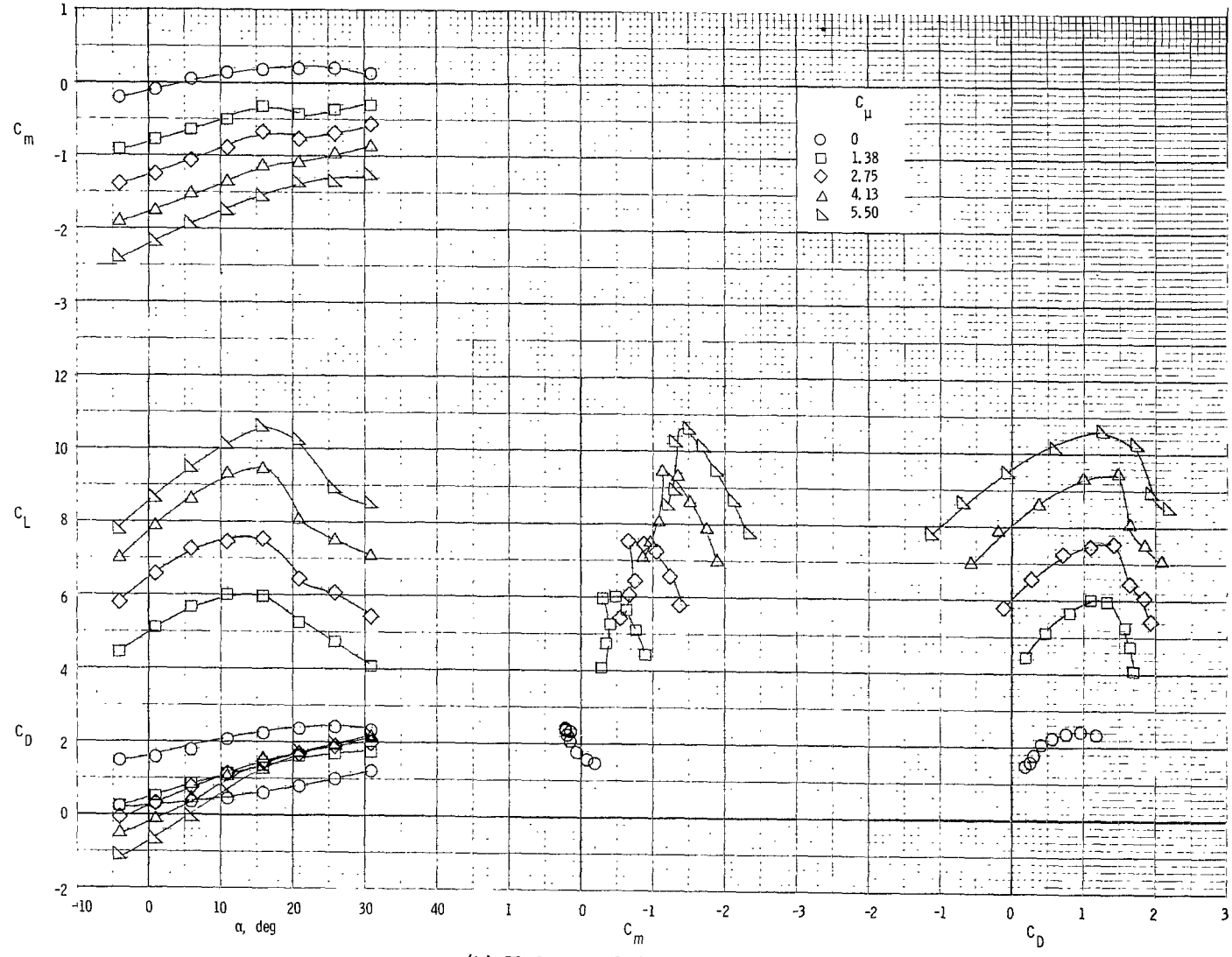

(b) Exhaust deflectors on.

Figure 42.- Concluded.

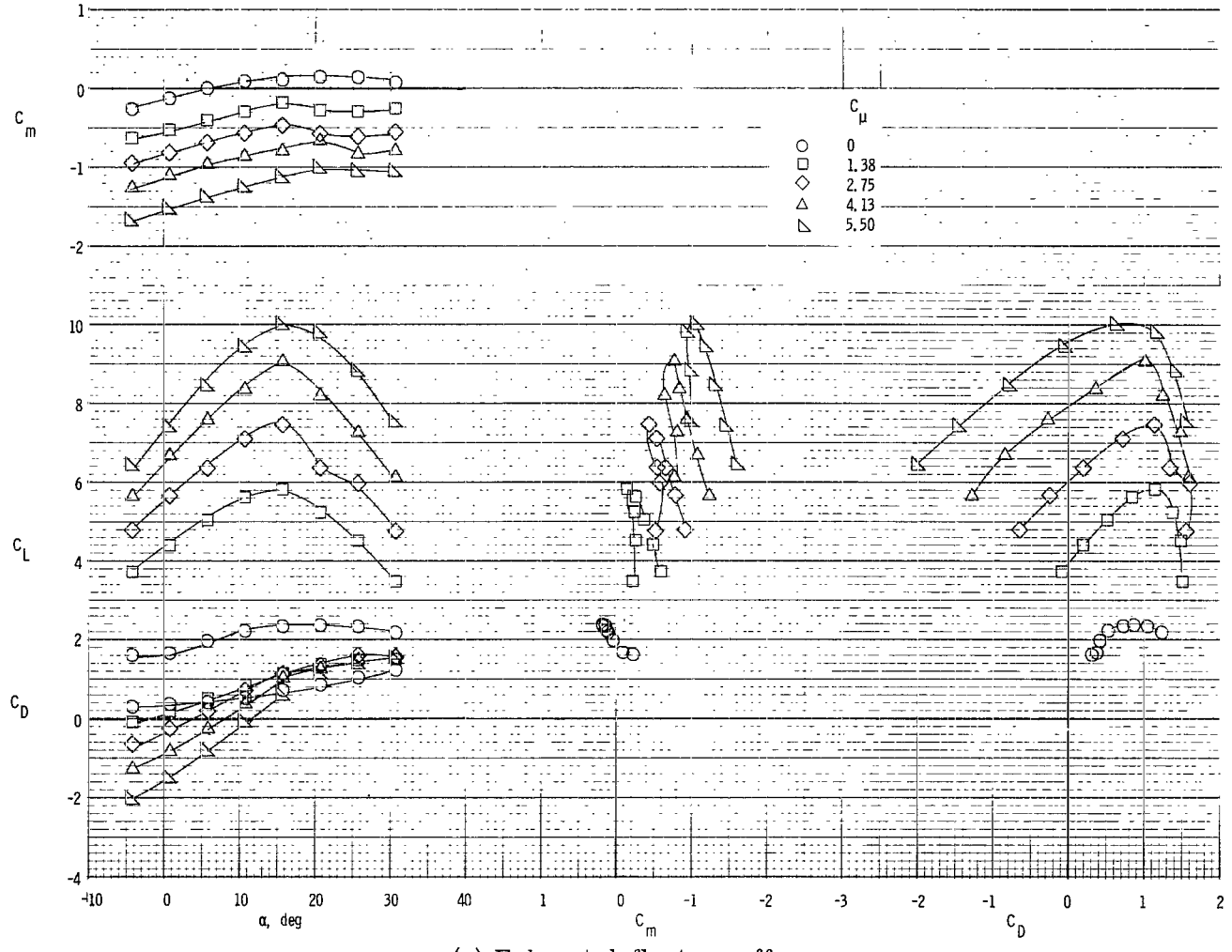

(a) Exhaust deflectors off.

Figure 43.- Longitudinal aerodynamic characteristics of model with engine position 4 and 0.02c flap overlap. $\delta_f = 55^o$; original leading-edge slat.

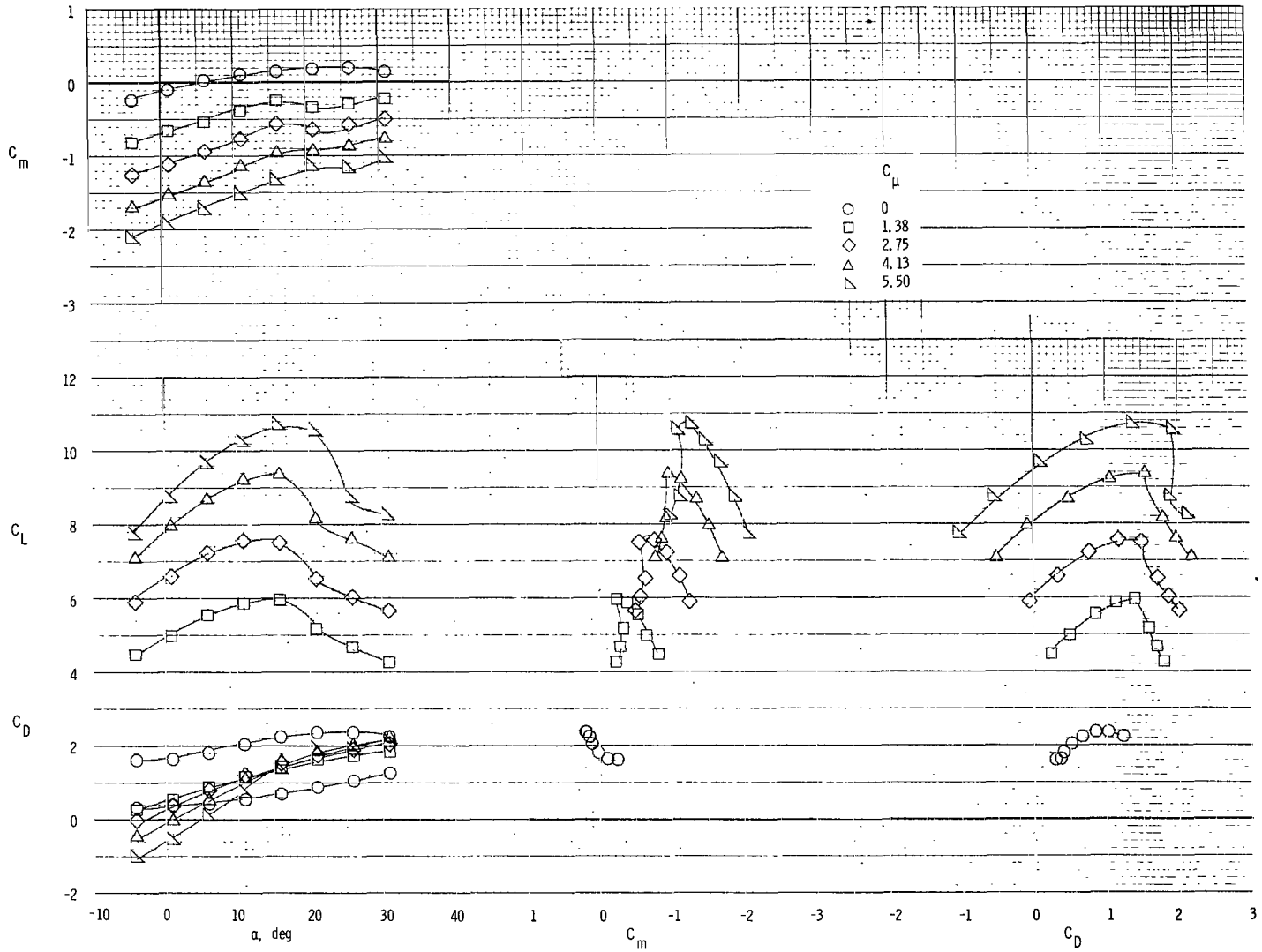

(b) Exhaust deflectors on.

Figure 43.- Concluded.

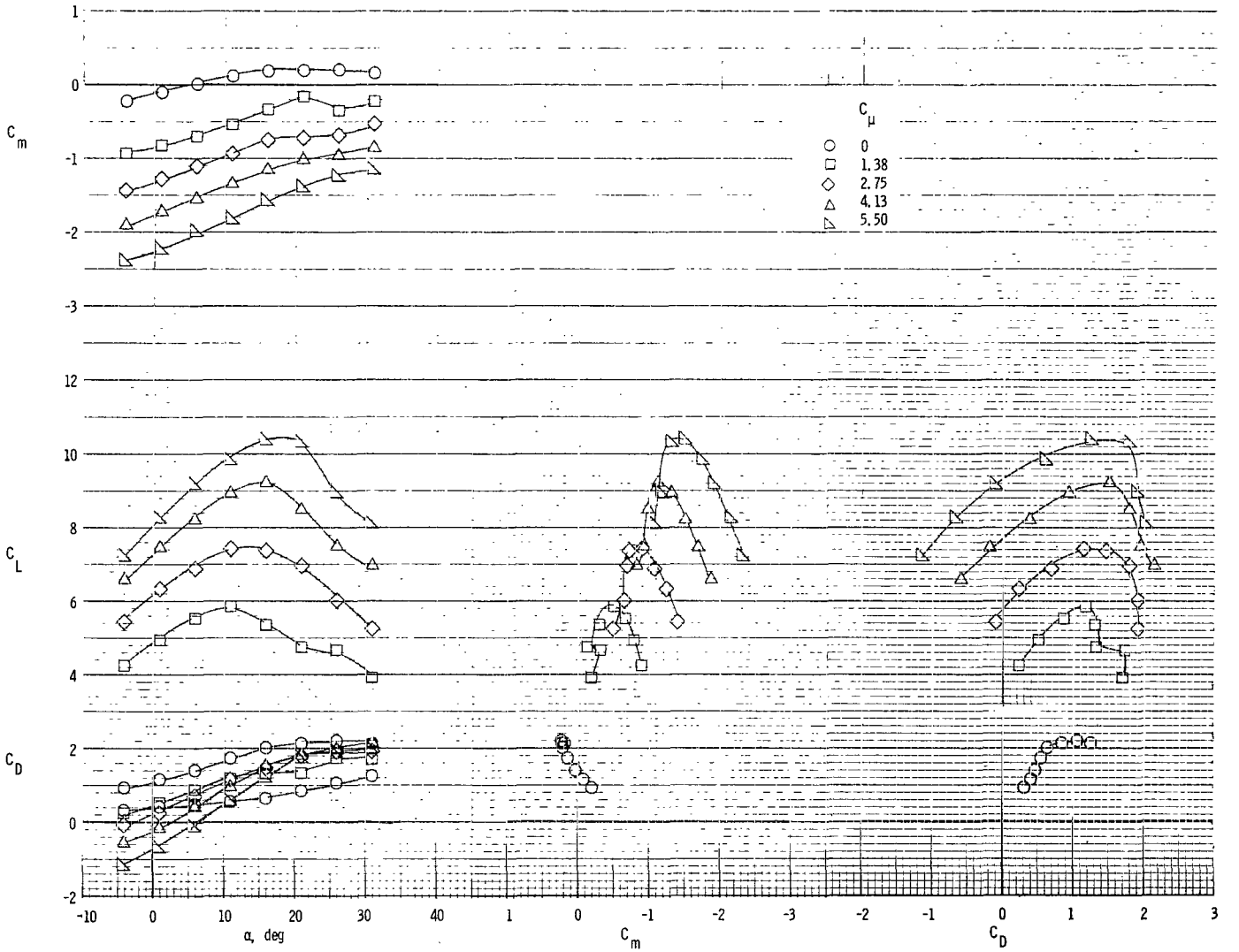

Figure 44.- Longitudinal aerodynamic characteristics of model with engine position 4 and -0.02c vane overlap. $\delta_f = 55^o$; deflectors on; original leading-edge slat.

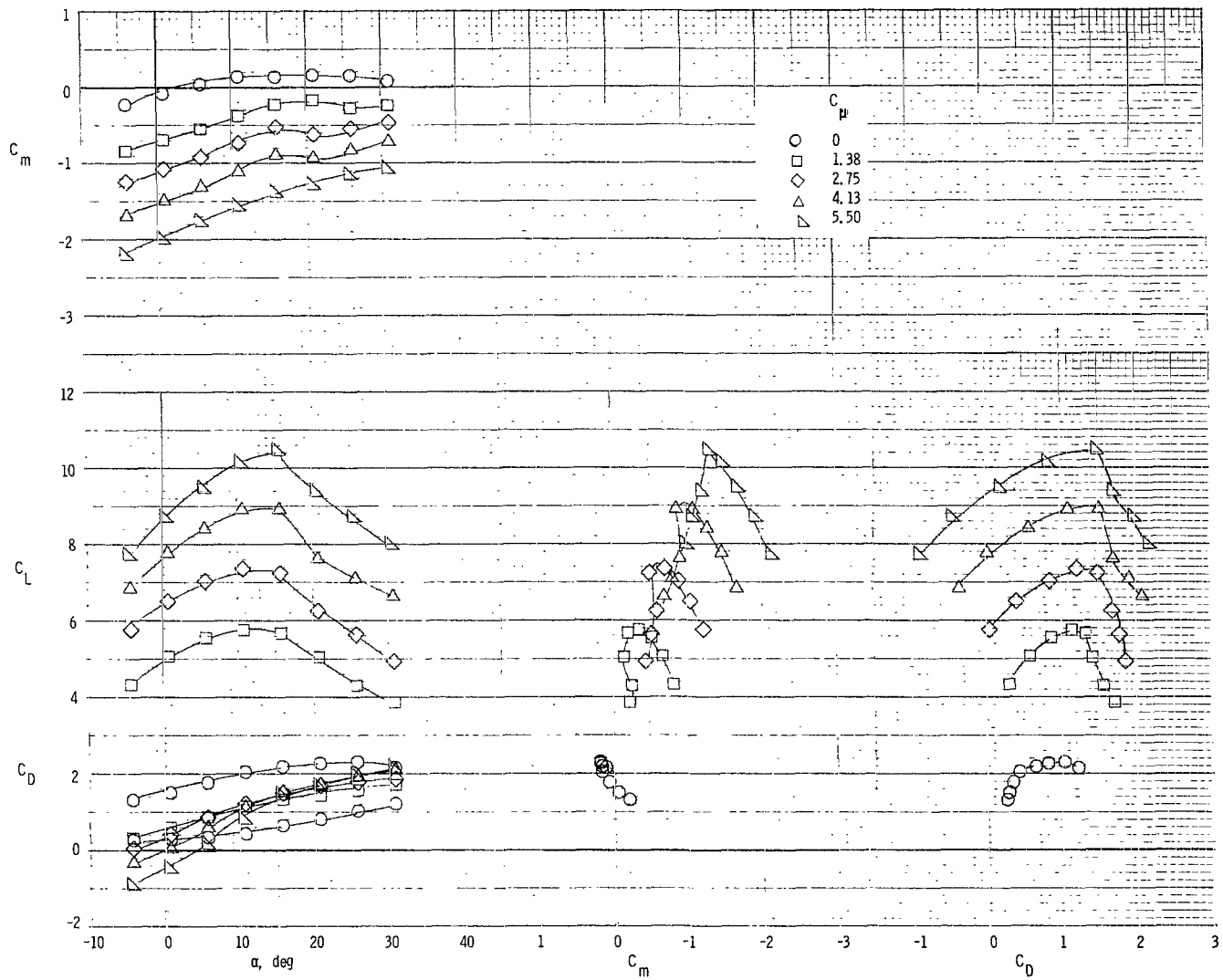

Figure 45.- Longitudinal aerodynamic characteristics of model with engine position 4 and 0.02c vane overlap. $\delta_f = 55^o$; deflectors on; original leading-edge slat.

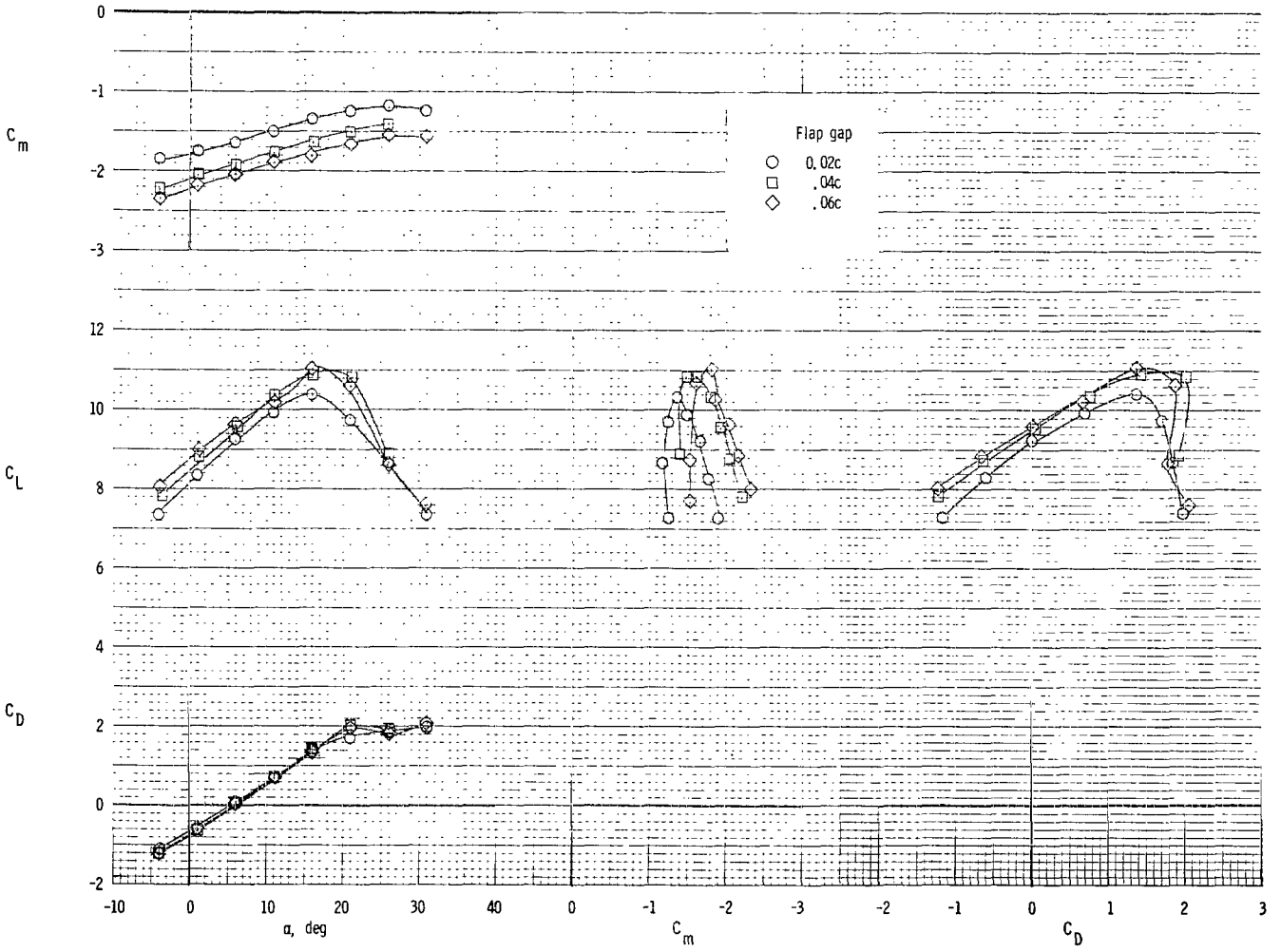

(a) Exhaust deflectors off.

Figure 46.- Summary of flap gap effect for engine position 1. $\delta_f = 55^o$; original leading-edge slat; $C_\mu = 5.50$.

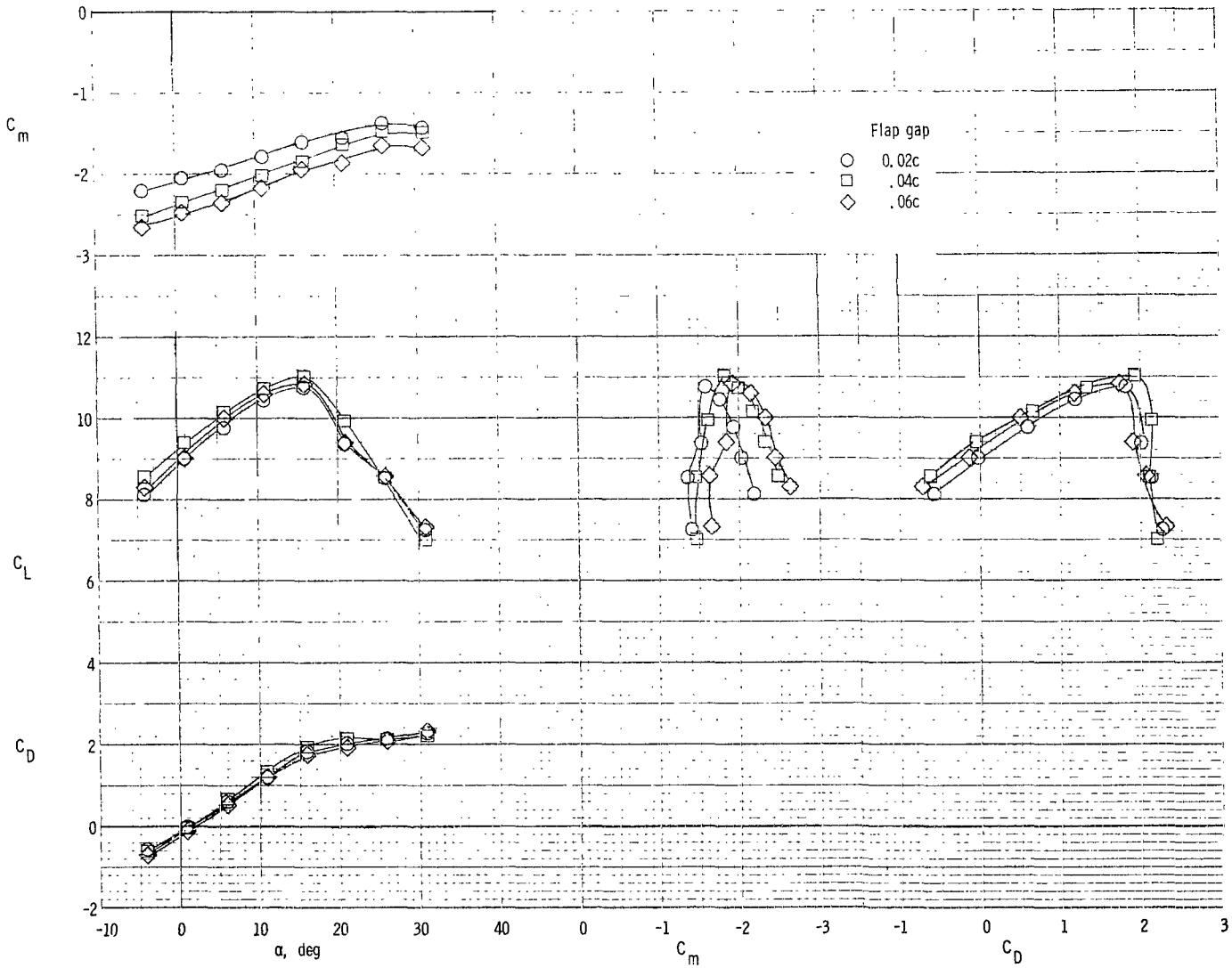

(b) Exhaust deflectors on.

Figure 46.- Concluded.

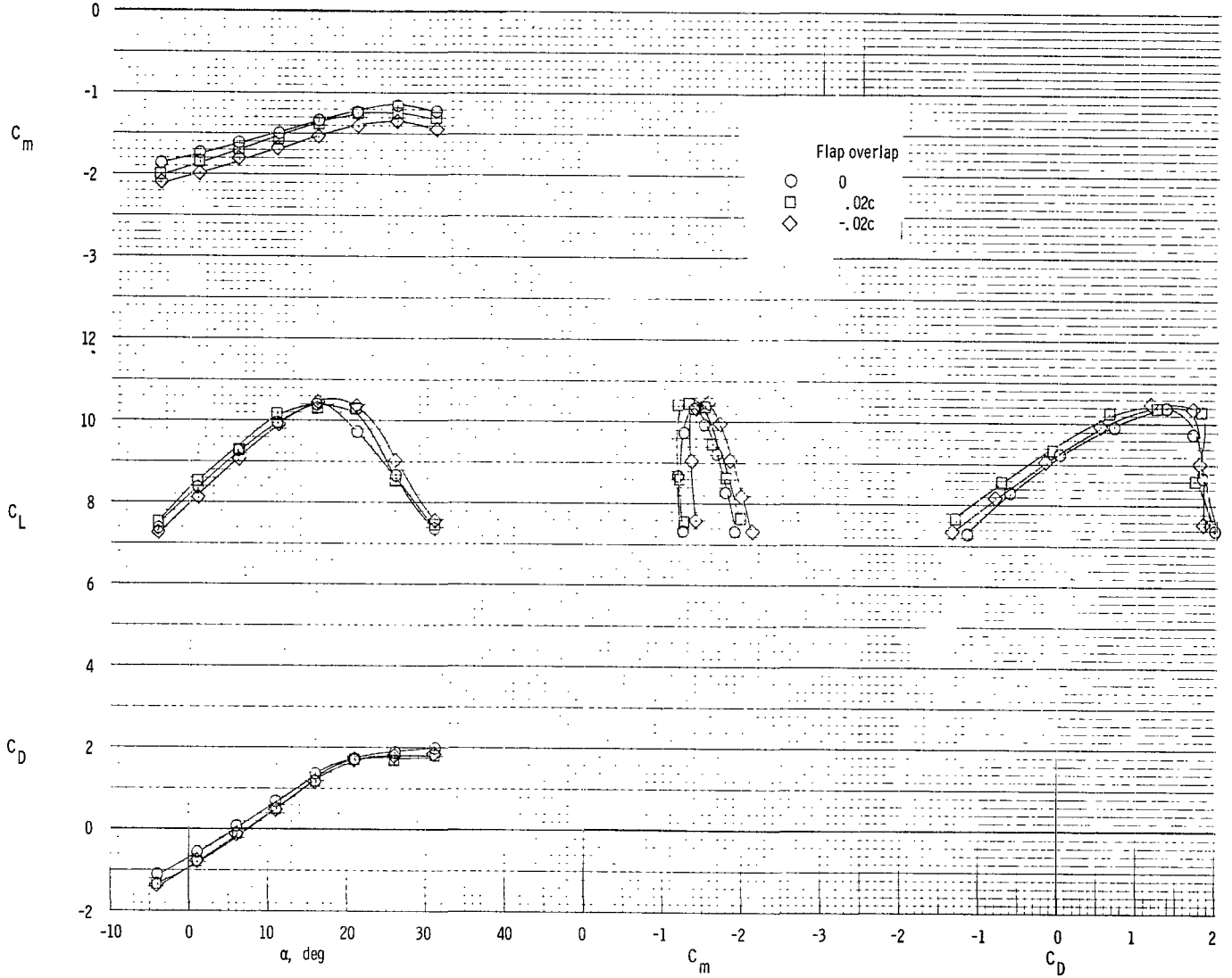

(a) Exhaust deflectors off.

Figure 47.- Summary of flap overlap effect for engine position 1. $\delta_f = 55^o$; original leading-edge slat; $C_\mu = 5.50$.

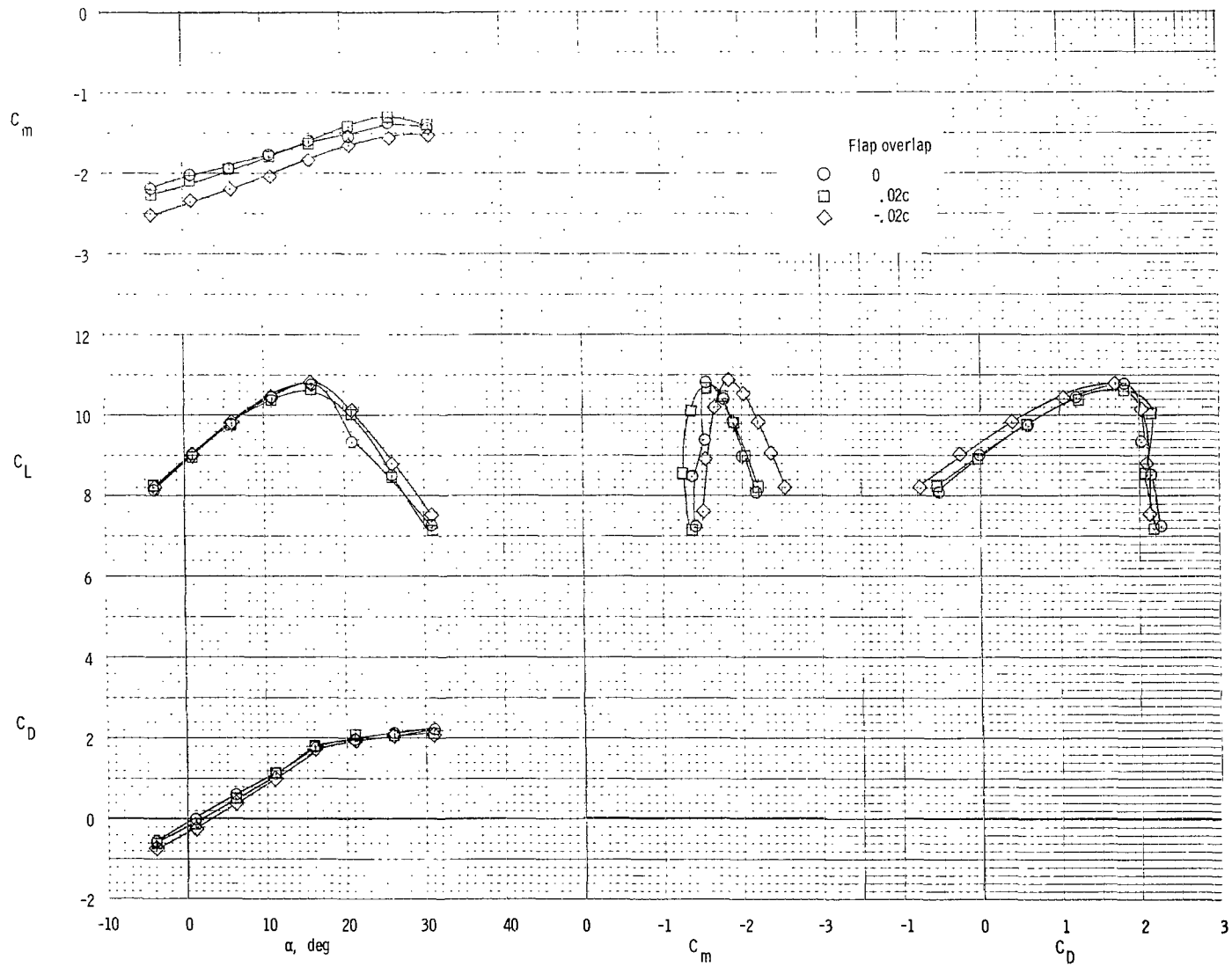

(b) Exhaust deflectors on.

Figure 47.- Concluded.

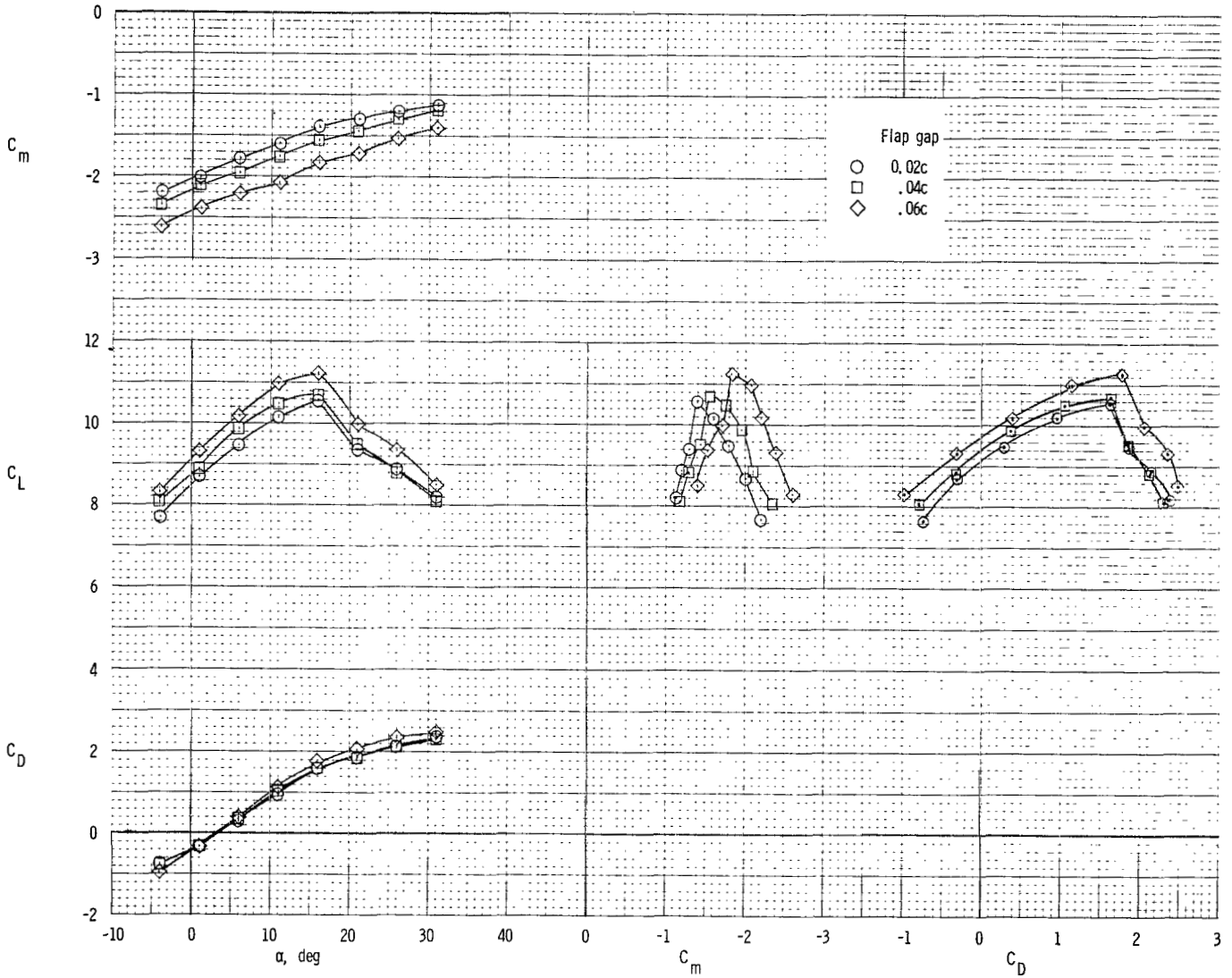

Figure 48.- Summary of flap gap effect for engine position 4 with exhaust deflectors. $\delta_f = 55^o$; original leading-edge slat; $C_\mu = 5.50$.

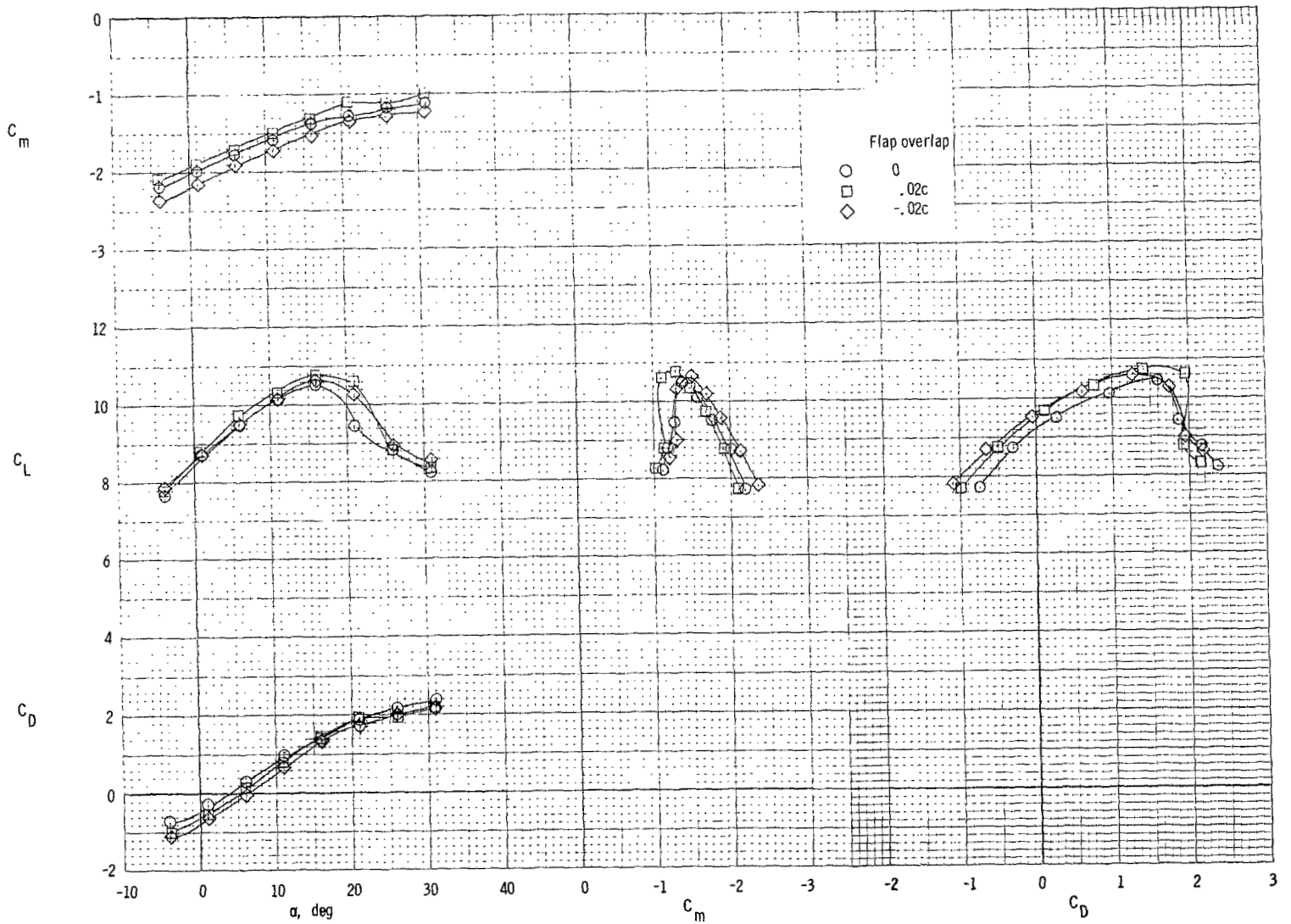

Figure 49.- Summary of flap overlap effect for engine position 4 with exhaust deflectors. $\delta_f = 55^o$; original leading-edge slat; $C_\mu = 5.50$.

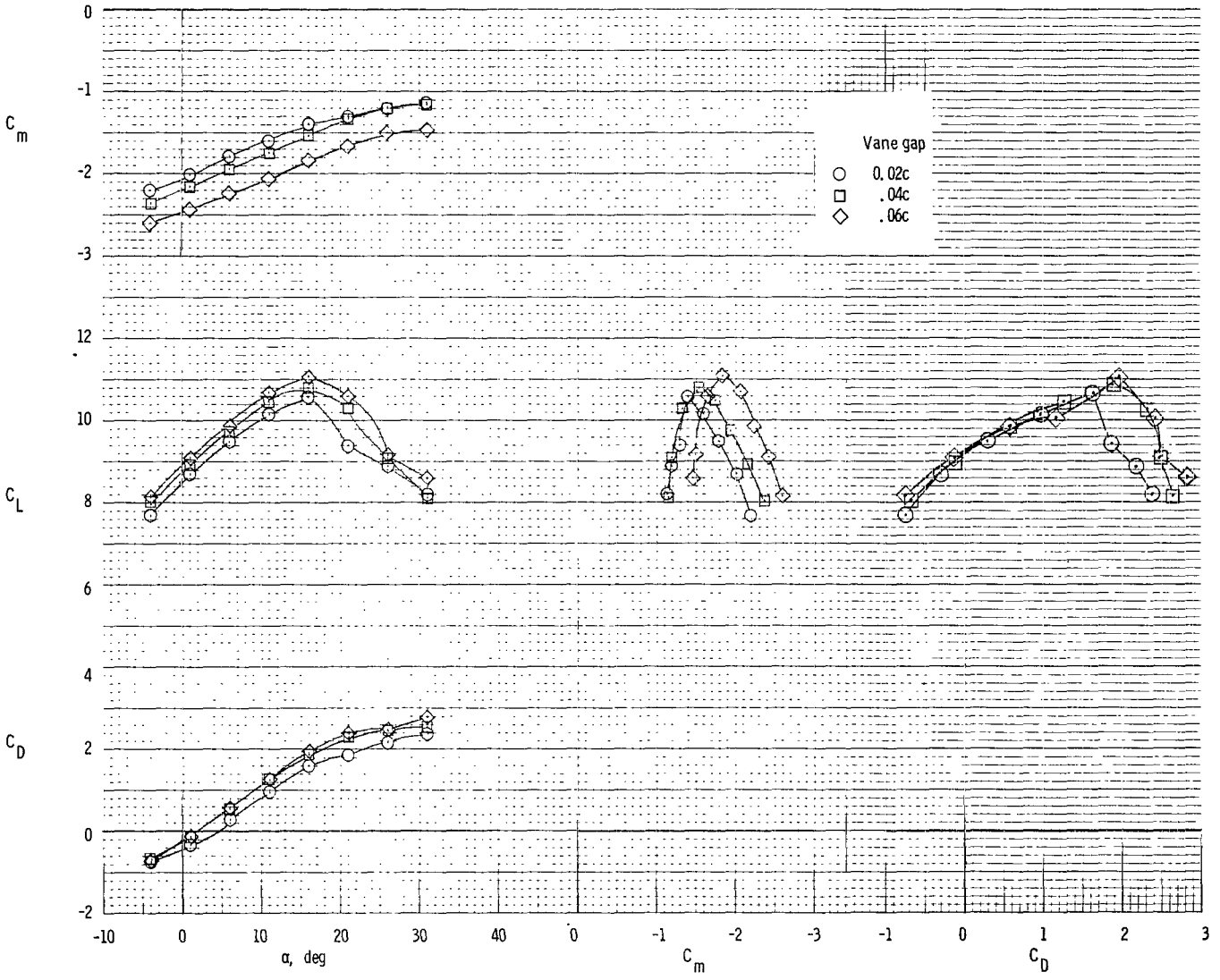

Figure 50.- Summary of vane gap effect for engine position 4 with exhaust deflectors. $\delta_f = 55^o$; original leading-edge slat; $C_\mu = 5.50$.

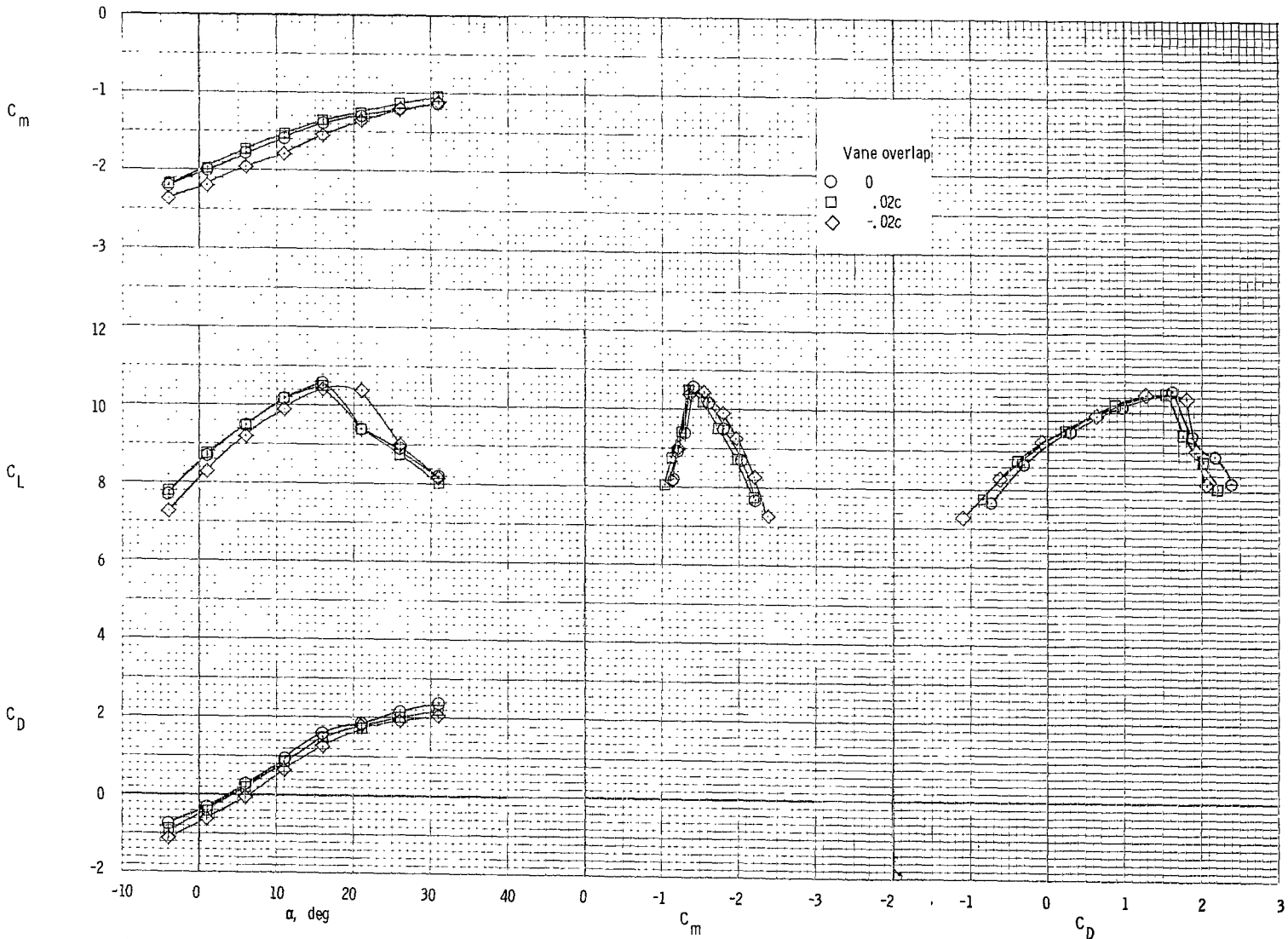

Figure 51.- Summary of vane overlap effect for engine position 4 with exhaust deflectors. $\delta_f = 55^o$; original leading-edge slat; $C_\mu = 5.50$.

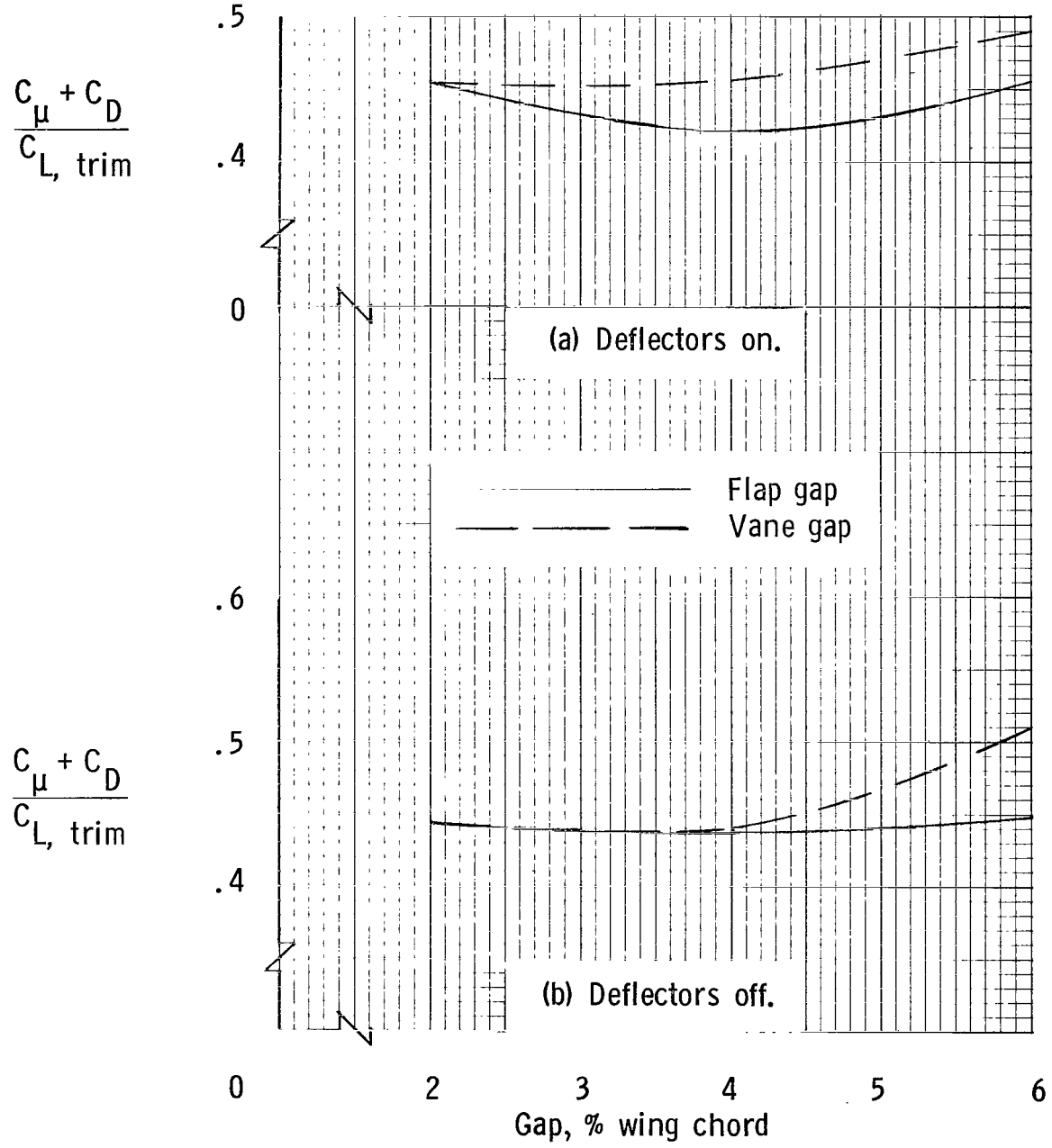

Figure 52.- Variation of $\frac{C_\mu + C_D}{C_{L,trim}}$ with flap gap and vane gap. Engine position 1; $\delta_f = 55^o$; $C_{L,trim} = 5$; $\gamma = 0^o$; $\alpha = 0^o$.

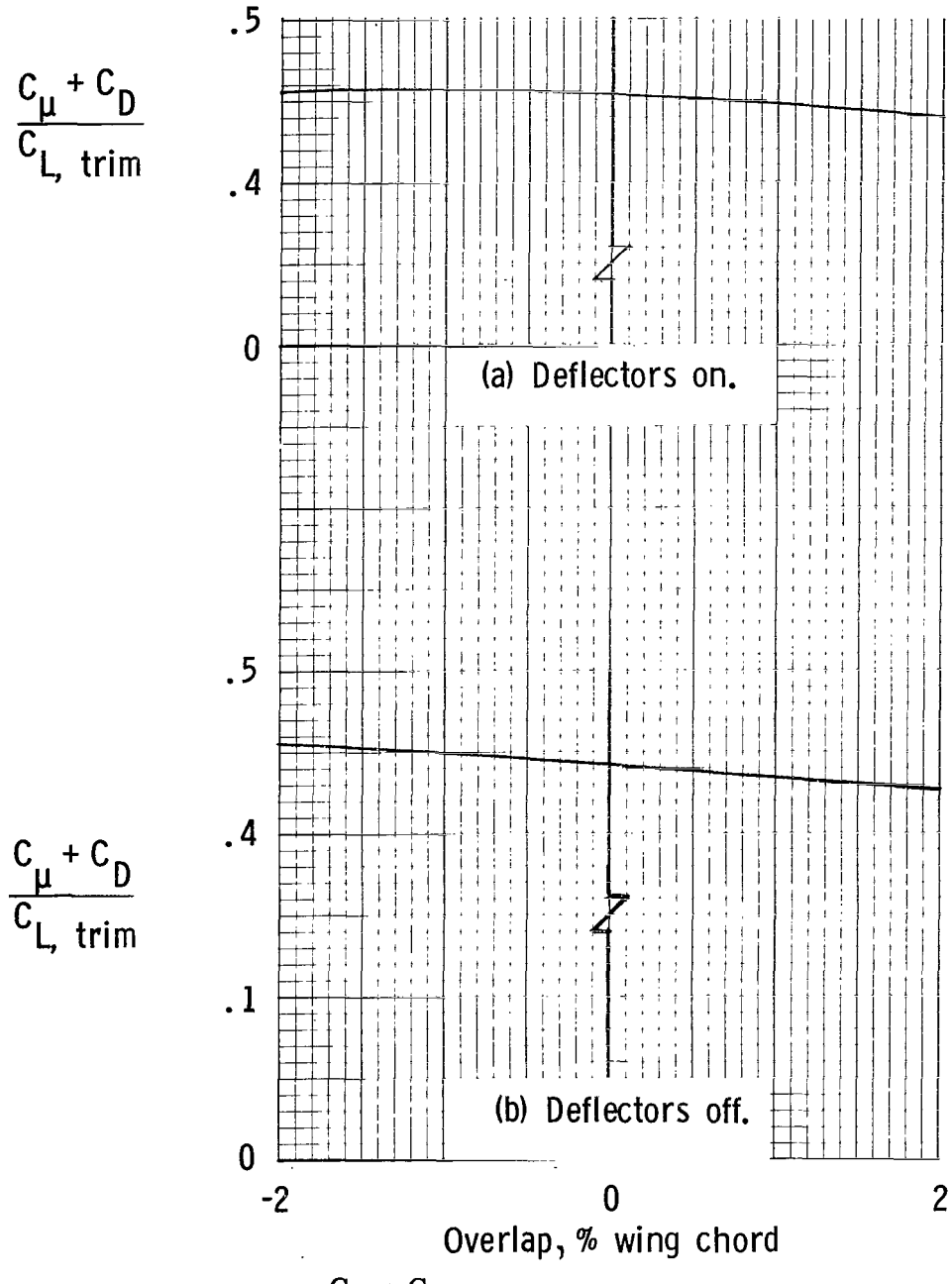

Figure 53.- Variation of $\frac{C_\mu + C_D}{C_{L,trim}}$ with flap overlap. Engine position 1; $\delta_f = 55^o$; $C_{L,trim} = 5$; $\alpha = 0^o$; $\gamma = 0^o$.

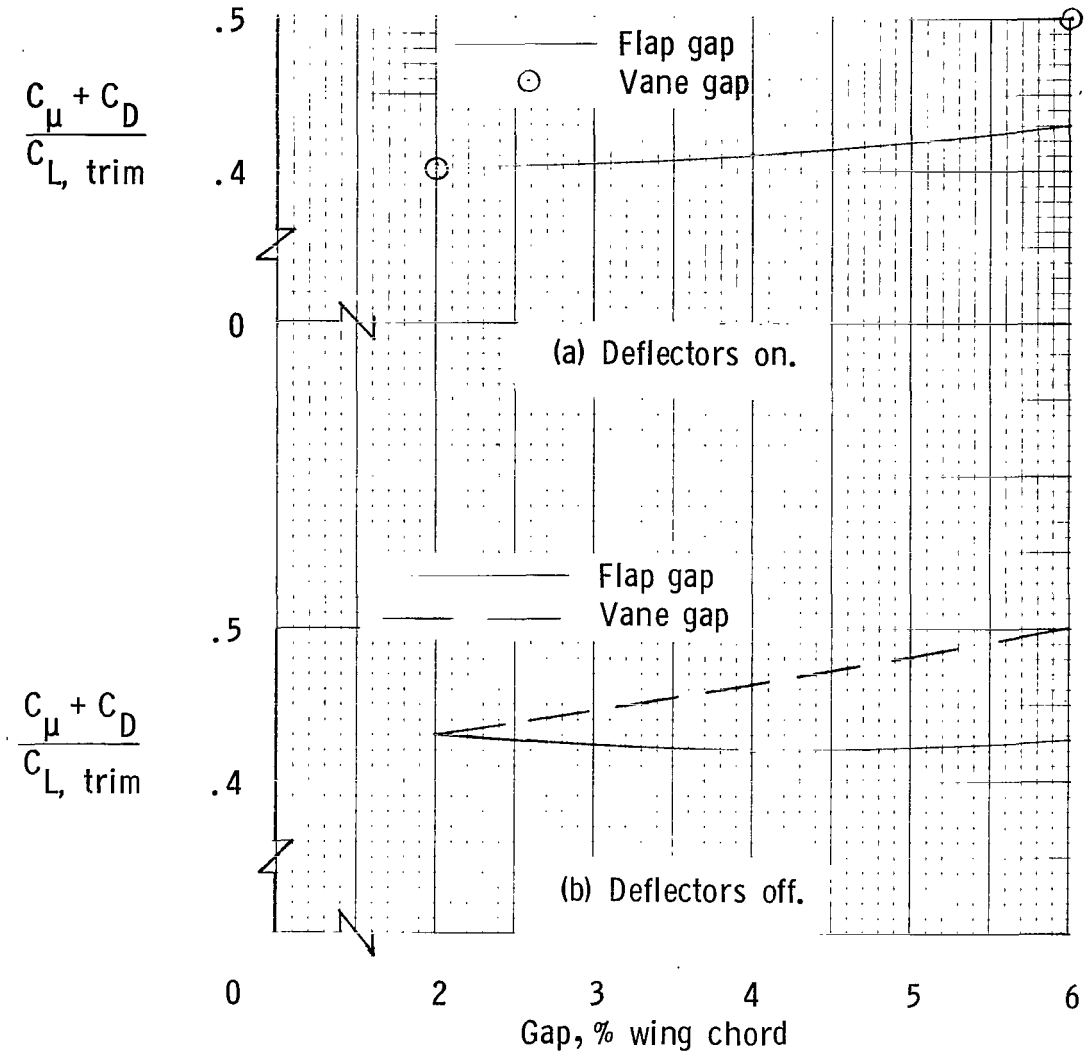

Figure 54.- Variation of $\frac{C_\mu + C_D}{C_{L,trim}}$ with flap gap and vane gap. Engine position 4; $\delta_f = 55^o$; $C_{L,trim} = 5$; $\alpha = 0^o$; $\gamma = 0^o$.

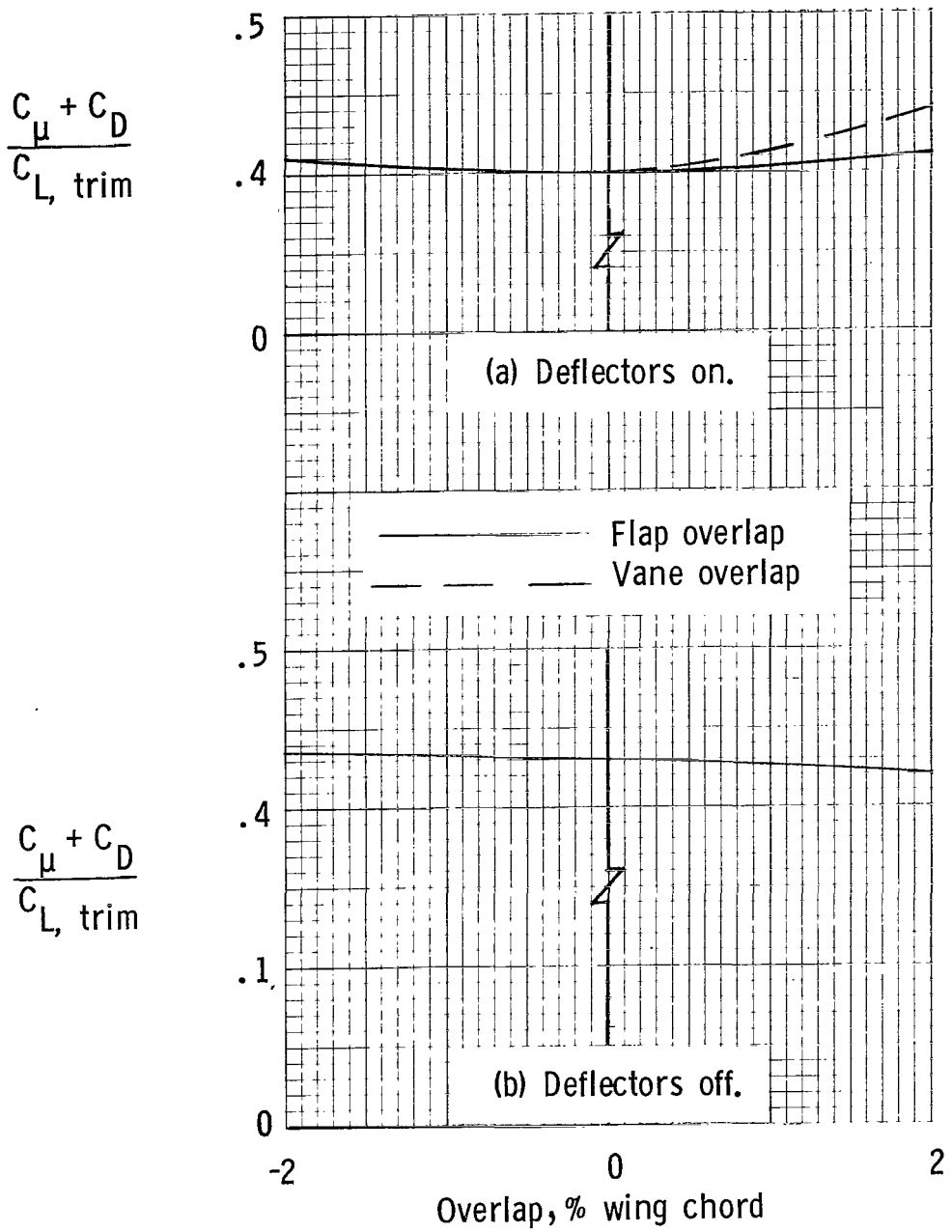

Figure 55.- Variation of $\frac{C_\mu + C_D}{C_{L,trim}}$ with flap overlap and vane overlap. Engine position 4; $\delta_f = 55^o$; $C_{L,trim} = 5$; $\alpha = 0^o$; $\gamma = 0^o$.

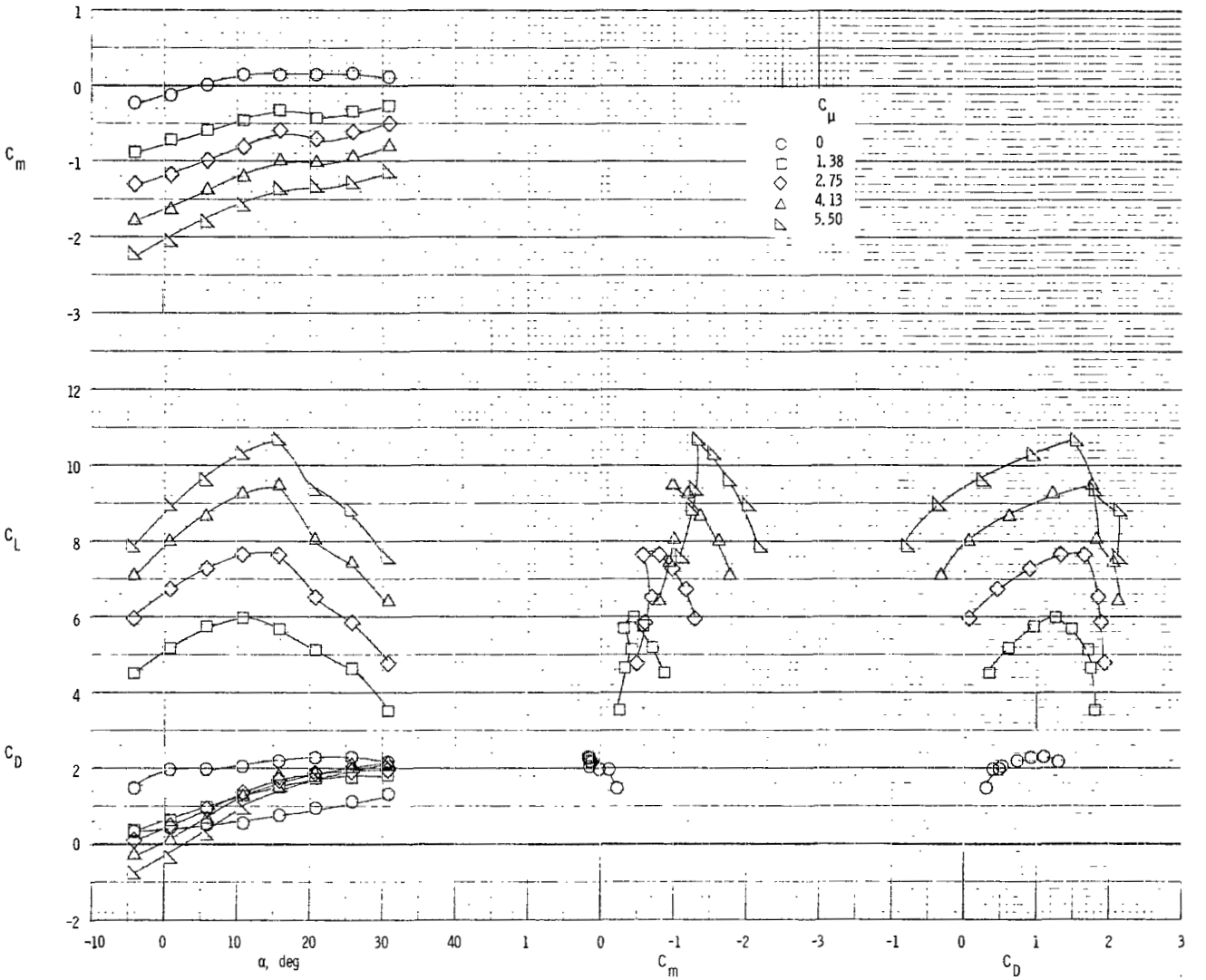

Figure 56.- Longitudinal aerodynamic characteristics of model with leading-edge slat deflected 55°, 0.19c slat chord, and 0.01c slat gap. Engine position 4; exhaust deflectors on; $\delta_f = 55^\circ$.

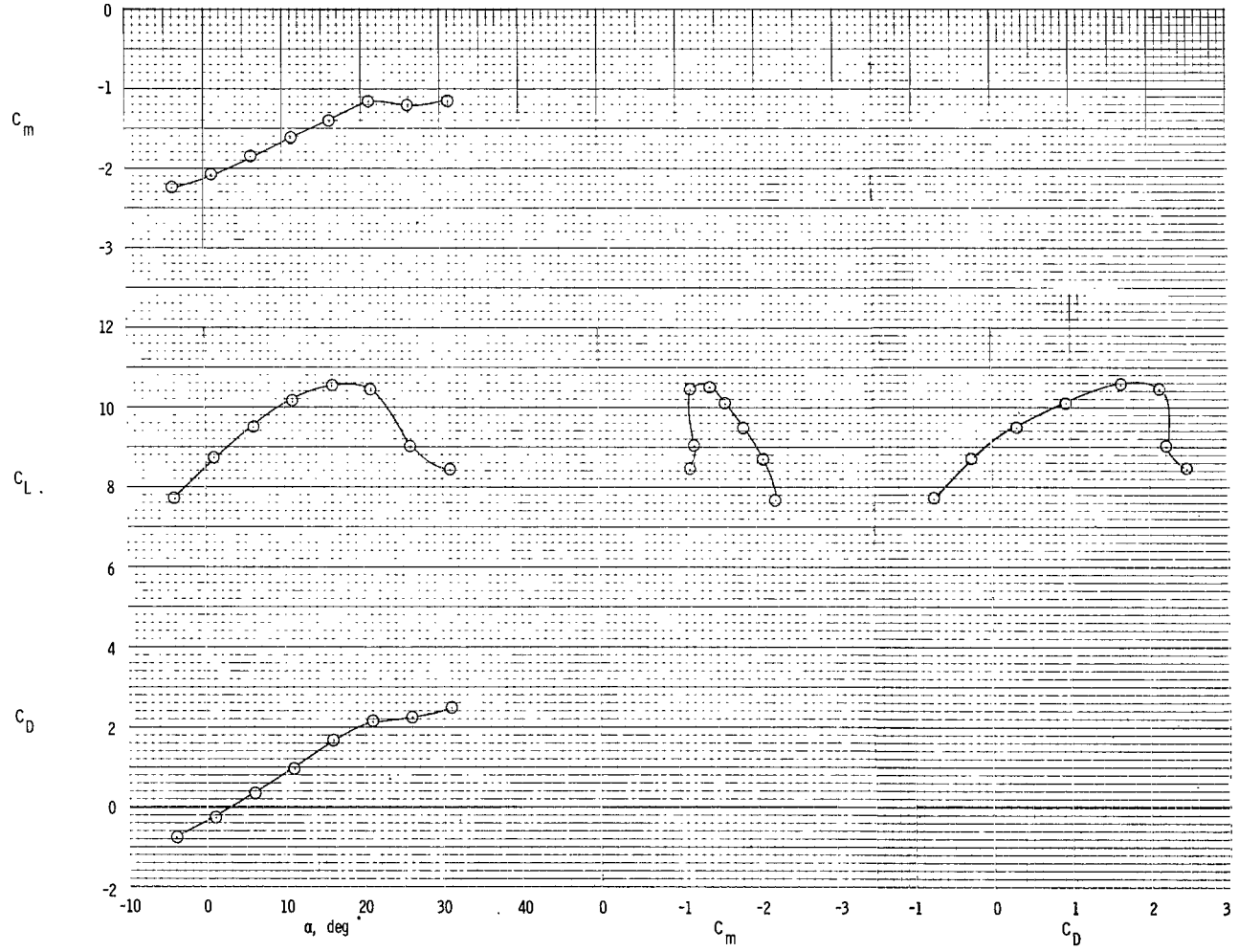

Figure 57.- Longitudinal aerodynamic characteristics of model with leading-edge slat deflected 55^o, 0.19c slat chord, and 0.03c slat gap. Engine position 4; exhaust deflectors on; $\delta_f = 55^o$; $C_\mu = 5.50$.

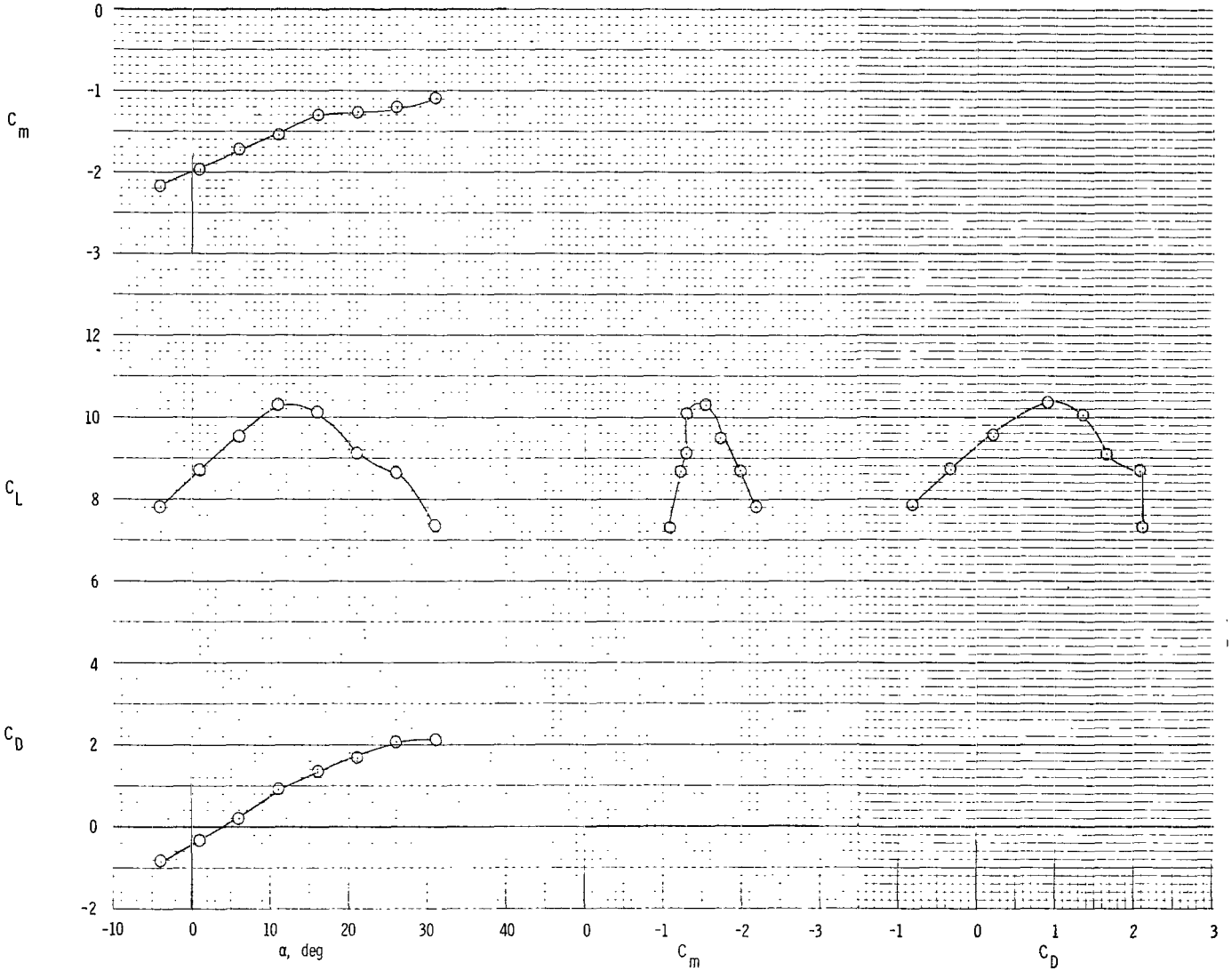

Figure 58.- Longitudinal aerodynamic characteristics of model with leading-edge slat deflected 45°, 0.19c slat chord, and 0.02c slat gap. Engine position 4; exhaust deflectors on; $\delta_f = 55°$; $C_\mu = 5.50$.

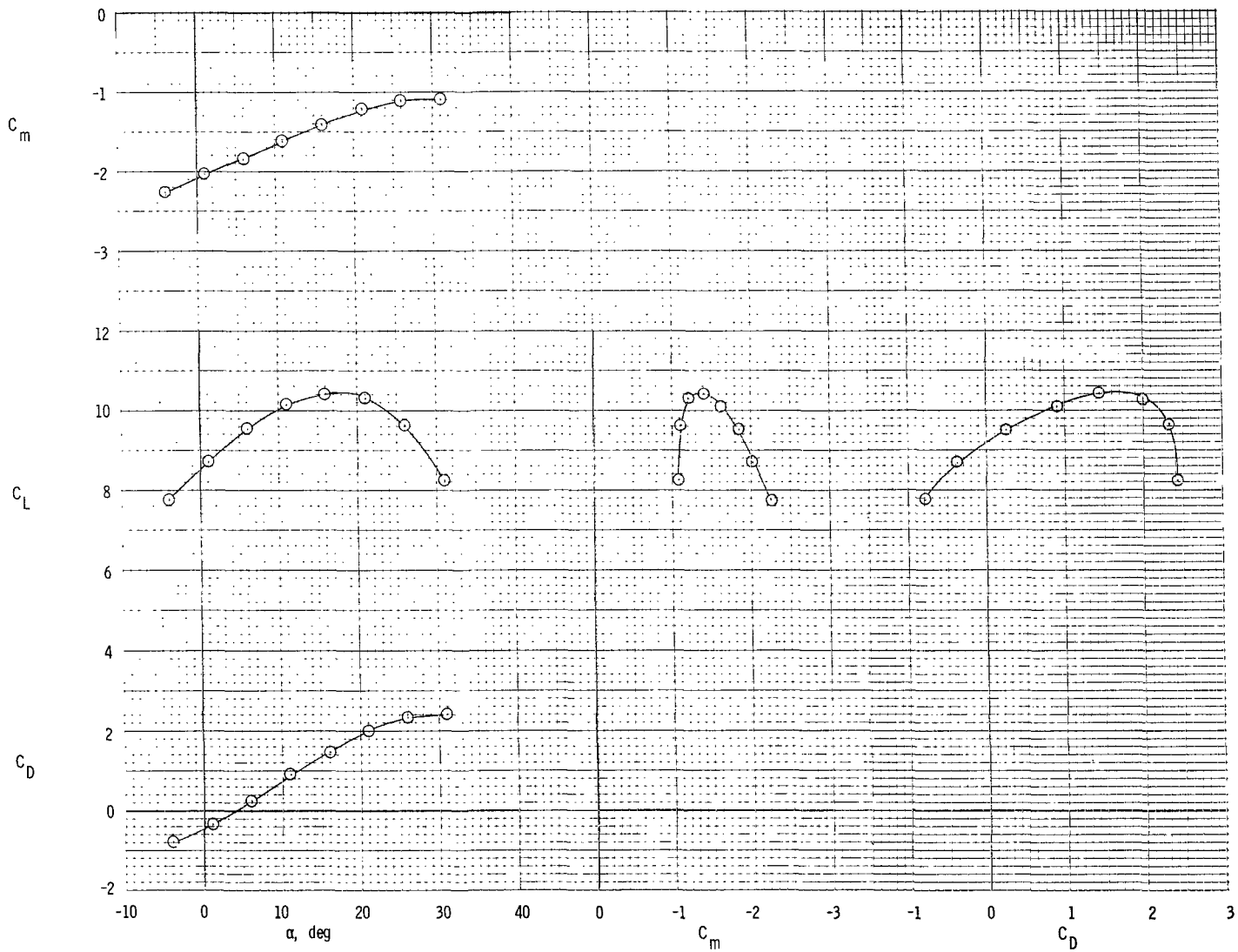

Figure 59.- Longitudinal aerodynamic characteristics of model with leading-edge slat deflected 65°, 0.19c slat chord, and 0.02c slat gap. Engine position 4; exhaust deflectors on; $\delta_f = 55°$; $C_\mu = 5.50$.

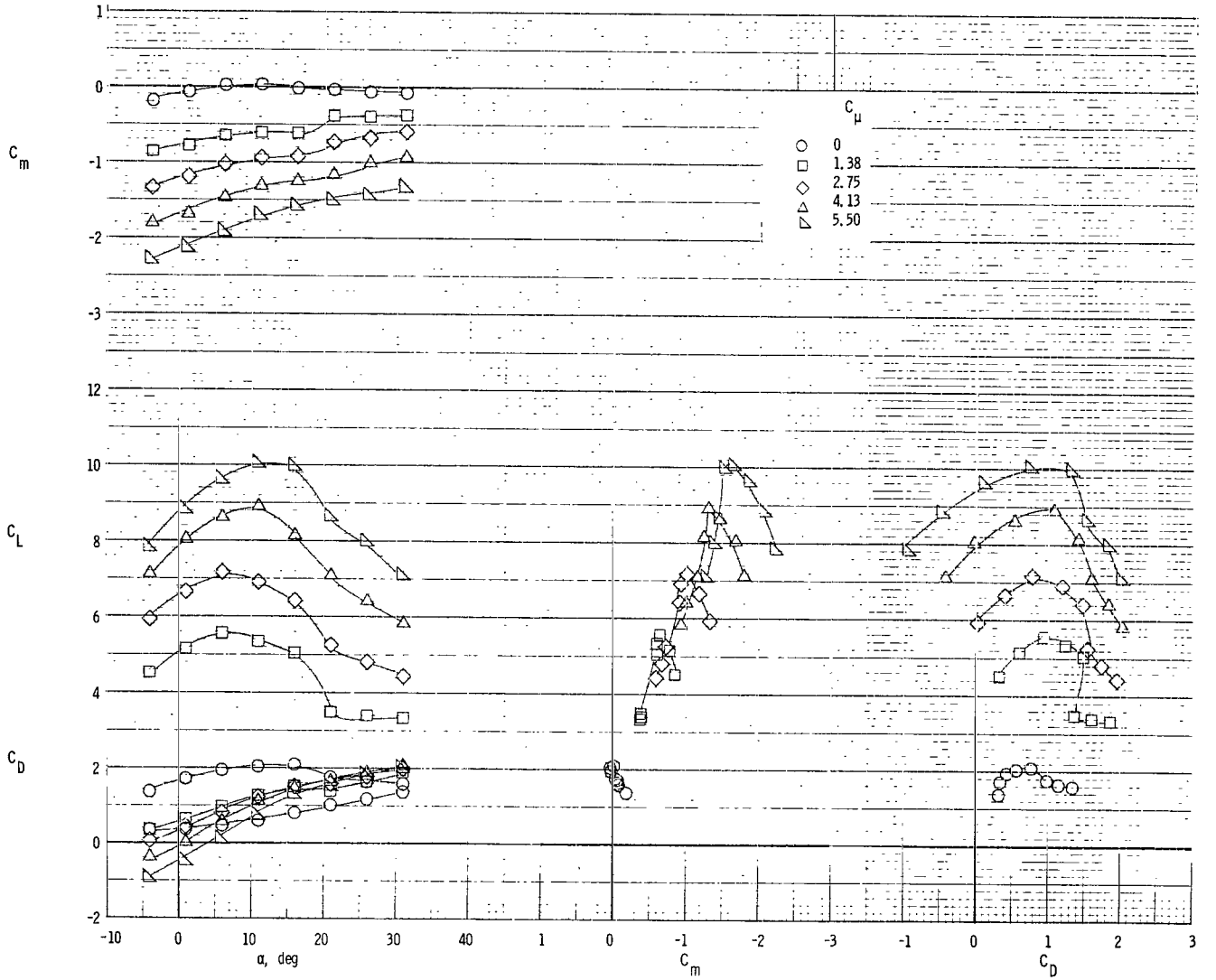

Figure 60.- Longitudinal aerodynamic characteristics of model with leading-edge slat removed. Engine position 4; exhaust deflectors on; $\delta_f = 55^o$.

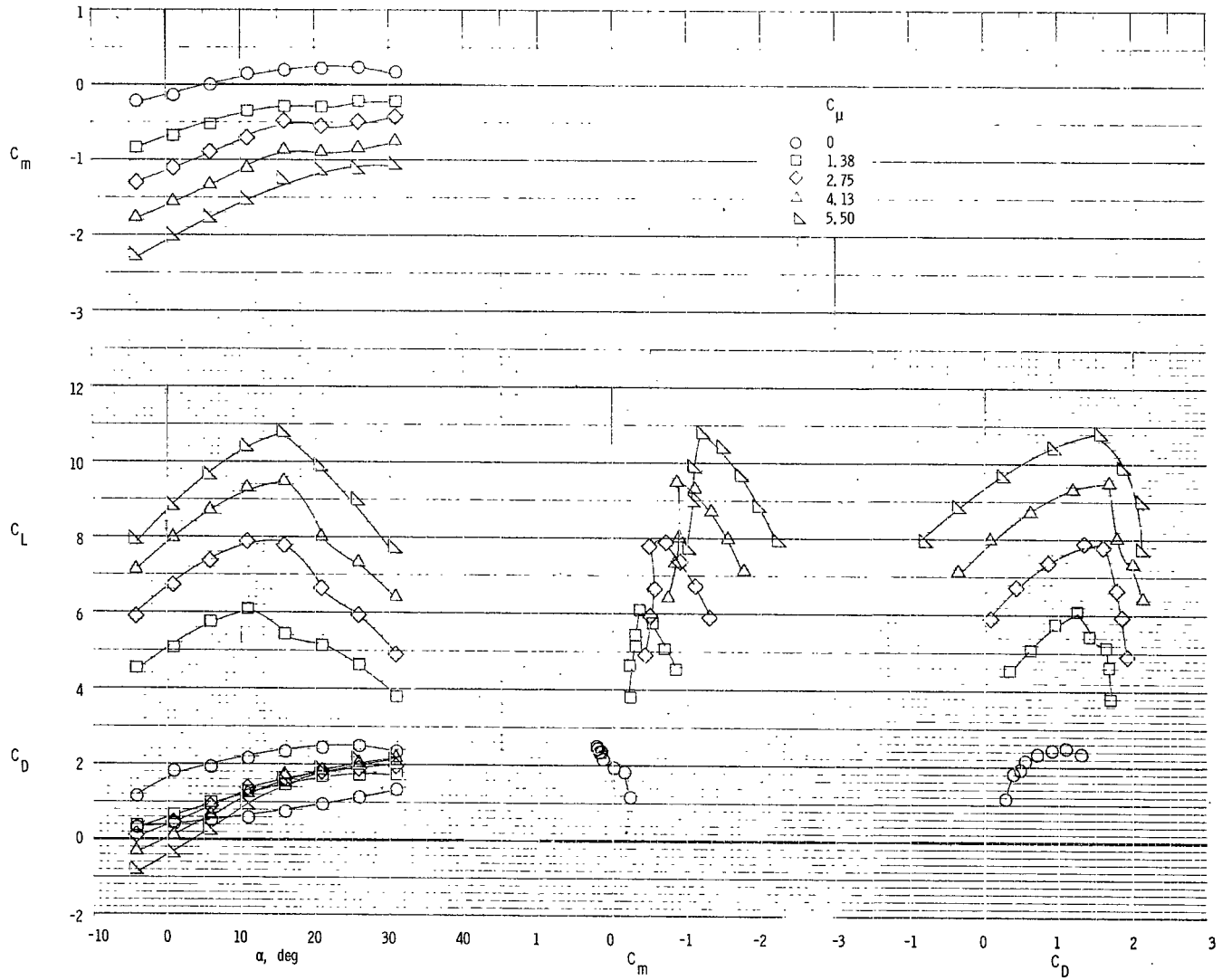

Figure 61.- Longitudinal aerodynamic characteristics of model with leading-edge slat deflected 55°, 0.25c slat chord, and 0.02c slat gap. Engine position 4; exhaust deflectors on; $\delta_f = 55°$.

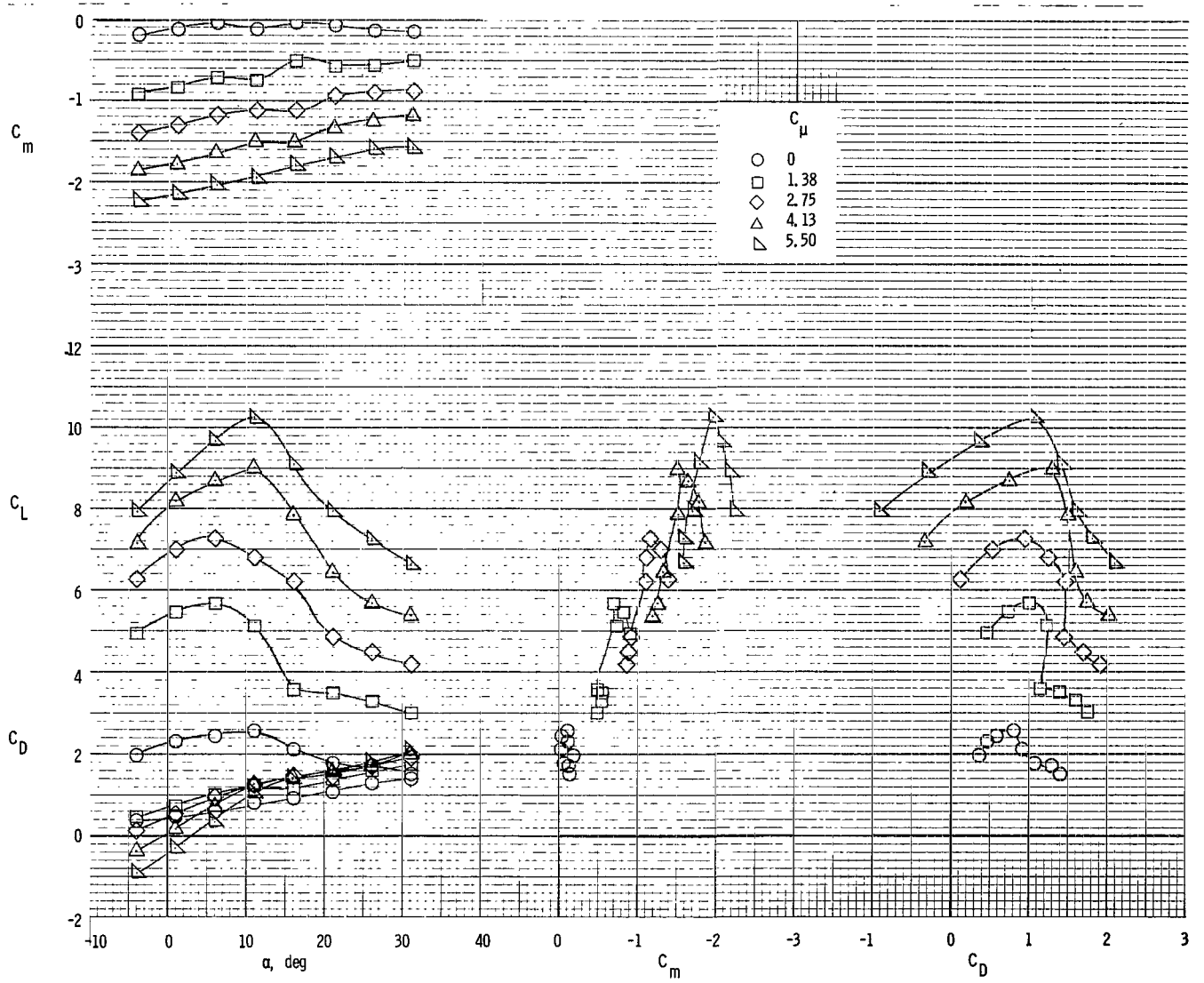

Figure 62.- Longitudinal aerodynamic characteristics of model with leading-edge slat removed. Engine position 1; exhaust deflectors off; $\delta_f = 55^o$.

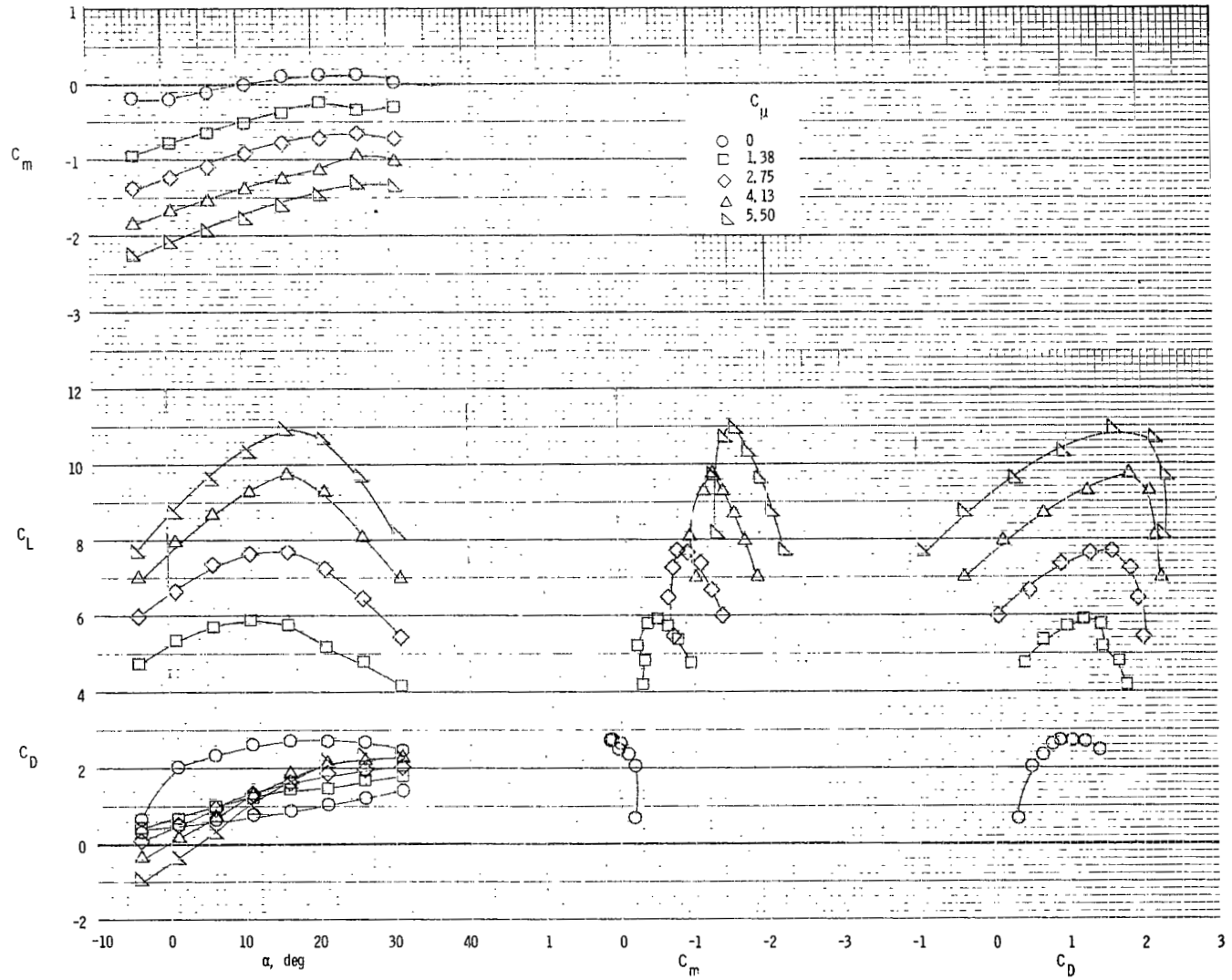

Figure 63.- Longitudinal aerodynamic characteristics of model with leading-edge slat deflected 55°, 0.25c slat chord, and 0.02c slat gap. Engine position 1; exhaust deflectors off; $\delta_f = 55°$.

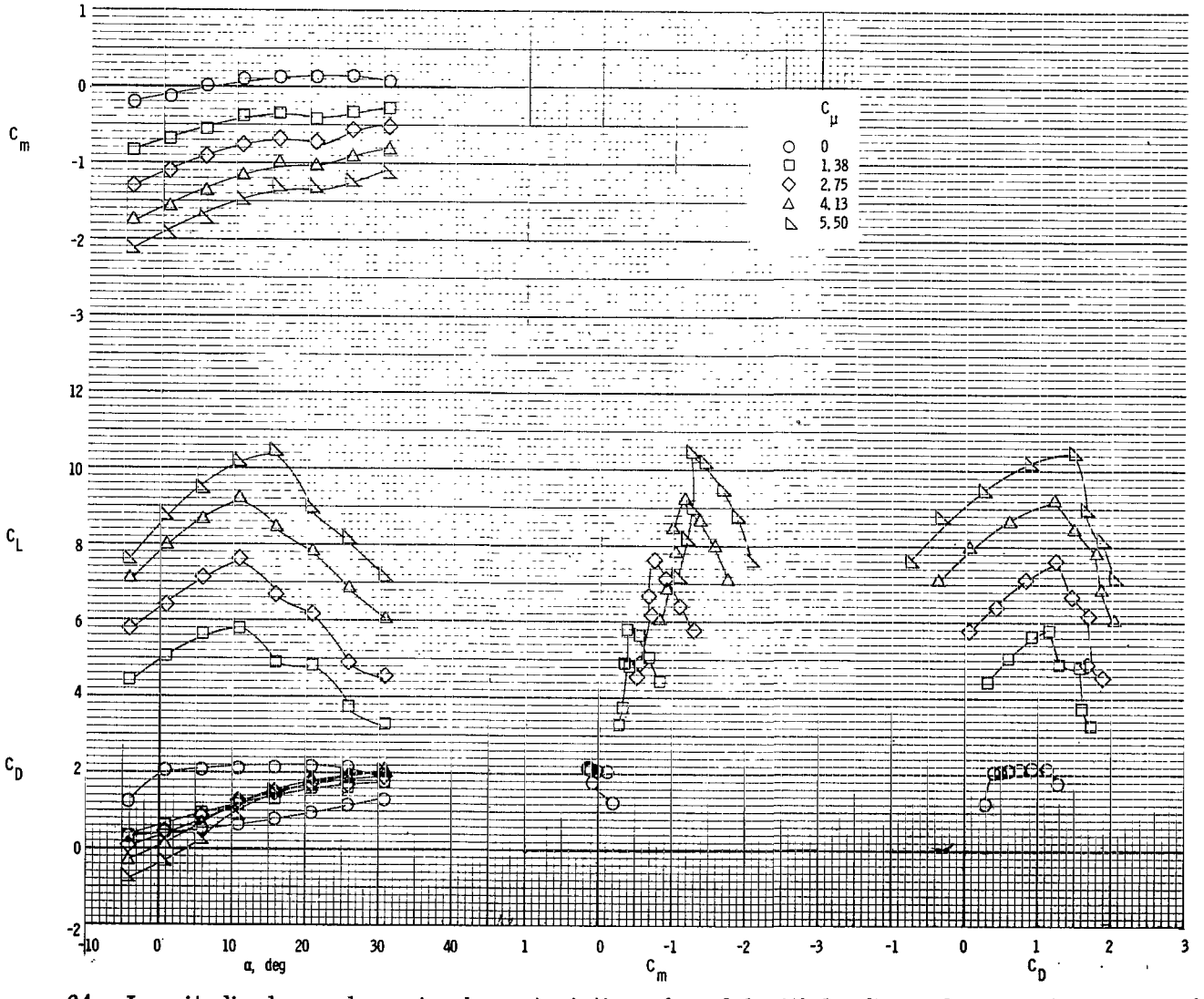

Figure 64.- Longitudinal aerodynamic characteristics of model with leading-edge slat deflected 55°, 0.19c slat chord, and slot sealed. Engine position 4; exhaust deflectors on; $\delta_f = 55^o$.

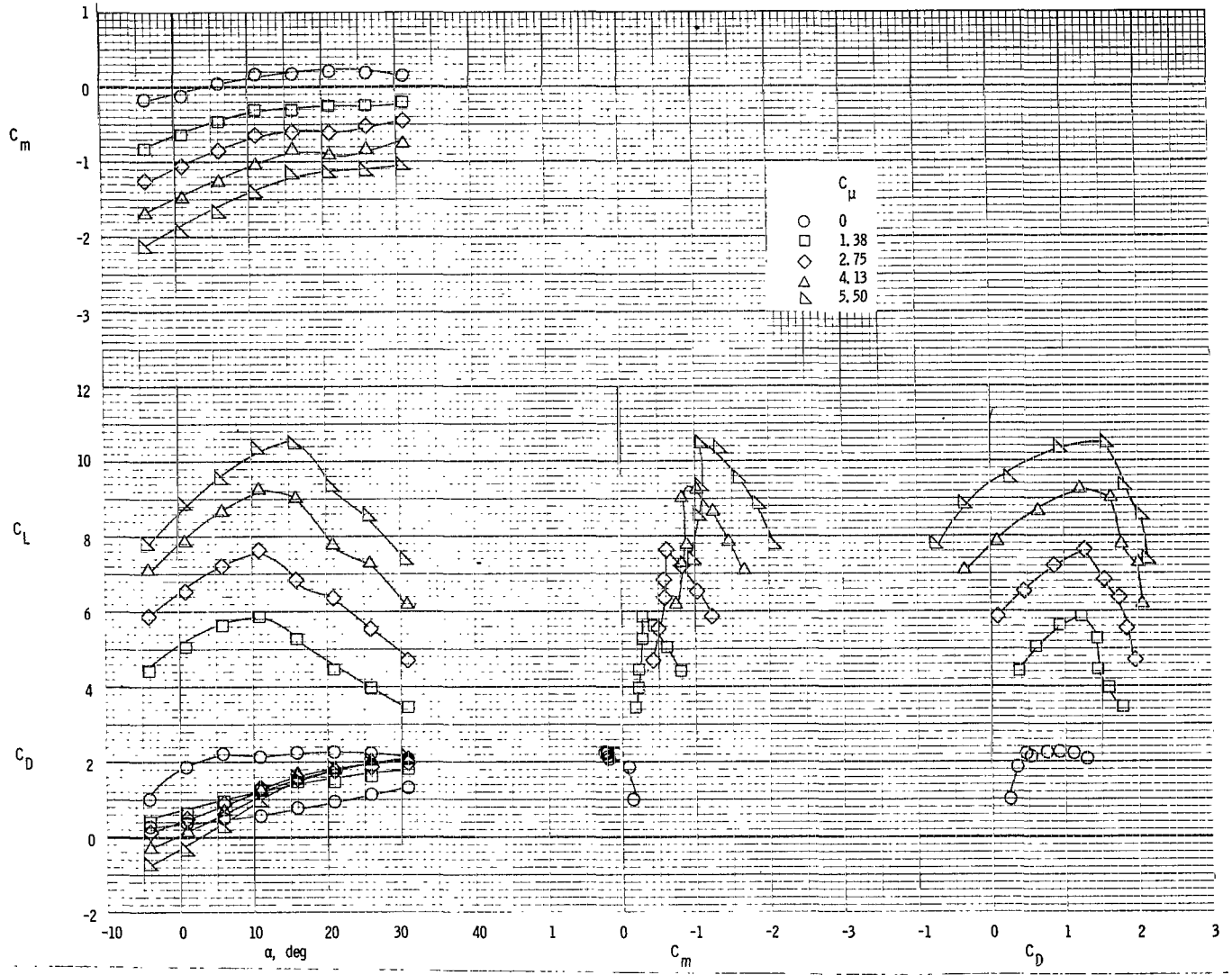

Figure 65.- Longitudinal aerodynamic characteristics of model with leading-edge slat deflected 55°, 0.25c slat chord, and slot sealed. Engine position 4; exhaust deflectors on; $\delta_f = 55^o$.

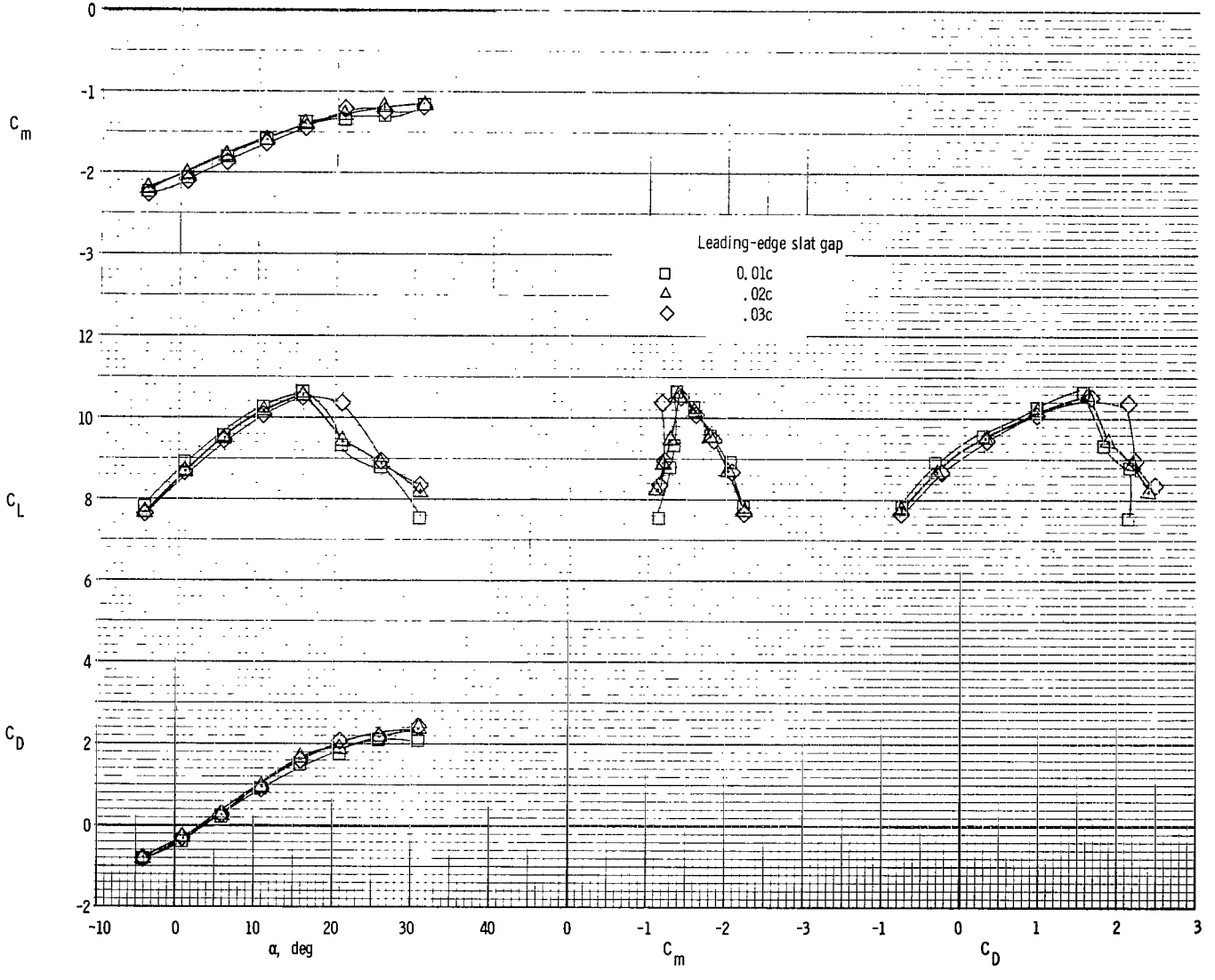

Figure 66.- Effect of leading-edge slat gap on longitudinal aerodynamic characteristics of model. Engine position 4; exhaust deflectors on; $\delta_f = 55^o$; $C_\mu = 5.50$; $\delta_s = 55^o$; slat chord, 0.19c; slat overlap, 0.

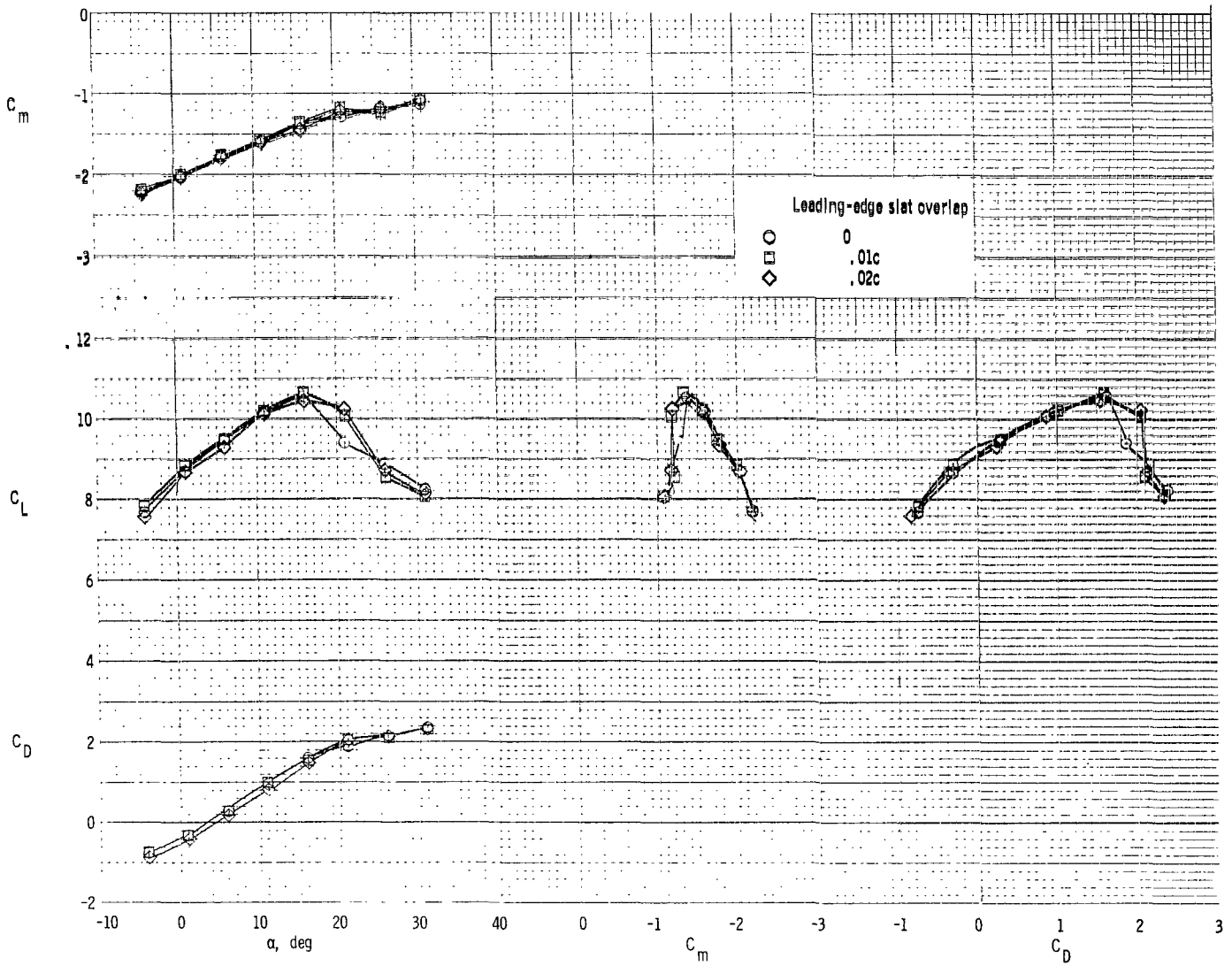

Figure 67.- Effect of slat overlap on longitudinal aerodynamic characteristics of model. Engine position 4; exhaust deflectors on; $\delta_f = 55^o$; $C_\mu = 5.50$; $\delta_s = 55^o$; slat chord, 0.19c; slat gap, 0.02c.

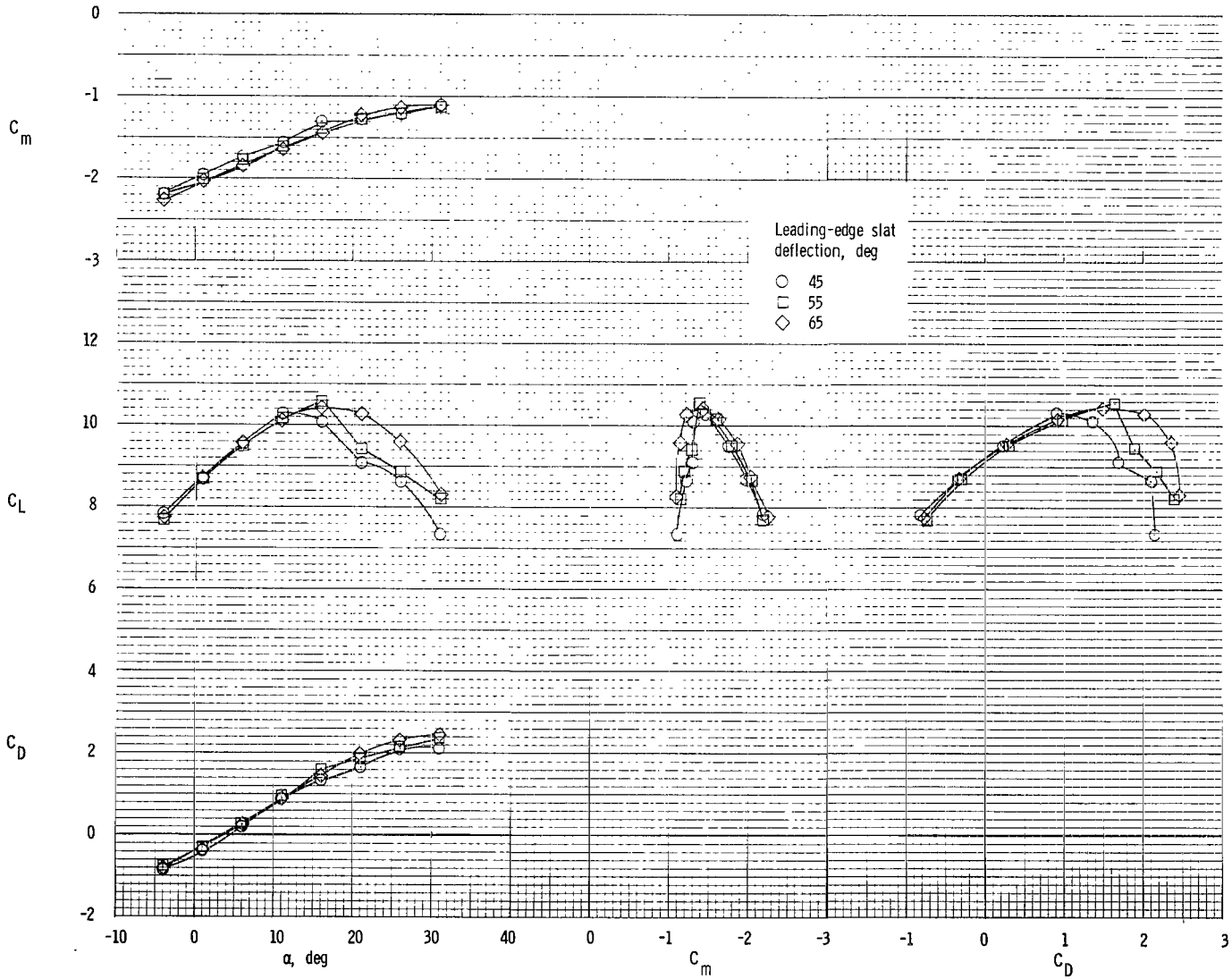

Figure 68.- Effect of leading-edge slat deflection on longitudinal aerodynamic characteristics of model. Engine position 4; exhaust deflectors on; $\delta_f = 55^o$; $C_\mu = 5.50$; slat chord, 0.19c; slat gap, 0.02c; slat overlap, 0.

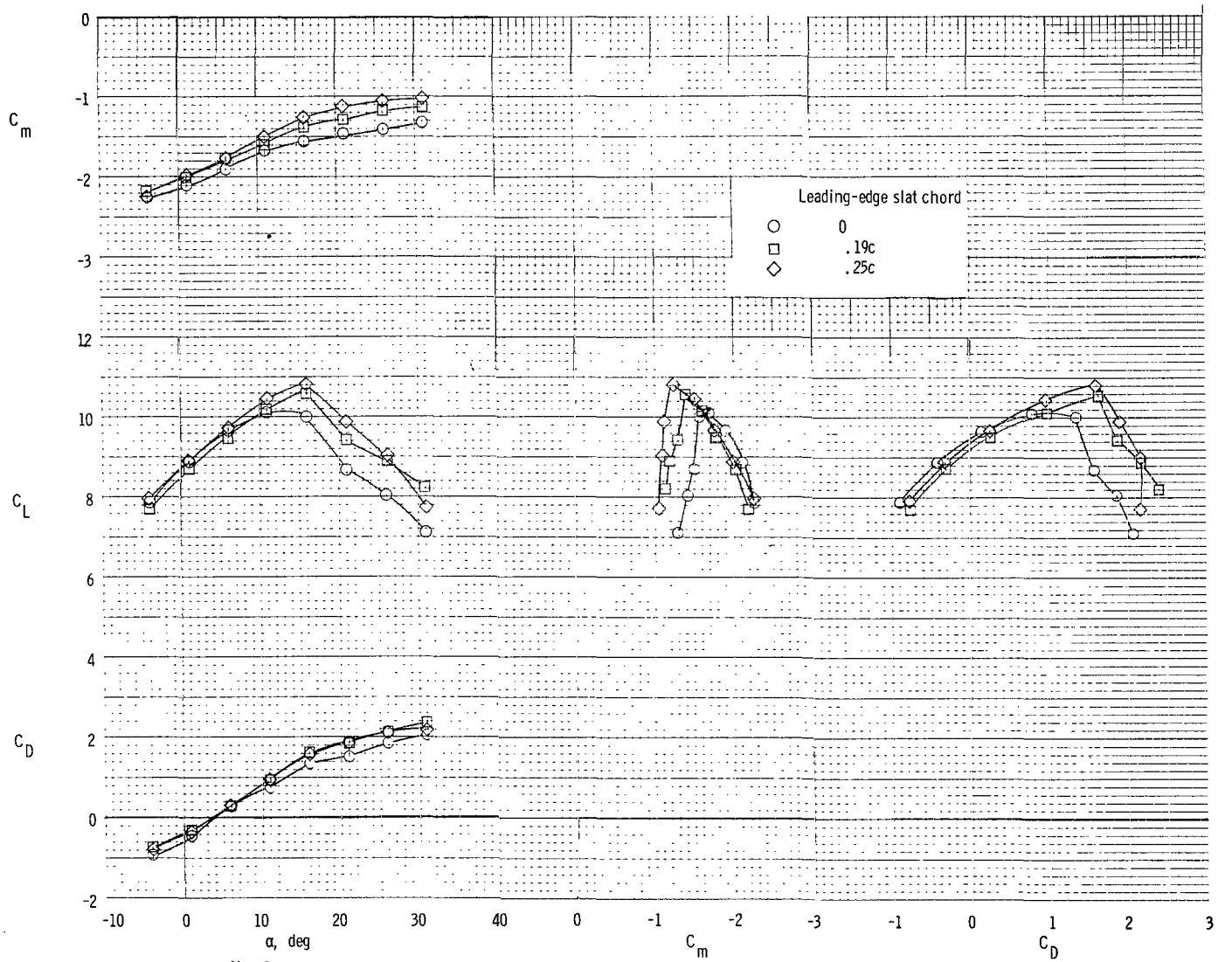

Figure 69.- Effect of leading-edge slat chord on longitudinal aerodynamic characteristics of model. Engine position 4; exhaust deflectors on; $\delta_f = 55^o$; $C_\mu = 5.50$; $\delta_s = 55^o$; slat gap, 0.02c; slat overlap, 0.

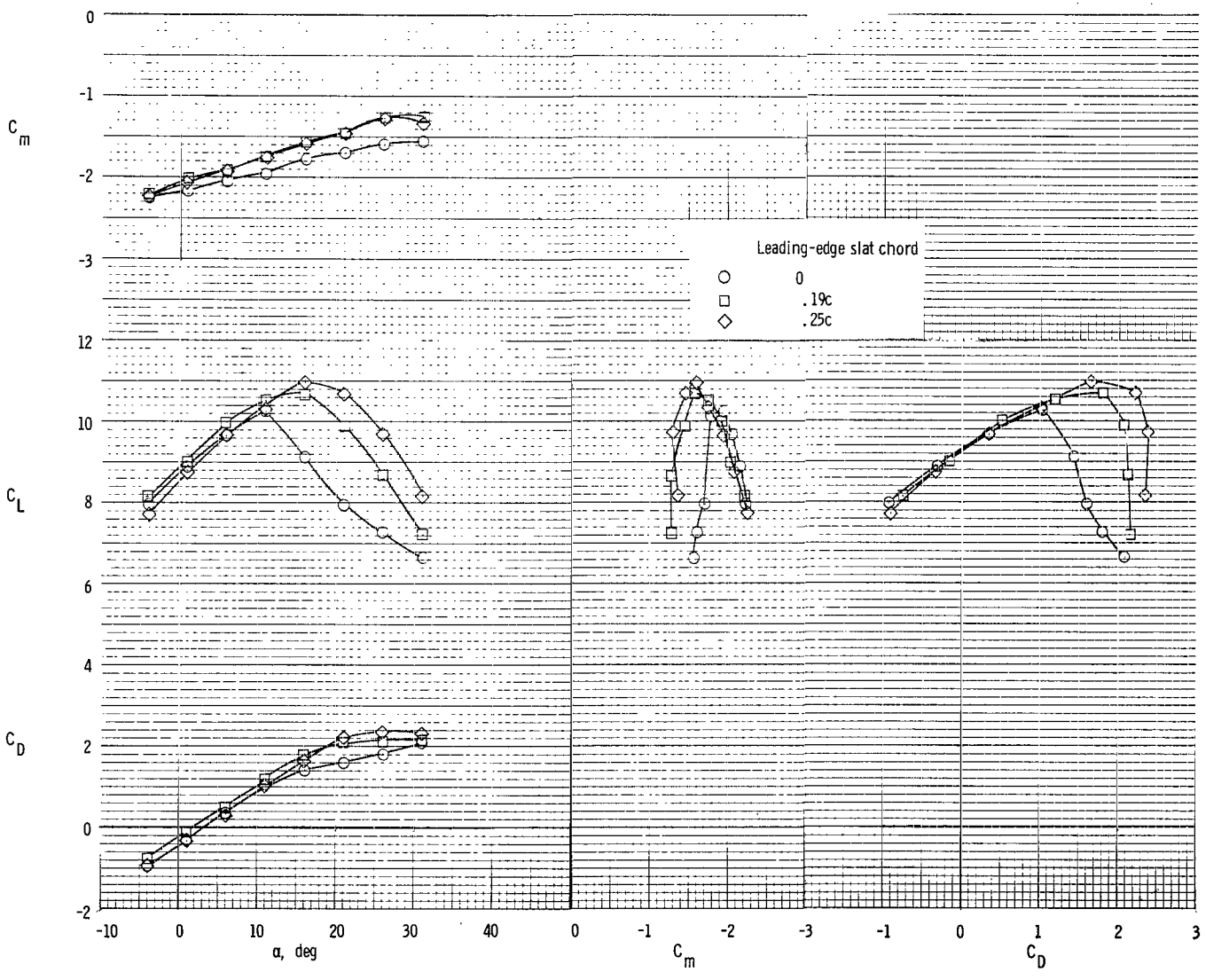

Figure 70.- Effect of leading-edge slat chord on longitudinal aerodynamic characteristics of model. Engine position 1; exhaust deflectors off; large-vane—large-flap double-slotted flap; $\delta_f = 55^o$; $C_\mu = 5.50$; $\delta_s = 55^o$; slat gap, 0.02c; slat overlap, 0.

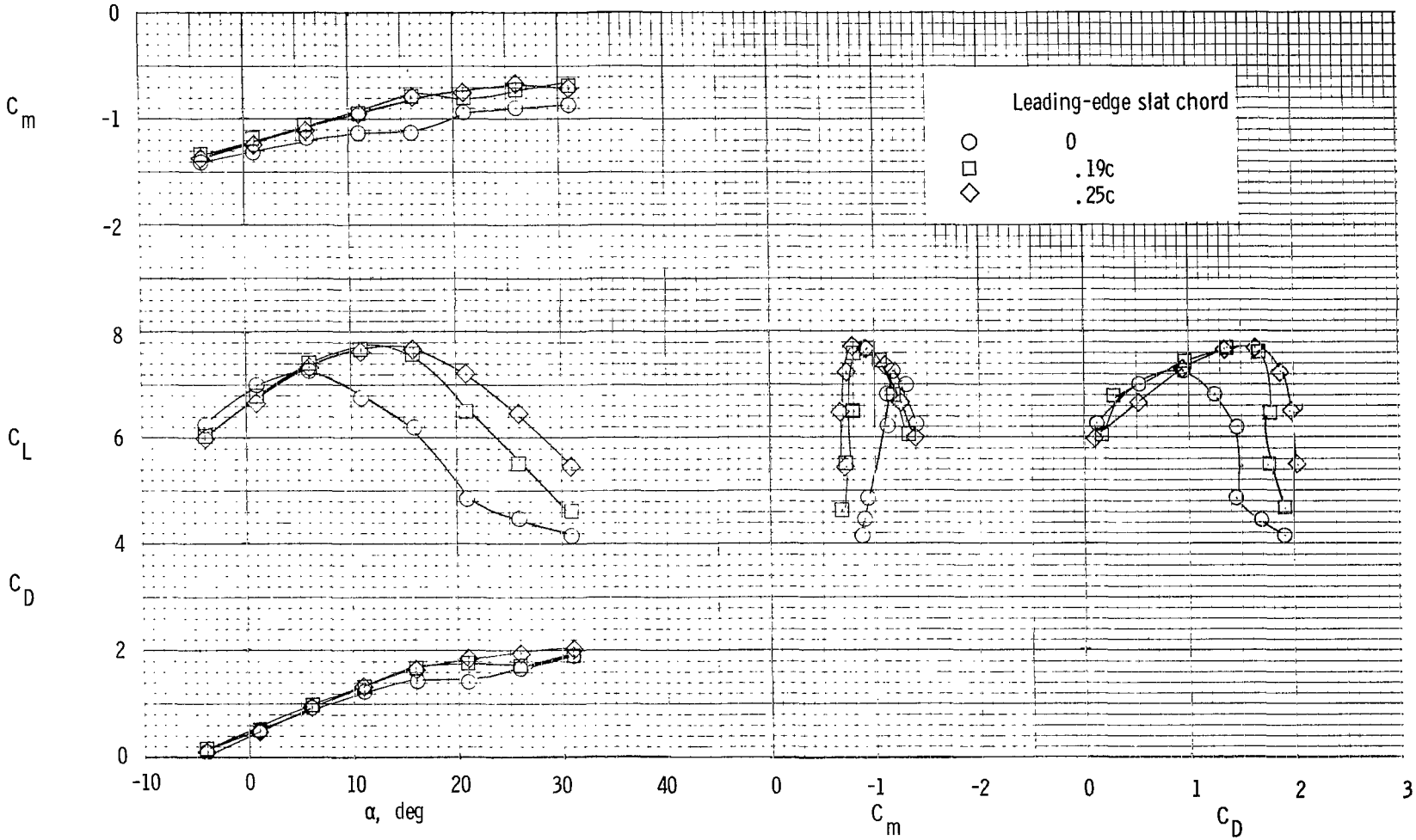

Figure 71.- Effect of leading-edge slat chord on longitudinal aerodynamic characteristics of the model. Engine position 1; exhaust deflectors off; large-vane—large-flap double-slotted flap; $\delta_f = 55^o$; $C_\mu = 2.75$; $\delta_s = 55^o$; slat gap, 0.02c; slat overlap, 0.

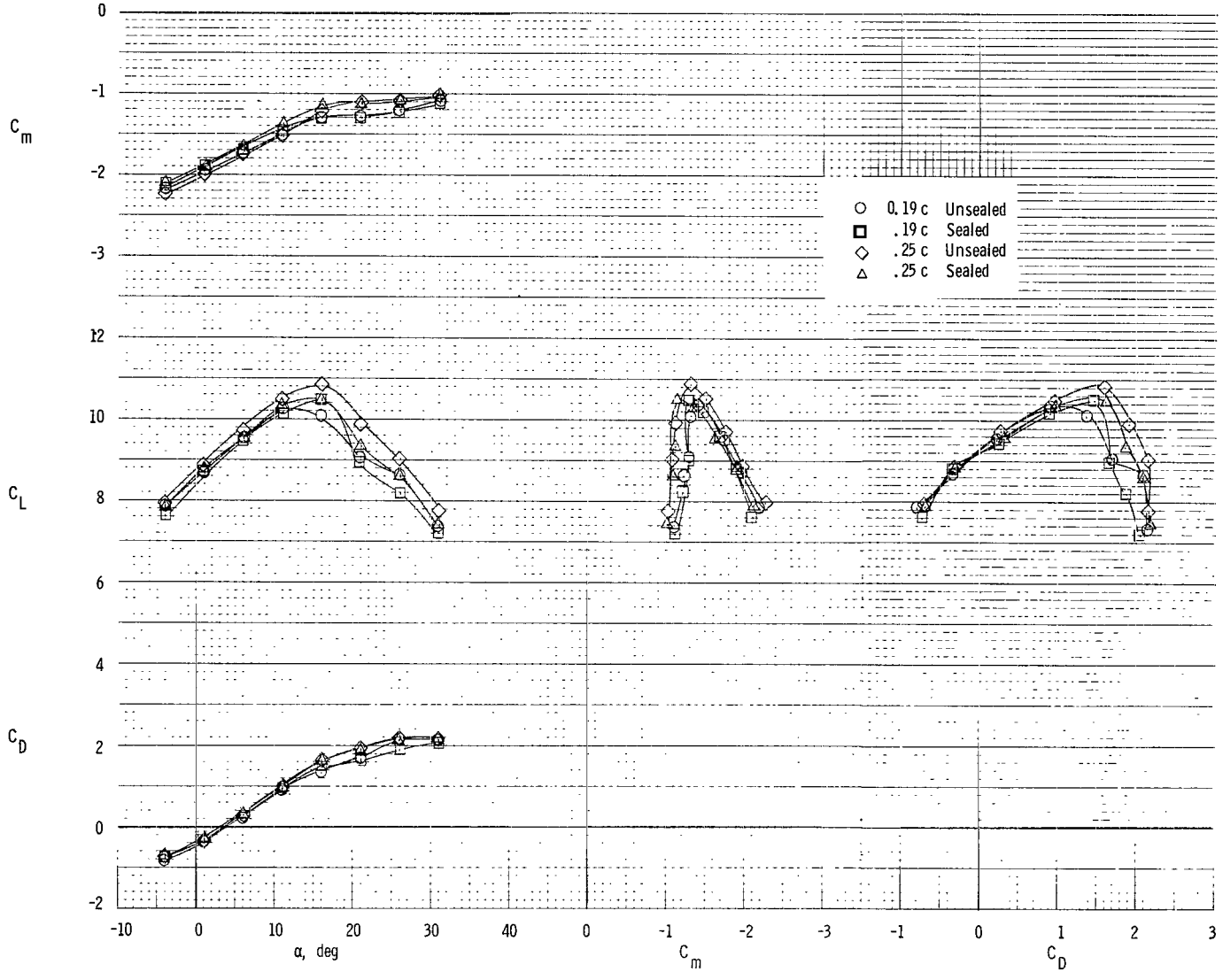

Figure 72.- Summary of effect of sealing leading-edge slat on longitudinal aerodynamic characteristics of model. Engine position 4; exhaust deflectors on; $\delta_f = 55^o$; $\delta_s = 55^o$; $C_\mu = 5.50$.

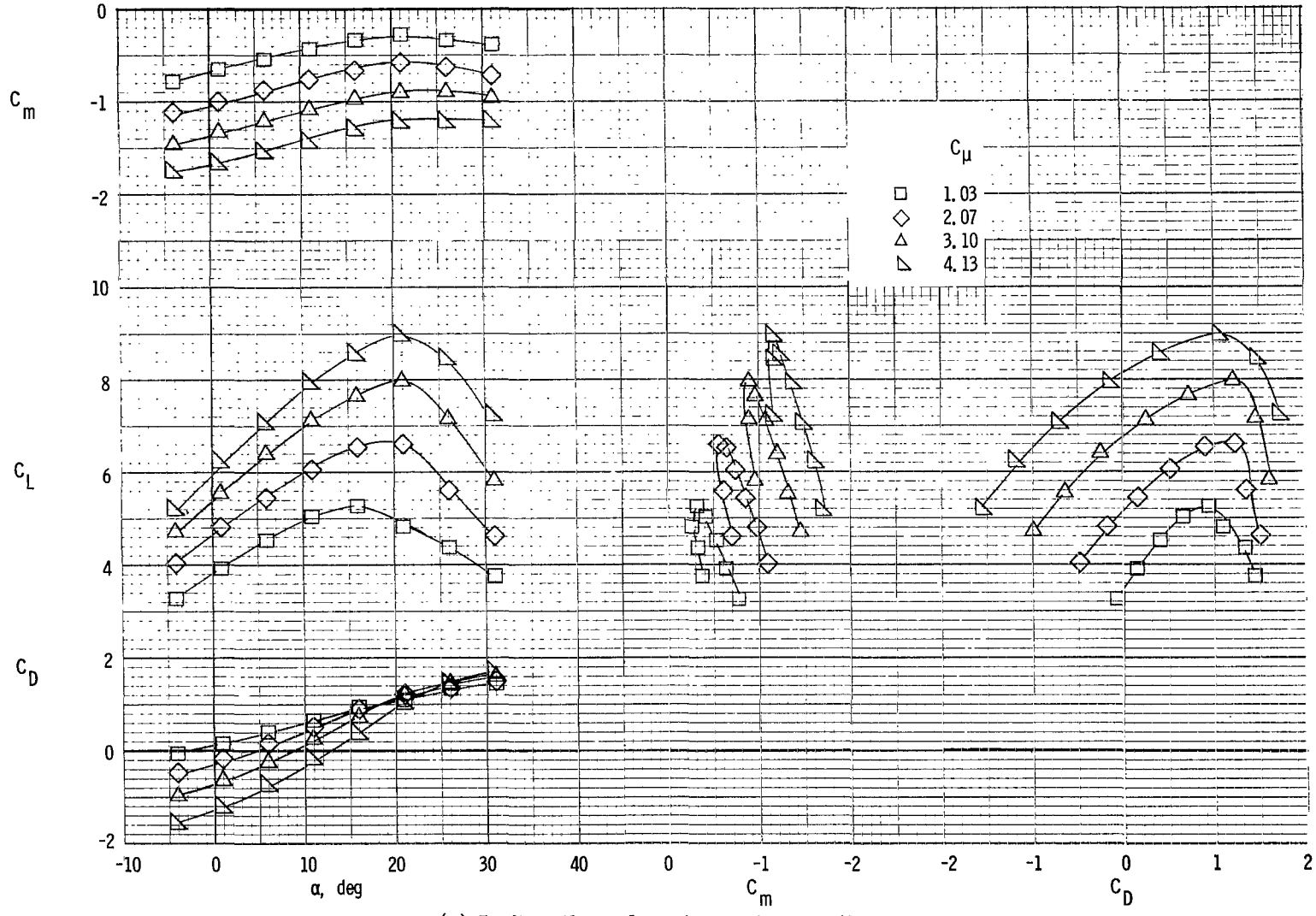

(a) Left outboard engine not operating.

Figure 73.- Longitudinal aerodynamic characteristics of model in an engine-out condition. Engine position 1; exhaust deflectors off; $\delta_f = 55^o$.

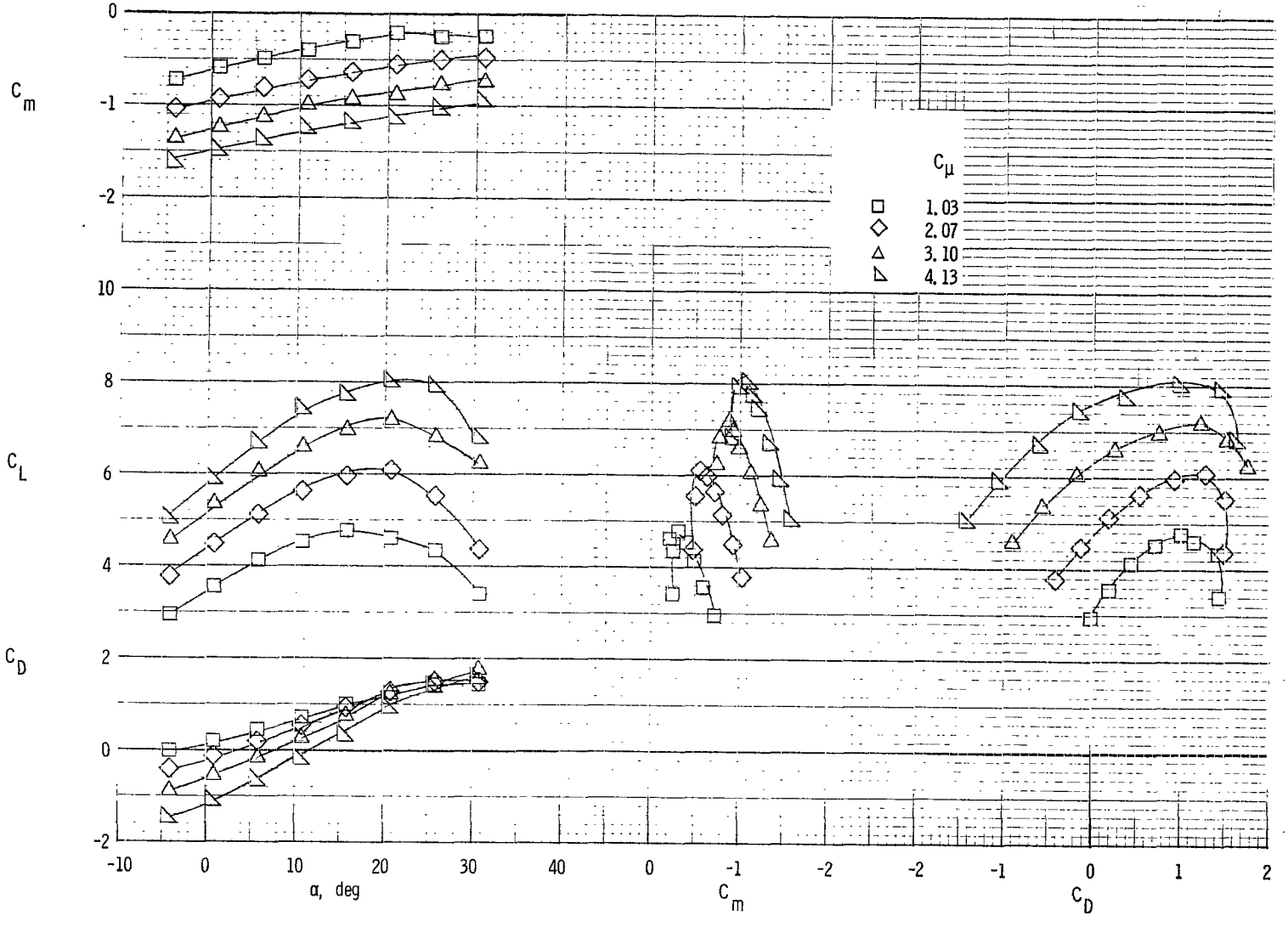

(b) Left inboard engine not operating.

Figure 73.- Continued.

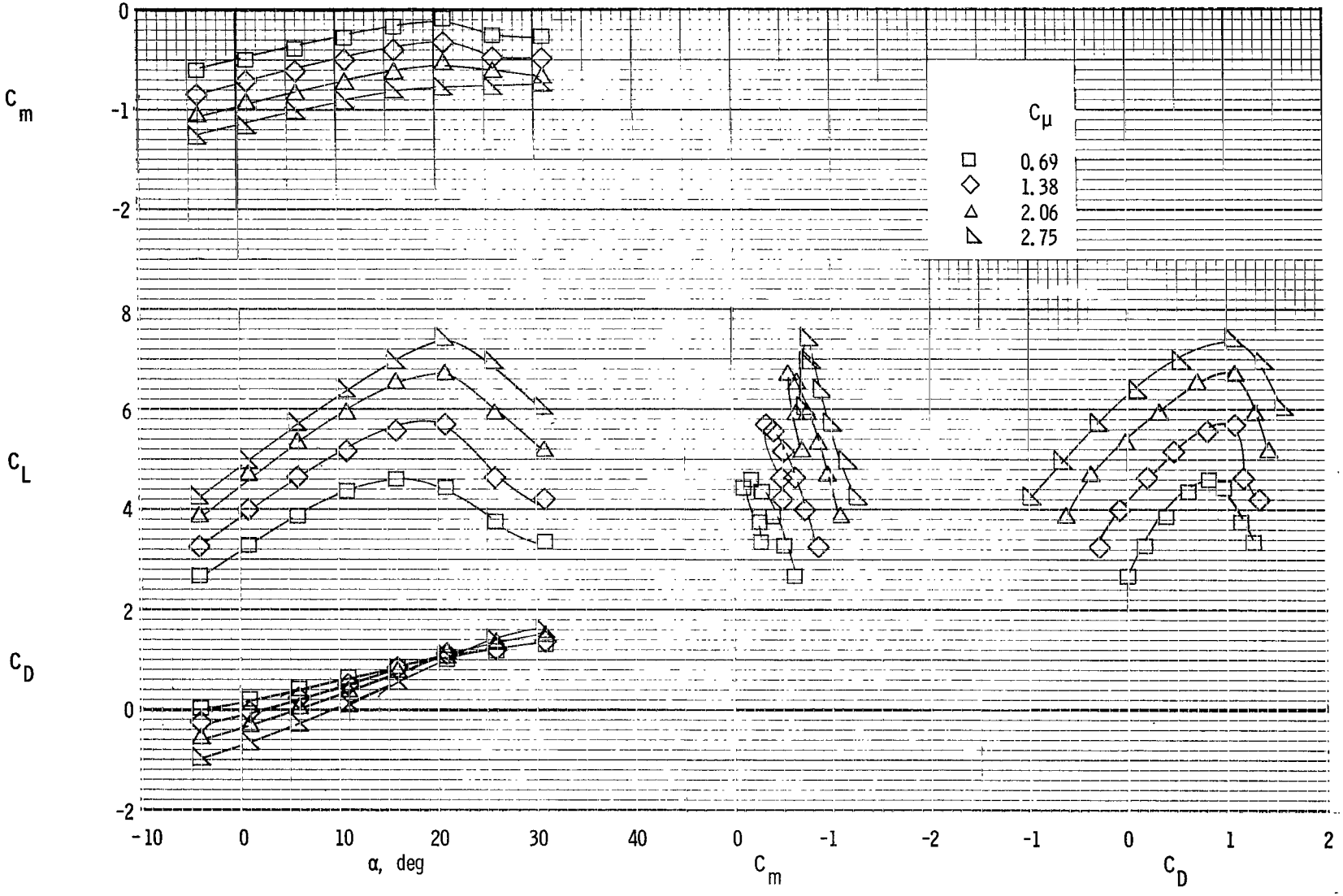

(c) Left and right outboard engines not operating.

Figure 73.- Concluded.

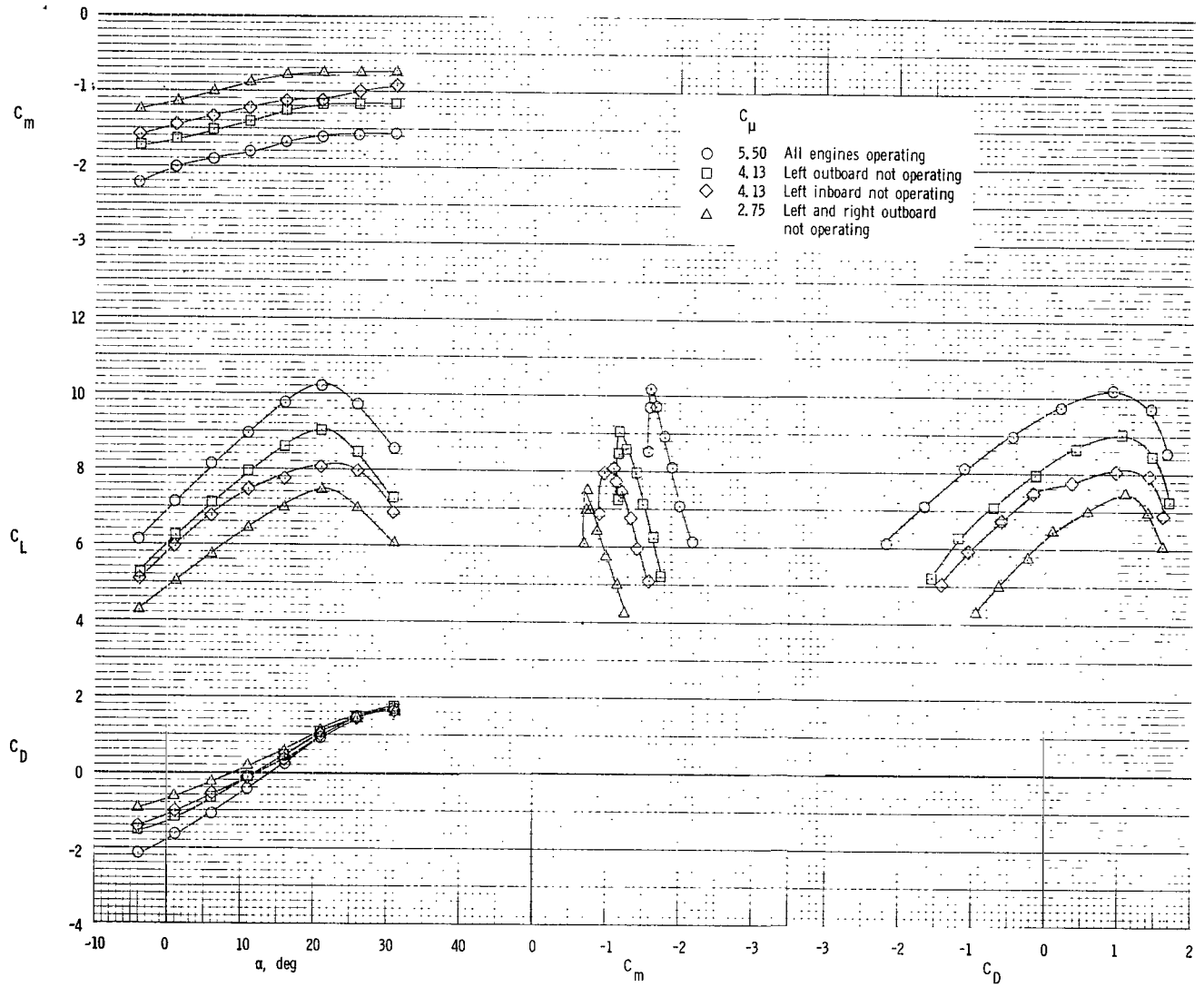

Figure 74.- Summary of engine-out effect on longitudinal aerodynamic characteristics of model. Engine position 1; exhaust deflectors off; $\delta_f = 55^o$.

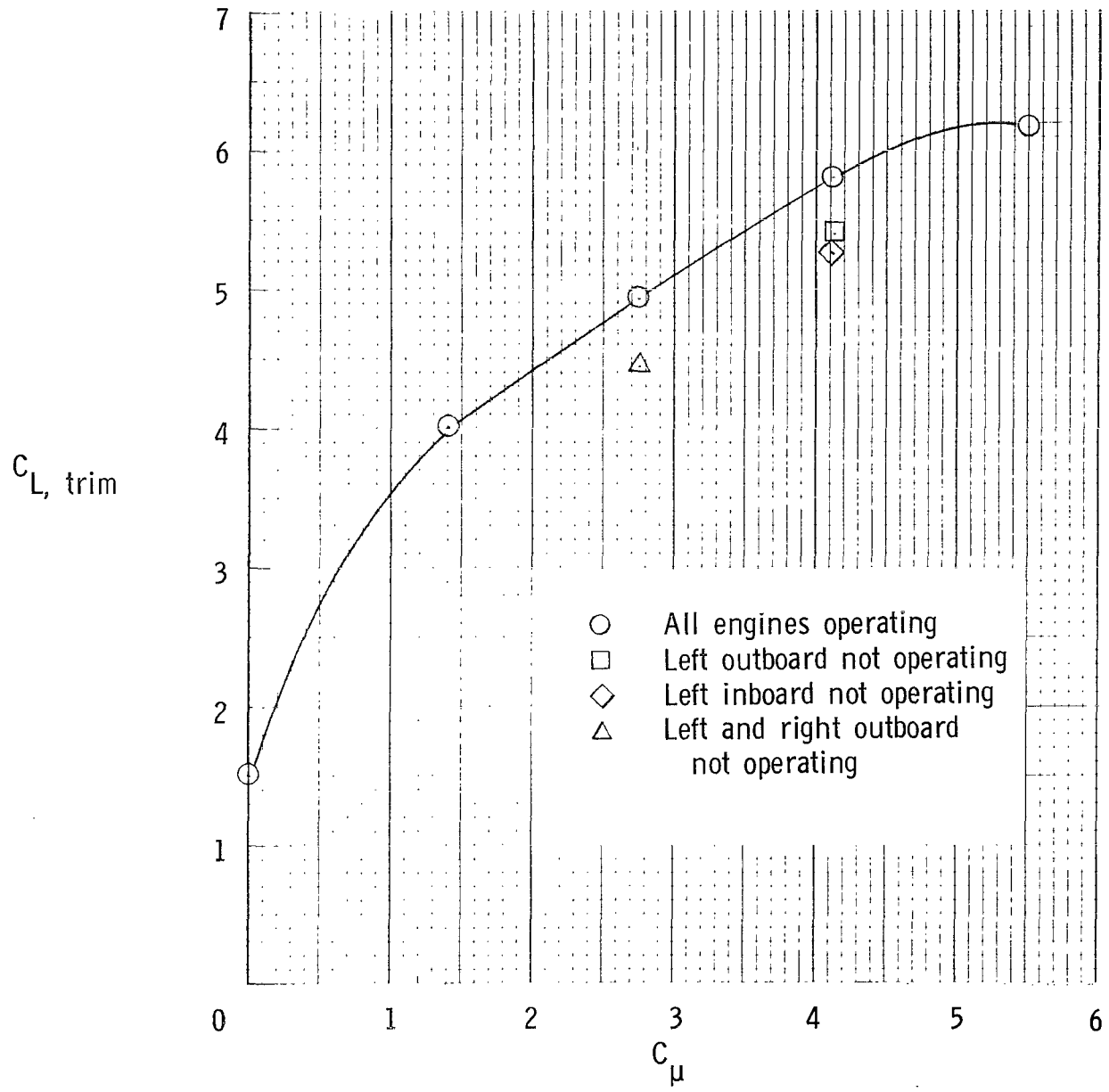

Figure 75.- Effect of engine-out condition on trim lift. Engine position 1; exhaust deflectors off; $\delta_f = 55^o$.

NASA-Langley, 1971 —— 2 L-7581

"The aeronautical and space activities of the United States shall be conducted so as to contribute . . . to the expansion of human knowledge of phenomena in the atmosphere and space. The Administration shall provide for the widest practicable and appropriate dissemination of information concerning its activities and the results thereof."

—NATIONAL AERONAUTICS AND SPACE ACT OF 1958

NASA SCIENTIFIC AND TECHNICAL PUBLICATIONS

TECHNICAL REPORTS: Scientific and technical information considered important, complete, and a lasting contribution to existing knowledge.

TECHNICAL NOTES: Information less broad in scope but nevertheless of importance as a contribution to existing knowledge.

TECHNICAL MEMORANDUMS: Information receiving limited distribution because of preliminary data, security classification, or other reasons.

CONTRACTOR REPORTS: Scientific and technical information generated under a NASA contract or grant and considered an important contribution to existing knowledge.

TECHNICAL TRANSLATIONS: Information published in a foreign language considered to merit NASA distribution in English.

SPECIAL PUBLICATIONS: Information derived from or of value to NASA activities. Publications include conference proceedings, monographs, data compilations, handbooks, sourcebooks, and special bibliographies.

TECHNOLOGY UTILIZATION PUBLICATIONS: Information on technology used by NASA that may be of particular interest in commercial and other non-aerospace applications. Publications include Tech Briefs, Technology Utilization Reports and Technology Surveys.

Details on the availability of these publications may be obtained from:

SCIENTIFIC AND TECHNICAL INFORMATION OFFICE

NATIONAL AERONAUTICS AND SPACE ADMINISTRATION

Washington, D.C. 20546